SPATIOTEMPORAL MODELING OF PM2.5 OXIDATIVE POTENTIAL USING SOURCE IMPACT AND MODEL FUSION TECHNIQUES

A Dissertation
Presented to
The Academic Faculty

by

Josephine T. Bates

In Partial Fulfillment
of the Requirements for the Degree
Doctor of Philosophy in the
School of Civil and Environmental Engineering

Georgia Institute of Technology
August 2018

SPATIOTEMPORAL MODELING OF PM2.5 OXIDATIVE POTENTIAL USING SOURCE IMPACT AND MODEL FUSION TECHNIQUES

Approved by:

Dr. Armistead Russell, Advisor
School of Civil and Environmental Engineering
Georgia Institute of Technology

Dr. Joseph Brown
School of School of Civil and Environmental Engineering
Georgia Institute of Technology

Dr. James A. Mulholland
School of Civil and Environmental Engineering
Georgia Institute of Technology

Dr. Howard Chang
Department of Biostatistics and Bioinformatics
Emory University

Dr. Rodney Weber
School of Earth and Atmospheric Sciences
Georgia Institute of Technology

Date Approved: June 01, 2018

For Gunner, my curious little learner

ACKNOWLEDGEMENTS

I would like to express my sincere appreciation for everyone that I met throughout my graduate career. I would like to thank my committee members, Dr. Armistead Russell, Dr. James Mulholland, Dr. Rodney Weber, Dr. Joseph Brown, and Dr. Howard Chang, for serving on my PhD committee and providing priceless guidance and constructive criticism for my work. I would like to especially acknowledge my advisor, Dr. Armistead Russell, for teaching me more than I ever thought that I could know about air quality, modeling, and critical thinking. I am privileged to have learned from such a great teacher. I would also like to thank Dr. James Mulholland for not only serving on my PhD committee but also leading the CEE graduate student council with Robert Simon, a council that gives a meaningful voice to graduate students. I also owe an incredible debt to all other professors at Georgia Tech and Emory University as well as Russell group members for the enthusiastic learning environment, support, and friendships that have been offered over the years. I would like to thank those who funded the research presented in this dissertation, including the U.S. EPA and ARCS foundation. Finally, I would like to acknowledge my friends and family for their unwavering support and willingness to listen to me talk about my work. To my brother and sister-in-law, for always welcoming me home with fun and games. To my mom, for your unwavering support in my life decisions. To my dad, for showing me the world so that I can care more about it. To Ben, for never doubting that I would reach my dreams even when I doubted myself. To all my friends in Georgia and elsewhere, for keeping me grounded and always smiling.

TABLE OF CONTENTS

ACKNOWLEDGEMENTS iv

LIST OF TABLES viii

LIST OF FIGURES xi

SUMMARY xv

CHAPTER 1. Introduction 1

CHAPTER 2. Review of acellular assays of ambient particulate matter oxidative potential: methods and relationships with composition, sources, and health effects 8
2.1 Introduction 9
2.2 Overview of Measurement Methods 12
2.2.1 Measuring Particle-Bound ROS 13
2.2.2 Measuring Oxidative Potential (OP) 15
2.3 OP in Epidemiologic Analyses 19
2.4 Effects of PM Characteristics on OP 24
2.4.1 Species Composition 24
2.4.2 Source Contribution 35
2.5 Size Distribution 43
2.6 Synthesis and Recommendations for Future Research 44

CHAPTER 3. Reactive oxygen species generation linked to sources of atmospheric particulate matter and cardiorespiratory effects 49
3.1 Introduction 50
3.2 Methods 52
3.2.1 Sample Collection and Analysis 52
3.2.2 Source Apportionment 55
3.2.3 Linear Regression 55
3.2.4 Historical DTT estimation 58
3.2.5 Epidemiologic Modeling 59
3.3 Results and Conclusions 61
3.3.1 Source Contribution to DTT activity 61
3.3.2 Health Analysis 65

CHAPTER 4. Source impact modeling of spatiotemporal trends in $PM_{2.5}$ oxidative potential across the eastern United States 69
4.1 Introduction 70
4.2 Methods 73
4.2.1 Sample Collection and Analysis 73
4.2.2 $PM_{2.5}$ Source Impact Estimation 74
4.2.3 Regression Development 78
4.3 Results and Discussion 81

4.3.1 Source Impacts on OP^{DTT} 81
4.3.2 Spatial Variation in Estimated OP^{DTT} across the Eastern United States 85
4.3.3 Temporal Trends in Estimated OP^{DTT} 89
4.3.4 Uncertainty Analysis in OP^{DTT} Regression 90
4.4 Conclusion 94

CHAPTER 5. Spatial downscaling of CMAQ $PM_{2.5}$ using fine-scale vehicle emissions and concentration data in a statistical model 96
5.1 Introduction 97
5.2 Method 100
5.2.1 Spatial Downscaler Development 100
5.2.2 Inputs for Atlanta Application 103
5.3 Results 107
5.4 Discussion and Conclusions 111

CHAPTER 6. Application and evaluation of two model fusion approaches to obtain ambient air pollutant concentrations at a fine spatial resolution (250m) in Atlanta 113
6.1 Introduction 113
6.2 Methods 118
6.2.1 Model Fusion Methods 120
6.2.2 Methods for Developing Inputs for Application of Model Fusion Techniques to Atlanta, GA 123
6.3 Results 126
6.3.1 Monitoring Data for Evaluation 129
6.3.2 Evaluation of Model Fusion Methods 130
6.3.3 Comparison of Model Fusion Results to OBS-CMAQ 135
6.3.4 Sensitivity Analyses 139
6.4 Discussion 140

CHAPTER 7. Intraurban spatial variation in oxidative potential driven by vehicle emissions in Atlanta 144
7.1 Introduction 145
7.2 Methods 147
7.2.1 $PM_{2.5}$ sampling and DTT analysis 147
7.2.2 Dispersion Modeling 148
7.2.3 $PM_{2.5}$ Model Fusion Process 150
7.2.4 Estimation of OP^{DTT} spatial fields 154
7.3 Results 155
7.4 Discussion 158

CHAPTER 8. Summary of conclusions and future research 161
8.1 Summary of Conclusions 161
8.2 Future Research 165
8.2.1 OP^{DTT} measurements for further evaluation of source impact results 165
8.2.2 Updated Source Impact Analysis 167

8.2.3 Integrating new measurements and updated modeling for intraurban pollutant concentration estimates 169
8.2.4 Global OP research initiatives 170

Appendix A. Supplemental material for chapter 3 172

Appendix B. Supplemental material for chapter 4 174

Appendix C. Supplemental material for chapter 6 186

Appendix D. Supplemental material for chapter 7 195

References 196

LIST OF TABLES

Table 2-1 Reported results of tested associations between OP assays and health endpoints. Associations that were reported to be stronger for OP than PM concentration in at least one study are marked with an *. No significant negative (protective) associations were reported by any study. 19

Table 2-2 Species showing evidence of an impact on OP, either using correlation analyses, measuring OP of pure solutions, or exposing ambient samples to metal chelators (note there is no differentiation with the use of SLF or not). 27

Table 3-1 Pearson correlation coefficients between DTT activity and CMB-estimated sources for the 2012-2013 period. 62

Table 3-2 Regression coefficients and standard errors for each source in the DTT regressions with normalized data[a]. 64

Table 4-1 Average source impact estimates on species in μg m^{-3} after applying primary and secondary corrections with spatial and temporal interpolation. Averages are available across the entire eastern United States modeling domain (Eastern US) and at locations of monitoring data that the regression was trained on (OP^{DTT} measurement sites). 78

Table 4-2 Regression coefficients and standard errors for the regression with all source impacts included (ALL) and for the final regression with only source impacts that significantly impact OP^{DTT} (FINAL). All values [except the intercept (int) in (10^{-2}) $nmol_{DTT}$ min^{-1} m^{-3}] are in units (10^{-2}) $nmol_{DTT}$ min^{-1} μg_{source} for ease of comparison of standard errors to coefficients. 80

Table 4-3 Pearson's correlation coefficients between final adjusted source impacts and OP^{DTT} across all measurements sites. 81

Table 4-4 Regression coefficients and standard errors for sensitivity models 1 and 2 in the sensitivity analysis. All values are in units (10^{-2}) $nmol_{DTT}$ min^{-1} μg_{source} for ease of comparison of standard errors to coefficients. 92

Table 5-1 Beta coefficients for spatial and temporal predictors with standard errors in parentheses. Each coefficient applies for one interquartile range increase in each predictor variable. 108

Table 5-2	Root mean squared error of CMAQ results, the *ARC* model run, and the *RLINE* model run averaged over all sites over the entire study period.	109
Table 5-3	Evaluation statistics for the three model runs with different inputs and/or training data sets.	109
Table 6-1	Evaluation statistics are the median, with minimum and maximum in parentheses, of year-specific averages (2003 through 2008) of the statistics for eight, five, and five monitors for $PM_{2.5}$ ($\mu g/m^3$), CO (ppb), and NOx (ppb), respectively, located in Atlanta, GA. Statistics are available for OBS-CMAQ, additive ($PM_{2.5}$) and multiplicative (NOx and CO) model fusion results using OBS-CMAQ and OBS-RLINE as inputs (*Model Fusion*), and additive ($PM_{2.5}$) and multiplicative (NOx and CO) model fusion results with OBS-RLINE and CMAQ simulations that have not been adjusted using daily observations, representing a 100% withholding, as inputs (*Model Fusion Withholding*).	131
Table 6-	Median of spatial Pearson's correlation coefficients over the study period with minimum and maximum in parentheses. Values are estimated using the annual averages of available observation sites and additive ($PM_{2.5}$) and multiplicative (NOx and CO) model fused results (250m resolution) with OBS-CMAQ and OBS-RLINE as inputs, OBS-CMAQ (12km resolution), and OBS-RLINE simulations (250m resolution) during the years 2003 through 2008.	137
Table 7-1	Normalized mean biases of OP^{DTT} estimates using different source impacts at each measurement site.	158
Table A-1	Coefficients, standard errors (in parentheses) and *p* values for the DTT regression with all sources and for the regression with only sources that have statistically significant coefficients used to create the historical DTT estimates for the epidemiologic study.	172
Table A-2	Pearson correlation coefficients between volume normalized DTT (DTTv, nmol min^{-1} m^{-3}) and species concentration and mass normalized DTT (DTTm, nmol min^{-1} μg^{-1}) and species concentration measured from June 2012 – April 2013.	173
Table B-1	A description of each of the 16 emission source categories used in the CMAQ-DDM modeling.	174
Table B-2	Normalized mean biases in $PM_{2.5}$ species after bias correction algorithms and temporal interpolation have been applied.	178

Biases presented in the table are averaged over all CSN and SEARCH sites (146 sites) across the eastern United States and across the OP^{DTT} measurement sites (4 sites).

Table B-3 Pearson's linear correlation coefficients between CMAQ-DDM source impacts used in regression development. 178

Table C-1 Monitor information, including network names, whether the monitor is located in an urban or rural location, and years that data are available. If there is no month listed, data are available for the entire year. 190

Table C-2 Evaluation statistics for model fused estimates of $PM_{2.5}$ ($\mu g/m^3$), CO (ppb), and NOx (ppb) using each model fusion method. 192

LIST OF FIGURES

Figure 2-1 Intrinsic OP^{DTT} (median and standard deviations) of various emission sources studied in either ambient or chamber conditions at locations worldwide plotted on a log scale. The size fractions of average ambient PM are defined as: quasi-ultrafine ($\leq PM_{0.18}$), fine ($\leq PM_{2.5}$), and coarse ($\leq PM_{10}$).Measured DTT activity plotted against DTT activity estimated using the regression model. This data is for the 2012-2013 period. The R^2 between estimated and measured DTT is 0.49. 38

Figure 3-1 Measured DTT activity plotted against DTT activity estimated using the regression model. This data is for the 2012-2013 period. The R^2 between estimated and measured DTT is 0.49. 57

Figure 3-2 Daily estimated DTT activity of WS-$PM_{2.5}$ from Aug 1998 to Dec 2009 calculated using the regression. The pie chart shows the average contribution of each source over the time period. 63

Figure 3-3 Effect of ROS (by estimated DTT activity) on ED visits for (a) asthma/wheeze and (b) congestive heart failure in the Atlanta 5 county area, from Aug 1, 1998 to December 31, 2009, with 0—2 day lag. The model labeled "DTT only" or "$PM_{2.5}$ only" illustrates the results from the model run only with DTT activity or total $PM_{2.5}$ mass as the exposure variable, respectively. The model labeled "DTT and $PM_{2.5}$" illustrates the results from the two-pollutant model, in which both DTT activity and total $PM_{2.5}$ mass were used as exposure variables. 67

Figure 4-1 Average of (a) CMAQ-derived and bias corrected $PM_{2.5}$ in $\mu g\ m^{-3}$ (average 6.3 $\mu g\ m^{-3}$ with minimum 0.5 $\mu g\ m^{-3}$ and maximum 131.7 $\mu g\ m^{-3}$) and (b) estimated OP^{DTT} in $nmol_{DTT}\ min^{-1}\ m^{-3}$ (average 0.30 $nmol_{DTT}\ min^{-1}\ m^{-3}$ with minimum 0.13 $nmol_{DTT}\ min^{-1}\ m^{-3}$ and maximum 14.1 $nmol_{DTT}\ min^{-1}\ m^{-3}$) from June 1, 2012 to July 30, 2013 across the eastern United States. 85

Figure 4-2 Specific source impacts on OP^{DTT} across the Eastern United States averaged from June 1, 2012 to July 30, 2013, including (a) on-road gasoline (b) on-road diesel (c) fires and (d) natural gas combustion. Note, the plots have different color scales so that spatial distributions are visible. 87

Figure 4-3 Estimated contribution of source impacts to apportioned OP^{DTT} averaged from June 1, 2012 through July 30, 2013. 88

Figure 4-4 Daily source impacts on estimated OP^{DTT} across (a) all measurement sites (CSN and SEARCH sites across eastern United States) and at (b) OP^{DTT} measurement site in Atlanta, GA from June 1, 2012 through July 30, 2013. 90

Figure 5-1 Locations of $PM_{2.5}$ monitors in Atlanta, GA used in this study. Observational data from these monitors are used in the statistical downscaling model training data set. 103

Figure 5-2 (a) Link-based $PM_{2.5}$ emissions in g/m/day for a representative day in 2010 obtained from ARC and (b) 2005 annual average RLINE $PM_{2.5}$ concentrations 106

Figure 5-3 2005 annual-average $PM_{2.5}$ concentration fields estimated by the statistical downscaler at the 25,289 grids in Atlanta, GA. The results include the *ARC-Obs* model run (left), the *ARC* model run (middle), and the *RLINE* model run (right). Higher concentrations are in red and lower concentrations are in blue. 110

Figure 6-1 Additive model fusion steps and results for 2005 annual average $PM_{2.5}$. First, the fine resolution (250m) OBS-RLINE field is averaged to a 12km grid matching the OBS-CMAQ grid (b), which is subtracted from the OBS-CMAQ 12km field (a). These results are spatially interpolated to 250m resolution matching the OBS-RLINE grid resolution (c) and then added to the 250m resolution OBS-RLINE field (d) to provide a 250m resolution model-fused annual average $PM_{2.5}$ field (e). Note: each plot has a different color scale in order to show the spatial distributions clearly. 128

Figure 6-2 Multiplicative model fusion results for annual averages of 1 h maximum CO (ppb) (left) and NOx (ppb) (right) for the year 2005. 128

Figure 6-3 Density scatter plots of annually averaged model fusion estimates at each 250m grid cell versus annual average OBS-CMAQ values at the corresponding grid cells during the years 2003-2008 for (a) 24 h average $PM_{2.5}$ ($\mu g/m^3$) by additive method, and (b) 1 h maximum CO (ppb) and (c) 1 h maximum NOx (ppb) by multiplicative method. A higher density of points is in yellow and lower density in blue. Black lines represent 1:1 lines. 138

Figure 7-1 Locations of OP^{DTT} measurement sites in Atlanta, GA. 148

Figure 7-2 2011 annual-average OBS-RLINE of the impacts of on-road emissions to primary $PM_{2.5}$ ($\mu g\ m^{-3}$) in Atlanta, GA. 150

Figure 7-3 CMAQ-DDM ($\mu g\ m^{-3}$) identified vehicle source impacts (on-road gasoline + on-road diesel) on $PM_{2.5}$ in Atlanta, GA (extracted from previously developed data for eastern United States (J. Bates, 153

Weber, et al., 2018)) averaged from June 1, 2012 through April 30, 2013.

Figure 7-4 Model fused $PM_{2.5}$ ($\mu g\ m^{-3}$) from vehicles in Atlanta,GA , averaged from June 1, 2012 through April 30, 2013. 154

Figure 7-5 Estimated OP^{DTT} (nmol min^{-1} m^{-3}) due to (a) on-road vehicles and (b) all sources (fires, natural gas, on-road vehicles, regional) in Atlanta, GA averaged from June 1, 2012 through April 30, 2013. Note the differences in color bar on each plot to better show spatial distribution. 156

Figure 8-1 Annual average contributions to apportioned OPDTT in Atlanta, GA for 1999 (left) and 2009 (right). 165

Figure A-1 Results from an experiment comparing the DTT activity of a blank filter (filter 1) to filters with water-soluble sulfate (filters 2-7) showing that there is no significant difference between the blank filters and water-soluble sulfate filters. 173

Figure B-1 Locations of CSN and SEARCH monitoring sites within the study domain whose data were used to minimize bias in CMAQ-DDM estimates. CSN sites are represented as black dots and SEARCH sites are represented as red asterisks. SEARCH site locations are also where OP^{DTT} measurement sites are. 180

Figure B-2 Measured OP^{DTT} versus regression-estimated OP^{DTT} with the 1:1 line in red. 181

Figure B-3 OP^{DTT} driven by natural gas combustion, on-road diesel, and on-road gasoline (no fire impacts) averaged from June 2012 to July 2013. 181

Figure B-4 Temporal trends in source impacts on estimated OP^{DTT} at the Atlanta, GA measurement site. Note: The plots are on different y-scales to show daily variations in OP^{DTT}. 183

Figure B-5 Temporal trends in source impacts on estimated OP^{DTT} across the modeling domain. Note: The plots are on different y-scales to show daily variations in OP^{DTT}. 184

Figure B-6 OP^{DTT} estimated using source impacts and coefficients in sensitivity models 2 ((a) and (b)) and 3 ((c) and (d)), with ((a) and (c)) and without ((b) and (d)) fire impacts to see the spatial distributions without large concentrations from wildfires. 185

Figure C-1 Multiplicative model fusion steps and results for 2005 annual average CO. First, the fine resolution (250m) OBS-RLINE field is averaged to a 12km grid matching the OBS-CMAQ grid (b). OBS-CMAQ 12km field (a) is divided by the 12km OBS-RLINE (b). These results are spatially interpolated to 250m resolution matching the OBS-RLINE grid resolution (c) and then multiplied by the 250m resolution OBS-RLINE field (d) to provide a 250m resolution model-fused annual average CO field (e). 187

Figure C-2 Multiplicative model fusion steps and results for 2005 annual average NOx. First, the fine resolution (250m) OBS-RLINE field is averaged to a 12km grid matching the OBS-CMAQ grid (b). OBS-CMAQ 12km field (a) is divided by the 12km OBS-RLINE (b). These results are spatially interpolated to 250m resolution matching the OBS-RLINE grid resolution (c) and then multiplied by the 250m resolution OBS-RLINE field (d) to provide a 250m resolution model-fused annual average NOx field (e). 188

Figure C-3 Annual average $PM_{2.5}$ concentrations ($\mu g/m^3$) estimated using the additive model fusion process for each year of the study period (2003 through 2008). 189

Figure C-4 Annual average 1-hr maximum NOx concentrations (ppb) estimated using the multiplicative model fusion process for each year of the study period (2003 through 2008). 189

Figure C-5 Annual average 1-hr maximum CO concentrations (ppb) estimated using the multiplicative model fusion process for each year of the study period (2003 through 2008). 190

Figure D-1 Estimated OP^{DTT} of fires (top) and natural gas combustion (bottom) in Atlanta, GA. 195

SUMMARY

Exposure to elevated levels of air pollution can lead to cardiorespiratory disease, birth defects, and cancer. However, observational air quality data are spatially and temporally sparse due to high cost of monitors, limiting the scope of epidemiologic analyses and introducing error in exposure assessments. This dissertation presents the developments, evaluations, and applications of multiple mathematical and computational modeling approaches for estimating spatiotemporal fields of air pollutant concentrations where and when monitoring data are not available.

First, source apportionment techniques with multivariate regression analyses are used to estimate long-term (years 1998—2010) and large-scale (eastern United States) spatiotemporal trends in a novel pollutant metric, fine particulate matter ($PM_{2.5}$) oxidative potential measured with a dithiothreitol assay (OP^{DTT}). OP^{DTT} measures a particle's ability to catalytically generate reactive oxygen species while simultaneously depleting a body's antioxidant defenses, leading to oxidative stress and, in turn, inflammation in the respiratory tract and cardiovascular system. Two different source apportionment techniques are used to estimate source impacts on OP^{DTT}: the source-receptor Chemical Mass Balance (CMB) method and the photochemical air quality model with sensitivity analysis CMAQ-DDM (Community Multiscale Air Quality Model with Direct Decoupled Method). CMB is applied to an OP^{DTT} measurement site in Atlanta, GA at which advanced ensemble-based source profiles had previously been developed. CMAQ-DDM is applied across the eastern United States and data assimilation techniques are used to minimize biases in source impact estimates. Two OP^{DTT}-predictive models are developed by relating OP^{DTT} measurements to either CMB or CMAQ-DDM derived $PM_{2.5}$ source impacts using

multivariate regression analyses with backwards selection. The CMB-based model is applied to daily $PM_{2.5}$ CMB source impacts from August 1998 through December 2010 to obtain an historical time series of daily 24 h averaged estimated OP^{DTT} at one site in Atlanta, GA. The CMAQ-DDM source impact model is applied to daily $PM_{2.5}$ CMAQ-DDM source impacts from June 2012 to July 2013 to estimate daily 24 h averaged OP^{DTT} across the eastern United States. The estimated historical time series of ambient OP^{DTT} in Atlanta, GA is used in a health study showing that OP^{DTT} is more linked to asthma/wheezing and congestive heart failure emergency department visits than $PM_{2.5}$ mass. In other words, OP^{DTT} exposure drives a positive, significant risk ratio in two-pollutant models with both OP^{DTT} and $PM_{2.5}$ exposure, while $PM_{2.5}$ does not, even though OP^{DTT} estimates are likely more uncertain than $PM_{2.5}$ measurements, implying OP^{DTT} is a useful, health-relevant air pollutant metric. The OP^{DTT} estimates across the eastern United States are developed for future regional or multi-city health analyses. Both source apportionment regression approaches find that out of the sixteen tested emission sources, vehicle (both gasoline and diesel) and biomass burning emissions are the major contributors to ambient OP^{DTT} levels. Biomass burning, including wildfires and prescribed burning, is the largest overall contributor to ambient OP^{DTT} levels in these studies, driving its spatial and temporal trends.

Second, statistical downscaling techniques and model fusion approaches are developed and applied to simulate intraurban air pollutant concentrations [OP^{DTT}, $PM_{2.5}$, carbon monoxide (CO), and nitrogen oxides (NOx)] at a fine spatial resolution (250m) in Atlanta, GA. These methods attempt to capture steep concentration gradients driven by vehicle emissions on roadways that are not captured by models with coarse grid resolutions

(like CMAQ) or limited observational data but can affect exposures. The statistical model is developed under a Bayesian Hierarchal framework to downscale 12km CMAQ data to geocoded locations using annual-averaged link-based vehicle emissions or 250m resolution dispersion model data from RLINE (Research LINE model—a link-based dispersion model for near-surface releases of primary, inert pollutants) as land-use regression variables. However, there is limited observational data on which to train the model, and the CMAQ and RLINE data are correlated, so estimated $PM_{2.5}$ concentration fields in Atlanta, GA are unphysical with lower concentrations on roadways than in rural areas. Further work modeling daily RLINE and collecting near-road $PM_{2.5}$ monitoring data for the model training data set is suggested to produce a successful statistical downscaler under this framework.

Due to the current limitations of the statistical downscaler, two model fusion techniques are also developed to estimate air pollutant concentrations at a fine spatial resolution within Atlanta, GA. These approaches combine 12km CMAQ data, which provide the daily data along with chemistry and regional emissions, and 250m RLINE data, which provide the fine spatial resolution data of primary pollutants on an annual basis, that have been previously fused with observations to optimize model estimates. Two slightly different model fusion techniques are developed due to biases in CMAQ and RLINE: an additive model that is applied to $PM_{2.5}$ and a multiplicative model that is applied to CO, NOx, and OP^{DTT}. The model-fused air pollutant concentration fields in Atlanta, GA show peaks on roadways and steep spatial gradients. Overall, model-fused concentration estimates for $PM_{2.5}$, NOx, and CO have higher temporal and spatial correlations with monitoring data than observation-fused CMAQ or RLINE alone, suggesting that the

model-fused estimates provide the most accurate data out of currently available modeling data for epidemiologic and environmental justice studies investigating effects of intraurban air pollution exposures, particularly as they relate to impacts of vehicle emissions on health. Model-fused OP^{DTT} results show peaks on roadways that can affect exposures but contributions from other sources, like biomass burning and natural gas combustion, cause a more spatially homogeneous field compared to other pollutants (e.g., CO and NOx). The OP^{DTT} results also suggest that the intrinsic OP^{DTT} of vehicle emissions may vary spatially. These model fusion methods are computationally fast and can be easily applied to other models, study areas, spatial resolutions, and pollutants, allowing their use in a broad range of future research projects.

The methods and spatiotemporal fields presented in this dissertation can be valuable tools for future epidemiologic and environmental justice studies investigating the utility of OP^{DTT} as a useful health metric and the impacts of disproportionate air pollution exposure on minority communities in urban environments resulting from heterogeneous pollutants emitted by vehicles.

CHAPTER 1.

INTRODUCTION

The World Health Organization reports that ambient air pollution is the fifth leading cause of premature death and disability (Lim et al., 2012). Specifically, fine particulate matter ($PM_{2.5}$) is estimated to have contributed to 3.2 million premature deaths in 2010 and to roughly 5% of all cardiorespiratory deaths across the globe (Lim et al., 2012). One critical difficulty with studying air pollution health effects is estimating pollutant exposures for epidemiologic studies. Misidentifying exposure can lead to significant biases in health risk assessments, especially in long-term cohort studies (Goldman et al., 2011). Further, inaccurately estimating intraurban spatial variations in air pollutant concentrations affects environmental justice studies researching the impacts of disproportionate exposures of populations and individuals to pollution. Air quality monitoring data are often too sparse to capture the spatial and temporal variabilities in air pollutant concentrations, so air quality modeling is often used to provide spatially and temporally resolved air pollutant estimates that monitors do not capture. However, models can be limited by coarse grid resolutions incapable of capturing steep spatial gradients in pollutant concentration or may lack chemistry for secondary pollutant formation. Further, current models do not capture all atmospheric contaminants or pollutant properties relevant to health, such as oxidative potential (OP) of $PM_{2.5}$. With a changing particulate matter composition with an increasing biogenic fraction due to dropping anthropogenic emissions, it may become more important to measure and model health-relevant components of $PM_{2.5}$ rather than total $PM_{2.5}$ mass as each $PM_{2.5}$ component may not have similar impacts on health. OP is a potentially useful

metric for measuring the components of particulate matter that drive adverse health outcomes. This dissertation presents the developments, evaluations, and applications of source impact models capable of estimating long-term and large-scale spatiotemporal trends in OP as well as modeling methods developed to estimate urban air pollutant concentrations, including $PM_{2.5}$, carbon monoxide (CO), nitrogen oxides (NO_2 + NO = NOx), and OP, at a fine spatial resolution. Developing long-term, large-scale, and fine-scale spatiotemporal fields of air pollutant concentrations is valuable for reducing uncertainty, assessing consistency of results across study areas, and improving accuracy, respectively, in exposure and epidemiologic analyses.

The first part of this dissertation describes the current state of knowledge on OP while building upon that research by developing models using source impact analyses that are applied to create spatiotemporal fields of OP of ambient $PM_{2.5}$ for health research, described in chapters 2 through 4. OP assays measure a particle's ability to catalyze redox reactions that generate reactive oxygen species (ROS) while depleting antioxidants *in vivo*, leading to an imbalance in ROS and the body's antioxidant defenses that results in oxidative stress. Oxidative stress can lead to DNA strand breakage and inflammatory responses in organs such as the lungs, heart, and brain (Baulig et al., 2003; Donaldson, Stone, Seaton, & MacNee, 2001; N. Li et al., 2003; Prahalad et al., 2001). OP integrates the biologically-relevant redox reactions of particulate matter species into one measurement. Studying source impacts on OP can assist with targeting health-relevant emissions for regulatory initiatives. The research presented in this dissertation is focused on Atlanta, GA and the eastern United States where $PM_{2.5}$, and, thus, OP are impacted by a multitude of emission sources with significant formation from photochemistry.

The second part of this dissertation focuses on developing methods for estimating urban air pollutant concentrations near roadways at a fine spatial resolution while also capturing the atmospheric chemistry and regional emissions that impact the more spatially homogenous "urban background" concentrations and is presented in chapters 5 through 7. With over 66% of the world's population projected to live in cities by 2050, accurately estimating intraurban air pollution is critical for epidemiology and environmental justice work (United Nations, Department of Economic and Social Affairs, & Population Division, 2014). Two modeling techniques are developed to incorporate the strengths of regional-scale photochemical air quality models and fine-scale dispersion models while limiting the disadvantages of each model and are applied to develop intraurban air quality estimates at a fine spatial resolution. Daily pollutant concentration fields in Atlanta at geocoded locations and 250m resolution are presented. These fine-scale spatial fields can capture the steep concentration gradients near roadways necessary for exposure and health analyses focusing on vehicle emissions. A brief introduction specific to each chapter in this dissertation is presented below.

Chapter 2 assesses our understanding of particulate matter OP by reviewing the broad and growing global literature. A variety of acellular OP measurement techniques exist, including the dithiothreitol (OP^{DTT}), glutathione (OP^{GSH}), ascorbic acid (OP^{AA}), and electron spin resonances (OP^{ESR}) assays. Each assay responds differently to particulate matter species and emission source composition and appears to have different relationships with health outcomes. Each of the listed OP assays captures the redox reactions driven by metals, including copper, manganese, and iron (except OP^{DTT} does not capture Fenton chemistry driven by iron) that are found in vehicle emissions while OP^{DTT} also responds to

organic species, such as quinones, resulting from vehicle and biomass burning emissions. As organic species age, OP^{DTT} increases, which could impact population exposures to health-relevant particulate matter. Further, the species and source impacts on particulate matter drive the size distribution of OP. Based on the limited health research currently available, OP^{DTT} and OP^{GSH} appear to be the most relevant assays for cardiorespiratory health, including asthma/wheezing, congestive heart failure, lung cancer, and ischemic heart disease. OP^{AA} does not appear to measure particulate matter effects relevant to any health endpoints. Future work should include standardizing OP measurement techniques for more direct and effective comparison between studies and expanding measurements of OP^{DTT} and OP^{GSH} for more extensive epidemiologic studies looking at chronic and acute health endpoints beyond cardiorespiratory effects.

Chapter 3 presents the development of an empirical model for OP^{DTT} in Atlanta, GA using source impacts from the source-receptor Chemical Mass Balance (CMB) method. Multivariate regression with backward selection is used to relate CMB source impacts to OP^{DTT} measurements. The resulting model shows the importance of vehicle and biomass burning emissions to OP^{DTT} of ambient $PM_{2.5}$ in Atlanta. The model is applied to daily CMB-derived source impacts at the OP^{DTT} measurement site from August 1998 through December 2010 to estimate an unprecedentedly large temporal data set of OP^{DTT}, which is used in an epidemiologic analysis. This study highlights OP^{DTT} as a useful health indicator for certain cardiorespiratory endpoints, the importance of vehicles and biomass burning for health-relevant $PM_{2.5}$, and the capability to reconstruct a long time series of ambient OP^{DTT} using a source impact model developed using a regression analysis. As a

testament to the utility of this modeling approach, it has been used more recently by other groups internationally (Samuël et al., 2018).

Chapter 4 describes the spatiotemporal modeling of OP^{DTT} across the eastern United States. Building on the approach discussed in chapter 3, chapter 4 details the development, evaluation, and application of using chemical transport model-derived source impacts rather than CMB-derived source impacts to model regional spatial trends in ambient OP^{DTT} for use in multi-city epidemiologic analyses. CMB is limited to a specific observational site with speciated measurements (in this case, Atlanta, GA), so CMAQ-DDM (Community Multiscale Air Quality Model with Direct Decoupled Method) is used to generate source impacts across the eastern United States. Biases in these source impacts are reduced using data assimilation techniques. These bias-reduced source impacts are integrated with spatially-limited observations of OP^{DTT} from four measurement locations across Georgia and Alabama by using multivariate regression with backward selection. This work supports that out of the sixteen tested source impacts (agriculture, aircraft, biogenics, coal combustion, dust, fuel oil, fires, metal processing plants, natural gas combustion, on-road and non-road gasoline vehicles, on-road and non-road diesel vehicles, seasalt, other, and residential wood combustion), on-road vehicle and fire emissions are significant contributors to OP^{DTT}, consistent with previous work presented in chapter 3 as well as from other work globally. Overall, this chapter presents a method for using limited observations with source impact analyses to develop a model capable of estimating OP^{DTT} across a large study domain.

Chapter 5 presents the development and application of a spatial statistical downscaling model developed under a Bayesian hierarchal framework that uses

observations to train coefficients for daily 12km CMAQ data and annual-averaged 250m dispersion model data from RLINE or on-road vehicle emissions developed by the Atlanta Regional Commission (ARC) to simulate $PM_{2.5}$ concentrations at geocoded locations. In other words, the fine-scale emissions and dispersion model data are used as land-use regression variables to downscale 12km CMAQ data. The advantage of this method is computational efficiency, the ability to estimate concentration estimates at geocoded locations, and built-in uncertainty analysis. However, when using annual-averaged RLINE data as an input parameter, the statistical downscaler predicts unphysical spatial concentration gradients with lower concentrations on roadways than in rural areas. The hypothesized reasons for these unphysical results, including lack of observational data for the training set and covariation between CMAQ and RLINE, are discussed.

Chapter 6 describes the development, evaluation, and application of two model fusion methods used to simulate air pollutant concentrations in Atlanta, GA from 2003 through 2008 at a 250m resolution. Two slightly different models are developed due to biases in CMAQ and RLINE: an additive model that is applied to $PM_{2.5}$ and a multiplicative model that is applied to CO and NOx. A sensitivity analysis using each model for estimating each pollutant is presented. Each method fuses daily 12km CMAQ and annual-average 250m RLINE data that were each previously adjusted with observations to minimize biases. CMAQ provides the daily temporal data as well as photochemically formed secondary pollutants and regional source impacts while RLINE provides the fine spatial variation in primary roadway pollution. The resulting model fused pollutant concentration fields have high concentrations on roadways and steep spatial gradients, in line with available observations, and are being used in environmental justice, city planning,

and health studies. These model fusion methods are flexible and fast tools that can be applied to other pollutants, models, and study areas of interest for future research.

Chapter 7 presents a brief analysis of spatial variation of daily water-soluble OP^{DTT} within Atlanta, GA from June 2012 through July 2013. OP^{DTT} concentrations are estimated at a 250m resolution using the multiplicative model fusion method described in chapter 6 with daily $PM_{2.5}$ on-road vehicle impacts from CMAQ-DDM and annual-average primary $PM_{2.5}$ RLINE estimates. The model fused results represent the primary and secondary $PM_{2.5}$ resulting from vehicle emissions and are multiplied by an estimated intrinsic OP^{DTT} value for vehicle sources. This vehicle-driven OP^{DTT} is then added to OP^{DTT} of other sources, including fires, natural gas combustion, and regional sources, that are calculated by multiplying source-specific intrinsic OP^{DTT} by their respective spatially interpolated $PM_{2.5}$ source impacts. The results presented provide initial insight into within-city variation of OP^{DTT} that could affect exposure analyses and suggest that intrinsic OP^{DTT} of vehicles may vary in space due to photochemical aging.

This dissertation concludes with a summary of the major findings of the above studies as well as proposed ideas for future work that would be valuable to improve upon the developed models and our understanding of the relationship between source impacts, OP, and health.

CHAPTER 2.

REVIEW OF ACELLULAR ASSAYS OF AMBIENT PARTICULATE MATTER OXIDATIVE POTENTIAL: METHODS AND RELATIONSHIPS WITH COMPOSITION, SOURCES, AND HEALTH EFFECTS

Abstract

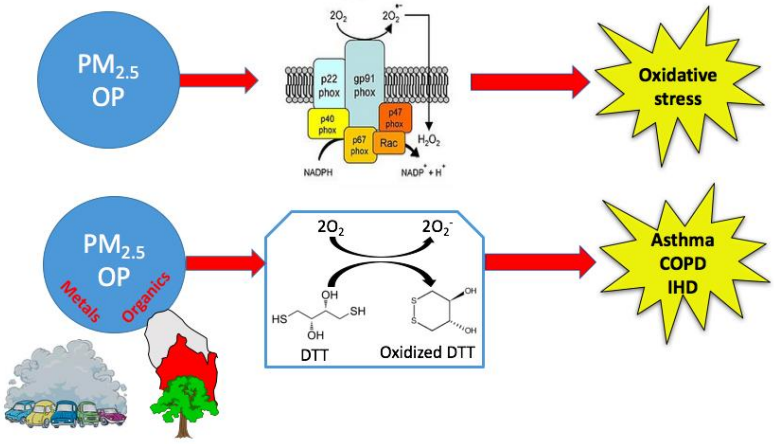

Oxidative stress is a potential mechanism of action for particulate matter (PM) toxicity and occurs when the body's antioxidant capacity cannot counteract harmful effects of reactive oxygen species (ROS) due to an excess presence of ROS. ROS can be bound on and/or within PM (particle-bound ROS) and/or catalytically generated *in vivo* by redox-active PM components (oxidative potential, OP). In this review, particle-bound ROS techniques are discussed briefly while acellular OP measurements are the focus because more ROS are generated catalytically *in vivo* than are present bound to particles. The most common OP measurement methods are discussed along with evidence for utility of OP

measurements in epidemiologic studies and PM characteristics that drive different responses between assay types (such as species composition, emission source, and photochemistry). Dithiothreitol and glutathione OP assay measurements have significant associations with certain cardiorespiratory endpoints, such as asthma, ischemic heart disease, and lung cancer. Though more work is needed, OP shows promise for health studies as it integrates redox-active PM species that drive *in vivo* catalytic reactions leading to oxidative stress into one measurement and current work highlights the importance of metals, organic carbon (especially aged organic carbon), vehicles, and biomass burning emissions to OP.

2.1 Introduction

Extensive literature supports the association between airborne particulate matter (PM) and adverse human health effects, especially cardiorespiratory endpoints (Brunekreef & Holgate, 2002; Cesaroni et al., 2014; Delfino, Sioutas, & Malik, 2005; Donaldson et al., 2001; N. Li et al., 2003; Pope et al., 2002; Pope, Ezzati, & Dockery, 2009). However, the mechanisms of action are not completely understood. Growing evidence in cellular, animal model, and human biomarker studies show that PM exposure can induce oxidative stress, offering one potential mechanism of PM toxicity (Autrup et al., 1999; Ball, Straccia, Young, & Aust, 2000; Baulig et al., 2003; Dellinger et al., 2001; Donaldson et al., 2001; Kodavanti et al., 2002; N. Li et al., 2003; Prahalad et al., 2001; Saffari, Daher, Shafer, Schauer, & Sioutas, 2014a; Sorensen et al., 2003; Strak et al., 2012). Oxidative stress occurs when the concentration of reactive oxygen species (ROS) are in excess of the body's antioxidant capacity, leading to a redox state change in cells that, in turn, can initiate or exacerbate inflammation in the respiratory tract and cardiovascular systems, chemically

alter DNA, proteins, and lipids, and lead to cell and tissue damage or death (Baulig et al., 2003; Donaldson et al., 2001; N. Li et al., 2003; Prahalad et al., 2001). ROS are any oxygen-containing molecules that have one or more unpaired electrons, making them highly reactive, and include species like hydrogen peroxide (H_2O_2), superoxide radical (O_2^-), and hydroxyl radical ($^{\bullet}OH$). These species can be introduced to the body via PM inhalation with ROS directly bound to the particles ("particle-bound ROS") and/or by catalytic generation of ROS *in vivo* via cellular redox reactions stimulated by specific inhaled PM components (Dellinger et al., 2001; Obrien, 1991). The catalytic generation of ROS by such inhaled components with simultaneous depletion of antioxidants is defined in this paper as "oxidative potential" (OP).

The recent development of acellular assays for OP has led to a rapid rise in OP measurements worldwide. Common acellular OP assays include electron spin (or paramagnetic) resonance (OP^{ESR}), dithiothreitol (OP^{DTT}), ascorbic acid (OP^{AA}), and glutathione assays (OP^{GSH}). OP^{ESR} measures the generation of $^{\bullet}OH$ via electron spin resonance while OP^{DTT}, OP^{AA}, and OP^{GSH} measure the depletion rate of antioxidants (AA, GSH, urate (UA)) or chemical proxies for cellular reductants (DTT), which is proportional to the generation rate of ROS. Particle-bound ROS measurements use fluorescence-based techniques to measure concentrations of specific ROS, usually H_2O_2 or $^{\bullet}OH$, on and/or within a PM sample. The development of particle-bound ROS measurement methods precedes the development of acellular OP assays, but recent literature showing the relevance of OP to health has pushed current and future research towards using OP assays. Further, the concentrations of particle-bound ROS are often much smaller than the concentrations of ROS catalytically generated by PM components *in vivo*, meaning OP-

active PM components may be more related to oxidative stress and observable adverse health endpoints.

OP measurements integrate multiple aspects of PM, including species composition, bioavailability of chemical species (specifically metals) for reactions, synergistic interactions between chemical species and emission source impacts, redox cycling by complex organics, and oxidative stress delivered by surfaces, making it an advantageous health metric. Current epidemiologic analyses using acellular assays suggest that exposure to PM with high OP affects cardiorespiratory health (Abrams et al., 2017; J. T. Bates et al., 2015; Janssen et al., 2015; Yang et al., 2016). In fact, OP has been found to be more strongly associated with acute cardiac and respiratory endpoints than fine PM concentration in multiple studies, suggesting that OP may be a more relevant health metric than PM mass for certain outcomes of interest (Abrams et al., 2017; J. T. Bates et al., 2015; Weichenthal, Crouse, et al., 2016). Understanding the current state of knowledge on acellular OP assays could guide future research investigating the epidemiologic relevance of various OP assays and further our understanding on the relationship between PM and health.

Different OP assays are sensitive to different PM species and pollutant mixtures from different emission sources. Metals can directly support electron transport that generates ROS while diminishing antioxidant levels and organic compounds can drive oxidative stress through redox cycling of quinone-based radicals (Ghio, Carraway, & Madden, 2012). In general, all OP methods are responsive to some metals, though not all assays capture every metal-induced redox reaction, making assays sensitive to different metals. For example, OP^{AA} is more sensitive to iron and copper and OP^{DTT} to copper and

manganese. OP^{DTT} is also sensitive to organic species, especially highly oxidized organics. Literature shows that PM related to vehicle emissions drives responses in all OP assays, most likely due to the high copper content in brake and tire wear, and biomass burning PM significantly contributes to OP^{DTT} due to its large oxidized aromatic (e.g., quinone) fraction. Further, chemistry, photochemical aging, and volatility of organic species can play significant roles in OP. Each of the described PM factors, including species and source composition and photochemical aging along with pH, affects the size distribution of OP measurements, which also varies by assay.

This review summarizes the current state of knowledge on the relationship between health endpoints and acellular OP measurements along with the sensitivities of various acellular OP assays to PM composition, emission source impacts, and size. Particle-bound ROS measurements are described in brief, but the focus is on OP due to the growing body of literature linking these assays to adverse health outcomes.

2.2 Overview of Measurement Methods

ROS can exist on and/or within PM or can be generated *in vivo* by constituents of inhaled particles chemically interacting with fluids and cells in the body. There are various methods to measure these two different phenomena. Particle-bound ROS techniques typically report levels in units of concentration (e.g. nmol H_2O_2 equivalents m^{-3}_{air}) while OP techniques use units of time rate-of-change of volume-based concentration (nmol or % depletion per min per m^3 of air), mass-based concentration (nmol or % depletion per min per μg of PM; sometimes referred to as intrinsic OP), or absorbance units. Volume-based

concentration rates of OP are relevant for epidemiologic studies while mass-based concentration rates of OP are useful for comparing between OP observational studies.

2.2.1 Measuring Particle-Bound ROS

Measurements of ROS present within and/or on PM are typically measured using fluorescence-based techniques adapted from intracellular ROS measurement techniques. These particle-bound ROS methods suspend particles in a reagent and measure the spectra of specific oxidation byproducts. Dichlorofluorescin (DCFH) is a non-fluorescent reagent that becomes fluorescent (DCF) when oxidized in the presence of ROS and is the most common probe used when quantifying particle-bound ROS (Antonini et al., 1998; Venkatachari, Hopke, Grover, & Eatough, 2005). Specifically, DCFH is mixed with Horseradish Peroxidase (HRP) in a sodium phosphate buffer prior to analysis to catalyze reactions. Then the DCFH-HRP reagent is added to each PM sample filter and the solution is sonicated to extract ROS in the particles. Finally, fluorogenic intensity of DCF is measured and converted to $nmol_{H2O2\text{-}eq}\ m^{-3}$ or $nmol_{H2O2\text{-}eq}\ \mu g^{-1}$ using least squares regression with a H_2O_2 calibration assay (Venkatachari et al., 2005). Other particle-bound ROS methods can vary by reagent type and concentration, mixing time and method, and fluorescence measurement technology. Other common reagents include the 9-(1,1,3,3,tetramethylisoindolin-2-yloxyl-5-ethynyl)-10-(phenylethynyl)anthracene (BPEAnit) probe, aminophenyl fluorescamine (APF) probe, and the 10-Acetyl-3,7-dihydroxyphenoxazine (Amplex Red) probe (Cohn, Simon, & Schoonen, 2008; Miljevic et al., 2010; Venkatachari & Hopke, 2008).

Molecular probes vary in their sensitivities to species. In general, the DCFH probe is the least specific method, reacting similarly with multiple ROS, including $^{\bullet}OH$, H_2O_2, peroxyl radicals, and peroxynitrite. This is largely due to the ease of abstraction of the hydrogen atom located at the 9' position of the DCFH molecule (Venkatachari & Hopke, 2008). APF reacts with $^{\bullet}OH$ but not peroxynitrite, unlike the DCFH and Amplex Red probes, making it potentially useful for specific $^{\bullet}OH$ measurements (Cohn et al., 2008).

Artifacts can occur using these techniques during sonication or development of reagents. Increased sonication of BPEAnit in dimethyl sulfoxide (DMSO) and of DCFH-HRP in 10/90 ethanol/water are correlated with an increase in fluorescence, implying sonication results in formation of ROS (Miljevic et al., 2014). The amount of ROS generated can be approximately two orders of magnitude higher than the values obtained for PM samples using the same probe (Miljevic et al., 2014). Particle-bound ROS measurements are also sensitive to pH, reagent concentration, and extraction method but not incubation temperature (Huang, Zhang, Zhang, Fang, & Schauer, 2016). According to Huang et al., (2016) (Huang et al., 2016) optimized performance in stability, reliability, and operability for offline particle-bound ROS measurements occurs at a pH of the phosphate buffer at 7.2 with the DCFH-HRP reagent at a concentration of 10μM DCFH + 0.5 unit/ml HRP.

One limitation of off-line particle-bound ROS measurements is the very short lifetime of ROS, ranging from only a few minutes to a day or longer, so off-line measurement techniques with delays of hours to days may severely underestimate true particle-bound ROS concentrations (Fuller, Wragg, Nutter, & Kalberer, 2014). Specifically, H_2O_2 bound to particles has been shown to significantly decrease over time

(Chen & Hopke, 2009; Hung & Wang, 2001; Wang, Kim, & Paulson, 2011). On-line measurement technologies have been developed to measure particle-bound ROS, in particular, three using DCFH (Fuller et al., 2014; King & Weber, 2013; Wang, Hopke, Sun, Chalupa, & Utell, 2011; Wragg et al., 2016). The main difference between the three on-line measurement techniques currently available is the particle collection method. One instrument collects PM in an aqueous HRP solution on a paper filter that then flows through Teflon tubing immersed in a water bath for 15 minutes (Fuller et al., 2014). This instrument was further developed to be portable (Online Particle-bound ROS Instrument, OPROSI) for automated continuous field deployment over many hours or days (Wragg et al., 2016). Another method uses a particle into liquid sampler (PILS), which allows particle collection at a high flow rate (Venkatachari & Hopke, 2008). The final method uses a mist chamber to collect particles (King & Weber, 2013). Even with online particle-bound ROS technologies, the growing epidemiologic evidence suggests OP measurements are potentially more relevant than particle-bound ROS measurements, pushing future research towards OP assays.

2.2.2 Measuring Oxidative Potential (OP)

OP is most commonly measured as the capacity of PM to oxidize target molecules over time (e.g., OP^{DTT}, OP^{AA}, OP^{GSH}). Assays using antioxidants, including OP^{AA} and OP^{GSH}, can be performed in a chemical assay or in surrogate lung fluid (SLF). Currently, all OP^{GSH} studies have been performed with SLF, but OP^{AA} has been measured in chemical and SLF environments. To differentiate if AA depletion was measured in SLF or not, subscripts will be used throughout this review (e.g., OP^{AA} versus OP^{AA}_{SLF}). Two other

techniques measure the actual generation of ROS over time rather than the depletion of target molecules using electron spin resonance (OP^{ESR}) or high-performance liquid chromatography (HPLC) with fluorescent probes. Different OP assays capture different redox reactions that lead to the generation of different ROS species. For example, OP^{ESR} and HPLC techniques measure the production rate of $^{\bullet}OH$ and/or H_2O_2, while antioxidant depletion assays (OP^{AA} and OP^{GSH}) have not been shown to be correlated with the generation of any specific ROS. OP^{DTT} is most correlated with O_2^- and H_2O_2 formation and is not correlated with $^{\bullet}OH$ generation (Xiong, Yu, Wang, Wei, & Verma, 2017).

OP^{ESR} measures the ability of PM to induce $^{\bullet}OH$ formation in the presence of H_2O_2 by measuring the electron paramagnetic resonance signals of the spin trap 5,5-dimethyl-1-pyrroline-*N*-oxide byproduct DMPO-OH quartet as the average of total amplitudes expressed in arbitrary units (A.U.) (Hellack et al., 2014; Shi et al., 2003). HPLC techniques measure the concentration of reduced byproducts of chemicals in SLF reacting with $^{\bullet}OH$ or H_2O_2, such as 2,3 dihydroxygenzoic acid (2,3 DHBA)—the hydroxyl radical adduct of salicylic acid, *p*-hydroxybenzoate (*p*-HBA)—forming from the reaction of $^{\bullet}OH$ with benzoate (BA), and parahydroxylphenyl acetic acid (POPHAA) dimer—a result of the oxidation of POPHAA by H_2O_2, at various time steps to measure $^{\bullet}OH$ or H_2O_2 generation over time (DiStefano et al., 2009; Donaldson et al., 1997; H. Shen, Barakat, & Anastasio, 2011). Disodium terephthalate (TPT)—which reacts with $^{\bullet}OH$ to form 2-hydroxyterephthalic acid (2 OHTA)—with a spectrofluorophotometer has also been used to estimate OP, specifically $^{\bullet}OH$ generation (Son et al., 2015; Xiong et al., 2017). BA is the most common probe, but it can bind with manganese potentially disrupting results.

However, •OH production from manganese seems to be negligible, so results should not be affected significantly (Charrier & Anastasio, 2011).

OP^{DTT} measures the depletion of a biologically relevant chemical due to oxidation rather than direct ROS production (Cho et al., 2005). DTT is a surrogate for the cellular oxidant NADPH, which reduces oxygen to O_2^-. Overall, the rate of O_2^- generation by a PM sample is measured by the rate at which DTT is consumed, which is proportional to the concentration of redox-active species in the PM sample. Specifically, solvent-extracted (e.g., in water or methanol) PM samples are incubated with DTT and a potassium phosphate buffer for times varying from 15 – 90 minutes. A small aliquot is removed from the mixture at designated times and mixed with 1% w/v Trichloraoacetic acid (TCA) to quench DTT reactions. The aliquot is mixed with 0.5 mL 5,5-dithiobis-(2-nitrobenzoic acid) (DTNB) to form 2-nitro-5-mercaptobenzoic acid (TNB) by reacting with the residual DTT, which is then measured using a spectrometer. The DTT consumption rate, otherwise known as DTT activity, is determined from the linear slope of DTT consumption and is used as a measure of OP (Cho et al., 2005; Fang et al., 2015). Work has been done to alter the DTT assay protocol for personal monitoring use, but most current studies focus on ambient or chamber PM samples (Sameenoi et al., 2013). The chemical OP^{AA} protocol is very similar to the OP^{DTT} protocol (Fang et al., 2016). Semi-automated OP^{DTT} and OP^{AA} assays have been developed to reduce labor intensity (Fang et al., 2015; Gao, Fang, Verma, Zeng, & Weber, 2017). Online systems for OP^{DTT} have also been developed to avoid filter sampling of PM that may lose reactive species before analysis and provide better temporal resolution (between 3 minutes and 3 hours) (Eiguren-Fernandez, Kreisberg, & Hering, 2017; Sameenoi et al., 2012). One system couples a PILS with microfluidic-

electrochemical detection of reduced DTT using a cobalt(II) phthalocyanine (CoPC) electrode (Koehler, Shapiro, Sameenoi, Henry, & Volckens, 2014; Sameenoi et al., 2012), while another uses a Liquid Spot Sampler (Eiguren-Fernandez et al., 2017). Offline systems are still the most common methods as online technologies have just recently been developed and require further evaluation.

The chemiluminescent reductive acridinium triggering (CRAT) assay measures the interaction of reductants, such as DTT or GSH, and oxidants. These chemicals act as reducing agents leading to the formation of H_2O_2, which in turn reacts with acridinium ester and emits light that can be used to quantify rates of H_2O_2 production (Zomer et al., 2011). CRAT is a relatively new technique that is not as commonly used as OP^{DTT} or OP^{AA}.

OP_{SLF}^{AA} and OP_{SLF}^{GSH} measure % depletion of antioxidants in SLF exposed to PM rather than directly from PM samples exposed only to the depletion chemical of interest. SLF is typically composed of multiple antioxidants, which is more indicative of realistic lung conditions; however, the composition of SLF varies by study and affects OP measurements. AA is the most critical component in SLF for reactions with metals (Charrier & Anastasio, 2011). The concentration of antioxidants in SLF is quantified at specific time intervals using HPLC and/or a DTNB-enzyme recycling to obtain % antioxidant depletion per unit time as a measure of OP (Godri, Duggan, et al., 2010; Jung, Guo, Anastasio, & Kennedy, 2006; S. X. Ma et al., 2015; Yang et al., 2016).

With the multitude of acellular OP assay types and varying protocols within an assay, results across studies can be difficult to compare. Choices of PM extraction solvent (water, methanol, SLF), PM filter type, incubation time, and metal chelator can affect OP

results. For example, OP^{AA}, OP^{DTT}, OP^{ESR}, and OP^{CRAT} are lower for PM measured on quartz filters than Teflon filters (Yang et al., 2014), and methanol can extract hydrophilic species and hydrophobic organic species, resulting in higher OP^{DTT} than water-soluble extracts (Rattanavaraha et al., 2011; Verma et al., 2012; Yang et al., 2014). Future research should focus on optimizing epidemiologically-relevant OP assays and standardizing methods across studies.

2.3 OP in Epidemiologic Analyses

To date, measurements of OP have been very limited both spatially and temporally, restricting the lengths of exposures for health studies relying on OP measurement data. There is a growing reliance on modeling approaches, such as land-use regression (LUR) and source impact regressions, to extend OP estimates where and when measurements are not available (J. T. Bates et al., 2015; Fang et al., 2016; Yang et al., 2016). Both modeled and measured OP have been found to be associated with cardiorespiratory outcomes (Table 1). In some cases, those associations have been stronger for OP than PM mass, supporting the hypothesis that oxidative stress is a mechanism of PM toxicity and OP is capturing the property of PM related to these health outcomes (Table 1). Based on current literature, OP^{DTT} and OP_{SLF}^{GSH} are the assays most relevant to health.

Fractional exhaled nitric oxide (FeNO), used as a measure of airway inflammation, has been used in the most OP epidemiologic studies with mixed results (Table 1). A human exposure study in the Netherlands found a significant association between OP^{ESR}, OP^{AA}, and OP^{DTT} and FeNO after 5 hours of exposure (to our knowledge, this is the only study to find a health association with OP^{AA}) (Janssen et al., 2015). Interestingly, in two-pollutant

models with exposure to two different OP measurements, effects of OP^{DTT} remained positive after adjustment for OP^{ESR} and OP^{AA} and vice versa, suggesting that the PM component drivers of OP^{DTT} and OP^{ESR} or OP^{AA} may have independent effects on FeNO. The same was not true for OP^{ESR} and OP^{AA} as they were too correlated to disentangle their effects. A longer follow-up study in the Netherlands using OP estimates from a LUR model did not find an association between FeNO and OP^{ESR} but did find an association between FeNO and OP^{DTT} (Yang et al., 2016). OP^{DTT} has also been associated with FeNO of healthy adults after 2 hours of exposure and in schoolchildren with persistent asthma in southern California with exposures lagged one and two days (Delfino et al., 2013; Janssen et al., 2015). The association of FeNO with OP^{DTT} in the schoolchildren study was nearly twice as strong as with other measures (macrophage ROS and traffic-related markers) (Delfino et al., 2013). AA oxidative burden [OB: calculated by multiplying $PM_{2.5}$ concentration by measured mass-based OP_{SLF}^{AA}; ($\mu g_{PM}\ m^{-3}$)* (%AA depletion μg_{PM}^{-1})] was reported to have a null association with FeNO (Maikawa et al., 2016). One limitation using OB is assuming an intrinsic OP measurement is applicable throughout the year to regional PM, but literature has shown that PM composition influences OP and is not static in time or space. Nevertheless, OP^{AA} has been found to have no association with other adverse health endpoints in multiple studies, including epidemiologic analyses on all-cause, respiratory, and cardiovascular mortalities, cardiorespiratory emergency department visits, myocardial infarction, and lung cancer mortality (Atkinson et al., 2016; Fang et al., 2016; Weichenthal, Crouse, et al., 2016; Weichenthal, Lavigne, Evans, Pollitt, & Burnett, 2016), suggesting that OP^{AA} may have limited utility in future epidemiologic studies.

Table 2-1. Reported results of tested associations between OP assays and health endpoints. Associations that were reported to be stronger for OP than PM concentration in at least one study are marked with an *. No significant negative (protective) associations were reported by any study.

Health Endpoint	**Assays with Positive Associations** (confidence interval does not include null)	**Assays with Null Associations** (confidence interval does include null)
Respiratory Health		
General	**DTT*** (Abrams et al., 2017)	
FeNO	**DTT*** (Delfino et al., 2013; Janssen et al., 2015; Yang et al., 2016) **ESR*** (Hogervorst et al., 2006; Janssen et al., 2015) **GSH_{SLF}** (Maikawa et al., 2016) **AA*** (Janssen et al., 2015)	**AA_{SLF}** (Maikawa et al., 2016; Strak et al., 2012) **ESR** (Yang et al., 2016) **GSH_{SLF}** (Strak et al., 2012)
Asthma/Wheeze	**DTT *** (Abrams et al., 2017; J. T. Bates et al., 2015; Fang et al., 2016)	**AA** (Fang et al., 2016) **AA_{SLF}** (Canova et al., 2014) **UA_{SLF}** (Canova et al., 2014) **GSH_{SLF}** (Canova et al., 2014)
Lung Cancer Mortality	**GSH_{SLF} *** (Weichenthal, Crouse, et al., 2016)	**AA_{SLF}** (Weichenthal, Crouse, et al., 2016)

Table 2-1 continued

All-cause Mortality		**AA$_{SLF}$** (Atkinson et al., 2016) **GSH$_{SLF}$** (Atkinson et al., 2016)
Cardiovascular Health		
Microvascular Function	**DTT** (Zhang et al., 2016)	
Myocardial Infarction	**GSH$_{SLF}$** (Weichenthal, Lavigne, et al., 2016)	**AA$_{SLF}$** (Weichenthal, Lavigne, et al., 2016)
Congestive Heart Failure	**DTT*** (J. T. Bates et al., 2015; Fang et al., 2016)	**AA** (Fang et al., 2016)
Ischemic Heart Disease	**DTT*** (Abrams et al., 2017)	
Chronic Obstructive Pulmonary Disease		**AA$_{SLF}$** (Canova et al., 2014) **UA$_{SLF}$** (Canova et al., 2014) **GSH$_{SLF}$** (Canova et al., 2014)
All-cause Mortality		**AA$_{SLF}$** (Atkinson et al., 2016) **GSH$_{SLF}$** (Atkinson et al., 2016)

OP^{DTT} has been linked with various acute cardiorespiratory endpoints beyond FeNO in multiple studies (Table 1). Markers of respiratory health, including forced

expiratory volume, asthma, and rhinitis, were more associated with LUR-estimated OP^{DTT} than $PM_{2.5}$ concentration in a 14-year study in the Netherlands (Yang et al., 2016). Another study utilized a 10-year data set of modeled OP^{DTT} in Atlanta, Georgia estimated via a regression with emission source impacts and found a significant, positive association between OP^{DTT} exposure and asthma/wheeze and congestive heart failure emergency department (ED) visits in both one- and two-pollutant models (the risk ratio for $PM_{2.5}$ was null in the two-pollutant model), suggesting that OP^{DTT} could explain much of the $PM_{2.5}$ impact on these two health endpoints (J. T. Bates et al., 2015). A similar, shorter term (196 days) epidemiologic study was conducted on OP^{DTT} measurements in Atlanta rather than modeled concentrations and showed a similarly significant link between OP^{DTT} exposure and asthma/wheezing and ischemic heart disease ED visits despite the small OP sample size (Abrams et al., 2017). Finally, particle size may play a role as a study in Los Angeles showed an inverse relationship between microvascular function in elderly adults and 5-day average OP^{DTT} of PM <0.18 μm but no association for OP^{DTT} of PM $0.18\mu m \leq D_P \leq 2.5\mu m$ or for OP^{DTT} of PM $2.5\mu m \leq D_P \leq 10\mu m$, (Zhang et al., 2016) though previously discussed studies in Atlanta and the Netherlands found cardiorespiratory outcome associations with OP^{DTT} of $PM_{2.5}$.

OB_{SLF}^{GSH} has been linked with both acute and chronic health endpoints, including myocardial infarction, FeNO, and lung cancer (Table 1). OB_{SLF}^{GSH} was more associated lung cancer mortality than $PM_{2.5}$ concentration (12% increase in risk compared to 5% for $PM_{2.5}$) (Weichenthal, Crouse, et al., 2016). Despite the positive associations found between OB_{SLF}^{GSH} and lung cancer mortality, a study in London found no association between OB_{SLF}^{GSH} and all-cause, respiratory, or cardiovascular mortality in any age group of adults (Atkinson

et al., 2016). Future work could obtain additional OP measurements for more robust studies and explore health endpoints beyond cardiorespiratory effects while focusing on the health-relevant OP assays, OP^{DTT} and OB_{SLF}^{GSH}.

2.4 Effects of PM Characteristics on OP

The growing literature on the relationship between OP and health, specifically OB_{SLF}^{GSH} and OP^{DTT} and cardiorespiratory endpoints, drives a need to investigate the effect of PM composition on OP to better understand the link between PM and health. Different OP assays capture the influence of different species and emissions sources on redox reactions and may also vary due to multicomponent interactions (e.g., between metals and organics and/or emission sources), causing the spatial and seasonal variations to vary between OP assays and OP measurements to not always correlate with each other when applied to the same PM. OP^{AA} and OP^{ESR} are often correlated due to their large metal influences but are not correlated with OP^{DTT}, which has a large organic species dependence (Fang et al., 2016; Visentin, Pagnoni, Sarti, & Pietrogrande, 2016; Yang et al., 2014). Rather, OP^{DTT} has been shown to be correlated with OP^{GSH} (Godri et al., 2011). OP^{DTT} is sensitive to vehicle and biomass burning emissions, while OP^{AA} and OP^{ESR} are most responsive to vehicle emissions. Overall, the responses of these assays to composition needs to be examined in order to correctly interpret the wealth of information these assays can provide, and multiple assays may need to be used jointly to more fully understand PM OP (Xiong et al., 2017).

2.4.1 Species Composition

2.4.1.1 Metals

Select metals have been shown to have significant effects on multiple OP assays at varying degrees. Insoluble and soluble transition metals have been correlated with •OH and H_2O_2 generation measured via OP^{ESR} and HPLC in PM samples worldwide (Alaghmand & Blough, 2007; Boogaard et al., 2012; Hellack et al., 2015; Janssen et al., 2014; Jung et al., 2006; Kunzli et al., 2006; S. X. Ma et al., 2015; H. Shen & Anastasio, 2011; H. Shen et al., 2011; Shi et al., 2003). Metal chelators reduced H_2O_2 and •OH production in ambient Californian PM samples by ~78% and ~97%, respectively (H. Shen & Anastasio, 2011; H. Shen et al., 2011). Specifically, iron (Fe(II) and Fe(III)) and soluble copper are critical to •OH generation and can synergistically increase •OH in SLF (Charrier & Anastasio, 2011; H. Shen & Anastasio, 2011; Vidrio, Jung, & Anastasio, 2008). In an OP^{ESR} study, the addition of desferrioxamine to ambient PM samples collected in Athens, Greece completely suppressed the DMPO-OH signal, showing the importance of iron to OP^{ESR} (Valavanidis, Salika, & Theodoropoulou, 2000). Soluble iron generates roughly six times more •OH in SLF than soluble copper (Charrier & Anastasio, 2011). Further, iron can play a synergistic role accelerating oxidation of organics and enhancing •OH generation through Fenton reactions (Y. Li, Zhu, Zhao, & Xu, 2012; Xiong et al., 2017). Cu (II) is more important for H_2O_2 production than Fe (II), but the rate of H_2O_2 generation in ambient particle extracts collected in California were lower than rates calculated from the measured soluble copper by 44 ± 22%, possibly due to H_2O_2 destruction by soluble iron or a reduction in soluble copper reactivity due to organic ligands in the PM (Charrier, McFall, Richards-Henderson, & Anastasio, 2014; H. Y. Shen & Anastasio, 2012). Soluble manganese and vanadium have shown effects on •OH generation measured with HPLC, but soluble cobalt, chromium, nickel, zinc, lead, and calcium showed no effect (Charrier & Anastasio, 2011;

Vidrio et al., 2008). •OH generation by metals soluble in SLF requires the presence of AA, and other antioxidants, like citrate and GSH, can have no effect or even inhibit •OH generation from metals like copper (Charrier & Anastasio, 2011; Vidrio et al., 2008).

Metals have a larger impact on OP beyond •OH and H_2O_2 production, as shown by OP^{DTT}, OP^{AA}, OP_{SLF}^{AA}, and OP_{SLF}^{GSH} studies. OP^{AA} and OP_{SLF}^{AA} have shown significant correlations with both soluble and total metals, including copper, manganese, lead, zinc, and iron (Fang et al., 2016; Godri, Duggan, et al., 2010; Janssen et al., 2014; Pant et al., 2015; Visentin et al., 2016). OP_{SLF}^{GSH} has been shown to increase with higher iron, lead, and aluminum content in ambient PM (Godri, Duggan, et al., 2010; Godri et al., 2011). OP_{SLF}^{GSH} and OP_{SLF}^{AA} both varied significantly between underground subway stations due to the presence of metallic trace elements like copper and antimony from brakes and pantographs but not from $PM_{2.5}$ concentration changes from ventilation, tunnel works, or station design, implying metal content may be more important than total $PM_{2.5}$ to these assays (Moreno et al., 2017). One study estimated that up to 45% of variation in mass-based OP^{DTT} of diesel exhaust particulate samples can be explained by soluble metals (Shinyashiki et al., 2009). However, OP^{DTT} is not affected by iron like OP^{AA} and OP_{SLF}^{GSH}, so OP^{DTT} may not fully capture ROS generated through Fenton chemistry or synergistic effects, specifically with regards to •OH generation (Xiong et al., 2017). Metals that do significantly impact OP^{DTT} include soluble copper and manganese. Charrier, et al. (2012) and Charrier, et al. (2015) estimate that up to 78% of the loss of DTT in ambient $PM_{2.5}$ and PM_1 samples collected in California was due to soluble copper and manganese (Charrier & Anastasio, 2012) (Charrier et al., 2015), but only ~40% of the volume-normalized OP^{DTT} of $PM_{2.5}$ in Atlanta was estimated to be due to soluble metals (Verma, Fang, et al., 2015). OP^{DTT} shows a

nonlinear response to soluble copper and manganese when concentrations of these metals are high, and varying compositions with different metal and organic fractions could explain the differences between California and Georgia (Charrier & Anastasio, 2012; Charrier et al., 2016). The volume-normalized OP^{DTT} of ambient quasi-ultrafine PM in Los Angeles and $PM_{2.5}$ in northern Italy were correlated with other metals, including chromium, vanadium, nickel, cadmium, and zinc, but other studies show no correlation between mass-normalized OP^{DTT} and these metals (Jeng, 2010; Saffari, Daher, Shafer, Schauer, & Sioutas, 2014b; Verma et al., 2012; Visentin et al., 2016; Xiong et al., 2017). Volume-normalized OP^{DTT} is often correlated with PM concentration, so correlations with metals other than manganese and copper should be interpreted with caution as the association may be due to similar variations in metal and PM concentrations rather than a significant causal relationship between OP^{DTT} and metals. Further, only the soluble forms of metals participate in redox reactions, so correlations between OP and total metals depends on the fraction of total metals that is soluble. Low particle pH due to the presence of ammonium sulfate can mobilize metals to react in OP assays (Fang, Guo, et al., 2017).

2.4.1.2 Organic Species

A limited number of the OP assays have been found to be sensitive to organic species, and those that are tend to be quite responsive. Many studies worldwide (United States, Greece, India, China) show a correlation between organic carbon (OC) and/or water-soluble organic carbon (WSOC) and OP^{DTT} of PM collected during different seasons (Cho et al., 2005; S. Hu et al., 2008; Jeng, 2010; Liu, Zhang, Liu, & Zhang, 2014; Patel & Rastogi, 2018; Velali et al., 2016; Verma, Fang, et al., 2015; Verma, Ning, et al., 2009; Verma et al., 2011; Vreeland et al., 2017). 88% of variability in volume-normalized OP^{DTT}

of quasi-ultrafine ambient PM in the Los Angeles basin has been explained by WSOC, water-insoluble organic carbon (WIOC), elemental carbon, and hopanes, and 60% of OP^{DTT} of water-soluble $PM_{2.5}$ in the southeastern United States has been attributed to organic aerosols (Saffari et al., 2014b; Verma, Fang, et al., 2015). Specifically, the hydrophobic fraction of water-soluble and water-insoluble organic aerosols contribute to mass-normalized OP^{DTT} (Verma et al., 2012). OP^{DTT} is often correlated with polyaromatic hydrocarbon species (PAHs) like phenanthrene and pyrene, which, when oxidized, form quinones that are known to be DTT active, including phenanthraquinone (PQ), 1,2-napthaquinone (1,2-NQ), and 1,4-NQ (in decreasing OP^{DTT} order) (Cho et al., 2005; Chung et al., 2006; McWhinney, Badali, Liggio, Li, & Abbatt, 2013; Xiong et al., 2017). PAHs that are converted to DTT-active quinones can be bound to the surfaces of soot, and black carbon coated in 1,4-NQ significantly increased mass-normalized OP^{DTT} compared to untreated black carbon particles (Antinolo, Willis, Zhou, & Abbatt, 2015; McWhinney, Badali, et al., 2013; Pant et al., 2015). The methanol extracts of OP^{DTT} are higher than water-soluble PM extracts because the less polar solvent can extract hydrophilic and hydrophobic organic species, although water-soluble organic PM components are still significant contributors to OP^{DTT} and may be more biologically available (Rattanavaraha et al., 2011; Verma, Fang, et al., 2015; Verma et al., 2012; Yang et al., 2014). Further, soluble forms of metals, including iron and copper, can synergistically increase the effects of quinones on OP in multiple assays, such as OP^{DTT}, OP^{ESR}, and $^{\bullet}OH$ generation in SLF, even if those assays are not sensitive to organic species (Charrier & Anastasio, 2015; Y. Li et al., 2012; Xiong et al., 2017). Soluble manganese has shown synergistic effects with quinones on OP^{DTT}, while soluble copper appears to have an antagonistic effect with

quinones on the same assay (Yu, Wei, Cheng, Subedi, & Verma, 2018). Contrarily, manganese appears to have an antagonistic relationship with quinones on $^{\bullet}OH$ generation (H. R. Yu et al., 2018), while quinones and soluble iron or copper react synergistically to form $^{\bullet}OH$ (H. R. Yu et al., 2018). Future work investigating the synergistic effects of species on different assays as well as the effect of organic species on OP assays, such as OP^{GSH}, would be useful to better understand impacts of PM composition on OP.

Table 2-2. Species showing evidence of an impact on OP, either using correlation analyses, measuring OP of pure solutions, or exposing ambient samples to metal chelators (note there is no differentiation with the use of SLF or not).

Assay	Species Driving Responses in OP Assay
DTT	**Metals**
	• **Soluble non-specific** (Shinyashiki et al., 2009) • **Soluble copper** (Charrier & Anastasio, 2012; Charrier et al., 2016; Charrier et al., 2015) • **Soluble manganese** (Charrier & Anastasio, 2012; Charrier et al., 2016; Charrier et al., 2015)
	Organics
	• **OC** (including WSOC and WIOC) (Cho et al., 2005; Fang et al., 2016; S. Hu et al., 2008; Jeng, 2010; Liu, Zhang, et al., 2014; Velali et al., 2016; Verma, Fang, et al., 2015; Verma, Ning, et al., 2009; Verma et al., 2011; Verma et al., 2012; Vreeland et al., 2017) • **PAH's and quinones** (Cho et al., 2005; Chung et al., 2006; McWhinney, Badali, et al., 2013; Totlandsdal, Lag, Lilleaas, Cassee, & Schwarze, 2015) • **HULIS** (Dou, Lin, Kuang, & Yu, 2015; Y. Ma et al., 2017a; Verma, Fang, et al., 2015; Verma et al., 2012; Verma, Wang, et al., 2015)

Table 2-2 continued

	Synergistic Effects
	• **Soluble manganese with quinones** (H. R. Yu et al., 2018)
GSH	**Metals**
	• **Total aluminum** (Godri, Duggan, et al., 2010) • **Total lead** (Godri, Duggan, et al., 2010) • **Total iron** (Godri et al., 2011)
AA	**Metals**
	• **Soluble copper** (DiStefano et al., 2009; Fang et al., 2016; Visentin et al., 2016) • **Total copper** (Janssen et al., 2014; Pant et al., 2015) • **Total iron** (Godri, Duggan, et al., 2010; Godri et al., 2011; Janssen et al., 2014) • **Soluble iron** (*53*) • **Total lead** (Godri, Duggan, et al., 2010) • **Total zinc** (Godri et al., 2011) • **Soluble manganese** (Visentin et al., 2016)
	Organics
	• **OC** (Calas et al., 2018)

Table 2-2 continued

ESR	**Metals**
	• **Total non-specific** (Alaghmand & Blough, 2007; Boogaard et al., 2012; Janssen et al., 2014; Kunzli et al., 2006) • **Soluble copper** (Hellack et al., 2015; Shi et al., 2003) • **Soluble iron** (Arangio, Tong, Socorro, Poschl, & Shiraiwa, 2016; Hellack et al., 2015; Y. Li et al., 2012; Makino, Hagiwara, Hagi, Nishi, & Murakami, 1990; Valavanidis et al., 2000) • **Soluble vanadium** (Shi et al., 2003)
	Synergistic Effects
	• **Soluble iron with anthraquinone** (Y. Li et al., 2012) • **Soluble iron with quinones** (Arangio et al., 2016)
$^{\bullet}$OH production measured via HPLC or fluorescence[1]	**Metals**
	• **Soluble non-specific** (DHBA, BA) (Jung et al., 2006) • **Soluble copper** (DHBA, BA, TPT) (Charrier & Anastasio, 2011; DiStefano et al., 2009; H. Shen & Anastasio, 2011; Son et al., 2015; Vidrio et al., 2008) • **Soluble iron** (BA) (Charrier & Anastasio, 2011; Vidrio et al., 2008) • **Total iron** (BA) (S. X. Ma et al., 2015) • **Soluble manganese** (BA) (Charrier & Anastasio, 2011; Vidrio et al., 2008) • **Soluble vanadium** (BA) (Charrier & Anastasio, 2011; Vidrio et al., 2008)
	Organics
	• **Quinones** (Xiong et al., 2017)

Table 2-2 continued

	Synergistic Effects
	• **Elemental iron with quinones** (TPT) (Xiong et al., 2017) • **Soluble iron with quinones or copper** (BA) (Charrier & Anastasio, 2015)
H_2O_2 production measured via HPLC or fluorescence[1]	**Metals**
	• **Soluble non-specific** (POPHAA) (H. Shen et al., 2011) • **Soluble copper** (POPHAA) (Charrier et al., 2014; Wang, Arellanes, Curtis, & Paulson, 2010) • **Soluble iron** (POPHAA) (Wang et al., 2010) • **Soluble zinc** (POPHAA) (Wang et al., 2010)
	Organics
	• **Quinones** (Xiong et al., 2017)

[1]probe denoted in parentheses

Photochemical aging of organic species has been found to be an important factor for particle-bound ROS and OP^{DTT}, particularly in conversion of PAH's to DTT-active quinones. The influence of chemical aging can be seen in spatial and temporal variations of OP. Volume-normalized OP^{DTT} per elemental carbon (EC) surface area was found to be 4-5x higher at an urban site than roadside side in Atlanta, suggesting that PAH-coated soot requires oxidation through aging to convert EC-surface-bound PAHs to redox-active quinones (Fang, Zeng, et al., 2017). Higher mass-normalized OP^{DTT} in Los Angeles was found for quasi-ultrafine PM samples collected in the afternoon when OC has a higher contribution from secondary processes than morning samples with fresh OC from rush hour

(Saffari et al., 2016; Verma, Ning, et al., 2009). Furthermore, aged emissions and oxygenated derivatives of species are often more correlated with OP than their precursor chemicals. Diesel $PM_{2.5}$ exhaust from shipping vessels exhibited higher •OH production in SLF for plume exhaust than freshly emitted particles (Kuang et al., 2017). Particle-bound ROS measured using a BPEAnit probe showed higher correlations with oxygenated OC than total OC of diesel and biodiesel fuels, and higher particle-bound ROS concentrations were found in aged diesel particle exhaust from common-rail engines than unaged diesel particle exhaust (Pourkhesalian et al., 2015; Stevanovic et al., 2013). The OP^{DTT} per mass OC of fresh trash-burning emissions in India was found to be an order of magnitude lower than OP^{DTT} of ambient air with significant aged components (Vreeland et al., 2016). The oxygenated derivative of 1,4-NQ (5-hydroxy-1,4-NQ) was found to be intrinsically similar or more DTT-active than its parent compound (McWhinney, Badali, et al., 2013; McWhinney, Zhou, & Abbatt, 2013; Verma, Wang, et al., 2015), and a study in the southeastern United States reported higher correlations between mass-based OP^{DTT} of water-soluble $PM_{2.5}$ and more-oxygenated organic aerosols (MO-OOA) than less-oxygenated organic aerosols, as identified by Aerosol Mass Spectrometry (AMS) (Verma, Fang, et al., 2015). Humic-Like Substances (HULIS) is composed of MO-OOA and is associated with a dominant fraction of mass-based OP^{DTT} of ambient $PM_{2.5}$ in the southeastern United States (Verma, Fang, et al., 2015). Correlations between OP^{DTT} of PM_{10} in Beijing, China and ammonium and nitrate, tracers of secondary processes, along with correlations of OP^{DTT} of total suspended particles in Milan, Italy and global radiation, a proxy for secondary oxidizing organics, further the conclusion that aging increases OP^{DTT} (Liu, Zhang, et al., 2014; Perrone et al., 2016). Exposure to ozone, a result of

photochemistry, increases ambient particle-bound ROS as shown by DCFH analyses of ambient PM samples of various size fractions in New York, Texas, and California (Khurshid, Siegel, & Kinney, 2014; Venkatachari et al., 2007; Venkatachari et al., 2005). Further, mass-based OP^{DTT} of oxidized flame soot has been found to be 1.5 – 2 times higher than soot not exposed to ozone (Holder, Carter, Goth-Goldstein, Lucas, & Koshland, 2012). Ozone-exposed black carbon exhibits a higher mass normalized OP^{DTT} than untreated black carbon, mostly likely due to quinone formation from soot-bound PAH oxidation by ozone (Antinolo et al., 2015; Pant et al., 2015). Sulfate is the only secondary species consistently found to not significantly contribute to OP^{DTT}, but secondary acids, like ammonium sulfate, can have an indirect effect on OP by reducing pH of an aerosol and, in turn, solubilizing metals that react in OP^{DTT} (J. T. Bates et al., 2015; Fang, Guo, et al., 2017; Fang et al., 2016; Pant et al., 2015; Patel & Rastogi, 2018).

Multiple chamber studies have investigated the effects of secondary organic aerosols (SOA) on OP. Certain species, especially quinone-derived SOA like naphthalene SOA, have been shown to have high mass-normalized OP^{DTT} (McWhinney, Badali, et al., 2013; McWhinney, Zhou, et al., 2013; Tuet et al., 2017). In general, anthropogenic SOA, like m-xylene SOA, toluene SOA, and naphthalene SOA, show higher intrinsic OP^{DTT} than biogenic SOA, such as isoprene SOA, α-pinene SOA, and β-caryophylene SOA (Jiang, Jang, Sabo-Attwood, & Robinson, 2016; Tuet et al., 2017). Conversely, H_2O_2 production in SLF measured with HPLC was higher for α-pinene and β-pinene SOA than toluene SOA (Wang, Kim, et al., 2011). Interestingly, adding DTT to the solution analyzed by HPLC increased H_2O_2 production from toluene SOA by a factor of 2.6 but had no effect on the pinene SOA (Wang, Kim, et al., 2011). Kramer, et al. (2016) reports that isoprene-

derived hydroxyl hydroperoxide (ISOPOOH) showed significantly higher mass-normalized OP^{DTT} than other isoprene-derived epoxides and SOA, suggesting the importance of organic peroxides to OP^{DTT} (Kramer et al., 2016). However, the impact of ISOPOOH was only half of the impact of 1,4-NQ (Kramer et al., 2016). It should be noted that the OP^{DTT} protocol in Kramer et al. (2016) used a different metal chelator than the original, more commonly used method developed in Cho et al. (2005) [EDTA in Kramer et al. (2016) and Chelex 100 resin in Cho et al. (2005)], which dampens the catalytic generation of certain PM species, like copper and manganese. Based on analyses performed at the Georgia Institute of Technology, the OP^{DTT} of 1,4-NQ using the Kramer et al. (2016) method is, on average, 1.3-1.5 times lower than the OP^{DTT} response for the same quinone using the Cho et al. (2005) method, reflecting that the Kramer et al. (2016) method may miss the effects of some species on DTT oxidation. Overall, although differences in chamber conditions and OP assay methods exist between studies, anthropogenic SOA seems to be more critical to OP^{DTT} than biogenic SOA.

Finally, volatility of organic molecules may play a significant role in OP with semi-volatile species significantly impacting OP^{DTT} and particle-bound ROS (Biswas et al., 2009; Miljevic et al., 2010). After heating ambient quasi-ultrafine PM samples from Los Angeles, essentially removing semi-volatile components, OP^{DTT} of the samples significantly decreased (Verma et al., 2011).

2.4.2 Source Contribution

Identifying emission sources that contribute to OP could be useful for developing air quality control strategies aiming to protect human health. Mass-normalized OP^{DTT} can

vary by a factor of 8 between sources identified using single-particle mass spectrometry (Charrier et al., 2015). High correlations between OP^{DTT} and benzo[g]pyrene (BgP), PAHs, alkanes, hopanes, and steranes along with transition metals that share similar vehicular sources with primary organics imply that vehicle exhaust contributes to OP^{DTT} (Cho et al., 2005)' (Saffari et al., 2014b; Shirmohammadi et al., 2016). Vehicular abrasion and brake and tire wear tracers, like metals, have been correlated with OP^{DTT} and OP^{AA} (Fang et al., 2016; Shirmohammadi et al., 2017). The inclusion of tailpipe emissions within 100m of traffic and break and tire wear PM_{10} emissions within 50m of traffic improved a land-use regression estimate of OP_{SLF}^{GSH} (Yanosky, Tonne, Beevers, Wilkinson, & Kelly, 2012). Further, the association between OP^{DTT} and brown carbon and/or levoglucosan suggests a biomass burning influence on OP (Samara, 2017; Verma et al., 2012). A thorough examination of emissions source impacts on OP could provide useful insights into the relationships between PM and health.

2.4.2.1 Vehicles

An extensive amount of laboratory and field studies have been conducted showing that diesel exhaust is a significant source of particle-bound ROS and OP (Akhtar et al., 2010; Alaghmand & Blough, 2007; Fujitani, Furuyama, Tanabe, & Hirano, 2017; McWhinney, Badali, et al., 2013; Valavanidis et al., 2000). The redox activity of diesel exhaust particles (DEP) can vary based on engine configuration, driving conditions, photochemical aging of exhaust (as previously discussed), and fuel type (Figure 1) (Fox et al., 2015). Research shows that microalgael biodiesel blends have smaller particle-bound ROS concentrations than regular diesel (Rahman et al., 2015). Further, volume-normalized OP^{DTT} was significantly lower for biodiesel exhaust compared to CARB ultra-low sulfur

diesel (Karavalakis et al., 2017). Conversely, other studies show an increase in particle-bound ROS and OP^{ESR} in biofuels compared to diesel (Godoi et al., 2016; Pourkhesalian et al., 2014). OP^{ESR} and OP^{DTT} capture different components of ROS generation, with OP^{ESR} focusing on $^{\bullet}OH$ production and OP^{DTT} measuring chemical depletion by oxidation, which may explain the discrepancy between results and emphasizes the importance of discerning which of the OP assays is relevant to health.

Control technologies like selective catalytic reduction (SCR) can reduce the impact of both diesel and biodiesel blends on OP and particle-bound ROS by reducing PM emissions (Godoi et al., 2016). Active and passive diesel particulate filters (DPF) and diesel oxidation catalysts have all demonstrated a removal of volume-normalized particle-bound ROS concentrations measured by a DCFH probe by more than 75% on average with passive DPF driving the largest reduction (~ 99%) (Pavovic, Holder, & Yelyerton, 2015). However, mass-normalized particle-bound ROS concentrations increased ~ 2-3 times in downstream particles after active DPF was installed (Pavovic et al., 2015). The EC/PM ratio was lower downstream of the active-DPF than the baseline vehicle, suggesting that the higher mass-normalized particle-bound ROS was associated with the higher fraction of organic compounds (Pavovic et al., 2015). Other studies have supported that DPF and other control technologies (e.g., SCR) decrease OP^{DTT} per distance travelled by 60-98% but can increase mass-normalized OP^{DTT} up to 3 times higher (Biswas et al., 2009; Geller et al., 2006). However, not all control technologies on all vehicle types cause higher mass-normalized OP^{DTT} (Biswas et al., 2009; Cheung et al., 2009). Interestingly, a large reduction in OP^{DTT} was seen following the use of a thermodenuder (150 °C) during collection of diesel exhaust with various control technologies, which may explain why

certain control technologies that are less effective at removing semivolatile species than refractory PM fractions reduce OP less (Biswas et al., 2009).

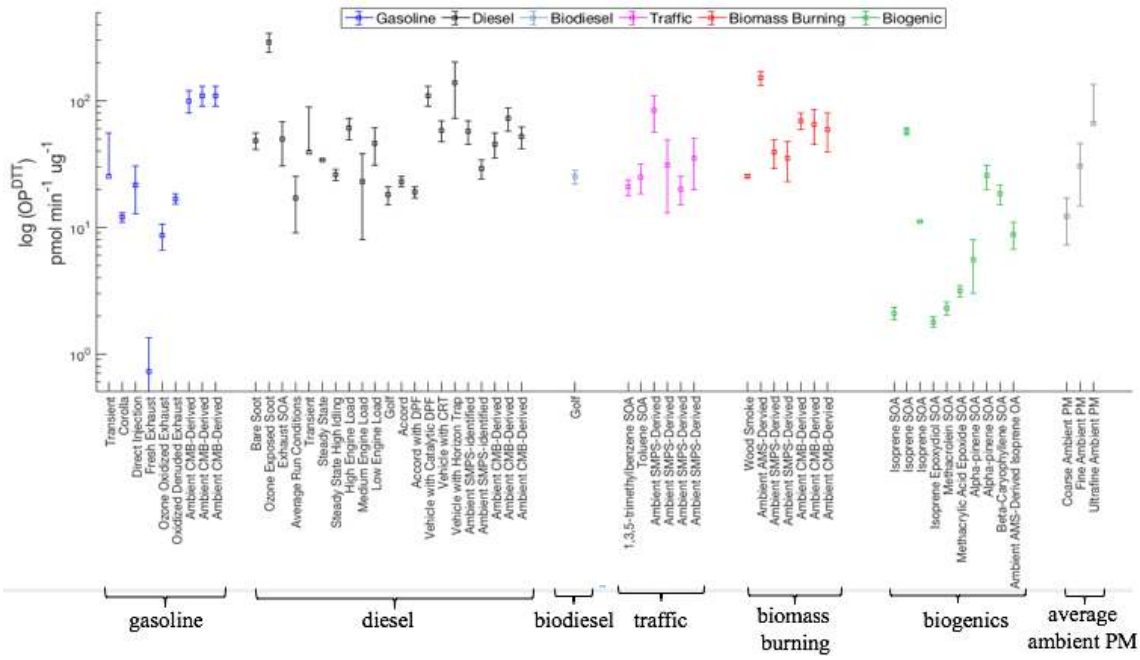

Figure 2-1. Intrinsic OP^{DTT} (median and standard deviations) of various emission sources studied in either ambient or chamber conditions at locations worldwide plotted on a log scale. The size fractions of average ambient PM are defined as: quasi-ultrafine ($\leq PM_{0.18}$), fine ($\leq PM_{2.5}$), and coarse ($\leq PM_{10}$).

Gasoline vehicles, and traffic emissions in general, have been associated with multiple OP assays, including OP^{DTT}, OP^{AA}, OP^{ESR}, OP_{SLF}^{AA}, and OP_{SLF}^{GSH} (J. T. Bates et al., 2015; Charrier et al., 2015; Fang et al., 2016; Fujitani et al., 2017; Shirmohammadi et al., 2016; Szigeti et al., 2015; Valavanidis et al., 2000). In the southeastern United States, multiple source apportionment studies using positive matrix factorization (PMF) and the chemical mass balance method (CMB) have shown that vehicular emissions contribute to volume-normalized OP^{DTT} and OP^{AA} uniformly throughout the year with contributions ranging between 12% and 32% for OP^{DTT} and ~45% for OP^{AA} (Fang et al., 2016; Verma et al., 2014). In Beijing, vehicle-derived HULIS accounted for up to 23% of ambient OP^{DTT}

(Y. Ma et al., 2017a). Light-duty gasoline vehicles were found have the highest intrinsic water-soluble OP^{DTT} (nmol min^{-1} μg_{source}^{-1}) out of 8 tested sources in Atlanta (J. T. Bates et al., 2015). In-vehicle concentrations of volume-normalized OP^{DTT} have been reported as 2 times higher than OP^{DTT} at stationary roadside monitoring sites (Vreeland et al., 2017). The largest contributors to OP^{AA} in Atlanta were reported to be traffic emissions and secondary process, such as metal mobilization by secondary acids, which also dominate summertime OP^{DTT} in the southeastern United States (Fang, Guo, et al., 2017; Fang et al., 2016; Verma et al., 2014). Vehicles were also found to be a dominant source of OP^{AA} in Chamonix, France (Samuël et al., 2018). Particle-bound ROS measured using a BPEAnit probe found higher correlations with total traffic count than traffic composition, implying that total traffic count may be more important than gasoline or diesel vehicle count (Crilley et al., 2012). Local traffic as a whole has also been a strong predictor in land-use regression (LUR) models for volume-normalized OP^{ESR} and OP^{DTT} in the Netherlands and OP_{SLF}^{GSH} in London (Yang et al., 2015; Yanosky et al., 2012). Further research is needed to investigate if the impacts of diesel and gasoline vehicles can be separated or if it is more useful to look at OP impacts of traffic as a whole.

Vehicle emissions can significantly affect spatial variability of OP. Volume-normalized OP^{DTT}, OP^{AA}, OP^{ESR}, and particle-bound ROS measurements (DCFH) were all found to be higher at an underground tunnel site than farm or urban background sites (Crilley et al., 2012; Janssen et al., 2014). OP^{ESR} of PM_{10} collected in Germany along a motorway showed ~1.4 times higher $^{\bullet}OH$ production rates downwind than upwind in 72% of the observations (Hellack et al., 2015). OP^{ESR} of PM_{10} samples in the Netherlands showed 3.6 times and 6.5 times higher $^{\bullet}OH$ generation rates at major roadways than urban

background and suburban background sites, respectively (Boogaard et al., 2012). OP^{DTT} has been shown to be more spatially homogeneous than OP^{AA} and OP^{ESR} (Janssen et al., 2014; Yang et al., 2015). Multiple studies report only slightly higher volume- and mass-normalized OP^{DTT} at roadways than urban background sites with ratios of roadway/urban background ranging from 1.1 to 1.2 for volume-normalized OP^{DTT} of PM_{10} in Europe, from 1.9 to 2.1 for mass-normalized OP^{DTT} of quasi-ultrafine PM in California, and ~1.1 for volume-normalized OP^{DTT} of water-soluble $PM_{2.5}$ in Atlanta (Gao et al., 2017; Jedynska et al., 2017; Saffari et al., 2014b; Saffari et al., 2016; Shirmohammadi et al., 2017; Yang et al., 2015). The inability of LUR models to capture spatial variability in volume-normalized OP^{DTT} in Europe may also be a sign of spatial homogeneity in OP^{DTT} (Jedynska et al., 2017; Perrone et al., 2016). Traffic emissions with heterogeneous spatial patterns may account for a larger fraction of OP^{ESR} and OP^{AA} than OP^{DTT} (which has contributions from more homogeneous sources like aged biomass burning), which may explain the increase in spatial homogeneity of OP^{DTT} compared to other OP measurements (Fang et al., 2016).

2.4.2.2 Biomass Burning

Biomass burning has a significant impact on OP^{DTT} (Figure 1). In a study looking at the effect of organic aerosols on OP^{DTT} of waster-soluble $PM_{2.5}$, biomass burning organic aerosols showed significantly higher intrinsic OP^{DTT} (151 ± 20 pmol min^{-1} μg_{source}^{-1}) than all other organic aerosols identified (next highest (36 ± 22 pmol min^{-1} μg_{source}^{-1})) (Verma, Fang, et al., 2015). Wildfires in California have been shown to significantly increase mass-based OP^{DTT} (Verma, Polidori, et al., 2009). Biomass burning has been reported as the largest contributor to volume-normalized OP^{DTT} of water-soluble $PM_{2.5}$ in Atlanta and Beijing (J. T. Bates et al., 2015; Y. Ma et al., 2017a). Biomass burning emissions drive

seasonal trends in OP^{DTT} in the southeastern United States, Greece, and France with higher concentrations in the winter/spring than fall/summer (J. T. Bates et al., 2015; Calas et al., 2018; Velali et al., 2016; Verma et al., 2014). Crop-burning does not seem to be a large contributor to mass-normalized OP^{DTT} of biomass burning and varies by crop type, with highest values for wheat straw burning followed by rice husk and straw burning and then barley straw burning (Fushimi et al., 2017). Trash burning, on the other hand, produces extremely redox-active particles. Water-soluble OP^{DTT} of trash burning in Bangalore, India exceeded 1000 nmol min^{-1} m^{-3} (most ambient measurements range between 0.1 and 1.7 nmol min^{-1} m^{-3}) and waste incineration contributed up to 21% of ambient HULIS-related OP^{DTT} in Beijing (Y. Ma et al., 2017a; Vreeland et al., 2016).

The relationship between biomass burning and OP^{AA} is less clear. A study in Atlanta using CMB and PMF for source apportionment of $PM_{2.5}$ showed that biomass burning does not significantly contribute to OP^{AA} , but a study in Chamonix, France using PMF on PM_{10} found a high contribution of biomass burning to OP_{SLF}^{AA} (Calas et al., 2018; Fang et al., 2016; Samuël et al., 2018). The discrepancy could be explained by different measurement sites (the biomass burning source may be more aged in Atlanta than Chamonix), the use of SLF extraction in the Chamonix-based study but water extraction in the Atlanta-based study, or different PM sample size fractions (e.g., metal-containing mineral dust lofted during burning may have a disproportionate effect on PM_{10} relative to $PM_{2.5}$)

2.4.2.3 Other Source Impacts

Road dust was reported to contribute roughly 12% of the volume-normalized OP^{DTT} of water-soluble $PM_{2.5}$ collected during the summer and fall in the southeastern United States (Verma et al., 2014). Dust storms and soil dust in China have contributed to volume-normalized OP^{DTT} of PM_{10} and $PM_{2.5}$ samples, respectively (Liu, Baumgartner, et al., 2014; Liu, Zhang, et al., 2014; Secrest et al., 2016). However, Saharan dust does not appear to significantly contribute to OP^{DTT} (Chirizzi et al., 2017). This difference may be driven by how much the PM samples have aged before collection, allowing acidic species, such as ammonium sulfate, to form and lower pH enough to solubilize metals and permitting time for internal mixing and dissolution.

OP^{DTT} of ship emissions has been measured between 0.01 and 0.04 nmol min^{-1} μg^{-1}, similar to some urban and traffic site measurements (Moldanova et al., 2013). PM_{10} from fireworks in London has been shown to have higher OP_{SLF}^{GSH} and OP_{SLF}^{AA} than traffic (Godri, Green, et al., 2010), but emission from these sources are very localized and may not impact OP of most ambient PM.

The contribution of biogenic emissions to OP^{DTT} is still under debate as ambient and chamber study results are mixed (Figure 1). Multiple source apportionment studies show that $PM_{2.5}$ isoprene-derived organic aerosols and secondary organic carbon from biogenic sources in the southeastern United States do not contribute significantly to OP^{DTT} of water-soluble $PM_{2.5}$ (J. T. Bates et al., 2015; Verma et al., 2014; Verma, Fang, et al., 2015). However, a recent study in Chamonix, France using PMF found primary and secondary biogenic species to have the highest intrinsic OP^{DTT} of PM_{10} out of all identified sources (Samuël et al., 2018). Bioaerosols, especially fungal spores, have recently been shown to cause significant depletion of DTT, which may disproportionately affect PM_{10}

compared to PM of smaller size fractions and may be causing the high intrinsic OP^{DTT} of biogenic aerosols in the Chamonix study (Samake et al., 2017). However, the authors caution that these biogenic sources contain black carbon from fossil fuel combustion, suggesting imprecision in the source apportionment approach.

2.5 Size Distribution

There is growing interest in the relationship between particle size and OP as size impacts the path of particles in the body after inhalation. In general, mass-normalized OP^{DTT} decreases with increasing particle size (Chirizzi et al., 2017; Janssen et al., 2014; Mugica et al., 2009; Ntziachristos, Froines, Cho, & Sioutas, 2007). Quasi ultrafine PM (<0.18μm) was found to have the highest intrinsic OP^{DTT} in multiple studies in Georgia and California (Cho et al., 2005; Fang, Zeng, et al., 2017; S. Hu et al., 2008; Jeng, 2010; N. Li et al., 2003). However, submicron PM ($0.17\mu m \leq D_P \leq 1.0\mu m$ in Fresno, California and $0.49\mu m \leq D_P \leq 1.0\mu m$ in Thessaloniki, Greece) was found to have larger mass-normalized OP^{DTT} than ultrafine PM (<0.17μm and <0.49μm, respectively) (Charrier et al., 2015; Samara, 2017). Based on a study in London, mass-normalized OP_{SLF}^{AA} appeared to have no significant dependence on particle size, but mass-normalized OP_{SLF}^{GSH} illustrated a slight increase with increasing particle size (Godri et al., 2011).

Volume-normalized OP, which is more relevant to health than mass-normalized OP, illustrates consistent peaks near 2 μm across studies. In Atlanta, water-soluble volume-normalized OP^{DTT} and OP^{AA} peaked within 1-2.5 μm (Fang, Guo, et al., 2017; Fang, Zeng, et al., 2017). Similarly, volume-normalized ambient OP^{DTT} in Los Angeles peaked between $0.18\ \mu m \leq D_P \leq 2.5\ \mu m$, and both volume-normalized OP_{SLF}^{GSH} and OP_{SLF}^{AA} in London peaked

between 1.9 μm ≤ D_P ≤ 10.2 μm (Godri et al., 2011; Zhang et al., 2016). The water-soluble fraction of volume-normalized OP^{DTT} and OP^{AA} in Atlanta was found to have a unimodal distribution due to fine-mode organics and coarse-mode metals mobilized by acidic species like sulfate in PM (Fang, Guo, et al., 2017; Fang, Zeng, et al., 2017). Water-insoluble volume-normalized OP^{DTT} illustrated a bimodal distribution, with both fine and coarse modes due to DTT active species absorbed on the surfaces of soot and non-tailpipe traffic dust, respectively (Fang, Zeng, et al., 2017). The distribution of volume-normalized OP^{DTT} varied between urban and roadside sites due to the difference in relative contributions of metals and oxygenated organics to PM. OP^{ESR} measurements show opposite trends of previously discussed OP^{DTT} results with higher production efficiency in larger size fractions, specifically 4.6 and 3.1 times higher in PM_{10} than $PM_{2.5}$ on a volume- and mass-normalized basis, respectively (Boogaard et al., 2012). H_2O_2 and $^{\bullet}OH$ generation measured with HPLC had higher rates in $PM_{2.5}$ than PM_{10} on a volume-normalized basis but an opposing trend on a mass-normalized basis (H. Shen & Anastasio, 2011; H. Shen et al., 2011). Overall, composition plays a significant role in OP size distribution and it appears that submicron and fine PM are most critical to mass-normalized and volume-normalized OP^{DTT}, respectively, but may not be the largest contributors for other assays, such as OP_{SLF}^{GSH} and OP^{ESR}.

2.6 Synthesis and Recommendations for Future Research

An increasing number of health studies have found relationships with OP, driving increased interest in acellular OP assays. OP captures the biologically relevant redox reactions driven by PM that can lead to oxidative stress, meaning it can be a useful multipollutant, multisource health indicator providing knowledge on the relationship

between PM and health beyond what PM mass measurements alone provide. With consistent reductions in anthropogenic emissions, aerosol composition will continue to change with a growing biogenic fraction, possibly causing the relationship between PM and various health outcomes to change. OP, however, should continue to be a strong predictor of adverse health as it only captures redox-active species and sources and may more closely capture PM components that are related to certain health endpoints than PM mass, as observed in multiple studies that show OP exposure to be a better predictor of certain adverse health endpoints (e.g. asthma/wheezing, lung cancer, and ischemic heart disease) than PM concentration (Abrams et al., 2017; J. T. Bates et al., 2015; Delfino et al., 2013; Weichenthal, Crouse, et al., 2016; Yang et al., 2016). Further, OP provides insight into specific processes that may mediate the health effects of PM, including aging (oxidation of quinones and solubilizing metals), and helps address specific questions relevant to regulatory initiatives, such as discerning best fuels and vehicle control technologies and what PM emission sources should be targeted for reduction. Finally, once there is a thorough understanding of what chemical species and interactions drive OP, we may be able to rely on just one measurement (OP) that integrates compositional effects rather than speciated measurements requiring a suite of instruments for certain types of health studies. It should be noted that OP only measures one potential mechanism of PM toxicity, oxidative stress, and other mechanisms are likely at work. Nevertheless, OP has shown promise within health studies and has potential advantages over PM concentration, and, thus, it is a critical area of research.

Based on current literature, OP^{DTT} and OP_{SLF}^{GSH} appear to be the most relevant OP assays to epidemiologic analyses as they both have been associated with acute and chronic

health endpoints, and in some cases, have been found to be more strongly associated with adverse cardiorespiratory outcomes than PM concentration. On the other hand, OP^{AA} has often been found to have null associations with health outcomes, so even though this assay may be informative for the ability of certain PM species to catalyze reactions, it does not seem to be relevant to health. More work is needed to confirm the associations between OP^{DTT} and OP_{SLF}^{GSH} and reported health outcomes, but it would also be valuable to investigate the potential associations of OP^{DTT} and OP_{SLF}^{GSH} with other health endpoints beyond cardiorespiratory effects, e.g. birth outcomes, motivated by observations of associations with PM in previous studies (H. H. Chang, Reich, & Miranda, 2012; Darrow, Klein, Strickland, Mulholland, & Tolbert, 2011; U.S. EPA, 2009). With a growing body of longer time-series data of OP, more thorough epidemiologic analyses on the effects of OP on chronic health could also be achieved. The impact of particle size on OP health associations is also of interest to inform regulatory initiatives.

The collected knowledge on species composition and emission source impact on OP could be useful for developing PM regulations aimed at protecting human health and guiding future research towards health-relevant species and sources. Copper is a critical metal in almost every OP assay, and OP^{DTT} appears to be the most sensitive assay to organics (especially oxidize organics), though more work is needed to investigate synergistic or antagonistic effects of various species and sources and the impact of organics on OP_{SLF}^{GSH} (less work has focused on compositional impacts on this assay compared to OP^{DTT}). Diesel vehicles are critical to OP due to metal and soot-bound quinone concentrations, though the relative importance of diesel and gasoline vehicles versus total traffic count has not been fully explored and may change with changing engine

configurations, control technologies, fuel types, and vehicle fleets. The large contribution from biomass burning drives temporal variation in OP^{DTT}. Future work investigating local and large-scale variations in OP driven by emissions could provide critical information for exposure studies.

When comparing OP studies, it is important to identify the particular method used. For example, some studies have modified the original OP^{DTT} method developed by Cho, et al. (Cho et al., 2005) by using different metal chelators, reaction times, PM filters, and extraction methods, which can affect the magnitudes of and potentially relative species/source contributions to OP^{DTT}. Different compositions of extraction fluids affect OP^{DTT} of ambient PM (Calas et al., 2017), and the composition of SLF significantly impacts the sensitivities of antioxidant depletion assays to various species with AA being the most critical antioxidant in SLF for OP responses to metals. For epidemiologic studies, both water-soluble and SLF studies (OP^{DTT} and OP_{SLF}^{GSH}) have shown significant associations with adverse health outcomes, so the advantages or disadvantages of using SLF from a health research standpoint are not clear at this time. Overall, care should be taken when comparing study results and designing research.

Ultimately, developing "standard" methods for different OP assays that use consistent PM size fractions would improve upon the value of comparing studies as well as provide a clearer picture of the effects of PM on OP. Overall, the current studies have suggested that OP^{DTT} and OP_{SLF}^{GSH} may be the most relevant OP assays for cardiorespiratory health, and traffic and biomass burning emissions significantly impact OP assays due to their metal and organic components. Longer term measurements in multiple locations

focusing on OP^{DTT} and OP_{SLF}^{GSH} would be valuable for future epidemiologic analyses to determine the mode of action of PM toxicity, to confirm associations with cardiorespiratory endpoints, to identify associations with non-cardiorespiratory endpoints, and to help target strategies to better improve health. With a growing measurement database allowing for more epidemiologic and source apportionment studies, OP may be a useful multipollutant, multisource indicator for elucidating potential relationships between PM and adverse health impacts associated with the oxidative stress mechanism.

CHAPTER 3.

REACTIVE OXYGEN SPECIES GENERATION LINKED TO SOURCES OF ATMOSPHERIC PARTICULATE MATTER AND CARDIORESPIRATORY EFFECTS

Abstract

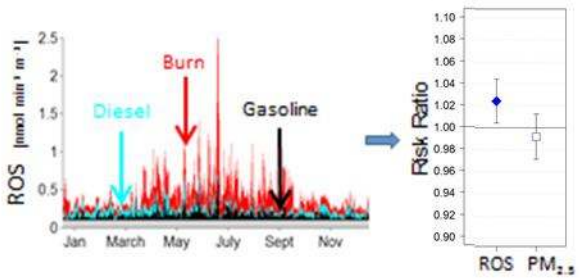

Exposure to atmospheric fine particulate matter ($PM_{2.5}$) is associated with cardiorespiratory morbidity and mortality, but the mechanisms are not well understood. We assess the hypothesis that $PM_{2.5}$ induces oxidative stress in the body via catalytic generation of reactive oxygen species (ROS). A dithiothreitol (DTT) assay was used to measure the ROS-generation potential of water-soluble $PM_{2.5}$. Source apportionment on ambient (Atlanta, GA) $PM_{2.5}$ was performed using the chemical mass balance method with ensemble-averaged source impact profiles. Linear regression analysis was used to relate $PM_{2.5}$ emission sources to ROS-generation potential and to estimate historical levels of DTT activity for use in an epidemiologic analysis for the period of 1998−2009. Light duty gasoline vehicles (LDGV) exhibited the highest intrinsic DTT activity, followed by biomass burning (BURN) and heavy-duty diesel vehicles (HDDV) (0.12 ± 0.02, 0.074 ±

0.01, and 0.061 ± 0.03 nmol min^{-1} μg^{-1}_{source}, respectively). BURN contributed the largest fraction to total DTT activity over the study period, followed by LDGV and HDDV (43, 22, and 17%, respectively). DTT activity was more strongly associated with emergency department visits for asthma/wheezing and congestive heart failure than $PM_{2.5}$. This work provides further epidemiologic evidence of a biologically plausible mechanism, that of oxidative stress, for associations of adverse health outcomes with $PM_{2.5}$ mass and supports continued assessment of the utility of the DTT activity assay as a measure of ROS-generating potential of particles.

3.1 Introduction

Air pollution exposure is one of the world's leading environmental health risks, causing approximately 7 million deaths worldwide in 2010 (Lim, Vos, & Flaxman, 2013). Fine particulate matter ($PM_{2.5}$) is a prevalent air pollutant, and epidemiologic studies show that exposure to $PM_{2.5}$ increases risk for cardiorespiratory morbidity and mortality (Brunekreef & Holgate, 2002; Delfino et al., 2005; Pope et al., 2009). However, the mechanisms of toxicity are not well understood. Reactive oxygen species (ROS) either transported on particles or catalytically generated by particles through redox reactions are suspected to cause injurious cellular responses. This work focuses on the catalytic generation of ROS by $PM_{2.5}$. It is hypothesized that $PM_{2.5}$ inhalation can induce oxidative stress, leading to a variety of health effects, by catalyzing the generation of ROS in excess of the antioxidant capacity of the body (Baulig et al., 2003; Donaldson et al., 2001). Small-scale health studies have linked particulate matter ROS-generating potential to inflammation and decreased lung capacity, although inconsistent results highlight the need

for a more comprehensive population-level epidemiologic analysis (Delfino et al., 2013; Hogervorst et al., 2006; Janssen et al., 2015).

ROS-generating potential of $PM_{2.5}$ may vary by $PM_{2.5}$ composition. For example, quinones and transition metals have been shown to catalyze redox reactions in the body (Ghio et al., 2012). Biomass burning organic aerosols and highly-oxidized organic aerosols have been identified as having high intrinsic toxicities with regard to ROS-generating abilities (Verma, Fang, et al., 2015). This study aims to identify emission sources of $PM_{2.5}$ that have the ability to catalytically generate ROS and investigate the relationship between these particles and human health. Identifying sources of redox-active $PM_{2.5}$ rather than species is important for policy development and provides an additional understanding of the compounds involved in ROS generation.

A variety of methods are available for measuring the capacity of $PM_{2.5}$ to catalyze redox reactions. The dithiothreitol (DTT) assay is a commonly used acellular assay because its response correlates well with biological markers like hemeoxygenase (HO-1) expression in cells and exhaled nitric oxide fraction in human subjects (Ghio et al., 2012; Hogervorst et al., 2006). Water-soluble and water-insoluble fractions of particulate matter exhibit different mechanisms of action in the body, (Verma, Fang, et al., 2015) and while both components are important, this research focuses on the water-soluble fraction. A DTT assay was used in this study to quantify ROS-generation potential of water-soluble $PM_{2.5}$ (WS-$PM_{2.5}$). Source apportionment techniques were used with linear regression analyses to assess intrinsic DTT activity of $PM_{2.5}$ sources. The model was used to simulate historical trends in ambient DTT activity for use in epidemiologic studies. Developing better

indicators of the potential of $PM_{2.5}$ to impact health facilitates optimization of air pollution control strategies.

3.2 Methods

3.2.1 Sample Collection and Analysis

Atlanta is a major urban population center with relatively high emissions of $PM_{2.5}$ from a variety of sources (including mobiles sources, biomass burning, etc.) and secondary aerosol formation, making it a suitable U.S. location to study particle toxicity. Additionally, it is the site of detailed work identifying source impacts on $PM_{2.5}$ (Balachandran et al., 2012), which have also been used in prior health studies (Gass, Balachandran, Chang, Russell, & Strickland, 2015; J. A. Sarnat et al., 2008). Sampling was conducted at a Southeastern Aerosol Research and Characterization (SEARCH) site in Atlanta [Jefferson Street (JST)] from June 2012 to April 2013. Ambient $PM_{2.5}$ was collected using a high-volume sampler (HiVol, Thermo Anderson, nondenuded, nominal flow rate 1.13 m^3/min, $PM_{2.5}$ impactor). Prebaked 8 x 10" quartz filters were used for particle collection. Samples were taken from 12 pm (noon) to 11 am, creating 23 h integrated samples. All samples were wrapped in prebaked aluminum foil and stored in freezers (-18 °C) until ROS-generation analysis. Filter extraction processes were similar to those described in detail by Verma et al. (2014) . In brief, 1 in. punches were extracted in 15 mL of deionized water via sonication in a water bath for 30 min. Each extract was filtered using a polytetrafluoroethylene (PTFE) 0.45 μm pore syringe filter to remove insoluble materials and fibers. These WS-$PM_{2.5}$ samples were used in the DTT analysis.

A semi-automated cell-free DTT assay instrument was developed and used to measure the rate at which ambient WS-$PM_{2.5}$ catalytically generates ROS (J. T. Bates et al., 2015), creating a uniquely large data set of 196 23 h integrated measurements. DTT acts as a surrogate of the biological reducing agents nicotinamide aldenine dinucleotide (NADH) and reduced nicotinamide adenine dinucleotide phosphate (NADPH), and the ROS-generating potential of ambient WS-$PM_{2.5}$ was quantified by the DTT consumption rate (i.e. DTT activity). The method of measuring DTT activity is described in detail by Cho et al. (2005) . Briefly, the rate of DTT consumption was measured from a mixture of 100 μM DTT, a WS-$PM_{2.5}$ filter sample (3.5 mL) collected using the HiVol sampler, and potassium phosphate buffer (0.1 mL, pH 7.4). This mixture was incubated in a ThermoMixer (Eppendorf North America, Inc., Hauppauge, NY, USA) at 37 °C. DTT consumption was measured at five time steps (4, 13, 23, 30, and 41 min). For each, a 100 μL aliquot was mixed with 1 mL of 1% (w/v) trichloroacetic acid (TCA) to quench the reaction, and 0.5 mL 5,5'-dithiobis(2-nitrobenzoic acid) (DTNB) and 2 mL of tris(hydroxymethyl)-aminomethane (Tris) buffer [0.08 M with 4 mM ethyl-enediaminetetraacetic acid (EDTA)] were added to form 2-nitro-5-mercaptobenzoic acid (TNB) by reacting with the residual DTT. A spectrometer was used to measure the light absorption of this product to quantify the remaining DTT concentrations. The measurements at the five time-steps, along with the initial DTT concentration, were used to estimate a linear slope parameter representing the DTT consumption rate (nmol min^{-1}) associated with the aerosol sample collected from a known volume of ambient air. Volume-normalized DTT (DTTv) is the rate of moles of DTT consumed per minute per volume of air sampled (nmol min^{-1} m^{-3}). Mass-normalized DTT (DTTm), with units of nmol min^{-1}

μg^{-1}, was determined by dividing DTTv for each day by total 23 h $PM_{2.5}$ mass measured from a tapered elemental oscillating microblance (TEOM). The recently developed analytical system allowed for automated measurements at a rate of one sample per hour and the ability to generate large DTT data sets at a reasonable cost (J. T. Bates et al., 2015).

Other air quality data, including total species concentrations [organic carbon (OC), elemental carbon, ions, and metals], were used for source apportionment of total $PM_{2.5}$. Different measurements had to be used for source apportionment than the filters for DTT analysis because the source profiles used in the chemical mass balance (CMB) method were based on total species concentrations, whereas only water-soluble species were measured from the DTT filters. The measurements of total species concentrations were collected at JST over the same time period as the DTT filter collection (June 2012 to April 2013) using methods detailed in Hansen et al. (2006) , Edgerton et al. (2005) , and Hansen et al. (2003) . In brief, total $PM_{2.5}$ was collected using a Rupprecht & Patashnick model 2025 sequential FRM monitor. The 24 h integrated samples (from midnight to midnight) were collected daily on Teflon filters (47 mm diameter and 2 µm pore size) and were collected, processed, and analyzed according to FRM protocols ("Appendix L to Part 50-Reference Method for the Determination of Fine Particulate Matter as PM2.5 in the Atmosphere," 2001). A particle composition monitor (PCM) built by Atmospheric Research & Analysis, Inc. was used to measure sulfate, nitrate, ammonium, OC, and black carbon (BC) every 3 days. 24 h integrated samples of ions were collected on Teflon filters (47 mm diameter and 2 µm pore size) and analyzed using ion chromatography. 24 h integrated samples of OC and BC were collected on quartz filters (37 mm diameter) and measured using thermal/optical reflectance. Denuders (annular for the ions and activated

carbon honeycomb for OC and BC) were used for removal of select gases. Flow through the PCM was maintained at 16.7 L/min. Metals, including aluminum, calcium, copper, iron, potassium, manganese, lead, silicon, titanium, and zinc, were measured from the FRM filter samples using X-ray fluorescence. These measurements were available daily.

3.2.2 Source Apportionment

Using collocated measures of total $PM_{2.5}$ and $PM_{2.5}$ species (ions, carbon, and metals), $PM_{2.5}$ source impacts were constructed. Source apportionment was performed on the ambient $PM_{2.5}$ measurements using the CMB model version 8.2 with month-specific ensemble-based source profiles for $PM_{2.5}$ that combined source impacts from three receptor-based models (CMB-LGO, CMB-MM, and Positive Matrix Factorization) and a chemical transport model (Community Multi-scale Air Quality model) (Balachandran et al., 2012; Gass et al., 2015; J. A. Sarnat et al., 2008). Sources in these profiles include light-duty gasoline vehicles (LDGV), heavy-duty diesel vehicles (HDDV), soil dust (SDUST), biomass burning (BURN), ammonium sulfate (AMSULF), ammonium bisulfate (AMBSULF), ammonium nitrate (AMNITR), and not otherwise apportioned organic carbon (OTHER_OC), which mostly contains secondary biogenic carbon. To correct for temporal misalignment between DTT measurements collected from noon to 11 am and source impact estimates from midnight to midnight, the sources identified were linearly interpolated to the time period over which the DTT filters were taken.

3.2.3 Linear Regression

The impact of specific sources of $PM_{2.5}$ on DTT activity was estimated using a multivariate linear regression model (Figure 3-1). The regression identifies the

relationship between the measured times series of WS-$PM_{2.5}$ DTT activity and the estimated time series of source impacts on total $PM_{2.5}$. The use of total $PM_{2.5}$ for sources in the regression was required for applying the regression to previous years for which source impacts were only available for total $PM_{2.5}$ and not WS-$PM_{2.5}$. $PM_{2.5}$ sources rather than species were investigated in this work for the following reasons: First, the ROS-generation potential of emission sources circumvents the problem that some of the bulk species measurements actually represent many species that are expected to have different health impacts. For example, what is measured as OC encompasses many different chemical species, including those expected to significantly generate ROS (e.g., quinones and other humic-like substances) versus those less so (Charrier & Anastasio, 2012; Cho et al., 2005; Verma et al., 2012). Additionally, the chemical composition of OC varies seasonally; therefore, the ROS-generation potential per unit of OC is not stable over time (Verma, Fang, et al., 2015). This leads to the second reason of using sources: stability of the model over time. The composition of sources, such as vehicle emissions and biomass burning, is more constant over time, and the source profiles used in this work are consistent from 1998 to 2013; therefore, a model trained on 2012-2013 data can be used to backcast estimates to earlier years. Finally, using source impacts rather than species significantly reduces the number of independent variables in the model, many of which are highly correlated when using just species.

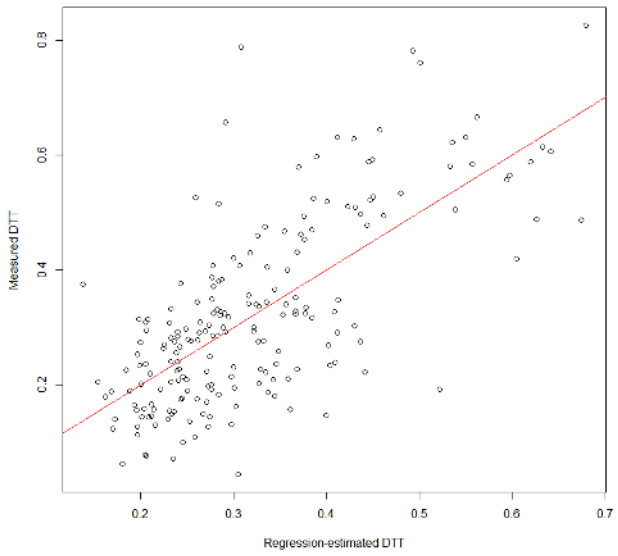

Figure 3-1. Measured DTT activity plotted against DTT activity estimated using the regression model. This data is for the 2012-2013 period. The R^2 between estimated and measured DTT is 0.49.

DTT activity was treated as the dependent variable, with sources as the independent variables. All programming was conducted using the statistical software package R 3.0.2. The assumption of a linear relationship between DTT activity and sources was supported by graphs of joint probability density functions (jpdf) between measured DTT activity of WS-$PM_{2.5}$ and concentrations of each individual source impact that illustrated linear relationships. An *F* test was used to assess the significance of each source impact in the model on estimating DTT activity. Coefficients of sources with *p* values of the *F* statistic >0.05 were not considered statistically significant. Using a backward elimination approach, the least significant source was removed from the model and least squares regression was performed again with one fewer independent variable. This process was repeated until only significant coefficients remained (Table A-1). Ammonium sulfate was not included in the model because additional work performed during this study and by others show that sulfate alone is not DTT-active. This was

supported by direct laboratory experiments of a sulfate-containing solution in which DTT activities of blank filters and filters with only sulfate were compared and found to be similar (Figure A-8-2). We also performed regression analyses in which source impacts had been normalized to a standard deviation of one to investigate the sensitivity of DTT activity to each source and provide further evidence of the differing contributions to DTT activity of each source impact.

3.2.4 Historical DTT estimation

The DTT activity model was used to backcast estimated water-soluble DTT activity of daily $PM_{2.5}$ for the greater metropolitan Atlanta area for the period from August 1998 to December 2009 (a period during which DTT activity measurements were not available but daily speciated air quality measurements were available, allowing source apportionment of $PM_{2.5}$). It was assumed that the chemical composition of $PM_{2.5}$ source impacts has not changed significantly over time so that source profiles could be applied to all years from 1998 to 2013. Vegetation in Georgia has not changed significantly over the past decade, making biomass burning source profiles relatively stable. Additionally, the EC/OC ratio (the main driver of vehicle source profiles) of average vehicle fleets in the 20 county non-attainment Atlanta calculated using MOVES 2010 are only ~20% different between previous years (averaged over 1998—2009) and 2012 (U. S. Environmental Protection Agency, 2009). These reasons, along with the reasons for using source impacts in the linear regression, support using a model trained on 2012—2013 data to backcast DTT estimates for earlier years. Additionally, it was assumed that the DTT activity estimated at one location (JST) using the regression applies to the 5 county metro Atlanta area used in the epidemiologic study because DTT activity per volume of air has been shown to be spatially

uniform (Verma et al., 2014). To obtain estimates of DTT activity from 1998 to 2009, daily concentrations of $PM_{2.5}$ from each source were multiplied by their respective coefficients in the model and then summed to estimate daily total DTT activity. This resulting DTT time series was then used in an epidemiologic analysis to investigate the link between DTT activity and emergency department (ED) visits for asthma/wheezing and congestive heart failure.

3.2.5 Epidemiologic Modeling

We conducted time series analyses using modeling methods and control for confounding variables employed in our previously reported epidemiologic analyses (Gass et al., 2015; Strickland et al., 2010; Winquist, Schauer, Turner, Klein, & Sarnat, 2015) to characterize epidemiologic associations between health events and $PM_{2.5}$, estimated DTT activity, and measures of $PM_{2.5}$ species at JST. The outcome was the daily number of ED visits with a primary International Classification of Disease, 9th Revision, (ICD-9) code of asthma or wheeze (493 and 786.07) or congestive heart failure (428) for a patient with a home ZIP code within the Atlanta 5 county metro area (Fulton, DeKalb, Gwinnett, Cobb, Clayton) recorded in an Atlanta hospital from Aug 1, 1998 to Dec 31, 2009 (other outcome groups that are not presented here include chronic obstructive pulmonary disease, pneumonia, and ischemic heart failure; in preliminary examinations, none of these showed significant associations with DTT activity or with $PM_{2.5}$ mass). Over the study period, 263,665 and 70,587 ED visits were recorded for asthma/wheezing and congestive heart failure, respectively. The primary air quality variables of interest were 24 h averaged estimated DTT activity and 24 h averaged $PM_{2.5}$ from JST (models were run for each of these variables separately as well as models with both variables included). Because health

effects of pollution may be observed over several subsequent days, the exposures were modeled as lag 0—2 (average pollutant level for that day, the previous day, and the day before). This analysis was modeled as a Poisson generalized linear regression allowing for over-dispersion using SAS 9.4 statistical software (SAS Institute, Cary, NC).

The covariates in this model were chosen on the basis of prior knowledge of variables that could potentially act as temporal confounders between ED visits and daily pollution levels. Models controlled for temporal trends using transformed cubic splines with monthly knots. Linear, quadratic, and cubic terms were included for mean daily dew point (lag 0—2), maximum daily temperature, and minimum daily temperature (lag 1—2). Other variables included indicators of hospital contribution time periods (not all hospitals provided data for the whole time period August 1998 to December 2009; the model controlled for the subset of days that the data for each hospital was available for), season of year, day of week, and holiday indicators. Interaction terms were included between season and maximum temperature (linear, quadratic, and cubic) and between season and day of week because the effects of the latter variables can change according to season. The use of the maximum temperature from that day as well as the lagged minimum temperature was based on previous analyses showing that this temperature control was highly predictive of ED visits while minimizing covariate collinearity. Sensitivity analyses were conducted varying age category (pediatric ED visits versus all ED visits), geographic extent (20 county Atlanta area versus 5 county Atlanta area), and ICD code priority (any asthma/wheeze or congestive heart failure code versus primary asthma/wheezing or congestive heart failure code). Results for these analyses remained similar to those presented.

Risk ratios and their 95% confidence intervals were calculated for estimated DTT activity in a single pollutant model, total $PM_{2.5}$ in a single pollutant model, and estimated DTT activity and total $PM_{2.5}$ in a two-pollutant model for lag 0—2. The risk ratios represent the relative risk of ED visits per unit increase in DTT activity or $PM_{2.5}$ mass. The interquartile ranges (IQR, a measure of variability that reflects the difference between the 75^{th} percentile and the 25^{th} percentile of a distribution) of DTT activity and $PM_{2.5}$ were used as exposure units. For example, if the risk ratio was 1.08, an increase in pollution by 1 IQR unit would increase the risk of ED visits for the illness in question by 8%. The two-pollutant model allows for the assessment of health outcome associations of DTT activity controlling for total $PM_{2.5}$ mass, providing additional evidence that any measured association with health outcomes represents the effects of ROS-generating potential.

3.3 Results and Conclusions

3.3.1 Source Contribution to DTT activity

This paper investigates the differing ROS-generation capabilities of various source impacts on $PM_{2.5}$ and their relationships to acute health effects. First-level analysis on the relationship between DTT activity and $PM_{2.5}$ looked at the correlation coefficients between DTT activity, species, and $PM_{2.5}$ source impacts (Table 3-1 and Table A-2). Volume-normalized DTT activity (DTTv, nmol min^{-1} m^{-3}) was positively correlated with $PM_{2.5}$ (R = 0.57), indicating that one or more components of this pollutant contribute to its ROS-generating capability. The negative correlation between DTT activity normalized by $PM_{2.5}$ mass (DTTm, nmol min^{-1} μg^{-1}) and total $PM_{2.5}$ (R = -0.25) suggests that certain species,

such as sulfate, that contribute to total $PM_{2.5}$ mass do not on their own contribute much to the ROS-generating capability. These correlations support the regression results.

Table 3-1. Pearson correlation coefficients between DTT activity and CMB-estimated sources for the 2012-2013 period.

	Total $PM_{2.5}$	LDGV	HDDV	SDUST	BURN	AMSULF	AMBSLF	AMNITR	OTHER OC
DTTv nmol min^{-1} m^{-3}	0.57	0.56	0.27	0.18	0.63	0.30	-0.02	0.32	0.08
DTTm nmol min^{-1} μg^{-1}	-0.25	0.34	-0.29	0.25	0.25	-0.16	-0.29	0.22	-0.47

Advanced analysis involved the development of a regression relating DTT activity of WS-$PM_{2.5}$ to total $PM_{2.5}$ source impacts. The model was developed using DTT activity measurements in Atlanta, GA from June 2012 to April 2013 and source impacts estimated from the CMB method applied to collocated total $PM_{2.5}$ and species measurements, leading to a linear relationship between the ROS activity of WS-$PM_{2.5}$ (DTTa) and source impacts on total $PM_{2.5}$:

$$DTTa = 0.066 + 0.12\,LDGV + 0.061\,HDDV + 0.074\,BURN \qquad (3\text{-}1)$$

DTTa acts as a multi-pollutant, multi-source indicator, a measure integrating across species and sources with respect to their oxidative potential. Equation (3-2) has an R^2 of 0.49 and mean squared error of DTT activity of 0.013 nmol min^{-1} m^{-3} (4.0% of mean of measurements). Cross-validation was performed to evaluate this model. A total of 10% of the DTT measurements was removed; the regression coefficients were reevaluated; and the

mean-squared error was calculated. This process was repeated 50 times, and the average mean-squared error over 50 iterations was 0.011 nmol min^{-1} m^{-3} (3.4% of the mean of measurements).

From this analysis, we find that gasoline vehicle emissions exhibited the highest intrinsic DTT activity, as shown by their coefficient in the regression (nmol min^{-1} μg^{-1}_{source}), which is consistent with studies showing links between DTT activity and oxygenated OC and metals (Cho et al., 2005; Verma et al., 2014; Verma, Fang, et al., 2015). Diesel particles have been shown to be DTT-active; however, most of the DTT activity occurs in the water-insoluble fraction of diesel particles (Verma et al., 2012) and, thus, was not measured in this work and is not captured by our approach, consistent with its relatively low intrinsic activity (i.e. lowest coefficient in the model). The high intrinsic DTT activity of biomass burning is most likely driven by its high oxygenated OC content (Verma et al., 2014; Verma, Fang, et al., 2015).

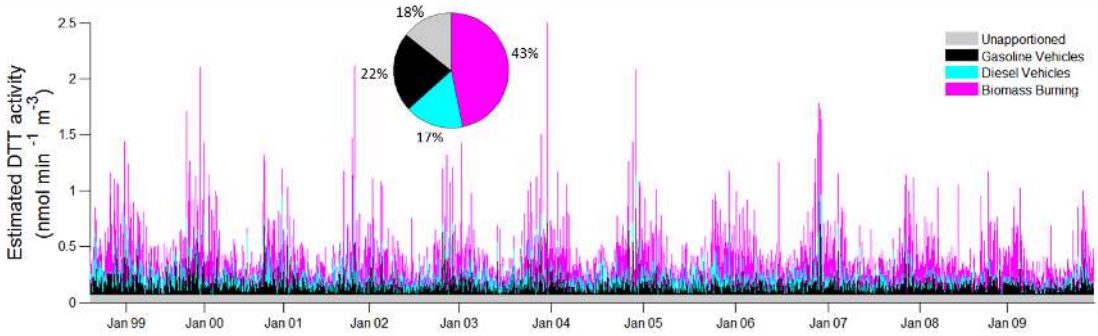

Figure 3-2. Daily estimated DTT activity of WS-$PM_{2.5}$ from Aug 1998 to Dec 2009 calculated using the regression. The pie chart shows the average contribution of each source over the time period.

While gasoline vehicles exhibited the highest intrinsic toxicity in this analysis, biomass burning accounted for the highest fraction of total estimated DTT activity on a per volume of air basis (Figure 3-2). Biomass burning, light-duty gasoline vehicles, and heavy-duty diesel vehicles contributed 43, 22, and 17% (standard deviations: 16, 11 and 11%), respectively. Results from measurements and estimated historical DTT activity suggest a strong seasonal trend, with higher values in the winter than summer, driven mostly by biomass burning emissions. The largest source of biomass burning $PM_{2.5}$ in Atlanta is prescribed burns, occurring primarily from winter to early spring (Tian et al., 2009). This, along with the lower wintertime mixing heights, results in a strong seasonal trend in DTT activity. Mobile source emissions are more evenly spread throughout the year.

Table 3-2. Regression coefficients and standard errors for each source in the DTT regressions with normalized data[a].

	LDGV	HDDV	BURN	AMSULF	AMBSLF	OTHER_OC
DTTv nmol min^{-1} m^{-3}	0.33 (<0.01)	0.13 (0.018)	0.44 (<0.01)	-	-	-
DTTm nmol min^{-1} μg^{-1}	0.22 (0.068)	-	0.21 (0.078)	-0.25 (0.077)	-0.28 (0.077)	-0.32 (0.092)

[a]Standard errors are in parentheses. The coefficients for SDUST and AMNITR were not statistically significant and were not included in the regressions.

Normalized regressions were used to further investigate sensitivity of DTT activity to each source, and results suggest that gasoline vehicles and biomass burning drive the variation in DTT activity of WS-$PM_{2.5}$ (Table 3-2). The negative coefficients in the normalized DTTm regression provide further evidence that ammonium sulfate is not significantly DTT-active. Although OC is usually correlated with DTT activity,

OTHER_OC (linked to secondary OC formation)(Balachandran et al., 2012) identified during source apportionment was not found to be a significant contributor to DTT activity, likely because it consists mostly of biogenic components derived from isoprene and terpene oxidation, which are not as DTT-active as biomass burning and mobile source WS-$PM_{2.5}$ (Verma, Fang, et al., 2015).

Uncertainties in the DTTa regression arise from measurement error, interpolation of data, source apportionment, and possible incomplete source information in the model. A non-zero intercept in the DTTa regression is an indicator of model misspecification, which could arise from a missing source. The intercept is partly due to artifacts collected on the undenuded filters used for the DTT analysis and smaller contributions from other sources. Regressions between OC from the undenuded filters used for DTT analysis and OC from the denuded SEARCH data set used for source apportionment were created to investigate the presence of positive artifacts that may affect DTT activity, leading to the following relationship:

$$OC_{DTT\_Filter} = 1.48 * OC_{SEARCH\_Filter} \ (R^2 = 0.72) \quad (3\text{-}2)$$

Equation (3-2) indicates that the filters used for DTT analysis had on average ~1.5 times the concentration of OC as the denuded filters used for source apportionment, consistent with the presence of a positive OC artifact on the DTT filters.

3.3.2 Health Analysis

The health model used daily $PM_{2.5}$ source impacts from 1998 to 2009 to produce daily DTT activity estimates for an epidemiologic analysis on acute health effects. The

average estimated DTT activity over the time period was 0.44 nmol min^{-1} m^{-3}, with a standard deviation of 0.24 nmol min^{-1} m^{-3}. The IQR for estimated DTT activity and $PM_{2.5}$ were 0.21 nmol min^{-1} m^{-3} and 8.3 µg m^{-3}, respectively. Time series analyses using emergency ED visit data showed that estimated DTT activity was positively associated with ED visits for both asthma/wheeze and congestive heart failure (Figure 3-3). The risk ratio for DTT activity of WS-$PM_{2.5}$ in a two-pollutant model (with DTT activity and total $PM_{2.5}$) for asthma/wheeze was 1.015 [95% confidence interval (CI) = 1.002—1.027] per IQR increase. The risk ratio for WS-$PM_{2.5}$ DTT activity with total $PM_{2.5}$ in a two-pollutant model for congestive heart failure was 1.024 (95% CI = 1.004—1.044) per IQR increase. Each risk ratio was significant at a 95% level. Estimated DTT activity was the only single pollutant measure out of several tested pollutant measures ($PM_{2.5}$, O_3, elemental carbon, and OC) that exhibited a significant link to congestive heart failure. Further, in two-pollutant models with DTT activity and $PM_{2.5}$, included in the model simultaneously, estimated DTT activity was significantly associated with asthma/wheeze and congestive heart failure, while $PM_{2.5}$ was not associated with these outcomes (Figure 3-3). These results are interesting in that DTT activity is likely not estimated as well as $PM_{2.5}$ is measured, and overall, they provide support that DTT activity may be a driver of health effects from $PM_{2.5}$.

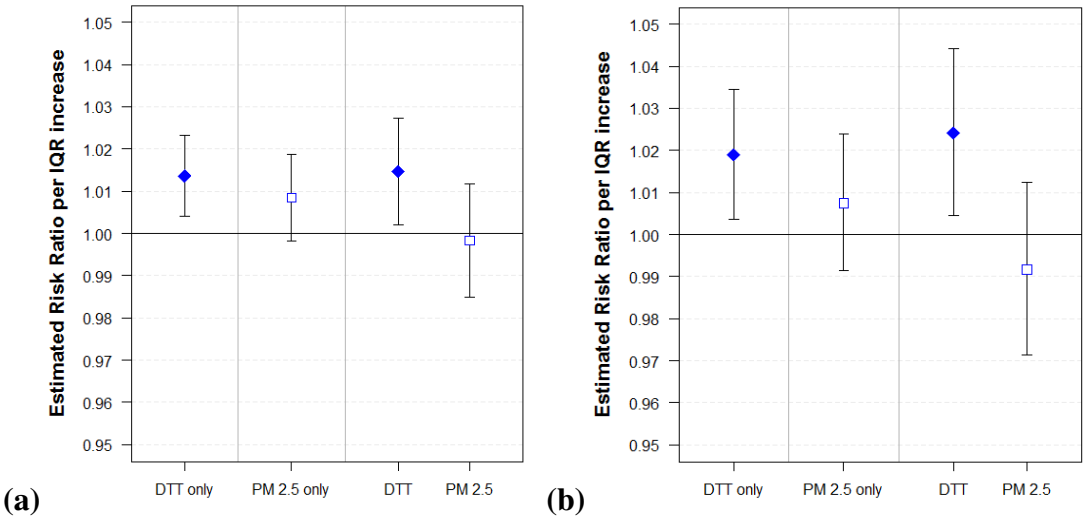

Figure 3-3. Effect of ROS (by estimated DTT activity) on ED visits for (a) asthma/wheeze and (b) congestive heart failure in the Atlanta 5 county area, from Aug 1, 1998 to December 31, 2009, with 0—2 day lag. The model labeled "DTT only" or "$PM_{2.5}$ only" illustrates the results from the model run only with DTT activity or total $PM_{2.5}$ mass as the exposure variable, respectively. The model labeled "DTT and $PM_{2.5}$" illustrates the results from the two-pollutant model, in which both DTT activity and total $PM_{2.5}$ mass were used as exposure variables.

The observed associations between estimated DTT activity and cardiorespiratory ED visits are consistent with the hypothesis that oxidative stress is a mechanism of particle toxicity. Furthermore, the association between estimated DTT activity and asthma/wheeze and congestive heart failure and a lack of association between $PM_{2.5}$ and these health effects in the two-pollutant models support the interpretation that endogenous ROS-generation potential may be a property of particulate matter responsible, in part, for detrimental health effects. Thus, DTT activity may be a helpful multipollutant, multisource indicator of the potential health consequences of $PM_{2.5}$ exposure, complementary to $PM_{2.5}$ mass.

DTT-active components of ambient WS-$PM_{2.5}$ potentially pose a larger risk to human health than the components that do not significantly generate ROS, which is

supported by the observed association between estimated DTT activity and asthma/wheeze and congestive heart failure ED visits. Given the potential implications of these results on assessing the effectiveness of control strategies and regulations, verification of the study results and advancements in this research area are important. Much of the mass in $PM_{2.5}$ is sulfate and, in many locations, biogenically-derived secondary OC (Hidy et al., 2014), which have water-soluble fractions that are not as DTT active as other species. The links between ROS, biomass burning and vehicles as sources, and both respiratory and cardiovascular health outcomes can focus controls on those sources.

This study is the first to estimate population-level health effects of a measure of ROS activity and to use an epidemiologic approach to linking $PM_{2.5}$ ROS to health endpoints. Our results suggest that reducing pollutant emissions associated with WS-$PM_{2.5}$ DTT activity may measurably decrease ED visits associated with asthma and wheezing attacks and congestive heart failure. Additional studies exploring DTT/health associations in other populations or using spatially distributed measurements could also be useful for elucidating the relationship between DTT activity and health outcomes. By presenting further evidence of oxidative stress as a potential mechanism for particle toxicity, this work provides epidemiologic evidence of a biologically plausible mechanism for the observed associations of $PM_{2.5}$ concentration with cardiorespiratory effects.

CHAPTER 4.

SOURCE IMPACT MODELING OF SPATIOTEMPORAL TRENDS IN $PM_{2.5}$ OXIDATIVE POTENTIAL ACROSS THE EASTERN UNITED STATES

Abstract

Oxidative potential (OP) of particulate matter measures the ability of particles to catalytically generate reactive oxygen species while simultaneously depleting antioxidants, leading to oxidative stress and, in turn, inflammation in the respiratory tract and cardiovascular system. OP measurements have been linked with adverse cardiorespiratory endpoints, such as asthma/wheezing, lung cancer, and ischemic heart disease. However, measurements of OP are limited, restricting the area over which epidemiologic analyses can be performed. In this work, a modeling approach is developed and evaluated that uses limited measurements of water-soluble OP and $PM_{2.5}$ source impact analysis to estimate OP over a large spatial domain (eastern United States). The dithiothreitol (DTT) assay was used to measure daily OP of water-soluble $PM_{2.5}$ from June 2012 to July 2013 across four sites in the southeastern United States. Daily $PM_{2.5}$ source impacts were estimated using CMAQ-DDM during the same time period and related to OP^{DTT} measurements via multivariate linear regression. This regression was then applied to spatial fields of daily CMAQ-DDM source impacts across the eastern United States to provide daily spatially-varying OP^{DTT} estimates. Backward selection during regression development showed vehicle and biomass burning emissions to be significantly predictive of OP^{DTT}, as observed in previous studies. The fire source impact was the largest contributor to OP^{DTT} (29%)

across the study domain during the study time period, and both spatial and seasonal variations were largely driven by fires. Vehicular impacts, especially diesel impacts, were more significant in urban areas. This CMAQ-DDM modeling approach provides a powerful tool for integrating OP measurements from multiple locations and times into a model that can provide spatiotemporal exposure fields of OP^{DTT} across a wide spatial domain for use in health analyses, and the results presented offer insight into the large-scale spatial distribution of OP^{DTT} driven by emission source impacts.

4.1 Introduction

Fine particulate matter ($PM_{2.5}$) is estimated to have contributed to 3.2 million premature deaths in 2010 and to roughly 5% of all cardiorespiratory deaths across the globe, but the biological mechanisms are not fully understood (Lim et al., 2012). There is growing evidence that particulate matter exposure can induce systemic oxidative stress in the body, leading to inflammation in various organ systems (Baulig et al., 2003; Donaldson et al., 2001; Strak et al., 2012). Oxidative stress occurs when there is an imbalance of reactive oxygen species (ROS) and antioxidant defenses. Various acellular assays exist to measure the ability of PM components to initiate and/or propagate redox reactions that catalytically generate ROS while simultaneously depleting antioxidants, otherwise known as the oxidative potential (OP) of PM, and may characterize biologically relevant components of $PM_{2.5}$ that can lead to oxidative stress. The dithiothreitol (DTT) assay is a commonly used acellular OP measurement technique, and multiple epidemiologic analyses have illustrated links between OP^{DTT} and acute cardiorespiratory endpoints, including asthma and wheezing attacks, congestive heart failure, ischemic heart disease, and microvascular function (Abrams et al., 2017; J. T. Bates et al., 2015; Yang et al., 2016;

Zhang et al., 2016). In a large fraction of those studies, OP^{DTT} was found to have a higher risk ratio than $PM_{2.5}$ mass in both one- and two-pollutant models, suggesting that the redox reactions that the OP^{DTT} assay captures are, at least partially, responsible for some of the observed PM-related health impacts. However, due to the constraints on current measurement technologies, epidemiologic research using OP^{DTT} measurements in the United States has been restricted to specific urban sites in California and Georgia (Abrams et al., 2017; Delfino et al., 2013; Zhang et al., 2016). Having a capability to estimate OP^{DTT} in locations where measurements are not available could provide valuable data for extensive epidemiologic analyses across larger study domains, offer insight into population exposures to OP^{DTT}, and guide decision-making on future locations of interest for OP^{DTT} measurements to better capture spatial variability.

A limited number of studies have attempted to estimate OP where and when measurements are not available. Land-use regression (LUR) modeling has been used in Europe to simulate OP using various assays, including OP^{DTT} (Jedynska et al., 2017; Yang et al., 2015). However, LUR models developed for one site may not be applicable to other locations. The objective of the current work is to develop a modeling approach more generally applicable to multiple locations at urban and regional scales and identify source impacts on OP. Previous studies have shown that emission source impacts can successfully be used as explanatory variables in regression analyses to estimate OP^{DTT} (J. T. Bates et al., 2015; Fang et al., 2016; Samuël et al., 2018). Multiple source apportionment techniques exist and have been used to investigate source impacts on OP^{DTT} in previous work, including the Chemical Mass Balance (CMB) method, single-particle mass spectrometry, and Positive Matrix Factorization (PMF), but these methods are limited to identifying

source impacts at one location (J. T. Bates et al., 2015; Charrier et al., 2015; Samuël et al., 2018; Verma et al., 2014). Here, a linear regression modeling approach is used with a photochemical air quality modeling approach for source impact analysis to estimate OP^{DTT} across a large spatial domain extending beyond the locations of limited observational data. Utilizing source impacts rather than individual species reduces the number of predictor variables and the challenge of collinearity between independent variables. Further, source impact analyses can provide useful information for regulatory initiatives along with elucidating the effects of bulk species, such as organic carbon (OC), on OP as their effects relate to different sources.

OP^{DTT} of water-soluble $PM_{2.5}$ was measured using a semi-automated instrument at four locations in the southeastern United States as part of the Southeastern Center for Air Pollution and Epidemiology (SCAPE) study (J. T. Bates et al., 2015). $PM_{2.5}$ source apportionment was performed during the same time period of the OP^{DTT} measurements across the eastern United States. Biases in source impacts were minimized using two data assimilation techniques (Y. Hu et al., 2014; C. E. Ivey, Holmes, Hu, Mulholland, & Russell, 2016). Linear regression analysis was used to relate these bias-corrected source impacts at the measurement sites to OP^{DTT} observations, and the final model was applied to source impact predictors across the entire modeling domain to estimate OP^{DTT} across the eastern United States. These results provide estimates of the large-scale spatiotemporal trends in OP^{DTT} and add to the growing knowledge on the relationships between emission sources and OP^{DTT}. Further, while the approach has been applied to OP^{DTT} measurements, other OP assay measurements (e.g., using ascorbic acid or electron spin resonance) could be used in a similar fashion.

4.2 Methods

4.2.1 Sample Collection and Analysis

OP^{DTT} measurements during SCAPE have been described in detail previously (J. T. Bates et al., 2015; Verma et al., 2014). Briefly, $PM_{2.5}$ was collected on pre-baked 8 x 10 in. quartz filters using non-denuded Thermo Anderson high-volume samplers at four locations in the southeastern United States, two urban [Atlanta, GA (ATL) and Birmingham, AL (BHM)] and two rural [Yorkville, GA (YRK) and Centerville, AL (CTR)] sites, all of which were part of the Southeastern Aerosol Research and Characterization Study (SEARCH) network sites (Hansen et al., 2003) (Figure B-1). Samples in ATL were taken daily from June 2012 through April 2013 from 12 pm (noon) to 11 am DST (23 h integrated samples) while a trailer was deployed with a high-volume sampler to the three other sites on a monthly basis: June 2012 and December 2012 at YRK and June 2013 to July 2013 at CTR and BHM (same collection hours). OP^{DTT} was analyzed using a semi-automated instrument based on the DTT assay protocol described in Cho et al. (2005) (J. T. Bates et al., 2015).

Total $PM_{2.5}$ concentration and speciated measurements, including 11 elements (Na, Al, Si, K, Ca, Ti, Mn, Fe, Cu, Zn, Pb) and five major components (OC, elemental carbon (EC), nitrate, ammonium, sulfate), were needed for the data assimilation techniques used for bias reduction in source apportionment analyses (described in detail later). These speciated measurements were obtained from the U.S. Environmental Protection Agency's Chemical Speciation Network (CSN) (142 sites) across the eastern United States and from

the SEARCH network at the OP^{DTT} measurement sites (4 sites) (Figure B-1). The methods for speciated analysis at CSN sites is detailed in Solomon et al., (2014), and speciated analysis techniques at SEARCH sites are described in detail in Hansen et al. (2003), Edgerton et al. (2005), and Hansen et al. (2006). Measurements were screened for validity using species specific detection limits (DL) and uncertainties.

4.2.2 $PM_{2.5}$ Source Impact Estimation

Source apportionment of $PM_{2.5}$ was performed using a hybrid chemical transport-receptor model approach with a secondary species bias correction algorithm to obtain best estimates with minimized biases (S. Hu et al., 2008; Y. Hu et al., 2014). First, $PM_{2.5}$ and relevant species (OC, EC, nitrate, ammonium, sulfate) were modeled using the Community Multiscale Air Quality model (CMAQ) version 5.0.2, and gridded sensitivities of those species to source-specific emissions were estimated using the direct-decoupled method (CMAQ-DDM) applied to three-dimensional air quality models and extended to include the capability to follow PM (Byun & Schere, 2006; Cohan, Hakami, Hu, & Russell, 2005; Dunker, 1981, 1984; Napelenok, Cohan, Hu, & Russell, 2006). Simulations were run with the CB05 chemical mechanism using a 12 km x 12 km resolution grid with 13 vertical layers of different thicknesses. The Weather Research Forecast (WRF) model version 3.6.1 was applied with 35 vertical layers to generate the necessary meteorological fields. Emissions were processed using the Sparse Matrix Operator Kernel for Emissions (SMOKE) version 3.6 with the 2011 National Emissions Inventory and grouped into 16 source-specific categories: agriculture (AG), aircraft (AC), biogenic (BI), coal (CL), dust (DU), fire (FI—including wildfire, prescribed burning, and agricultural burning), fuel oil (FO), metal processing (MT), natural gas combustion (NAT), non-road gasoline (NG),

non-road diesel (ND), on-road gasoline (OG), on-road diesel (OD), other (OT—any remaining unapportioned emissions), residential wood burning (WO), and seasalt (SS) (detailed description of each source in Table B-1)(CEP, 2003). These categories were grouped from previous work dividing SMOKE emissions into 33 source specific categories using SCC codes (Y. Hu et al., 2014). The final source impact estimates include primary and secondary $PM_{2.5}$ contributions by source. CMAQ-DDM was applied to a domain covering a majority of the eastern continental United States and parts of Canada during the OP^{DTT} measurement time period (June 2012 through July 2013) to estimate sensitivity of $PM_{2.5}$ and major components (OC, EC, nitrate, ammonium, sulfate) to each emission source. Source impacts on relevant metals (any metals measured at the OP^{DTT} sites, including: Na, Al, Si, K, Ca, Ti, Mn, Fe, Cu, Zn, Pb) were assessed by applying source-specific $PM_{2.5}$ composition profiles from SPECIATE to daily $PM_{2.5}$ source-specific impacts.

Biases in daily CMAQ-DDM source impacts were minimized using a hybrid chemical transport-receptor model approach (Y. Hu et al., 2014). Because emission source impacts are not measured directly, this technique utilizes a receptor model approach with CMAQ-DDM source impacts to minimize biases in primary species (relevant metals, EC, and primary OC). This method is described in detail in Hu et al. (2014) . Briefly, CMAQ-DDM estimates are designated as the "baseline" source impacts ($SA_{i,j}^{base}$) for species *i* and source *j*. These baseline estimates are inputs to the objective equation (4-1), along with speciated measurements (c_i^{obs}), simulated species concentrations from CMAQ (c_i^{sim}), and uncertainties of those two inputs ($\sigma_{c_i^{obs}}$ and $\sigma_{c_i^{sim}}$).

$$X^2 = \sum_{i=1}^{N} \left[\frac{\left[c_i^{obs} - c_i^{sim} - \sum_{j=1}^{J} SA_{i,j}^{base} (R_j - 1) \right]^2}{\sigma_{c_i^{obs}}^2 + \sigma_{c_i^{sim}}^2} \right] + \Gamma \sum_{j=1}^{J} \frac{ln(R_j)^2}{\sigma_{\ln(R_j)}^2} \quad (4\text{-}1)$$

The optimization equation is run for each day that measurements are available at each observational site in order to optimize R_j by minimizing the objective function X^2. R_j values are linear day-specific and site-specific adjustment factors for each source *j*. Adjustment calculations are constrained by the uncertainties of species observations, uncertainties in CMAQ modeled species concentrations, and uncertainties in source contribution due to emission errors expressed as the log of the estimated uncertainty ($\sigma_{c_i^{obs}}$, $\sigma_{c_i^{sim}}$, $and\ \sigma_{\ln(R_j)}$, respectively) so that source impact adjustments vary with uncertainty in species. In other words, the uncertainties weight the adjustment of source impacts so that components with larger uncertainties are weighted less, allowing more uncertain species and source impacts to vary more. R_j is also constrained between 0.1 and 10 due to the similarities between source categories leading to possible collinearities that could create unrealistic source impact adjustments. Γ is a term introduced to balance the two sides of equation (4-1). Nonlinear optimization using sequential quadratic programming is employed to minimize this objective function (Fletcher, 1987; Gill, Murray, & Wright, 1981).

In this work, R_j values were calculated for 146 measurement sites across 202 days with available speciated data for specific sites resulting in 12,211 data points with 17 species on which to perform the optimization. Voronoi tessellation was used to spatially interpolate these R_j values from the 146 speciated measurement sites to all 12km x 12km

CMAQ-DDM grids. R_j values were also linearly temporally interpolated across days without speciated measurement data when R_j could not be calculated. Final interpolated R_j values were applied to $SA_{i,j}^{base}$ at each 12km x 12km CMAQ-DDM grid to obtain daily primary adjusted source impacts and to reconstruct daily simulated species concentrations across the modeling domain using the following equations:

$$SA_{i,j}^{adj} = R_j * SA_{i,j}^{base} \quad (4\text{-}2)$$

$$c_i^{adj} = c_i^{sim} + \sum_{j=1}^{J} SA_{i,j}^{base} * \left(R_j - 1\right) \quad (4\text{-}3)$$

Secondary species, including ammonium, sulfate, nitrate, and secondary OC, can comprise a large fraction of $PM_{2.5}$ and have seasonal and spatial biases in CMAQ, so source impacts were further adjusted using a secondary species correction algorithm described in detail in Ivey, et al. (2016) . Briefly, this method reduces biases in the secondary species to zero at observation sites using a data assimilation technique that weights the differences between observations and simulated species by the magnitude of source impacts and distributes this weighted difference across source impacts. This secondary species correction method along with the hybrid chemical-transport receptor model achieve optimized estimates of CMAQ-DDM $PM_{2.5}$ source impacts across the eastern United States. Previous evaluation has shown that these methods greatly reduce biases in modeled species concentrations and result in source impacts that are in line to prior studies where measurements are available (Y. Hu et al., 2014; C. Ivey, Holmes, Hu, Mulholland, & Russell, 2014; C. E. Ivey et al., 2016). Normalized mean biases for bulk species (EC, OC, nitrate, ammonium, and sulfate) all fell to ≤ 27%. Certain trace metals (specifically titanium and calcium) were the most uncertain species due to emissions uncertainties

(Table B-2). For total $PM_{2.5}$, from which the source impacts used in OP^{DTT} regression development are derived [equation (4-4)], the normalized mean biases were -5.4% across the modeling domain and -1.5% at OP^{DTT} measurement sites during the study time period (Table B-2).

Table 4-1. Average source impact estimates on species in µg m^{-3} after applying primary and secondary corrections with spatial and temporal interpolation. Averages are available across the entire eastern United States modeling domain (Eastern US) and at locations of monitoring data that the regression was trained on (OP^{DTT} measurement sites).

	AC	AG	BI	CL	DU	FI	FO	MT	NAT	OG	NG	OD	ND	OT	SS	WO
Eastern US	0.02	0.35	0.35	0.86	0.35	0.74	0.55	0.07	0.34	0.39	0.17	0.29	0.38	0.83	0.08	0.30
OP^{DTT} measurement sties	0.04	0.21	0.30	1.2	0.34	0.49	0.68	0.37	0.41	0.75	0.18	0.60	0.54	1.33	0.09	0.22

***Abbreviations: Agriculture (AG), Aircraft (AC), Biogenic (BI), Coal (CL), Dust (DU), Fire (FI), Fuel Oil (FO), Metal Processing (MT), Natural Gas Combustion (NAT), Non-road Gasoline (NG), Non-road Diesel (ND), On-road Gasoline (OG), On-road Diesel (OD), Other (OT), Residential Wood Burning (WO), and Seasalt (SS)**

4.2.3 Regression Development

The impacts of specific emission sources on OP^{DTT} of $PM_{2.5}$ were estimated using multivariate linear regression analyses. The sixteen identified CMAQ-DDM source impacts at each OP^{DTT} measurement site were related to OP^{DTT} observations using methods similar to those developed in Bates, et al. (2015) but applied to multiple OP^{DTT} measurement sites and using more source impacts. Source-specific intrinsic OP^{DTT} were

assumed to be similar across measurement locations, and thus OP^{DTT} data from all four measurement sites were used in one regression. Doing so enabled sufficient data for regression training and ensured availability of sufficient OP^{DTT} measurements per season so that specific sources that were dominant during specific seasons (such as prescribed burning in the winter) were not missed. In model development, OP^{DTT} was the dependent variable and 16 CMAQ-DDM source impacts the independent variables. First, each source impact was included in the regression, resulting in an R^2 of 0.48 (adjusted R^2 of 0.43) (Table 4-2). Next, each source impact with a negative coefficient was removed from the regression as a negative association was assumed physically unreasonable because the DTT assay should only measure positive or null associations between $PM_{2.5}$ and OP^{DTT}. Then, backwards selection was used to remove source impacts that did not significantly impact OP^{DTT}. One by one, the source with the coefficient with the highest *p* value above the selection criteria (*p* value ≤ 0.05) was removed and the regression was re-run until all coefficients had a *p* value within the selection criteria. A tight selection criteria was used because the causal relationships between source impacts and OP^{DTT} were of more interest than prediction performance, though performance remained relatively high even with the strict selection criteria (adjusted R^2 of 0.35). Sensitivity analysis with a looser selection criteria was performed and is discussed in detail later. The final regression was applied to daily source impacts at a 12km x 12km resolution across the eastern United States to estimate spatiotemporal trends in OP^{DTT} across a wide study domain.

Table 4-2. Regression coefficients and standard errors for the regression with all source impacts included (ALL) and for the final regression with only source impacts that significantly impact OP^{DTT} (FINAL). All values [except the intercept (int) in (10^{-2}) $nmol_{DTT}$ min^{-1} m^{-3}] are in units (10^{-2}) $nmol_{DTT}$ min^{-1} μg_{source} for ease of comparison of standard errors to coefficients.

	Int (10^{-2})	**AC** (10^{-2})	**AG** (10^{-2})	**BI** (10^{-2})	**CL** (10^{-2})	**DU** (10^{-2})	**FI** (10^{-2})	**FO** (10^{-2})	**MT** (10^{-2})	**NAT** (10^{-2})	**OG** (10^{-2})	**NG** (10^{-2})	**OD** (10^{-2})	**ND** (10^{-2})	**OT** (10^{-2})	**SS** (10^{-2})	**WO** (10^{-2})
ALL *coefficient*	14.1	-113.1	-2.2	3.0	1.3	0.1	13.7	-1.1	2.8	7.3	2.1	30.8	5.6	-1.4	-0.1	-22.7	4.8
Standard error	2.9	24.0	3.7	2.1	1.7	1.4	2.1	1.7	2.4	2.8	0.8	9.7	3.7	4.4	1.5	24.7	2.9
FINAL *coefficient*	17.3	-	-	-	-	-	11.1	-	-	5.8	2.2	-	6.7	-	-	-	-
Standard error	1.7	-	-	-	-	-	1.9	-	-	2.3	0.8	-	2.4	-	-	-	-

***Int: intercept**

A comparison between regression results using CMAQ-DDM source impacts and previous results using CMB source impacts at the Atlanta measurement site was performed to evaluate the consistency of source impacts identified as significant to OP^{DTT} using various source apportionment techniques. To achieve this, the CMAQ-DDM source impacts were grouped into source impacts similar to those identified by CMB, including biomass burning ($BURN_{CMB}$), gasoline vehicles (GAS_{CMB}), and diesel vehicles ($DIES_{CMB}$). The CMAQ-DDM source impacts FI and WO were grouped into biomass burning ($BURN_{CMAQ}$), OG and NG into gasoline vehicles (GAS_{CMAQ}), and OD and ND into diesel vehicles ($DIES_{CMAQ}$), and the regression was re-run with these 3 source impacts along with the other CMAQ-DDM source impacts (AC, AG, BI, CL, DU, FO, MT, NAT, OT, and

SS) using the same methods described earlier for the measurement site in Atlanta, GA to enable direct comparison with the CMB results [equation (4-6)]. Results are discussed below.

4.3 Results and Discussion

4.3.1 Source Impacts on OP^{DTT}

First-level analysis on the relationship between OP^{DTT} and $PM_{2.5}$ source impacts used Pearson's linear correlation analyses (Table 4-3). OP^{DTT} shows the highest correlation with fire, natural gas combustion, and vehicle (OG, NG, OD, ND) source impacts. Previous work has reported on the correlations between these OP^{DTT} measurements and species (Abrams et al., 2017; J. T. Bates et al., 2015; Verma et al., 2014).

Table 4-3. Pearson's correlation coefficients between final adjusted source impacts and OP^{DTT} across all measurements sites.

	AC	AG	BI	CL	DU	FI	FO	MT	NAT	OG	NG	OD	ND	OT	SS	WO
OP^{DTT}	-0.05	0.19	-0.01	0.25	-0.06	0.44	0.08	0.00	0.39	0.34	0.26	0.40	0.39	0.15	0.24	0.17

A regression equation was developed using the methods described earlier to further investigate the relationship between source impacts and OP^{DTT} as well as to produce a model than can simulate OP^{DTT} across the entire study domain where measurements do not yet exist. The model was trained on a total of 187 OP^{DTT} data points [equation (4-4)]:

$$OP^{DTT} = 0.17 + 0.11*FI + 0.056*NAT + 0.022*OG + 0.067*OD \qquad (4\text{-}4)$$

This model has an R^2 of 0.36 (adjusted R^2 of 0.35) and a mean squared error of 0.011 $nmol_{DTT}$ min^{-1} m^{-3} (3.6% of mean of measurements) (Figure B-2). Cross-validation with 10% withholding was performed as an evaluation of the model robustness. The process of training the regression on a random sampling of 90% of the data was repeated 50 times, and the average mean-squared error over those iterations was found to be ~ 0.008 $nmol_{DTT}$ min^{-1} m^{-3} (2.6% of the mean of measurements). The R^2 compares well to previously reported LUR models in Europe that have a median R^2 of 0.33 across LUR models of different regions (Jedynska et al., 2017).

The large, non-zero intercept (accounting for roughly 56% of the OP^{DTT} across the modeling domain and during the modeling period) implies model misspecification. It is mostly likely due to uncertainties in measurements and source apportionment but may also be due to missing sources and filter artifact issues. The $PM_{2.5}$ samples used for OP^{DTT} analyses were collected without the use of a denuder, allowing semivolatile species to condense onto the filter, and semivolatile species have been shown to have significant impacts on OP^{DTT} (Biswas et al., 2009). The artifactual condensation of OP^{DTT}-active semivolatile organic species is not captured well by this CMAQ-DDM source apportionment method that uses data assimilation of OC measurements taken with a denuder. Along with the semivolatile species, an unspecified source, such as bioaerosols, which have recently been shown to impact OP^{DTT} (Samake et al., 2017), as well as the potential synergistic relationships between sources that are not captured using the multivariate linear modeling approach, may be responsible for part of the unnapportioned OP^{DTT} driving the intercept.

Multiple studies have shown results of the importance of gasoline and diesel vehicles and biomass burning to OP^{DTT} in the southeastern United States using various source apportionment methods, including PMF, CMB, and Aerosol Mass Spectrometry (AMS) measurements (J. T. Bates et al., 2015; Verma et al., 2014; Verma, Fang, et al., 2015). Equation (4-4) further supports this conclusion using CMAQ-DDM source apportionment. Natural gas combustion also has a substantial impact in equation (4-4), but little work has been performed investigating the OP of this source. Natural gas combustion, as modeled here, has very little primary $PM_{2.5}$ but leads to increased nitrate formation and the associated ammonium which have both been correlated with OP^{DTT} in Beijing, China (Liu, Zhang, et al., 2014). However, in the Indo-Gangetic Plain, ammonium, nitrate, and sulfate were negatively correlated with OP^{DTT} (Patel & Rastogi, 2018). Without more evidence, it is unknown at this time if the significant, positive relationship between CMAQ-DDM identified natural gas combustion and OP^{DTT} is due to a realistic causal link or if this source is a marker for secondary processes and/or season due to similar temporal trends between these two variables with higher values in the winter than summer.

A previous study showed success estimating OP^{DTT} in Atlanta, GA over a long time period using CMB source impacts, which was found to have a positive link with cardiorespiratory endpoints, so we compared the CMAQ-DDM regression technique to the CMB-derived regression to evaluate the consistency of results.

$$OP^{DTT} = 0.095 + 0.12 * GAS_{CMB} + 0.061 * DIES_{CMB} + 0.074 * BURN_{CMB} \quad (4\text{-}5)$$

R^2=0.49 (J. T. Bates et al., 2015)

$$OP^{DTT} = 0.12 + 0.023 * GAS_{CMAQ} + 0.063 * DIES_{CMAQ} + 0.12 * BURN_{CMAQ} \quad (4\text{-}6)$$

R^2=0.41

Each final regression resulted in the same significant source impacts with *p* values <0.05, suggesting consistency between methods. Equations (4-5) and (4-6) support the conclusion that fires and vehicle sources, specifically on-road diesel and on-road gasoline vehicles, significantly contribute to OP^{DTT} in Atlanta, GA, even when different source apportionment methods are used. The coefficient for diesel vehicles are remarkably similar between equations (4-5) and (4-6). The $BURN_{CMB}$ coefficient is roughly half the $BURN_{CMAQ}$ coefficient; however, the total magnitude of $BURN_{CMAQ}$ is roughly half the magnitude of $BURN_{CMB}$, so overall contribution of BURN to OP^{DTT} is consistent between the two models. The largest difference between equations (4-5) and (4-6) is the coefficients for gasoline vehicles. CMAQ-DDM captures the secondary formation of both OC and nitrate, leading to additional $PM_{2.5}$ mass from this source; so, GAS_{CMAQ} is, on average, roughly twice GAS_{CMB}. However, the coefficient for GAS_{CMAQ} is less than half of the coefficient for GAS_{CMB}, so the differences in GAS coefficients between equations (4-5) and (4-6) cannot be driven purely by differences in magnitudes of the source alone. The inconsistency between the two gasoline vehicle source coefficients could be driven by a difference in source apportionment formulations: CMAQ-DDM is based on sensitivity of $PM_{2.5}$ to 2011 source specific NEI emissions, and CMB is based on *a priori* source profiles developed using 2001 and 2002 measurement data, while recent measurements of more advanced technology vehicles show changes in those profiles. Nevertheless, the fact that the same emission sources were significant in both models after backward selection strongly supports that these sources are critical to OP^{DTT}. Further, the sources in the regressions are consistent with previous studies showing high source-specific OP^{DTT} for

biomass burning and vehicle sources (J. Bates, Fang, et al., 2018; Charrier et al., 2015; Velali et al., 2016; Verma et al., 2014; Verma, Fang, et al., 2015), further suggesting that the CMAQ-DDM source impact derived model [equation (4-4)] is capturing the correct sources relevant to OP^{DTT}.

4.3.2 Spatial Variation in Estimated OP^{DTT} across the Eastern United States

Equation (4-4) was applied to daily adjusted CMAQ-DDM source impacts across the eastern United States. Although measurements of OP^{DTT} were isolated to the southeastern United States, developing the spatial fields for the eastern United States assumes that the source specific intrinsic OP^{DTT} is applicable across the eastern United States. This is supported by studies in California, Japan, China, France, and Greece that have shown that vehicles and biomass burning contribute to OP^{DTT} with relatively similar OP^{DTT} levels (when comparably measured) (J. Bates, Fang, et al., 2018; Charrier et al., 2015; Fujitani et al., 2017; Y. Ma et al., 2017b; Samuël et al., 2018; Velali et al., 2016; Verma, Polidori, et al., 2009).

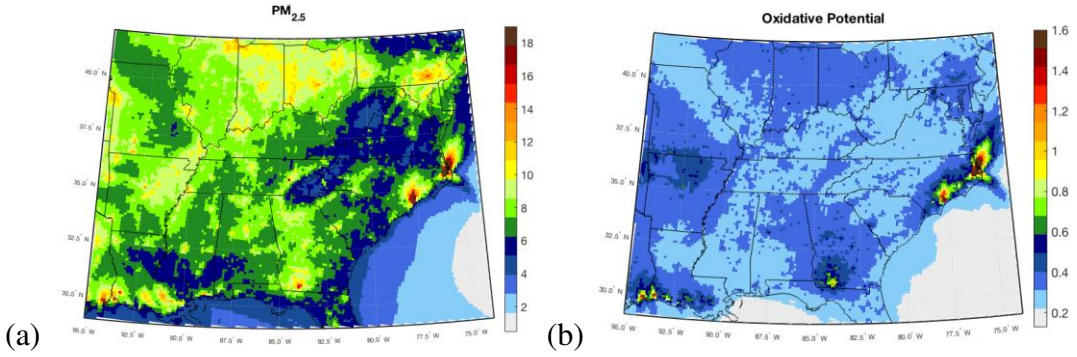

Figure 4-1. Average of (a) CMAQ-derived and bias corrected $PM_{2.5}$ in μg m^{-3} (average 6.3 μg m^{-3} with minimum 0.5 μg m^{-3} and maximum 131.7 μg m^{-3}) and (b) estimated OP^{DTT} in $nmol_{DTT}$ min^{-1} m^{-3} (average 0.30 $nmol_{DTT}$ min^{-1} m^{-3} with

minimum 0.13 $nmol_{DTT}$ min^{-1} m^{-3} and maximum 14.1 $nmol_{DTT}$ min^{-1} m^{-3}) from June 1, 2012 to July 30, 2013 across the eastern United States.

Although the $PM_{2.5}$ and OP^{DTT} spatial distributions have somewhat similar patterns, there are some key differences due to differences in source contributions. The spatial variation in water-soluble OP^{DTT} is mainly driven by fires (south Georgia, eastern North Carolina), which are the largest overall contributors to estimated OP^{DTT} during this time period due to their large concentrations and high coefficient in equation (4-4) (Figure 4-1). The large contribution of fires to overall OP^{DTT} across the eastern United States modeling domain is consistent with previous studies performed in Atlanta, GA finding prescribed burning to be a major factor of OP^{DTT} of ambient $PM_{2.5}$ (J. T. Bates et al., 2015; Verma et al., 2014). The high concentrations of fire-driven OP^{DTT} in south Georgia (Figure 4-2) is driven by a significant acreage of prescribed burning (1,412,869 acres were approved by permits to be burned in the southwestern corner of Georgia during the years 2012 and 2013, which represents ~50% of the total acreage allowed to be burned in Georgia during that time period, even though that area only represents 21% of the counties in Georgia). Other modeled fire hotspots, specifically in North Carolina and Texas, capture wildfires that occurred in these states in November 2012 and March through April 2013 (NOAA National Centers for Environmental Information, 2012). Because the $PM_{2.5}$ concentrations during these fires were so high, a spatial distribution of estimated OP^{DTT} driven by only natural gas combustion, on-road diesel, and on-road gasoline is presented (Figure B-3) to show patterns in estimated OP^{DTT} driven by sources with more consistent concentrations over time. Further, although the wildfires have been shown to create $PM_{2.5}$ with high OP^{DTT} (Verma, Polidori, et al., 2009), the largest $PM_{2.5}$ concentrations from fires were outside of the OP^{DTT} measurement locations and not captured by the OP^{DTT} observations that the

model [equation (4-4)] was trained on. The OP^{DTT} measurement sites have higher on-road vehicle source impacts and lower fire impacts, on average, than across the eastern United States (Table 4-1), so $PM_{2.5}$ composition of these sites may not be representative of locations with the highest OP^{DTT} (e.g. where wildfires occur). Most of the fire impacts captured at OP^{DTT} measurement sites are likely prescribed and residential burning or aged emissions from larger fires (Tian et al., 2009). Therefore, the very high OP^{DTT} estimates at wildfires is uncertain, and future OP^{DTT} measurements during wildfires would be useful to evaluate model results and the applicability of equation (4-4) to other locations in the study domain.

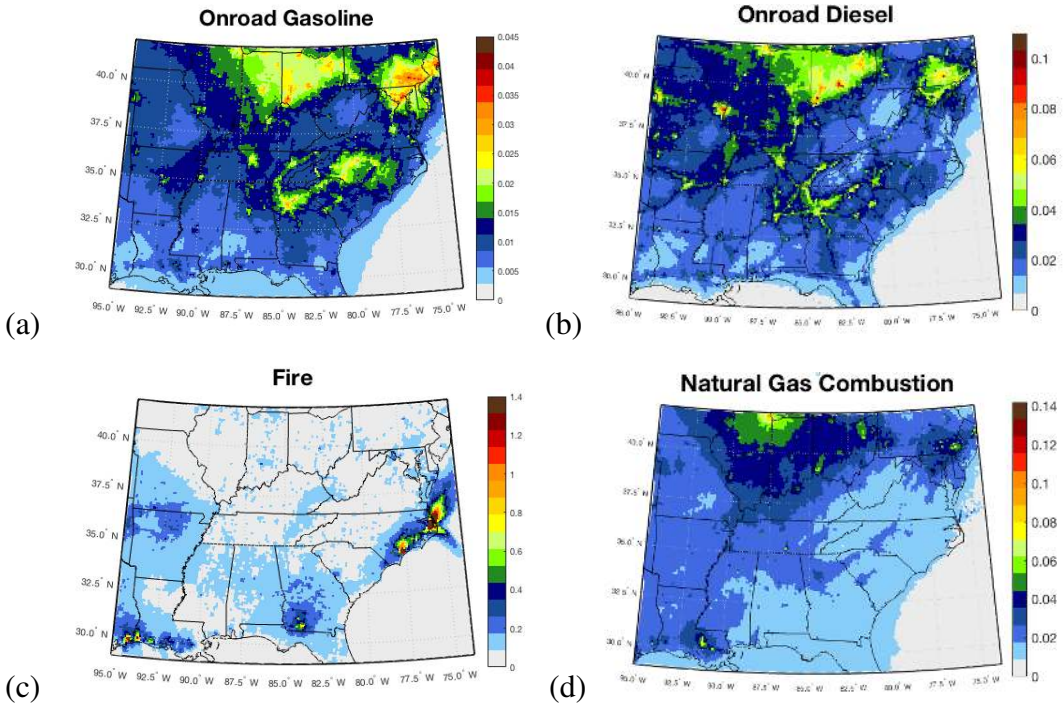

Figure 4-2. Specific source impacts on OP^{DTT} across the Eastern United States averaged from June 1, 2012 to July 30, 2013, including (a) on-road gasoline (b) on-road diesel (c) fires and (d) natural gas combustion. Note, the plots have different color scales so that spatial distributions are visible.

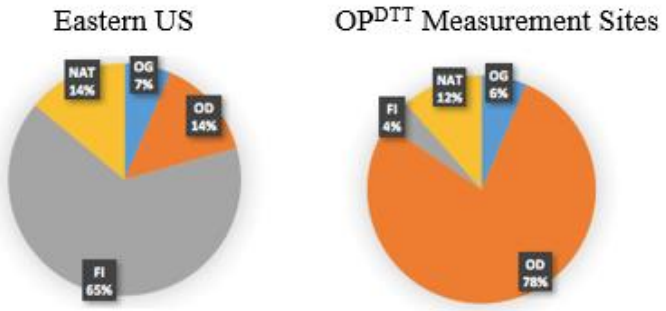

Figure 4-3. Estimated contribution of source impacts to apportioned OP^{DTT} averaged from June 1, 2012 through July 30, 2013.

On-road vehicle emissions concentrate OP^{DTT} in urban areas. The large contribution of diesel vehicles to OP^{DTT} at the measurement sites is most likely driven by the dominance of diesel vehicles in Atlanta, GA and Birmingham, AL (Figure 4-3).

Very limited OP^{DTT} measurements exist to evaluate modeling results outside of the Southeast. Two studies have reported volume-normalized OP^{DTT} in Illinois, specifically at the University of Illinois at Urbana-Champaign (Wang, Plewa, Mukherjee, & Verma, 2018; Xiong et al., 2017). ~25 samples were taken between June 2016 and June 2017 during different seasons, with OP^{DTT} measurements ranging between 0.1 and 0.2 nmol min^{-1} m^{-3}, which is in agreement with the combined diesel, gasoline, and fire impacts from the model-estimated OP^{DTT} in Illinois. Further, the average estimated OP^{DTT} at the CSN and SEARCH sites from June 2012 through July 2013 is 0.34 nmol min^{-1} m^{-3} with a range from 0.15 nmol min^{-1} m^{-3} to 1.4 nmol min^{-1} m^{-3}, which is in line with water-soluble OP^{DTT} measurements taken near CSN and SEARCH sites in Georgia (0.12—0.60 nmol min^{-1} m^{-3}) (Fang et al., 2016) and California (0.13—1.7 nmol min^{-1} m^{-3}) (Eiguren-Fernandez et al., 2010; Verma, Ning, et al., 2009).

4.3.3 Temporal Trends in Estimated OP^{DTT}

Temporal trends in estimated OP^{DTT} show large day to day variability, also seen in measurements (Figure 4-4, Figure B-4, Figure B-5). In Atlanta, GA, estimated OP^{DTT} has the highest monthly averages from November 2012 to March 2013 (excluding February) driven, in part, by prescribed burning. Previous studies have shown that OP^{DTT} in Atlanta, GA is driven by biomass burning with higher values in winter and spring, when prescribed burning is more frequent (and allowed in counties surrounding Atlanta), than in summer and fall (J. T. Bates et al., 2015). Further, the largest spikes in estimated OP^{DTT} in Atlanta, GA are driven by fires and occur during the prescribed burning legal period.

Temporal trends in OP^{DTT} across the eastern United States agree with the seasonal trends of measured and modeled OP^{DTT} in Atlanta, GA. OP^{DTT} values are, on average, highest in the winter months November 2012 through December 2012 and March 2013. The seasonal trend across the modeling domain is, again, driven by fire emissions due to their large contribution to OP^{DTT} during the study time period (Figure 4-4, Figure B-4, Figure B-5).

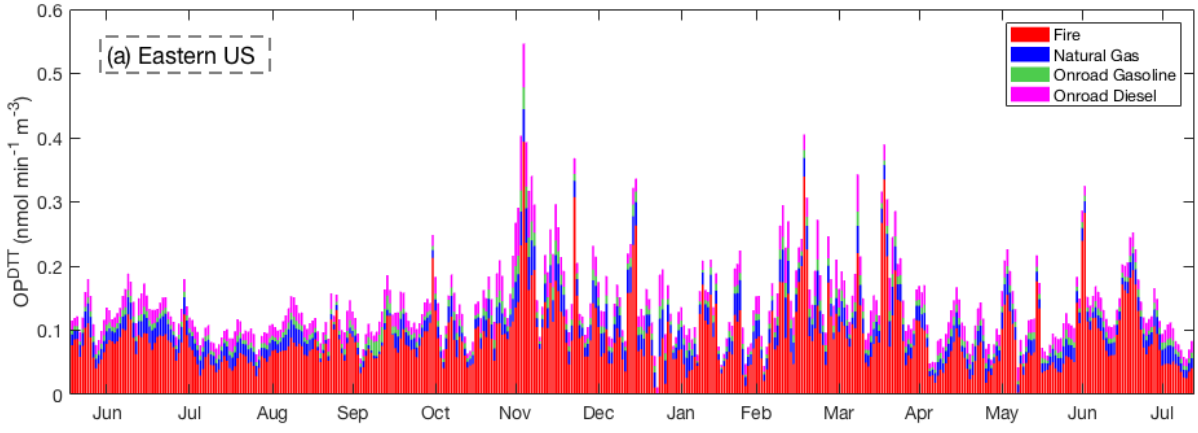

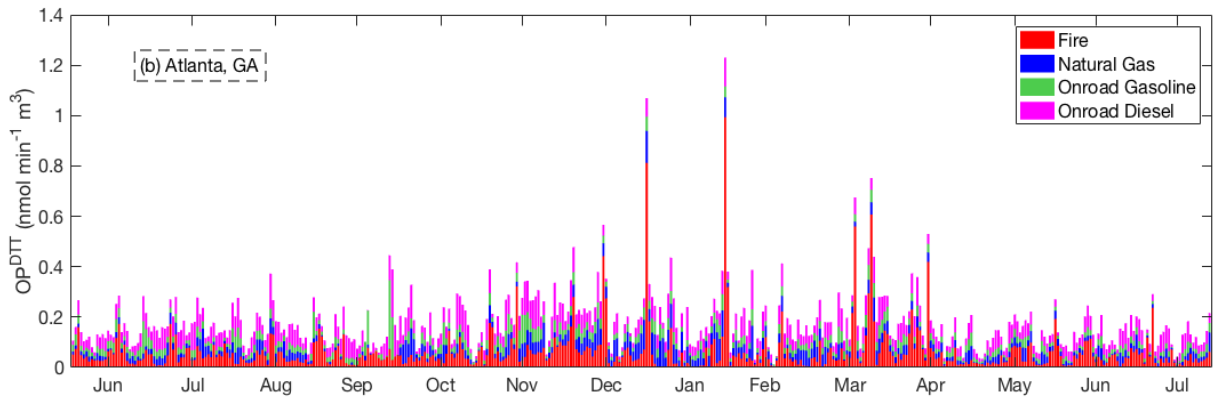

Figure 4-4. Daily source impacts on estimated OP^{DTT} across (a) all measurement sites (CSN and SEARCH sites across eastern United States) and at (b) OP^{DTT} measurement site in Atlanta, GA from June 1, 2012 through July 30, 2013.

4.3.4 Uncertainty Analysis in OP^{DTT} Regression

One limitation of using CMAQ-DDM source impacts in regression analyses is the possibility of correlation between source impacts. In this study, on-road diesel and non-road diesel were highly correlated (Pearson's linear correlation coefficient of 0.69) (

Table B-3). Therefore, due to the presence of covariance in these model parameters, a sensitivity analysis was performed by changing which source impacts were used as independent variables. After backwards selection, each excluded source was added back to the model [equation (4-4)] to develop twelve new regressions with five source impacts (fires, natural gas combustion, on-road diesel, on-road gasoline, and the added source). Coal combustion, residential wood burning, and biogenics each slightly increased the R^2 of the model compared to equation (4-4) and had positive coefficients with p values <0.11 (all other sources had p values > 0.15 or negative coefficients). Additionally, previous studies have shown causal relationships, either directly or indirectly, between OP^{DTT} and

byproducts of coal combustion, residential wood burning, and biogenic emissions, so additional models were developed using combinations of these three variables (J. T. Bates et al., 2015; Fang, Guo, et al., 2017; Samuël et al., 2018). When coal combustion and biogenics were included in the model either together or with all three variables (coal combustion, biogenics, and residential wood burning), neither source remained significant at a p value ≤ 0.10 level. When biogenics and residential wood burning were included (sensitivity model 1), both sources remained significant at a p value ≤ 0.10 level and the R^2 slightly increased to 0.38 (Table 4-4). When coal and residential wood burning were included (sensitivity model 2), again, both sources remained significant (at p value ≤ 0.05 level), while natural gas combustion lost significance (p value of 0.17), so NG was removed, resulting in an R^2 of 0.38 and the lowest intercept of any model (Table 4-4). The lower intercept implies that sensitivity model 2 captures more of the source impacts on water-soluble OP^{DTT}. Nevertheless, with the available OP^{DTT} measurement data, equation (4-4) was selected as the best model to be applied for spatial mapping of OP^{DTT} across the eastern United States because of the backwards selection process. The spatial distributions of OP^{DTT} estimated using equation (4-4) and each sensitivity model (Figure B-6) are highly correlated (Pearson's linear correlation coefficients; equation (4-4) & sensitivity model 1: 0.995, equation (4-4) & sensitivity model 2: 0.996, sensitivity model 1 & sensitivity model 2: 0.998).

Table 4-4. Regression coefficients and standard errors for sensitivity models 1 and 2 in the sensitivity analysis. All values are in units (10^{-2}) $nmol_{DTT}$ min^{-1} μg_{source} for ease of comparison of standard errors to coefficients.

	Int (10^{-2})	**BI** (10^{-2})	**CL** (10^{-2})	**FI** (10^{-2})	**NAT** (10^{-2})	**OG** (10^{-2})	**OD** (10^{-2})	**WO** (10^{-2})
Sensitivity Model 1 *coefficient*	14.9	3.9	-	11.4	5.6	2.3	6.4	5.4
Standard error	1.9	2.0	-	1.9	2.4	0.8	2.4	2.8
Sensitivity Model 2 *coefficient*	14.0	-	3.3	11.6	-	2.2	6.9	6.4
Standard error	2.1	-	1.3	1.9	-	0.8	2.3	2.6

Including coal and residential wood burning results in the model with the highest R^2 and lowest intercept, even though natural gas combustion was removed from the model, suggesting that the relationship between natural gas combustion and OP^{DTT} in equation (4-4) may be due to similar seasonal variations rather than a causal relationship. Further, coal combustion results in significant sulfate, which has been shown to reduce pH of aerosols significantly, thus mobilizing metals and having an indirect positive effect on OP^{DTT} (Fang, Guo, et al., 2017) while not having significant OP^{DTT} activity itself. Coal combustion also includes trace metals, such as selenium, that have unknown effects on OP^{DTT} due to lack of research. Future work could investigate whether the link between coal combustion and OP^{DTT} is direct, indirect, or both. Furthermore, when *p* value constraints are relaxed (*p* value ≤ 0.10 rather than ≤ 0.05), residential wood burning is included in both sensitivity analysis models. This source is a biomass burning source, similar to fires, which have been

shown to significantly impact OP^{DTT} (J. T. Bates et al., 2015; Y. Ma et al., 2017b; Samuël et al., 2018; Velali et al., 2016; Verma et al., 2014; Verma, Fang, et al., 2015). The difference in coefficients between residential wood burning and fires may be driven by different fuel types. Residential wood burning may produce lower OP^{DTT}, driving a lower and more uncertain coefficient, or the localized nature of the emissions may be difficult to capture in a chemical transport model with 12 km grids and a regression trained on limited measurement sites. The spatially heterogeneous nature of the wildfires in the CMAQ-DDM impacts also presents uncertainty in the spatial distribution estimates of OP^{DTT} as equation (4-4) was trained on different types of fire impacts (mostly prescribed burns) than those that occurred in Texas and North Carolina.

Because on-road and non-road diesel were so highly correlated, testing was done replacing one variable for another in equation (4-4) and observing the changes in the regression coefficient. When on-road diesel was replaced with non-road diesel in the regression, non-road diesel remained significant with a p value ≤ 0.05 (coefficient of 0.084 $nmol_{DTT}\ min^{-1}\ \mu g_{ND}$ with a standard error of 0.028 $nmol_{DTT}\ min^{-1}\ \mu g_{ND}$) and the R^2 of the model changed insignificantly (R^2 of 0.366 within nonroad-diesel versus R^2 of 0.362 on-road diesel). Therefore, the effects of on-road versus non-road diesel may not be able to be differentiated using this method. A sensitivity analysis was performed by combining on-road and non-road diesel together into one diesel source, but the total source was not as predictive as using either one of the individual sources. Further, when both on-road and non-road diesel were included in the model, neither had significant coefficients.

4.4 Conclusion

In this work, a first-principles, chemical transport model-based source apportionment modeling method is used to estimate OP^{DTT} of water-soluble $PM_{2.5}$ across a large spatial domain, integrating the limited measurements of OP^{DTT}. Vehicles, including gasoline and diesel vehicles, and fires are critical emission sources to OP^{DTT}. Further research needs to be conducted on the impact of natural gas combustion on OP^{DTT}, perhaps differentiating the effect of natural gas combustion, secondary processing, and season. The direct and indirect effects of coal combustion may also be of interest, as well as the differences between OP^{DTT} of residential wood burning and fire emissions. The prevalence of the major sources of OP^{DTT} suggest widespread population exposures, especially in urban cities and areas with significant biomass burning, to $PM_{2.5}$ components that can potentially cause oxidative stress and lead to adverse health effects.

The approach presented in this work can incorporate multiple OP^{DTT} measurement locations and times. The biggest limitation of this modeling method is limited OP^{DTT} data availability. Model results are limited by the data that the model was trained on and the source impacts that affected measurement locations. Future measurements, especially beyond the southeastern United States and within large wildfires, can be incorporated to improve the robustness of the regression and to further evaluate modeling results. OP measurements of fresh and aged $PM_{2.5}$ from wildfires is a future area of research of interest for health. Additional observations throughout the study domain could also be used to test the assumption that source-specific intrinsic OP^{DTT} is similar spatially and temporally and a regression trained on data in Georgia and Alabama can be applied to other states. Further, training the model on additional OP^{DTT} measurements closer to localized emissions, such

as residential wood burning and non-road diesel at construction sites, could help the regression differentiate impacts of sources. Future work could utilize measurements using other OP assays, such as the glutathione assay or total OP^{DTT} (including water-soluble and insoluble components) rather than water-soluble OP^{DTT}. Overall, the source apportionment modeling method can be used to estimate OP^{DTT} (or other OP measurement methods) across larger spatial and temporal domains, which may be useful for future epidemiologic studies investigating the association between OP and various health endpoints.

CHAPTER 5.

SPATIAL DOWNSCALING OF CMAQ $PM_{2.5}$ USING FINE-SCALE VEHICLE EMISSIONS AND CONCENTRATION DATA IN A STATISTICAL MODEL

Abstract

Epidemiologic studies investigating the link between air pollution and human health require spatially and temporally resolved air quality data with minimal biases. Specifically, studies interested in adverse effects of traffic exposure would benefit from air quality data that can accurately capture how air pollutant exposures vary with distance to roadways. Current monitoring data cannot capture steep spatial gradients in pollutant concentrations due to sparse availability. Chemical transport model estimates are often at too coarse of a grid resolution to simulate high concentrations near roadways (≤500m), and fine-scale emissions and dispersion model data do not capture regional emissions or photochemical reactions, a major source of secondary pollutants like $PM_{2.5}$. This work develops a spatial statistical downscaling model under a Bayesian hierarchical framework to simulate comprehensive $PM_{2.5}$ concentrations resulting from local and regional sources as well as secondary formation at geocoded locations for a birth cohort analysis in Atlanta, GA. A statistical approach is utilized for its computational efficiency, specificity in output location, and ability to estimate uncertainties. The model is trained on observational data sets from nine locations and uses CMAQ, link-based roadway emissions and/or RLINE dispersion model results, and meteorology as predictors. Results show that the spatial distribution of $PM_{2.5}$ estimates is heavily dependent on the choice of fine-scale data inputs

(emissions or RLINE) and number of observational data points in the model training data set. Further, daily CMAQ was found to provide sufficient spatiotemporal information, so using annual-average dispersion model results in the statistical downscaling model framework led to unphysical results. The high spatial correlation between the CMAQ and RLINE concentration fields led to a negative RLINE coefficient, driving concentrations on roadways lower than concentrations in rural areas. Overall, the presented statistical downscaling method provides a basis for future fine-scale spatial modeling work, but the temporal resolution of RLINE inputs needs to be improved before successful application.

5.1 Introduction

Air pollution exposure presents a serious risk to human health with links to adverse outcomes like cardiorespiratory morbidity and mortality, decreased cognitive abilities, and lower infant birth weight (Brunekreef & Holgate, 2002; H. H. Chang et al., 2012; Darrow et al., 2011; Delfino et al., 2005; Fonken et al., 2011; Pope et al., 2009). Particularly, the link between traffic emissions and deleterious health is of growing concern due to increasing urbanization (HEI Panel on the Health Effects of Traffic-Related Air Pollution, 2010). However, population-based health studies on vehicle emissions have been limited by the lack of a dense air pollutant ground monitoring network. Air quality observations are often not available daily and do not capture intraurban variability in heterogeneous pollutant concentrations, leading to exposure measurement error in populations living near roadways (Gryparis, Paciorek, Zeka, Schwartz, & Coull, 2009; S. E. Sarnat et al., 2010; Wilson, Kingham, Pearce, & Sturman, 2005). Air quality modeling can create spatially and temporally resolved concentration fields, providing estimated concentrations where and when measurements are not available. However, air quality model estimates are often at a

coarser grid resolution than the spatial resolution of health data used in epidemiologic studies or do not incorporate all emissions and chemistry necessary for predicting total pollutant concentration. For example, photochemical air quality models like CMAQ (Community Multiscale Air Quality model) incorporate local and regional emissions as well as secondary chemical formation but typically do not capture the steep spatial gradients in heterogeneous pollutants emitted from traffic due to their use of coarse grid resolutions (typically 4-36 km). Dispersion models and vehicle emission data can capture steep spatial gradients in pollutants emitted on roadways but often do not model chemistry or regional emissions. A spatial downscaling method linking fine scale dispersion model outputs or vehicle emissions to photochemical air quality model simulations that include local and regional emissions and chemistry for secondary formation could be used to improve exposure assessment for advanced, spatially resolved epidemiologic analyses. This method could incorporate the strengths of both dispersion and photochemical air quality models while minimizing their biases and limitations.

Multiple methods exist to improve spatial resolution of air quality model estimates by combining air quality model outputs, including coupled modeling, hybrid methods, and land-use regression techniques. Coarse-grid chemical-transport models, such as CMAQ and EMEP (European Monitoring and Evaluation Programme), with grid sizes ranging from 4km x 4km to 50 km x 50 km have been coupled with meteorological and dispersion models with fine grid scales, such as AERMOD (AMS/EPA Regulatory Model), HAPEM (Hazardous Air Pollutant Exposure Model), and ADMS (Atmospheric Dispersion Modeling System), to capture variability within chemical-transport model grid cells (Beevers et al., 2013; Isakov, Irwin, & Ching, 2007; Theobald, Simpson, & Vieno, 2016).

Hybrid methods add estimates of background pollution obtained from monitoring data or photochemical air quality models with zeroed out emissions to fine spatial resolution dispersion model data to estimate pollutant concentrations at scales as small as 100m x 100m (Arunachalam et al., 2014; Shih Ying Chang et al., 2017; Dionisio et al., 2013; Stein, Isakov, Godowitch, & Draxler, 2007). Land-use regression variable models incorporate landscape characteristics, such as elevation and distance to roadways, with data from monitors and air quality models of various grid sizes (Marshall, Nethery, & Brauer, 2008; Michanowicz et al., 2016). Statistical downscaling is computationally less expensive than other methods that directly model unobserved pollutant spatiotemporal concentration fields (Fuentes & Raftery, 2005; Paciorek, 2012). Further, statistical downscaling under a Bayesian hierarchical modeling framework treats the intercept and the slope between $PM_{2.5}$ observations and modeled concentrations as spatially and temporally correlated random effects, overcoming the challenge of spatial misalignment between the point-referenced monitoring measurements and gridded air quality modeling data. Because intercepts and slopes are modeled as smooth spatial surfaces, pollutant concentrations can be estimated at any point location within a grid cell, which is useful for epidemiologic studies with resident-specific data. Finally, the use of a unified Bayesian hierarchical framework ensures that uncertainties in parameter estimates are fully accounted for and allows uncertainty propagation in the form of prediction intervals and prediction standard deviations that can be readily used in health impact studies. This work describes the development and evaluation of a statistical downscaling model developed under a Bayesian hierarchical framework that downscales coarse-grid photochemical air quality model

estimates using fine-scale roadway emissions or modelled pollutant concentrations to provide air pollutant concentration estimates at geocoded locations.

Statistical downscaling has previously been used to calibrate daily $PM_{2.5}$ and ozone concentrations from CMAQ and has been applied to investigate inconsistencies between climate model outputs and observations (Berrocal, Craigmile, & Guttorp, 2012; Berrocal, Gelfand, & Holland, 2010a, 2010b). Here, an existing statistical downscaler formulated under a Bayesian hierarchical framework that originally was used to estimate surface $PM_{2.5}$ from satellite-derived aerosol optical depth (AOD) is modified to use CMAQ and dispersion model data or roadway emission data to simulate daily $PM_{2.5}$ estimates at resident homes, specifically homes near roadways as vehicle pollution is of interest to human health (H. H. Chang, Hu, & Liu, 2014). Fine particulate matter ($PM_{2.5}$) is the pollutant of interest in this work due to its significant association with adverse health impacts (Darrow et al., 2011; Franklin, Zeka, & Schwartz, 2007; Pope et al., 2009). The model application in this study uses gridded 12km CMAQ estimates rather than AOD data with 250m roadway pollution data as land-use variables. The model is trained on available monitoring data to predict daily concentrations during 2005 at geocoded locations across Atlanta, GA where health data for a birth cohort analysis is available. Sensitivities of the model to input parameters were tested by using both roadway emissions and dispersion modeled traffic impacts as inputs.

5.2 Method

5.2.1 Spatial Downscaler Development

The model used in this work is based on previous work by Chang, et al. (2014) calibrating AOD measurements with $PM_{2.5}$ ground level observations using a Bayesian hierarchal approach. In this study, gridded CMAQ estimates, rather than AOD, are downscaled using $PM_{2.5}$ observations. The spatial statistical downscaling model takes the form:

$$PM_{2.5}(x,t) = \alpha_o(x,t) + \alpha_1(x,t)CMAQ(x,t) + \varepsilon(x,t) \quad (5\text{-}1)$$

where $\alpha_o(x,t)$ and $\alpha_1(x,t)$ account for the additive bias (intercept) and multiplicative bias (slope), respectively, and $PM_{2.5}(x,t)$ denotes the 24 h averaged $PM_{2.5}$ concentration from an air quality ground monitor at location *x* and on day *t*. *x* is a point-referenced geo-location. The intercept and slope are treated as spatially and temporally correlated random effects and are assumed to be location and day-specific, allowing $\alpha_o(x,t)$ and $\alpha_1(x,t)$ to be estimated at locations and on days without $PM_{2.5}$ measurements via spatial-temporal interpolation. Residual errors represented by $\varepsilon(x,t)$ are assumed to be independently normal with mean zero.

The spatio-temporal regression coefficients are defined by the following two second-level linear regression models:

$$\alpha_o(x,t) = \beta_o(x) + \beta_o(t) + \gamma_o Z_o \quad (5\text{-}2)$$

$$\alpha_1(x,t) = \beta_1(x) + \beta_1(t) + \gamma_1 Z_1 \quad (5\text{-}3)$$

where $\beta_i(x)$ and $\beta_i(t)$ denote the unobserved correlated random effects that capture the spatial and temporal trends, respectively, in the intercepts (for *i*=0) and slopes (for *i*=1). The parameters γ_o and $\gamma_1$are fixed-effect regression coefficients associated with land use

variables (including roadway emissions or modeled vehicle pollutant concentrations) and meteorological variables Z_0 and Z_1, respectively. By substituting equations (5-2) and (5-3) into equation (5-1), the vector γ_1 can be interpreted as the interaction effects between CMAQ and covariates Z_1 on $PM_{2.5}$ concentrations. Spatial random effects $\beta_o(x)$ and $\beta_1(x)$ are determined using a tapered exponential covariance structure that depends on distance from monitor, and temporal random effects $\beta_o(t)$ and $\beta_1(t)$ are modeled using a first-order random walk (H. H. Chang et al., 2014).

Statistical inference is carried out under a Bayesian framework with prior distributions being assigned to all unknown parameters. Details on variance selection can be found in Chang, et al. (2014) . Estimation is carried out using a Markov Chain Monte Carlo (MCMC) techniques. 50,000 iterations were used in the MCMC method, with the first 25,000 samples being discarded as pre-convergence burn-in. 500 samples from the distributions of the coefficients are applied to inputs at all other desired locations, creating a distribution of results with means and standard errors of the estimates at each site. All analyses are carried out in R version 2.15.0 using an analytic code we developed.

In the application of the model to Atlanta, GA, meteorological data from WRF (Weather Researching Forecast model), including wind speed and temperature, are used in equation (5-2) to determine the slope in equation (5-1). Either vehicle emissions or roadway concentration data are used to determine the intercept in equation (5-1) using equation (5-3). Vehicle emissions are obtained from the Atlanta Regional Commission (ARC) while roadway primary $PM_{2.5}$ concentrations are modeled using the dispersion model RLINE (Research LINE model). CMAQ and RLINE concentrations are adjusted to minimize biases using observational data with previously evaluated methods in Friberg, et

al. (2016) and Zhai, et al. (2016), respectively. ARC emissions and RLINE concentrations are provided to the downscaler at a 250m resolution, allowing the statistical downscaling model to use these inputs to downscale 12 km CMAQ data.

5.2.2 Inputs for Atlanta Application

5.2.2.1 Monitoring Data

The regression coefficients for CMAQ are trained on daily or every 3-day 24 h averaged observational $PM_{2.5}$ data at monitoring locations. Nine monitor locations around the Atlanta area are used, eight urban sites and one rural site (Figure 5-1).

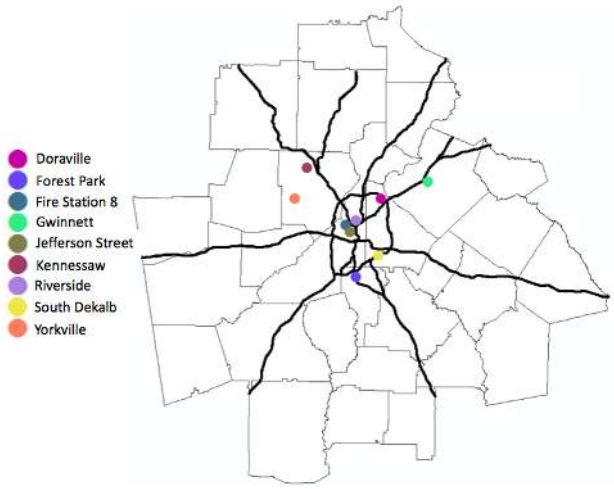

Figure 5-1. Locations of $PM_{2.5}$ monitors in Atlanta, GA used in this study. Observational data from these monitors are used in the statistical downscaling model training data set.

5.2.2.2 Meteorology

Daily meteorological data over the year 2005 are provided by the Weather Research and Forecasting Model (WRFv3.3.1, 13 vertical layers, Pleim-Xiu land surface model). Weather variables are included as spatial and temporal predictors in the multiplicative bias

terms [equations (5-3)]. Based on sensitivity analyses with various meteorological variables, wind speed and temperature were determined to be the most relevant meteorological variables to predicting $PM_{2.5}$ in this model, so only these variables are used in the application to Atlanta, GA.

5.2.2.3 CMAQ

CMAQ is a state-of-the-science Eulerian-grid regional chemical transport model (Byun & Schere, 2006). The use of CMAQ in the statistical downscaling model accounts for photochemical evolution of $PM_{2.5}$ as well as the impacts of regionally scaled sources. Daily $PM_{2.5}$ CMAQ results are obtained for the year 2005 at a 12km grid resolution from the Environmental Protection Agency's (EPA) PHASE CMAQ runs (CDC National Environmental Public Health Tracking Network, CMAQ v4.7, carbon bond mechanism CB05, 24 vertical layers, 2002 National Emissions Inventory (NEI) with the Sparse Operator Kernel Emissions (SMOKE), meteorology from WRF v3.3.1). The 12km CMAQ simulations had been previously blended with ambient ground observations to reduce bias using a method detailed in Friberg et al. (2016) . Briefly, the $PM_{2.5}$ spatiotemporal concentration dataset was built using weighted fields of (1) ratios of daily adjusted CMAQ result to annual mean observations and (2) a method obtaining temporal variance from observations and spatial structure from annual mean CMAQ values. The weight of the averages depends on distance to a monitor. This data fusion method and resulting CMAQ fields have been previously evaluated in Friberg et al. (2016) .

5.2.2.4 Fine-scale Vehicle Emissions and Concentrations

Fine-scale spatial distribution is defined by information from either ARC roadway emissions or EPA's RLINE vehicle pollutant concentration estimates. Roadway data was chosen in this application as an increasing number of environmental justice and epidemiologic studies, including birth cohort analyses, want pollutant concentration information near roadways for accurate exposure assessment. Each of these inputs are static variables representing an average day in 2010.

Hourly $PM_{2.5}$ emissions from vehicles are available for 43,712 individual highway links (e.g. sections of roadway) in Atlanta, GA based on ARC's 20-county activity-based travel demand model (D'Onofrio, 2016). These values are averaged over 24 hours and across the highway links, resulting in $PM_{2.5}$ data in g/m/day (assuming a representative weekday) (Figure 5-2). These values are then averaged over 250m grid cells for input into the statistical downscaling model. Emissions were developed using link-level information, including road type and location, traffic volume, and vehicle type and speed, with emission factors obtained from the Motor Vehicle Emission Simulator 2010b (MOVES20120b) (U. S. Environmental Protection Agency, 2012). More detail on Atlanta roadway emission development can be found in the Atlanta Roadside Emissions Exposure Study (D'Onofrio, 2016). $PM_{2.5}$ vehicle emissions are considered to have a lognormal distribution.

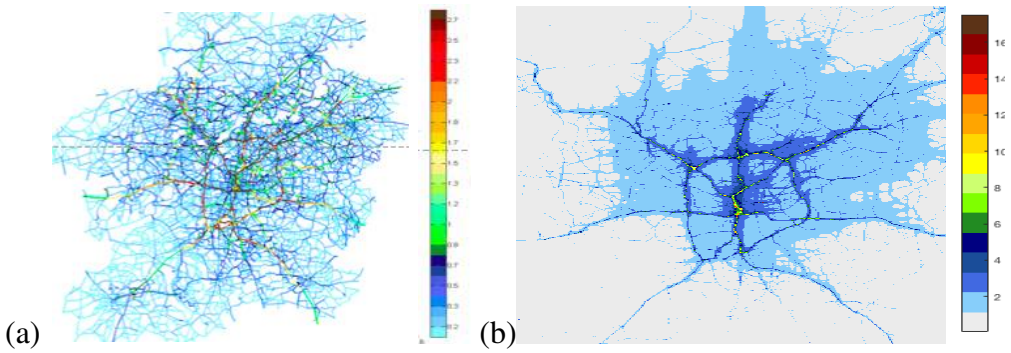

Figure 5-2. (a) Link-based $PM_{2.5}$ emissions in g/m/day for a representative day in 2010 obtained from ARC and (b) 2005 annual average RLINE $PM_{2.5}$ concentrations

Annual-average RLINE data used in this study is publicly available and the description of model specifications is available in Zhai, et al. (2016)(Figure 5-2). Briefly, RLINE was run with the 2010 ARC emissions previously described and hourly meteorology generated for the year 2005 using AERMET (Cimorelli et al., 2005; U.S. Environmental Protection Agency, 2004) and AERMINUTE (U.S. Environmental Protection Agency, 2015) with a modified version of the Stability ARray (STAR) method (U. S. Environmental Protection Agency, 1997) grouping meteorological variables into 78 categories that were then used to simulate annual average concentrations (S. Y. Chang et al., 2015; D'Onofrio, 2016; Zhai et al., 2016). $PM_{2.5}$ estimates from RLINE were calibrated using a linear regression of log-transformed RLINE with Chemical Mass Balance-Gas Constraint (CMB-GC) mobile source impact estimates derived using data from three monitor sites and *a priori* source profiles (Balachandran et al., 2012; Zhai et al., 2016). This calibration substantially reduced the normalized mean bias of the model results. Further description of RLINE calibration can be found in Zhai, et al. (2016) . Annual average RLINE results were used to provide the spatial pattern of mobile source impacts because results at finer temporal scales (e.g., hourly) were found to be biased during

periods with low dispersion. No major highways were opened or closed during this period, supporting the use of annual average 2010 emissions and RLINE concentrations to predict daily concentrations as each day should have similar spatial on-road emissions patterns.

5.3 Results

The statistical downscaling method [equation (5-1)] was applied to Atlanta, GA to obtain daily estimates of $PM_{2.5}$ during 2005 at geocoded locations where birth cohort data were available, resulting in 365 days with 25,289 estimates. The ability of the statistical downscaling model to simulate concentrations at specific locations reduces computational time by only producing results where necessary rather than at each grid cell in the study domain. The statistical downscaling model was run three times: once with ARC emissions as a land-use input in Z_0 (ARC), once with ARC emissions as a land-use input in Z_0 and less observational data used to train the coefficients (ARC - Obs), and once with RLINE concentration estimates a land-use inputs in Z_0 (RLINE). For the *ARC-Obs* model run, one in three day observations rather than daily data were used at a rural site (Yorkville, GA) over a period of four months, simulating what might be available at other measurement locations. These three model runs were used to test sensitivities of the statistical downscaling model to land-use inputs and the size of the observational training data set, i.e. the number of available observations. Each run used the meteorological variables wind speed and temperature from WRF and daily 12km CMAQ data as inputs.

For each model run, $PM_{2.5}$ concentration was found to be negatively associated with wind speed as advection removes particulate pollution from the area (Table 5-1). However, $PM_{2.5}$ was positively associated with CMAQ estimates, ARC emissions, and temperature.

Interestingly, the coefficient for RLINE was negative, suggesting a possible correlation between RLINE and CMAQ as both provide spatial information about pollutant concentration and may counter balance each other. The high coefficient for temperature was most likely driven by increased photochemistry in the summer, leading to an increase in secondary $PM_{2.5}$ formation most often in the form of ammonium sulfate.

Table 5-1. Beta coefficients for spatial and temporal predictors with standard errors in parentheses. Each coefficient applies for one interquartile range increase in each predictor variable.

	Intercept	CMAQ	ARC or RLINE	Temperature	Wind Speed
ARC - obs	-49.93 (±15.4)	4.33 (± 1.81)	1.17 (± 0.72)	3.06 (± 0.76)	-1.09 (± 0.24)
ARC	-50.02 (±14.9)	3.46 (± 1.81)	0.45 (± 0.66)	2.93 (± 0.69)	-1.25 (± 0.23)
RLINE	-48.40 (±16.1)	4.70 (± 2.00)	-0.45 (± 0.49)	2.92 (± 0.75)	-1.25 (± 0.23)

Furthermore, *p* values of all coefficients except those for ARC and RLINE (and CMAQ used in the ARC model run) are less than 0.05. Large *p* values for ARC and RLINE coefficients imply uncertainty in these coefficients and that the information that might be provided by the roadway emissions or RLINE is provided by other inputs, e.g., CMAQ, that also use roadway emissions for modeling $PM_{2.5}$ concentrations. However, including ARC or RLINE as land-use variables in the regression seem to improve model performance as root mean squared error is reduced (Table 5-2).

Table 5-2. Root mean squared error of CMAQ results, the *ARC* model run, and the *RLINE* model run averaged over all sites over the entire study period.

	CMAQ	ARC	RLINE
RMSE	6.40	2.68	2.32

The resulting estimates using different land-use variables have significantly different annual means and standard deviations averaged over the estimated 25,289 points (Table 5-3). These large differences in mean concentration and standard deviations are driven by the coefficients for CMAQ and the land-use variables ARC or RLINE, as the intercept and coefficients for other variables do not change greatly with varying inputs (Table 5-1). Further, there is a lack of correlation between the model runs with different land-use inputs (ARC or RLINE) (Table 5-3), suggesting the fine-scale data used in the model can significantly impact results.

Table 5-3. Evaluation statistics for the three model runs with different inputs and/or training data sets. Statistics are calculated using annual averages at each estimated location (25,289 points).

					Spearman Spatial Correlation Coefficients		
	Mean (SD)	**Median**	**Min**	**Max**	ARC	ARC - Obs	RLINE
ARC	15.68 (0.56)	15.66	12.97	17.37	1	0.83	0.28
ARC - Obs	17.73 (3.00)	16.27	9.32	26.98	0.83	1	0.25
RLINE	16.84 (0.95)	16.59	13.52	21.29	0.28	0.25	1

As with the means and standard deviations, the annually-averaged spatial distributions of $PM_{2.5}$ concentrations differ greatly between model runs (*ARC, ARC-Obs, RLINE)*. The spatial plots for the *ARC* and *ARC-Obs* model runs illustrate that the final estimates are heavily dependent on the number and values of observations (Figure 5-3). With very limited observational data that is highly concentrated in urban regions, the statistical downscaling model is sensitive to any changes in monitor inputs, especially in rural areas with fewer monitors.

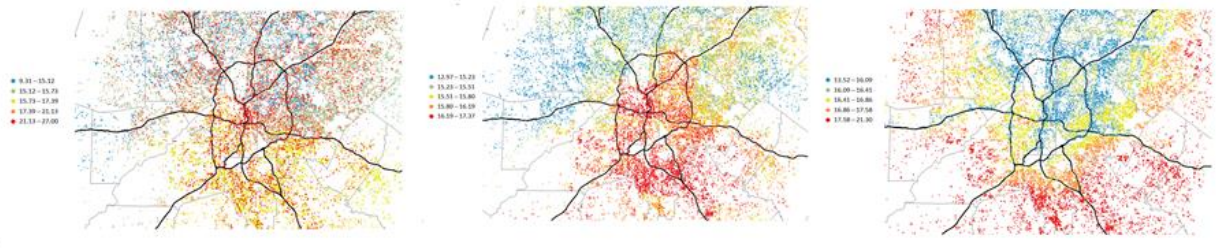

Figure 5-3. 2005 annual-average $PM_{2.5}$ concentration fields estimated by the statistical downscaler at the 25,289 grids in Atlanta, GA. The results include the *ARC-Obs* model run (left), the *ARC* model run (middle), and the *RLINE* model run (right). Higher concentrations are in red and lower concentrations are in blue.

Further, the spatial distribution of the concentration estimates for the RLINE run are unphysical (Figure 5-3). Lower concentrations of $PM_{2.5}$ are located on and near the highways, while higher concentrations are located in rural areas. This phenomenon results from the negative coefficient for RLINE (Table 5-1). CMAQ captures the spatial and temporal $PM_{2.5}$ trend well enough that RLINE, which only provides spatial information, does not provide additional information to the model. In other words, the statistical downscaling model relies most heavily on CMAQ while RLINE results are non-informative. Also, the RMSE of the statistical downscaling model with just CMAQ is significant and positive (Table 5-2), so including a correlated variable with a negative

coefficient would reduce the error. Even though the results of the RLINE model run perform well at the observational sites with lower RMSE than CMAQ (Table 5-2), it does not accurately predict concentrations at other locations due to the negative RLINE coefficient.

5.4 Discussion and Conclusions

The statistical downscaling method proved to be an efficient way to use CMAQ data in order to estimate $PM_{2.5}$ concentrations at specific geocoded locations. However, the results are highly sensitive to the size of the observational training data set and the land use variables used. The estimate for each geocoded location is based on one regression model that is trained on relatively few data points; therefore, these data points have to accurately represent the spatial distribution of the study area and downscaling results are sensitive to any changes. Additional measurements that better capture the spatial variation in $PM_{2.5}$ across the study domain, such as more observations in rural areas or near roadways, would be helpful.

Furthermore, though the statistical downscaling approach proved effective with ARC emissions as land use variables, the results were unphysical when using RLINE concentrations as a land use variable with lower $PM_{2.5}$ concentrations on the roadways than in rural areas. This phenomenon is driven by the negative RLINE coefficient in the model due to correlations between CMAQ and RLINE. Both CMAQ and RLINE data sets had previously been adjusted and calibrated using observations in the study area using methods described in Friberg, et al. (2016) and Zhai et al. (2016), respectively. Therefore, the statistical downscaling model may not have been able to differentiate the observation-

calibrated inputs with the observational training data set. Further, CMAQ and RLINE were correlated at the monitoring stations, and the the daily, observation-corrected CMAQ captured the spatio-temporal variability in $PM_{2.5}$ well enough that including annual-average, observation-calibrated RLINE as a land-use variable did not add additional information. Because CMAQ provided temporal information as well as spatial information, the model relied more heavily on CMAQ than the temporally static RLINE input, as shown by the higher coefficient (Table 5-1), which, along with the correlation between CMAQ and RLINE, led to a negative RLINE coefficient. Perhaps if RLINE was run on a daily basis, the model would perform better. Future work is needed to investigate the use of CMAQ and RLINE inputs that have not been calibrated with observations, using additional monitoring stations in the model training data set that were not used to calibrate CMAQ or RLINE, and/or using daily RLINE data. Overall, these results suggest that the statistical downscaling model approach would benefit from additional work improving temporal resolution of RLINE and obtaining more measurements for the observational training data set before RLINE and CMAQ are used together to predict pollutant concentrations at geocoded locations for health studies.

CHAPTER 6.

APPLICATION AND EVALUATION OF TWO MODEL FUSION APPROACHES TO OBTAIN AMBIENT AIR POLLUTANT CONCENTRATIONS AT A FINE SPATIAL RESOLUTION (250M) IN ATLANTA

Abstract

Epidemiologic studies rely on accurately characterizing spatiotemporal variation in air pollutant concentrations. This work presents two model fusion approaches that use publicly available chemical transport simulations, dispersion model simulations, and observations to estimate air pollutant concentrations at a neighborhood-level spatial resolution while incorporating comprehensive chemistry and emissions sources. The first method is additive and the alternative method is multiplicative. These approaches are applied to Atlanta, GA at a 250m grid resolution to obtain daily 24 h averaged $PM_{2.5}$ and 1 h max CO and NOx concentrations during the years 2003 through 2008 for use in health studies. The modeled concentrations provide comprehensive estimates with steep spatial gradients near roadways, secondary formation and loss, and effects of regional sources that can influence daily variation in ambient pollutant concentrations. Results show high temporal and spatial correlation and low biases across monitors, providing accurate pollutant concentration estimates for epidemiologic analyses.

6.1 Introduction

Air pollution has been linked to adverse health effects, including cardiorespiratory morbidity and mortality (Brunekreef & Holgate, 2002; Delfino et al., 2005; Pope et al., 2009) and adverse birth outcomes (H. H. Chang et al., 2012; Darrow et al., 2011). A limitation of many population-based health studies is the inability to estimate steep spatial gradients in intraurban pollutant exposures driven by local emission sources, like vehicle traffic on roadways. Simulation studies show that an inability to accurately capture spatial variability in heterogeneous pollutants can bias risk ratio estimates in epidemiologic studies (Goldman et al., 2011), and errors in exposure misclassification due to spatial variability assumptions are especially important for epidemiologic studies of long-term pollutant exposures (Wilson et al., 2005).

Reliance on air quality observational data for exposure analyses can introduce exposure measurement error because the lack of a dense monitoring network can result in unobserved spatial variation in pollutant concentrations (Gryparis et al., 2009; S. E. Sarnat et al., 2010; Wilson et al., 2005). Air quality modeling addresses this problem by creating spatially and temporally resolved concentration fields constructed from simulating emissions, chemistry, physics, and meteorology impacting pollutants. However, specific model results are often limited by either spatial resolution or an inability to capture complex chemistry and a vast array of emissions sources. Two types of emissions-based models are commonly used: chemical transport models and dispersion models (e.g., Gaussian plume and variants). Eulerian grid-based chemical transport models simulate the transport and chemical transformation of pollutants emitted from thousands of emissions sources over a large spatial domain. However, because all emissions are evenly distributed within one computational grid (often 36km^2 but seldom below 1km^2), these models do not

simulate local effects of individual sources and, thus, can miss steep spatial gradients that occur on scales < 1km. An example of a local source that can drive steep spatial gradients in pollutants is vehicles on roadways (Weijers, Khlystov, Kos, & Erisman, 2004). 59.5 million people lived within 500m of heavily trafficked roads in 2010, and $PM_{2.5}$ mass and component concentrations can double close to road sources (Beevers et al., 2013; Rowangould, 2013; Zhu, Hinds, Kim, & Sioutas, 2002). These high concentrations on roadways are not discernable using low resolution grids, leading to the need for additional exposure assessment methods to accurately characterize pollutant gradients in urban areas. Dispersion models can capture these gradients by using plume, puff, or particle representations but often do not take into account regional emissions or non-linear chemical reactions that contribute to the formation of major pollutants, like fine particulate matter ($PM_{2.5}$). They are also not used to derive daily estimates over large spatial domains (1000s of km's) due to model parameter limitations. Additionally, all types of models are subject to biases from model parameters and inputs. Therefore, neither chemical transport models nor dispersion models alone can estimate temporally and spatially resolved air pollutant concentration fields with comprehensive emission precursor information and chemistry. Reducing exposure misclassification by improving spatial and temporal resolution of air pollutant concentration estimates, reducing model biases, including emissions from all sources, and simulating chemistry in best-estimate simulations of concentrations is critical to minimizing error in epidemiologic studies.

Different methods have been utilized to reduce error and improve spatial resolution of air pollutant concentration estimates at unmonitored locations while maintaining chemistry and regional emission impacts. Land-use regression (LUR) variable models have

proven effective tools for fine-scale modeling by incorporating landscape characteristics, such as elevation and distance to roadway, with data from monitors and/or dispersion models (Marshall et al., 2008; Michanowicz et al., 2016). However, LUR models are specific to one study area with particular land-use characteristics. Other modeling approaches utilize various techniques to combine observations and/or different model outputs to represent intraurban air pollution. One method uses linear combinations of wavelet basis functions to blend data from monitors, the photochemical model CMAQ (Community Multiscale Air Quality model) (Byun & Schere, 2006), and the plume dispersion model AERMOD (AMS/EPA Regulatory Model) (Cimorelli et al., 2005; Crooks & Isakov, 2013) while another method nests the local dispersion model ADMS-Urban (McHugh, Carruthers, & Edmunds, 1997) in the regional photochemical model CAMx (Comprehensive Air Quality Model with Extensions) (ENVIRON International Corporation, 2014; Stocker, Hood, Carruthers, Seaton, & Jockel, 2014). "Hybrid" methods add fine-scale dispersion model outputs to broader-scale estimates of pollutant concentrations, often referred to as background concentrations. Previous hybrid studies have used observations from central monitoring stations after subtracting out concentrations due to local emissions for estimates of urban background (Stein et al., 2007). Other work utilized chemical transport models, like CMAQ, run without local emissions to determine urban background (Dionisio et al., 2013; Stein et al., 2007). An advanced method for calculating urban background was developed using space-time ordinary kriging to combine monitoring data, CMAQ, and CMAQ with zeroed out emissions (Arunachalam et al., 2014). These background estimates are added to model outputs from dispersion models like AERMOD and RLINE (Research LINE model)

(Snyder et al., 2013) and/or Lagrangian models like HYSPLIT (Hybrid Single Particle Lagrangian Integrated Trajectory model) that characterize primary concentrations from stationary and roadway sources (S. Y. Chang et al., 2017; Dionisio et al., 2013; Stein et al., 2007). Care must be taken with these hybrid methods to prevent double-counting of emissions in the dispersion models and background calculations. Here, methods are developed for fusing multi-model and observational data to estimate total pollutant concentrations from local and regional sources at a fine spatial resolution without needing to estimate the urban background *a priori* with a separate chemical transport model run without direct emissions of the pollutants of interest. Removing the need to simulate background concentrations using multiple photochemical air quality model runs and instead calculating urban background empirically can save computational time and prevent the methods from missing the chemistry and secondary formation or loss associated with local sources that chemical transport models cannot simulate if those emissions are zeroed out. We present the development of two novel, computationally efficient model fusion approaches to estimate air pollutant concentrations at a fine spatial resolution with comprehensive emissions and chemistry and their applications to the Atlanta, GA region.

Each model fusion method developed in this work uses mathematical combinations of outputs from a chemical transport model that provides chemistry and local and regional emission sources and a dispersion model that provides fine spatial resolution simulations of inert pollutants from a local source, along with limited observations as available. One method is an additive approach and the other is a multiplicative approach. Both methods are applied to Atlanta, GA using simulations from the chemical transport model CMAQ and RLINE. RLINE is a steady-state dispersion model that simulates near surface releases

of primary and chemically inert pollutants from line-sources, like vehicles on roadways (Snyder et al., 2013), and with 1.6 billion vehicles worldwide, the association between mobile source emissions and disease development is of particular concern (HEI Panel on the Health Effects of Traffic-Related Air Pollution, 2010). Emissions from road transportation are estimated to be the largest source contribution to premature deaths due to $PM_{2.5}$ pollution in the United States (Caiazzo, Ashok, Waitz, Yim, & Barrett, 2013), and previous studies have shown that resolving steep spatial gradients in pollutant concentration near roadways is beneficial to epidemiologic studies (S. Y. Chang et al., 2017). Results of the model fusion applications include a time series of daily concentration estimates of 1 h maximum carbon dioxide (CO) and nitrogen oxides ($NO + NO_2 = NOx$) and 24 h $PM_{2.5}$ at a 250m grid resolution across Atlanta, GA during the years 2003 through 2008. Although the applications of these methods focus on vehicles as local sources, the methods can be extended to other local, non-roadway facilities. Overall, the inclusion of comprehensive regional and local sources and chemistry with fine-scale spatial gradients can provide comprehensive estimates of pollutant concentrations, reducing biases in exposure estimates used for epidemiologic analyses. Results are currently being used in spatiotemporal epidemiologic analyses of birth outcomes associated with air pollution and city planning and environmental justice studies investigating the relationships between air pollution, health, socio-economic factors, and infrastructure characteristics (Davis et al., 2017).

6.2 Methods

This work describes the development of two novel methods that fuse data from multiple models and observations to create comprehensive estimates of air pollutant

concentrations at a fine spatial resolution. The two model fusion approaches combine results from a chemical transport model (CTM) and dispersion model (DISP) to obtain pollutant concentration estimates. The model fusion approaches are applicable to pollutants whose small scale spatial variation is captured by the dispersion model.

Although these model fusion methods could theoretically simulate many types of pollutants using inputs from different types of models, the specific applications of these methods presented in this paper fuse annual-average outputs from the local-scale dispersion model RLINE (250m resolution) and daily simulations from the regional-scale CMAQ model (12km resolution) (Byun & Schere, 2006) to estimate daily 24 h averaged $PM_{2.5}$ and 1 h maximum NO_x and CO concentrations at a 250m field resolution over Atlanta, GA from 2003 through 2008. CMAQ results are used as the CTM inputs because CMAQ is a state-of-the-science Eulerian-grid chemical transport model. RLINE is chosen as the dispersion model because roadway pollution is of interest to the epidemiologic analyses utilizing the results of this work and RLINE is a newly developed and well evaluated line-source model built to handle link-based emissions for roadways. Due to the presence of biases in both models, CMAQ and RLINE results were adjusted using observations and data fusion methods *a priori*, before model estimates were fused together (Friberg et al., 2016; Zhai et al., 2016). Such biases are present in the raw air quality model results due to model formulation (e.g., RLINE is subject to high biases under low dispersion conditions (Zhai et al., 2016), while CMAQ biases exist due to errors in numerical dispersion (Byun & Schere, 2006) and model inputs, like emissions data and meteorological fields). Both the data-fused CMAQ and observation-calibrated RLINE results for the pollutants of interest during the years 2003 through 2008 are publicly available and have been evaluated in

previous work (Friberg et al., 2016; Zhai et al., 2016). Although use of pre-calibrated CTM and DISP results is viewed as preferable due to biases in each individual model, it is not a prerequisite for the applications of these model fusion methods. Furthermore, while mobile sources are responsible for a majority of the urban-area emissions of NOx and CO, they have a smaller contribution to $PM_{2.5}$ concentrations in the area, which, along with high biases on and near roadways in RLINE results for NOx and CO, led to the development of slightly different model fusion approaches. One method uses an additive approach and is applied to provide daily concentration fields of particulate matter ($PM_{2.5}$), which includes substantial secondary source contributions that are relatively spatially homogeneous. The second method uses a multiplicative approach and is applied to estimate spatiotemporal fields of the gaseous pollutants CO and NOx which have steep concentration gradients near roadways. Both approaches were tested with all three pollutants as a sensitivity analysis (Table C-2).

6.2.1 Model Fusion Methods

6.2.1.1 Additive Method for Fine Particulate Matter ($PM_{2.5}$)

The first step in the additive model fusion method is to remove primary roadway $PM_{2.5}$ from the CTM estimates to avoid double counting of roadway emissions included in both the CTM and DISP outputs. To achieve this, the fine-scale DISP values are averaged into the coarser grid resolution matching the CTM computational grid (for clarity, the averaged DISP values at the coarser resolution will be referred to as $\overline{DISP}_{\text{coarse}}$). $\overline{DISP}_{\text{coarse}}$ $PM_{2.5}$ values, which represent primary roadway $PM_{2.5}$ concentrations, are subtracted from the CTM estimates, leaving an estimate of urban background (as defined as all secondarily

formed $PM_{2.5}$ and primary $PM_{2.5}$ from all sources excluding vehicles) at the CTM grid resolution. Next, results of this subtraction, i.e. the urban background at the coarse CTM resolution, are smoothed to the fine-scale grid resolution matching the DISP spatial resolution using a triangulation-based linear interpolation. These smoothed results represent urban background at a fine spatial resolution. Finally, because dispersion processes are linear, the initial DISP estimates are added to the interpolated urban background at each matching grid location, adding primary roadway $PM_{2.5}$ back into the estimates and producing the final pollutant concentration approximations at the same spatial resolution of the dispersion model [equation (6-1)].

$$PM_{2.5} = \left[(CTM - \overline{DISP}_{coarse})_{interpolated}\right] + DISP \qquad (6\text{-}1)$$

In equation (6-1), $PM_{2.5}$ is the $PM_{2.5}$ concentration estimates at the desired fine spatial resolution resulting from the model fusion method (which is the same resolution as the dispersion model), CTM is the chemical transport model $PM_{2.5}$ estimates, $\overline{DISP}_{\text{coarse}}$ is the DISP estimates averaged to match the grid resolution of the CTM, and DISP is the dispersion model estimates at the desired fine spatial resolution. To summarize, concentrations of primary roadway $PM_{2.5}$ are placed in their respective locations inside CTM grids after removing average roadway primary $PM_{2.5}$ from the CTM estimates to avoid double counting. The result is daily concentration estimates of total fine particulate matter incorporating chemistry and complete local and regional emissions at a fine spatial resolution that matches the DISP inputs.

6.2.1.2 Multiplicative Method for Gaseous Pollutants (CO and NOx)

In the application of the additive method to CO and NOx, it was found that biases in the input model data led to negative concentration estimates in urban background and final concentrations. The averages of the dispersion model estimates at the coarser grid resolution, i.e. the CTM grid resolution ($\overline{DISP}_{coarse}$), were higher than chemical transport model estimates at the same grid cell on certain days, leading to negative concentrations when $\overline{DISP}_{\text{coarse}}$ values were subtracted from CTM estimates (see Appendix C for details). In general, when specific locations within a 12km grid cell have concentrations much higher than background, leading to high $\overline{DISP}_{\text{coarse}}$ estimates, or background is small compared to the variation captured in the dispersion model, the additive method can lead to negative predictions due to errors in the model inputs.

To avoid this phenomenon, instead of subtracting, CTM estimates are divided by $\overline{DISP}_{\text{coarse}}$ values in the multiplicative method. This division results in linear adjustment factors for each grid cell at the coarser resolution. These adjustment factors physically represent the inverse fraction of total pollutant that is estimated to be primary from roadways. The spatial field of these adjustment factors is smoothed to the fine grid scale of the DISP estimates using triangulation based linear interpolation. Finally, each adjustment factor at the fine spatial resolution is multiplied by the DISP value at the matching grid cell to obtain final concentration estimates [equation (6-2)].

$$Gas = \left[\left({CTM}/{\overline{DISP}_{coarse}}\right)_{interpolated}\right] * DISP \qquad (6\text{-}2)$$

To summarize, this method rescales the DISP estimates using the linear relationship between CTM estimates and DISP values to obtain air pollutant estimates at the spatial resolution of the DISP simulations. If the linear adjustment factor is higher than one, the

total pollutant concentration estimated by the CTM is higher than the primary roadway concentration estimated by the $\overline{DISP}_{\text{coarse}}$, and the estimates from DISP will be scaled higher to match the total concentration. If the linear adjustment factor is below one, the $\overline{DISP}_{\text{coarse}}$ estimate of primary roadway pollutant concentration is higher than the CTM estimate of total pollutant concentration, implying that the DISP model is biased high, and the linear adjustment factor will scale the DISP estimate down. Although applications of the multiplicative method were limited to the gaseous pollutants NOx and CO, this method should be applied to any pollutant with biases in model input estimates (such as overly rapid vertical dispersion in CMAQ leading to biased low surface concentrations and excessive accumulation of pollutants due to wind direction aligning with roadway links in RLINE leading to biased high concentrations) that lead to higher $\overline{DISP}_{\text{coarse}}$ than the CTM estimates.

6.2.2 Methods for Developing Inputs for Application of Model Fusion Techniques to Atlanta, GA

6.2.2.1 Chemical Transport Model Input

CMAQ is a state-of-the-science Eulerian-grid regional chemical transport model incorporating emissions from a myriad of sources and complex chemistry, including gas/particle partitioning (Byun & Schere, 2006). The use of CMAQ in these model fusion methods accounts for photochemical evolution of the pollutants (loss and formation) as well as the impacts of regionally scaled sources. In Atlanta, specifically, much of the $PM_{2.5}$ is formed through secondary processes, such as the production of ammonium sulfate (Zhai, Mulholland, Russell, & Holmes, 2017), secondary organic aerosol (SOA) from both

anthropogenic and biogenic sources (Kleindienst et al., 2010), and CO from the photochemical degradation of biogenic emissions (Choi, Osterman, Eldering, Wang, & Edgerton, 2010; Hudman et al., 2008). For the model fusion applications, daily CMAQ fields for 24 h $PM_{2.5}$, maximum daily 1 h concentration of CO, and maximum daily 1 h concentration NOx during the years 2003 through 2008 were obtained from previous work by Friberg et al. (2016) that developed a data fusion method to optimize CMAQ outputs. In the Friberg et al. (2016) data fusion method, observational data is blended with the Environmental Protection Agency's (EPA) PHASE CMAQ runs at 12km resolution [CDC National Environmental Public Health Tracking Network, CMAQ v4.7, carbon bond mechanism (CB05), 24 vertical layers, emissions obtained from the 2002 National Emissions Inventory run with the Sparse Operator Kernel Emissions (SMOKE), meteorology obtained from the Weather Research and Forecasting Model (WRF) v3.3.1]. Briefly, the algorithm in Friberg et al. (2016) utilizes a weighted average of one method that corrects daily CMAQ estimates for annual- and seasonal-biases ($CMAQ_1$) and a second method the uses temporal variance from observations and spatial structure from the annual mean CMAQ field to obtain optimized air pollutant concentration fields ($CMAQ_2$). The weight of the averages is based on a temporal variance that weights the second method ($CMAQ_2$) heavier near monitors and the first method ($CMAQ_1$) heavier away from monitors. Further details on this method and evaluation of this observation-fused CMAQ data set can be found in Friberg et al. (2016). The resulting simulations, which we will refer to as "OBS-CMAQ", exhibit much less bias in the three pollutants of interest (daily 24 h $PM_{2.5}$ and 1 h maximum CO and NOx) than the raw EPA PHASE CMAQ simulations, providing more accurate inputs to the model fusion approaches than raw CMAQ. For

sensitivity analyses, the model fusion methods were also run with CMAQ outputs that were not calibrated with daily observations. Instead, CMAQ was only adjusted for annual means and seasonal biases using methods and regression coefficients described in detail in Friberg et al. (2016). In other words, the model fusion methods were run with $CMAQ_2$ results for a sensitivity analysis and an estimate of the performance of the model fusion methods away from monitors where $CMAQ_2$ is weighted more heavily in the OBS-CMAQ estimates.

6.2.2.2 Dispersion Model Input

RLINE is a steady-state line-source dispersion model developed by the U.S. EPA to simulate primary and chemically inert pollutants (Snyder et al., 2013). RLINE was chosen as the dispersion model for the application of these model fusion methods because it is designed to simulate primary concentrations from line-sources, such as mobile traffic. For the applications of the model fusion approaches, publicly available annual average RLINE fields during the years 2003 through 2008 developed in previous work were used (Zhai et al., 2016). Briefly, Zhai et al. (2016) ran RLINE using hourly meteorology generated for years 2003 through 2008 using AERMET (Cimorelli et al., 2005; U.S. Environmental Protection Agency, 2004) and AERMINUTE (U.S. Environmental Protection Agency, 2015) and link-based emissions from the Atlanta Regional Commission's (ARC) 20-county activity-based travel demand model (D'Onofrio, 2016). Zhai et al. (2016) utilized a modified version of the STability ARray (STAR) method to group meteorological variables, including wind direction, wind speed, and Monin-Obukhov length, into 78 categories to simulate annual mean impacts of on-road mobile sources on pollutant concentrations (S. Y. Chang et al., 2015; U. S. Environmental Protection Agency, 1997; Zhai et al., 2016). ARC emissions were only available for 2010

and, thus, were scaled to prior years to account for changes in vehicular traffic and emissions. Roadway link pattern and vehicle type distribution did not change significantly during the study time period and annual average MOVES emissions for the 20-county Atlanta area were available for each year of the study period, so MOVES emissions were used to calculate year-specific annual average link-based emissions via scaling of 2010 ARC emissions. Using these year-adjusted annual average link-based emissions and data on frequency of occurrence for each of the 78 meteorological categories for each year, annual average RLINE concentration estimates at 250m resolution were developed for 24 h $PM_{2.5}$ and 1 h maximum CO and NOx for the years 2003 through 2008 over Atlanta, GA.

The RLINE results were found to be biased high, so Zhai et al. (2016) developed a method to calibrate the results using linear regressions with observations, in this case using five monitors for CO and seven monitors for NOx in the Atlanta, GA area. $PM_{2.5}$ from RLINE was calibrated using a linear regression of log-transformed RLINE with Chemical Mass Balance-Gas Constraint (CMB-GC) mobile source impact estimates derived using data from three monitor sites and *a priori* source profiles (Zhai et al., 2016). This calibration substantially reduced the normalized mean bias of the model results, so these calibrated simulations, which we will refer to as "OBS-RLINE", were used in the model fusion approaches. Further description of RLINE calibration and evaluation of these methods and results can be found in Zhai et al. (2016).

6.3 Results

The additive and multiplicative model fusion methods were applied to obtain daily estimates of 24 h average $PM_{2.5}$ and 1 h maximum NOx and CO for Atlanta, GA during

the years 2003 through 2008. The general mathematical equations for the model fusion methods [equations (6-1) and (6-2)] can be rewritten to apply to the specific inputs used in this work, expressed in equations (6-3) and (6-4).

$$PM_{2.5}(x,d) = \left[\left(OBS\text{-}CMAQ(l,d) - \overline{OBS\text{-}RLINE}_{coarse}(l,y)\right)_{interpolated}\right] + OBS\text{-}RLINE(x,y) \qquad (6\text{-}3)$$

$$Gas(x,d) = \left[\left(OBS\text{-}CMAQ(l,d) \Big/ \overline{OBS\text{-}RLINE}_{coarse}(l,y)\right)_{interpolated}\right] * OBS\text{-}RLINE(x,y) \qquad (6\text{-}4)$$

In equations (6-3) and (6-4), pollutant concentration estimates are provided at 250m grid cells located at x for each day d, daily OBS-CMAQ and annual-average $\overline{OBS-RLINE}_{coarse}$ estimates are provided at 12km grid cell locations l, and annual-average OBS-RLINE estimates are provided for each year y. Equations (6-3) and (6-4) are specific to the model fusion applications presented in this work using previously developed OBS-CMAQ and OBS-RLINE data, but the methods could be applied to other models at various grid and time scales.

The additive and multiplicative model fusion methods are represented graphically for an example year (2005) (Figure 6-1, Figure C-1, Figure C-2).

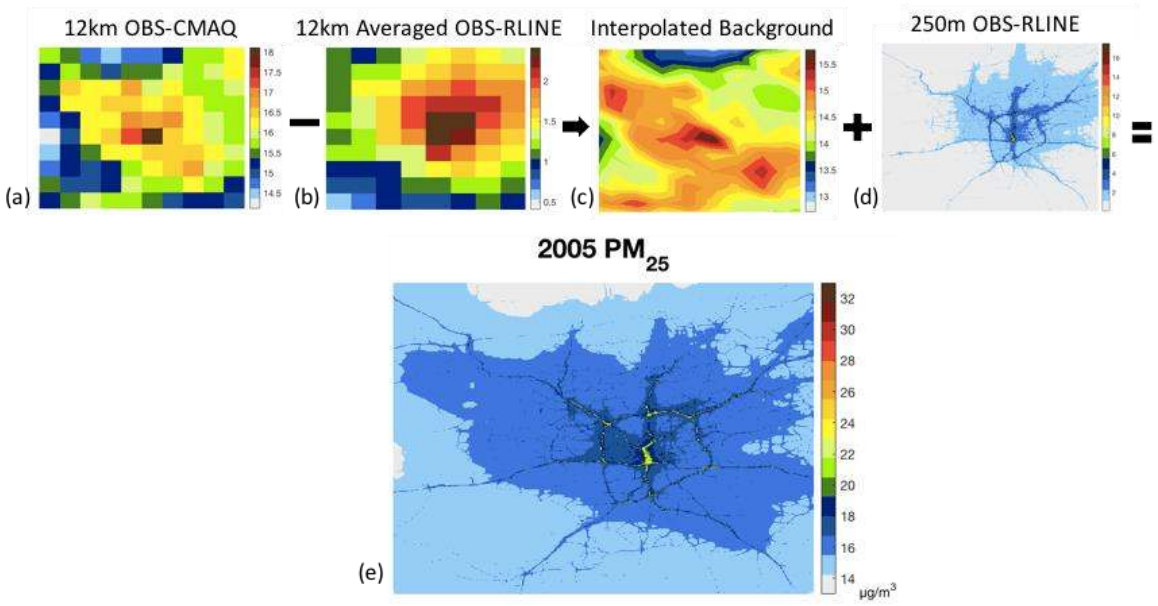

Figure 6-1. Additive model fusion steps and results for 2005 annual average $PM_{2.5}$. First, the fine resolution (250m) OBS-RLINE field is averaged to a 12km grid matching the OBS-CMAQ grid (b), which is subtracted from the OBS-CMAQ 12km field (a). These results are spatially interpolated to 250m resolution matching the OBS-RLINE grid resolution (c) and then added to the 250m resolution OBS-RLINE field (d) to provide a 250m resolution model-fused annual average $PM_{2.5}$ field (e). Note: each plot has a different color scale in order to show the spatial distributions clearly.

Annual average results for the same year are depicted for 1 h maximum NOx and CO using the multiplicative method (Figure 6-2).

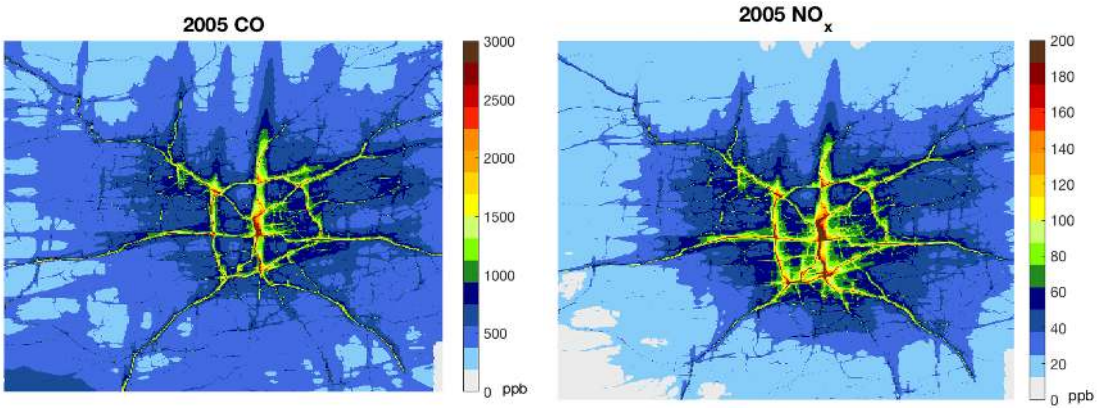

Figure 6-2. Multiplicative model fusion results for annual averages of 1 h maximum CO (ppb) (left) and NOx (ppb) (right) for the year 2005.

Plots of annual averages of each pollutant for all years of the study period can be found in the supplemental (Figure C-3, Figure C-4, Figure C-5). Major highways are clearly visible on spatial distribution maps of the resulting model fusion estimates for each pollutant (Figure 6-1, Figure 6-2, Figure C-3, Figure C-4, Figure C-5), indicating an ability of the model fusion methods to yield small-scale spatial gradients in pollutant concentration. Consistently high concentrations in the central part of Atlanta are due to vehicle emissions from the Downtown Connector where three interstates (I-20, I-85, and I-75) merge into one eight-lane highway [the busiest section experienced over 272,000 vehicles per day in 2005 (Cimorelli et al., 2005)], other roadway traffic in the region, a railyard, and other major sources west of the Downtown Connector.

6.3.1 Monitoring Data for Evaluation

Performances of OBS-CMAQ, OBS-RLINE, and model fusion results for each pollutant were evaluated using available urban and rural monitoring stations in the Atlanta region: eight monitors for $PM_{2.5}$, five monitors for CO, and five monitors for NOx. These same monitoring sites were used in the data assimilation methods to reduce bias in the model inputs (OBS-CMAQ and OBS-RLINE), but a sensitivity analysis was performed on the model fusion methods using CMAQ inputs that had not been adjusted with daily observations. Observations were taken from monitors that are part of the Central Speciation Network (CSN) and Southeast Aerosol Research and Characterization network (SEARCH) network and monitors operated by the Georgia Environmental Protection Department (GA EPD) (Table C-1) (Edgerton et al., 2005; Hansen et al., 2003; Paul A. Solomon et al., 2014). There were multiple $PM_{2.5}$ monitoring instruments at Yorkville and South Dekalb during the study period, so observations from each monitor were averaged into one value

for that site before evaluating model performance. Data were available daily or every 3 days, depending on the site, and available during the entire study time period (years 2003 through 2008) except for one $PM_{2.5}$ monitor and one CO monitor, each missing one year of data (Table C-1).

6.3.2 Evaluation of Model Fusion Methods

Results of the model fusion methods' applications to $PM_{2.5}$, NOx, and CO in Atlanta, GA were compared to monitoring data to assess and evaluate model fusion performance using the publicly available OBS-CMAQ and OBS-RLINE simulations (Table 6-1, Table 6-). These model fusion data are being used in current epidemiologic and environmental justice studies. Model fusion concentration estimates were compared to available site-day measurements paired in time and space during the entire study period (years 2003 through 2008). Evaluation statistics were calculated per available site-day for each monitor, averaged into annual values for each monitor, and then averaged over all monitoring sites for each year during the study period. The median, minimum, and maximum values over the time period are reported (Table 6-1).

Table 6-1. Evaluation statistics are the median, with minimum and maximum in parentheses, of year-specific averages (2003 through 2008) of the statistics for eight, five, and five monitors for $PM_{2.5}$ ($\mu g/m^3$), CO (ppb), and NOx (ppb), respectively, located in Atlanta, GA. Statistics are available for OBS-CMAQ, additive ($PM_{2.5}$) and multiplicative (NOx and CO) model fusion results using OBS-CMAQ and OBS-RLINE as inputs (*Model Fusion*), and additive ($PM_{2.5}$) and multiplicative (NOx and CO) model fusion results with OBS-RLINE and CMAQ simulations that have not been adjusted using daily observations, representing a 100% withholding, as inputs (*Model Fusion Withholding*).

	24-hr $PM_{2.5}$	*1-hr max CO*	*1-hr max NOx*
Mean			
OBS-CMAQ	16.4 (13.8—16.9)	748.2 (538.7—897.4)	58.4 (43.2—63.2)
Model Fusion	16.7 (13.7—17.0)	737.4 (528.5—890.7)	56.5 (41.6—61.0)
Model Fusion Withholding	17.0 (14.1—17.4)	745.3 (530.6—906.1)	57.3 (42.7—62.7)
Observations	15.7 (11.0—16.1)	787.8 (477.3—928.2)	68.8 (48.1—77.3)
RMSE[a]			
OBS-CMAQ	2.1 (1.8—2.6)	232.7 (182.2—326.4)	36.1 (31.2—39.1)
Model Fusion	1.9 (1.8—2.3)	206.3 (138.7—250.1)	36.8 (31.2—38.0)

Table 6-1 continued

Model Fusion Withholding	5.7 (5.4—6.0)	428.7 (310.5—505.1)	54.8 (52.2—65.4)
Mean Bias[b]			
OBS-CMAQ	0.8 (-0.08—1.2)	-42.9 (-86.8— -29.3)	-11.3 (-13.0— -4.0)
Model Fusion	1.0 (0.2—1.3)	-51.6 (-98.1— -36.5)	-13.9 (-15.3— -8.4)
Model Fusion Withholding	1.2 (0.7—1.8)	-50.5 (-84.5— -32.4)	-12.5 (-14.2— -7.1)
Normalized Mean Bias[c] *(%)*			
OBS-CMAQ	5.7 (-0.3—6.8)	3.4 (-0.3—12.7)	15.4 (9.3—37.1)
Model Fusion	6.9 (1.5—8.0)	0.2 (-1.7—8.4)	4.3 (0.9—22.2)
Model Fusion Withholding	7.8 (4.4—11.1)	1.1 (-2.2—10.1)	8.3 (4.4—26.5)
Mean Error[d]			
OBS-CMAQ	1.5 (1.3—1.8)	183.7 (154.1—267.6)	25.3 (22.4—26.5)

Table 6-1 continued

Model Fusion	1.5 (1.4—1.9)	143.5 (105.3—181.5)	24.9 (22.6—27.6)
Model Fusion Withholding	4.2 (3.8—4.3)	285.2 (210.0—369.5)	37.9 (32.6—43.6)
***Normalized Mean Error**[e] (%)*			
OBS-CMAQ	10.4 (8.5—11.4)	27.7 (22.5—37.0)	48.4 (44.6—64.6)
Model Fusion	9.9 (9.0—12.1)	23.8 (15.6—25.7)	39.6 (35.3—55.3)
Model Fusion Withholding	27.3 (26.5—29.1)	40.4 (36.4—45.0)	61.0 (59.5—74.7)
***Temporal R**[f]*			
OBS-CMAQ	0.98 (0.89—0.99)	0.93 (0.91—0.95)	0.98 (0.89—1.0)
Model Fusion	0.99 (0.92—0.99)	0.93 (0.92—0.95)	0.98 (0.89—1.0)
Model Fusion Withholding	0.77 (0.73—0.79)	0.54 (0.52—0.59)	0.60 (0.58—0.62)

[a]Root-mean squared error: $\sqrt{mean((C_m - C_o)^2)}$; C_o: daily observed concentration; C_m: daily modeled concentration

Table 6-1 continued

[b]Mean bias: $mean(C_m - C_o)$; C_o: daily observed concentration; C_m: daily modeled concentration

[c]Normalized mean bias: $\left(\frac{mean(C_m)}{mean(C_o)} - 1\right) * 100$; C_o: daily observed concentration; C_m: daily modeled concentration

[d]Mean error:$mean(|C_m - C_o|)$; C_o: daily observed concentration; C_m: daily modeled concentration

[e]Normalized mean error: $\frac{\sum|C_m - C_o|}{\sum C_o} * 100$; C_o: daily observed concentration; C_m: daily modeled concentration

[f]Pearson's correlation coefficient

Further evaluation of the model fusion algorithms was conducted by rerunning the model fusion methods for each pollutant over the entire study period (years 2003 through 2008) with CMAQ results that were adjusted for annual and seasonal biases using regression coefficients developed in Friberg et al. (2016) but do not incorporate the daily observations that were used in the evaluation. These results allow the evaluation of the model fusion approaches against daily observations without using those same observations in the model fusion inputs (OBS-CMAQ), providing a 100% withholding test for the model fusion results. This evaluation can be used to assess model fusion performance away from monitors that rely on CMAQ information more than observations due to the nature of the data fusion method used to develop OBS-CMAQ (Friberg et al., 2016). Even without fusing CMAQ inputs with daily observations, the model fusion methods perform well with median normalized mean biases of 7.8%, 1.1%, and 8.3% for 24 h average $PM_{2.5}$, 1 h maximum CO, and 1 h maximum NOx, respectively, across available observation site-days during the years 2003 through 2008 (Table 6-1). Temporal correlations were lower for the

100% withholding test than for the model fusion estimates with OBS-CMAQ (100% withholding model fusion R = 0.77, 0.54, and 0.60 for $PM_{2.5}$, CO and NOx, respectively; model fusion with OBS-CMAQ R = 0.99, 0.93, 0.98 for $PM_{2.5}$, CO and NOx, respectively) (Table 6-1). These results show that for temporal correlation, the inputs to the model fusion processes greatly impact evaluation statistics. The model fusion algorithms combine two model simulations and do not adjust them with observations to reduce biases, so adjustments with daily observations *a priori* increases temporal correlations. However, the biases and errors are relatively low for the 100% withholding test, indicating that the model fusion methods are generally unbiased in capturing concentrations away from monitors where the OBS-CMAQ inputs are not affected significantly by daily observations due to the data fusion method utilized and described in Friberg et al. (2016).

6.3.3 Comparison of Model Fusion Results to OBS-CMAQ

Performances of the applications of the model fusion methods to $PM_{2.5}$, CO, and NOx in Atlanta were compared to the performance of OBS-CMAQ to investigate the value of finer spatial resolution estimates (Table 6-1, Table 6-, Figure 6-3). The performance metrics between the model fusion results and OBS-CMAQ are comparable, which is to be expected as the performance of the model fusion methods relies heavily on model inputs, including OBS-CMAQ. There is general improvement in the medians and ranges of normalized mean bias and normalized mean error for model-fused 1 h maximum CO and NOx estimates compared to OBS-CMAQ estimates. These minimized biases and errors show the value in the model fusion methods' capabilities to incorporate OBS-RLINE information and obtain finer spatial resolution.

Performance metrics for 24 h averaged $PM_{2.5}$ do not vary significantly between OBS-CMAQ and model-fused results because mobile sources are not the dominant source of $PM_{2.5}$ in the region. Most of the $PM_{2.5}$ in the southeastern United States is secondary (including ammonium sulfate and secondary biogenic pollutants) (Zhai et al., 2017). OBS-RLINE only provides adjustments to the primary mobile source impacts while OBS-CMAQ and monitoring data include primary and secondary $PM_{2.5}$ from all sources, so OBS-RLINE contributes less information to total $PM_{2.5}$ than to total NOx and CO (which are dominated by vehicles emissions) driving the larger performance increase between model-fused and OBS-CMAQ NOx and CO compared to model-fused and OBS-CMAQ $PM_{2.5}$. Nevertheless, the model-fused $PM_{2.5}$ performs well compared to OBS-CMAQ simulations and provides results at a 16-times finer spatial resolution. In other words, the model fusion methods perform well and estimate steep spatial gradients in concentrations that cannot be simulated by OBS-CMAQ due to limitations of the coarse grid resolution.

Spatial correlation analyses illustrate the contribution of both OBS-CMAQ and OBS-RLINE to the model fusion results. Spatial correlation (Pearson's linear correlation coefficient) values were calculated across monitoring locations using annual averages during the years 2003 through 2008 (Table 6-).

Table 6-2. Median of spatial Pearson's correlation coefficients over the study period with minimum and maximum in parentheses. Values are estimated using the annual averages of available observation sites and additive ($PM_{2.5}$) and multiplicative (NOx and CO) model fused results (250m resolution) with OBS-CMAQ and OBS-RLINE as inputs, OBS-CMAQ (12km resolution), and OBS-RLINE simulations (250m resolution) during the years 2003 through 2008.

	Model Fusion	**OBS-CMAQ**	**OBS-RLINE**
24-hr avg. $PM_{2.5}$	0.60 (0.34—0.77)	0.61 (0.37—0.80)	0.38 (0.16—0.62)
1-hr max CO	0.98 (0.97—1.00)	0.84 (0.78—0.91)	0.96 (0.93—1.00)
1-hr max NOx	0.84 (0.76—0.89)	0.78 (0.72—0.83)	0.74 (0.68—0.77)

The spatial correlations for 1 h maximum CO and NOx multiplicative model fusion results are substantially higher than spatial correlations for OBS-CMAQ results due to the finer spatial resolution of the model-fused estimates, which incorporate OBS-RLINE results and more accurately capture the steep gradients in the pollutant concentrations. Furthermore, spatial correlations for model-fused estimates are larger than spatial correlation values for OBS-RLINE for each pollutant because the model fusion methods use OBS-CMAQ to capture chemistry and sources that OBS-RLINE does not account for, providing more comprehensive and accurate estimates (note that the OBS-RLINE median spatial correlation for $PM_{2.5}$ is low because this model only captures primary $PM_{2.5}$ from roadways, not total $PM_{2.5}$ from multiple primary sources and secondary processes that are captured by monitors). Thus, the simulations from both observation-fused models used as

inputs (OBS-CMAQ and OBS-RLINE) contribute to overall performance of the model fusion methods. Finally, the ranges of spatial correlations for 24 h averaged $PM_{2.5}$ are large and median values relatively small compared to NOx and CO because it is more difficult for models to capture small spatial variations. Secondary pollutant formation makes $PM_{2.5}$ more spatially uniform than NOx and CO, resulting in observations varying less between monitors.

Annual average model fusion estimates using OBS-CMAQ and OBS-RLINE as inputs were compared to annual average OBS-CMAQ simulations at each 250m grid cell across the entire spatial domain, rather than just monitoring locations, to investigate the effects of obtaining finer spatial resolution estimates across the study area. Many 250m model fusion results agree well with 12km OBS-CMAQ simulations, as shown by the majority of model fusion values falling near a 1:1 line with OBS-CMAQ values (Figure 6-3), but the 250m model fusion estimates capture more extreme concentrations (mostly at roadways) that are averaged out in 12km OBS-CMAQ simulations but captured by OBS-RLINE.

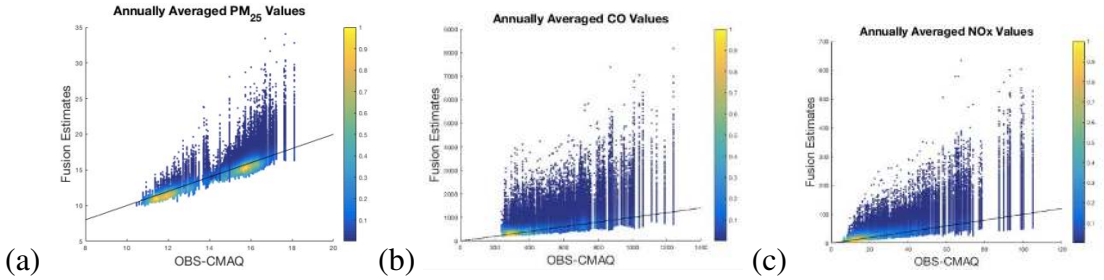

(a) (b) (c)

Figure 6-3. Density scatter plots of annually averaged model fusion estimates at each 250m grid cell versus annual average OBS-CMAQ values at the corresponding grid cells during the years 2003-2008 for (a) 24 h average $PM_{2.5}$ ($\mu g/m^3$) by additive method, and (b) 1 h maximum CO (ppb) and (c) 1 h maximum NOx (ppb) by multiplicative method. A higher density of points is in yellow and lower density in blue. Black lines represent 1:1 lines.

Vertical lines on the density scatter plots (Figure 6-3) show the ability of the model fusion methods to capture gradients within one 12km grid cell by illustrating the distribution of model fusion estimates for one OBS-CMAQ estimate. Many of the highest estimates are found directly on or near major roadways, which are in accordance with observations (Beevers et al., 2013; Cong, Qu, & Yang, 2016; J. Sarnat, 2017a).

6.3.4 Sensitivity Analyses

The multiplicative pollutant method was tested with 24 h average $PM_{2.5}$ to investigate the utility of the multiplicative pollutant model fusion method with other pollutants that have larger background contributions than NOx and CO. Overall performance for model fused 24 h average $PM_{2.5}$ estimates using the multiplicative method was poorer than the additive method (Table C-2). This lower performance results from the many sources of particulate matter contributing to urban background, so primary roadway $PM_{2.5}$ is being scaled by a heterogeneous mixture of particulate matter including both primary emissions and secondary formation. The multiplicative method can magnify errors when compared to the additive method. Additionally, the additive method was applied to 1 h maximum NOx and CO, in spite of the occasions when some of the final concentrations go negative, for comparison to the multiplicative approach. Overall, the statistics between the additive and multiplicative methods are comparable for NOx and CO, with a slightly more negative mean bias and higher mean error for the additive method. However, the incorrect negative concentration estimates using the additive approach persisted throughout the time period with 72% and 14% of the days for 1 h maximum NOx and CO, respectively, producing at least one 250m gird cell in the domain with a value below zero. Therefore, when determining which model fusion method to use for a specific pollutant, if

$\overline{DISP}_{\text{coarse}}$ values are higher than CTM values at certain locations due to biased high dispersion model outputs and/or biased low CTM values, the multiplicative model fusion method should be used to avoid unphysical results. In these cases, the background concentrations are often very low, i.e. a majority of the concentration of that pollutant is from primary vehicle emissions (when using RLINE as the dispersion model input). Otherwise, the additive model fusion method should be used to limit biases and errors. However, with relatively short run times, both model fusion methods can be tested and evaluated against observations to determine the best method on an individual basis.

6.4 Discussion

Capturing steep spatial gradients in pollutant concentrations near roadways is critical for exposure assessment in epidemiologic studies. Monitoring stations are too sparse to accurately capture spatial gradients in pollutant concentration and can miss very high concentrations near roadways. Some air quality models can estimate fine spatial resolutions (dispersion models) but do not simulate atmospheric chemistry processes or incorporate regional emission sources. Other models, like chemical transport models, can simulate atmospheric processing and comprehensive emission sources but typically at a coarse resolution (> 1km). The model fusion methods presented in this work utilize the strengths of both types of models (i.e., the regional chemical transport model CMAQ and the line dispersion model RLINE) and compares well to other air quality modeling techniques (H. Yu et al., 2018). The time limiting factor of these model fusion approaches is running the chemical transport model and dispersion model for inputs, but there is publicly available chemical transport and dispersion model data. These methods limit computational time by avoiding the need to re-run a chemical transport model with zeroed

out emissions to obtain background concentration estimates (Arunachalam et al., 2014; S. Y. Chang et al., 2017; Stein et al., 2007), presenting a relatively quick approach for obtaining finely-resolved spatial concentration estimates that avoids double counting of emissions. Fast run times allowed for the rapid development and evaluation of a long-term series of daily data for multiple pollutants. Additionally, by calculating "urban background" within the model fusion methods rather than *a priori* by zeroing out local emissions in CMAQ, the chemistry and secondary loss/formation that arise from the local emissions are not sacrificed.

Results shown in this paper are specific to daily 12km OBS-CMAQ and annual-averaged 250m OBS-RLINE inputs, but neither spatial nor temporal resolutions of both the inputs and outputs are fixed in these methods. Spatial resolution can change by adjusting the interpolation step. Additionally, these model fusion methods can be applied to other pollutants and can be used with simulations from different models as inputs if those data are more readily available or the focus of the study is capturing spatial gradients near local sources of emissions other than roadways.

There are three main limitations of the model fusion methods presented in this paper. First, the evaluation statistics, specifically temporal correlation, of these methods are dependent on the performance of the inputs. Specifically, in the applications presented in this paper, much of the daily variation in the results is due to the daily variation in the observations used to calibrate CMAQ. Although raw CMAQ, RLINE, or other model inputs can be used in the model fusion processes, a thorough evaluation of model inputs and adjusting these fields to reduce biases using methods such as the ones presented in Friberg et al. (2016) and Zhai et al. (2016) are recommended before resulting model fields

are fused in the model fusion methods. Additionally, fusing input CMAQ and RLINE with observations incorporates monitor information into estimating urban background and capturing the spatial gradients near roadways, which the model fusion methods alone do not achieve. Simulating steep spatial gradients in the dispersion model is critical because the fusion methods rely on the dispersion model inputs to capture all fine scale spatial variation in the pollutant of interest. Second, the interpolation step assumes that the urban background, as defined as pollution derived from all sources except the primary mobile fraction, can be linearly interpolated in space. If the urban background consists mostly of spatially uniform pollutants that vary smoothly in space, this assumption holds true. In Georgia, roughly 60% of the $PM_{2.5}$ mass is secondary, which is spatially smooth (Zhai et al., 2017). However, if the background pollution is dominated by spatially heterogeneous pollutants with strong local sources surrounded by steep spatial gradients that are not captured in the dispersion model inputs, this assumption may not hold true. In this work, NOx and CO are spatially heterogeneous in the study area, but the major local source driving this heterogeneity is vehicles and is captured by the OBS-RLINE inputs and is, thus, not included in urban background. Finally, for the multiplicative fusion method, the $DISP_{coarse}$ values must all be non-zero to avoid mathematical impossibilities due to division by zero. If $DISP_{coarse}$ is zero, implying that there is no primary pollutant in that coarse grid cell estimated by the dispersion model, i.e. if there is no primary pollution associated with vehicles on roadways using OBS-RLINE, the CTM value should be assumed as the total concentration of the area without undergoing the model fusion process, though this would not be expected to occur often and did not occur in these applications.

One limitation with evaluating these model fusion approaches is the lack of monitoring stations surrounding roadways. There is very limited near-roadway data to calibrate OBS-RLINE with to reduce bias in spatial gradient estimates. The lack of monitoring stations with daily data also limits the ability to evaluate the spatial gradients simulated by the model fusion methods on a daily basis using daily OBS-CMAQ and annual averaged OBS-RLINE as inputs. Nevertheless, these model fusion approaches compare well to available data and estimates near roadways are similar to measurements on roadways from other studies, including the more recent near-road monitoring study in Atlanta (J. Sarnat, 2017a).

Overall, the model fusion results capture high pollutant concentrations at roadways that OBS-CMAQ alone cannot while also retaining complex chemistry and contributions from sources that OBS-RLINE does not simulate. The fine spatial resolution of the resulting pollutant concentrations is useful for reducing exposure measurement error in health studies of spatially heterogeneous pollutants impacted by chemistry, such as studies investigating pollutant exposure while living in close proximity to roadways. More broadly, these model fusion results have many applications for epidemiologic analyses, city planning, and environmental justice studies that require pollutant concentration data at a fine spatial resolution.

CHAPTER 7.

INTRAURBAN SPATIAL VARIATION IN OXIDATIVE POTENTIAL DRIVEN BY VEHICLE EMISSIONS IN ATLANTA

Abstract

The link between vehicle emissions and health has been of increasing interest to epidemiologic and environmental justice studies due to the possibility of rapid urbanization leading to disproportionately high exposures in near-road environments. However, health studies on traffic exposure are impacted by the inability of observations to fully capture within-city spatial variability in pollutant concentration fields, especially steep spatial gradients near roadways. Observations for particulate matter (PM) oxidative potential (OP), a property of PM that measures a particle's ability to induce harmful redox reactions in the body, are especially limited as the development of acellular OP measurement techniques is relatively recent. Exposure to OP leads to higher risks for asthma/wheezing attacks, ischemic heart disease, and lung cancer than PM mass, and vehicle-derived PM from tailpipe emissions, brake/tire wear, and secondary formation have high intrinsic OP. This work develops and applies a model capable of estimating intraurban variability of OP driven by vehicle sources to better understand health impacts of traffic, particularly to vulnerable populations. A model fusion technique is used with dispersion and chemical transport model outputs to estimate vehicle-derived primary and secondary $PM_{2.5}$ in Atlanta, GA at a 250m resolution. These vehicle $PM_{2.5}$ estimates are multiplied by a vehicle-specific intrinsic OP value to estimate ambient levels of vehicle-derived OP. These vehicle-derived OP results are added to OP estimates from fires, regional sources, and

natural gas combustion that are interpolated to a fine spatial resolution to develop OP estimates of ambient PM from comprehensive emission sources for evaluation against measurements. Results show higher OP estimates near roadways, but other source impacts, like biomass burning and regional sources, make OP estimates more spatially homogeneous than estimated vehicle-derived $PM_{2.5}$ in Atlanta. The OP estimates are biased high at the roadside monitoring site but not at the urban monitoring site, possibly due to high biases in RLINE $PM_{2.5}$ on roadways or overestimation of intrinsic vehicle OP near highways. The intrinsic vehicle OP value may need to be differentiated for gasoline and diesel engines and/or be estimated as a spatially varying value to capture the effects of photochemistry on OP of vehicle PM emissions.

7.1 Introduction

Particulate air pollution has been associated with multiple health endpoints, including cardiorespiratory effects, adverse birth outcomes, and cancer (U.S. EPA, 2009). One limitation of epidemiologic studies on fine particulate matter ($PM_{2.5}$) is exposure error due to an inability of observational data to capture intraurban spatial variability driven by concentrated emission sources, such as vehicle emissions on heavily trafficked highways (Goldman et al., 2011). Air quality monitoring stations are spatially sparse due to cost limitations and are sited for regulatory purposes, e.g., to capture community-scale exposures. While the recently initiated near-road monitoring network is providing increased information on pollutant concentrations near certain busy highways, the near-road monitoring locations are very limited with only one or two locations in most larger cities and have been shown to be insufficient for capturing pollutant dynamics in areas near the monitors (J. Sarnat, 2017b). Together, this means that observational data lack the

information desired to characterize fine scale spatiotemporal pollutant concentrations wanted for epidemiology studies.

Dispersion models and model fusion techniques have previously been applied to estimate $PM_{2.5}$ concentrations in an urban environment at a fine spatial resolution. For example, RLINE (Research LINE model), a steady-state line-source model developed to model primary, chemically inert roadway concentrations, was applied in Atlanta and Detroit as part of health research and city planning efforts (D'Onofrio, 2016; J. Sarnat, 2017b; Snyder et al., 2013). A recently developed model fusion technique combined RLINE with CMAQ (Community Multiscale Air Quality model) to simulate daily $PM_{2.5}$ at a 250m resolution in Atlanta, GA without sacrificing secondary formation and regional source impacts (J. Bates, Pennington, et al., 2018). Because vehicle source impacts and secondary aerosol formation are critical for OP, this model fusion method was applied to vehicle source impacts from CMAQ-DDM to estimate intraurban spatial variability in vehicle-derived OP. First, the model fusion method was applied to estimate daily vehicle-derived $PM_{2.5}$ at a 250m resolution across Atlanta, GA. These daily fine-scale vehicle $PM_{2.5}$ fields were then multiplied by an intrinsic vehicle OP value and added to OP estimates of other sources, like biomass burning, to estimate the intraurban OP concentrations at a 250m resolution. The intrinsic vehicle OP value was obtained from previous studies that measured OP with a dithiothrietol (DTT) assay. OP^{DTT} has been shown to be associated with numerous acute cardiorespiratory effects, which is why modeling OP specifically using the DTT assay was chosen for this work (Abrams et al., 2017; J. Bates, Fang, et al., 2018; J. T. Bates et al., 2015; Fang et al., 2016; Yang et al., 2016; Zhang et al., 2016). Data

collected at three sites in Atlanta, GA are used with the model-fused OP^{DTT} estimates to evaluate the ability of the modeling method to capture within-city variability in OP^{DTT}.

7.2 Methods

The impact of vehicle emissions on intraurban spatial variability in OP^{DTT} was estimated using dispersion modeling and model fusion techniques. Briefly, OP^{DTT} was measured from water-soluble $PM_{2.5}$ filters collected at three locations within Atlanta, GA using an acellular DTT assay. Previously developed RLINE results were used in a model fusion algorithm with CMAQ-DDM identified vehicle source impacts to estimate the primary and secondarily-formed vehicle-related $PM_{2.5}$ in Atlanta, GA at a 250m resolution. Then, these results were multiplied by an intrinsic OP^{DTT} value for vehicle emissions to estimate vehicle-driven spatial variability of OP^{DTT} in Atlanta, GA. Fires and natural gas combustion-related $PM_{2.5}$, which have previously been identified as having impacts on OP^{DTT} (J. Bates, Weber, et al., 2018), were also multiplied by their intrinsic OP^{DTT} and added to the vehicle-derived OP^{DTT} to produce spatiotemporal fields of comprehensive water-soluble OP^{DTT} across Atlanta, GA.

7.2.1 $PM_{2.5}$ sampling and DTT analysis

Water-soluble $PM_{2.5}$ OP^{DTT} was measured at three sites in the Atlanta area using a semi-automated acellular DTT assay developed based on methods in Cho, et al. (2005) (J. T. Bates et al., 2015). Details of the measurement methods, study area, and results are found elsewhere (Tuet et al., 2017). Briefly, $PM_{2.5}$ was collected daily on pre-baked 8 x 10 in. quartz filters from 12 pm (noon) – 11 am using a non-denuded Thermo Anderson high-volume sampler. Details are described in Fang, et al. (2015) . Samples were collected

at three locations: Jefferson Street (JST) from June 2012 through April 2013, roadside site (RS) from September 2012 through October 2012 and January 2012 through February 2013, and Georgia Tech rooftop lab (GT) from July 2012 through August 2012 (Figure 7-1). RS is directly on the Downtown Connector, a strip of roadway where three interstates (I-20, I-85 and I-75) merge into one eight-lane highway (the busiest section experienced over 272,000 vehicles per day in 2005)(Georgia Department of Transportation, 2005). JST is an urban measurement site ~2.4km from the Downtown Connector next to a railyard and residential district. The GT site is on the roof of a three story building in the middle of Georgia Tech's campus, ~0.44km from the Downtown Connector (Figure 7-1).

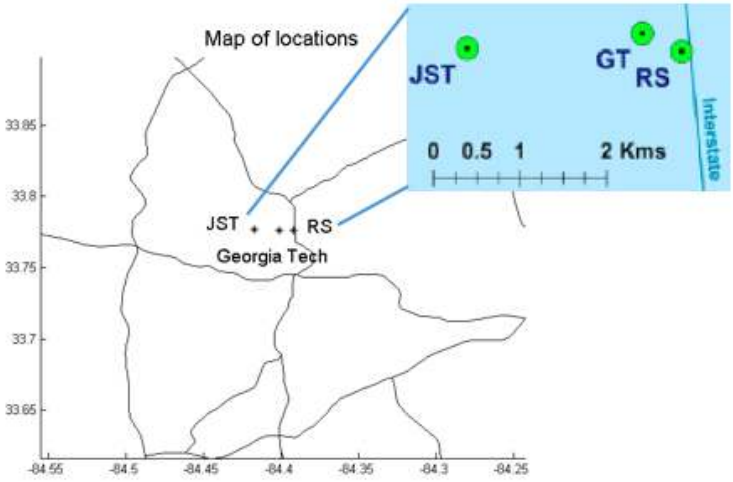

Figure 7-1. Locations of OP^{DTT} measurement sites in Atlanta, GA.

7.2.2 Dispersion Modeling

RLINE was chosen as the dispersion model for these analyses because it is an advanced, well-evaluated model designed to simulate primary concentrations from emissions of "line-sources", such as automobiles on highways. In Zhai et al. (2016),

annual-averaged primary roadway $PM_{2.5}$ was modeled for 2011 at a 250m resolution using RLINE with 2010 link-based emissions from the Atlanta Regional Commission's (ARC) 20-county activity-based travel demand model (D'Onofrio, 2016; Zhai et al., 2016). Roadway link pattern and vehicle type distribution did not change significantly between 2010 and 2011, so it was assumed that the spatiotemporal patterns of the 2010 emissions could be used with 2011 meteorology to produce 2011 air pollutant concentration data. RLINE was run with hourly meteorology generated using AERMET (Cimorelli et al., 2005; U.S. Environmental Protection Agency, 2004) and AERMINUTE (U.S. Environmental Protection Agency, 2015). A modified version of the STability ARay (STAR) method was used to group the meteorological variables wind direction, wind speed, and Monin-Obukhov length into 78 categories that were used with weighting techniques to generate annual-average fields (S. Y. Chang et al., 2015; U. S. Environmental Protection Agency, 1997; Zhai et al., 2016). High biases existed in the RLINE results due to over-accumulation of pollutants when wind direction aligns with roadway link, so Zhai, et al. (2016) developed a method to calibrate RLINE estimates with observations. A linear regression of log-transformed RLINE results with vehicle $PM_{2.5}$ identified using Chemical Mass Balance with Gas Constraint (CMB-GC) was used to correct RLINE primary $PM_{2.5}$ concentrations (Zhai et al., 2016). This calibration method substantially reduced normalized mean biases in the model results, so these calibrated simulations, which we will refer to as "OBS-RLINE", were used in these analyses. Further description of RLINE calibration and evaluation of these methods and results can be found in Zhai et al. (2016)

.

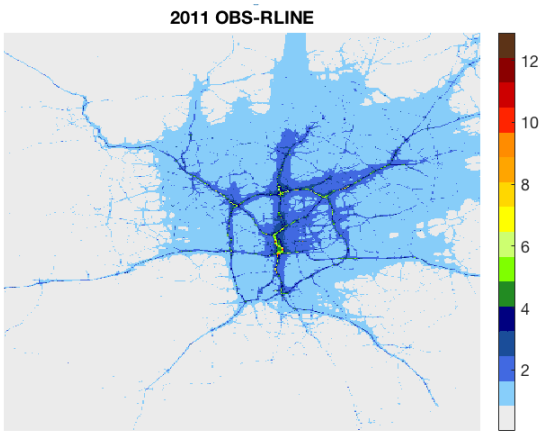

Figure 7-2. 2011 annual-average OBS-RLINE of the impacts of on-road emissions to primary $PM_{2.5}$ (µg m^{-3}) in Atlanta, GA.

7.2.3 $PM_{2.5}$ Model Fusion Process

Because RLINE does not simulate secondary formation of $PM_{2.5}$ from non-linear chemical reactions, and chemical aging has been shown to significantly impact the OP^{DTT} of aerosols (J. Bates, Fang, et al., 2018), a model fusion approach was applied to estimate vehicle-derived $PM_{2.5}$, including secondary formation. This model fusion approach and evaluation is described in detail in Bates, et al. (2018) . Briefly, this method combines dispersion and chemical transport (CTM) air quality model outputs to obtain air pollutant concentrations at the spatial resolution of the dispersion data. The CTM provides the regional sources, temporal variation, and chemical transformations of pollutants, while the dispersion model provides the fine spatial resolution of the impacts of roadway emissions on primary traffic-related air pollutants (TRAPs). First, the dispersion model data is averaged into the resolution of the CTM data. Then, the CTM data is divided by the CTM-grid resolution averaged dispersion model data, producing linear adjustment factors for the dispersion data. These adjustment factors are smoothed to the grid resolution of the dispersion model data using triangulation based linear interpolation and then multiplied by

the fine-scale dispersion model data. Overall, this method rescales the dispersion model data using the linear relationship between CTM estimates and dispersion values (J. Bates, Pennington, et al., 2018). In this work, OBS-RLINE is the dispersion model and CTM data is obtained from CMAQ with the direct-decoupled method (CMAQ-DDM) applied to three-dimensional air quality models and extended to include the capability to follow particulate matter (Byun & Schere, 2006; Cohan et al., 2005; Dunker, 1981, 1984; Napelenok et al., 2006).

Daily CMAQ-DDM data for on-road gasoline and on-road diesel $PM_{2.5}$ from June 2012 through April 2013 (during the OP^{DTT} measurement time period) were obtained from Bates, et al. (2018) . Briefly, on-road vehicle impacts were estimated for the eastern United States using CMAQ-DDM at a 12km x 12km grid resolution with 13 vertical layers of thickness, with chemistry from the Weather Research Forecasting (WRF) model v3.6.1 with 35 vertical layers and source-specific emissions from the Sparse Matrix Operator Kernel for Emissions (SMOKE) v3.6 with the 2011 National Emissions Inventory (CEP, 2003; Y. Hu et al., 2014). Biases in source impacts were reduced using two advanced data assimilation techniques: a CTM-receptor model hybrid method with speciated measurements and a secondary species correction algorithm (J. Bates, Weber, et al., 2018; Y. Hu et al., 2014; C. E. Ivey et al., 2016). These methods were previously applied and evaluated in Hu, et al. (2014) and Ivey, et al. (2016). Briefly, the CTM-receptor hybrid method adjusts source impacts using a receptor model based equation by minimizing biases in modeled primary species using speciated measurements (Y. Hu et al., 2014). The secondary species correction algorithm reduces biases in secondary species (ammonium, sulfate, nitrate, and secondary organic carbon) to zero at observation sites by distributing

weighted differences between modeled concentrations and speciated measurements across source impacts. The differences are weighted by source impact magnitudes. These adjusted CMAQ-DDM on-road gasoline and diesel source impacts were previously evaluated, finding that the data assimilation techniques greatly reduced biases in modeled species concentrations and resulted in source impacts that were in line with prior studies where measurements were available (J. Bates, Weber, et al., 2018; Y. Hu et al., 2014; C. E. Ivey et al., 2016). The Atlanta, GA area of the CMAQ-DDM modeling grid was isolated for the model fusion process applied in this work (Figure 7-3). On-road gasoline and on-road diesel were combined into one vehicle source to match the $PM_{2.5}$ concentrations estimated by RLINE.

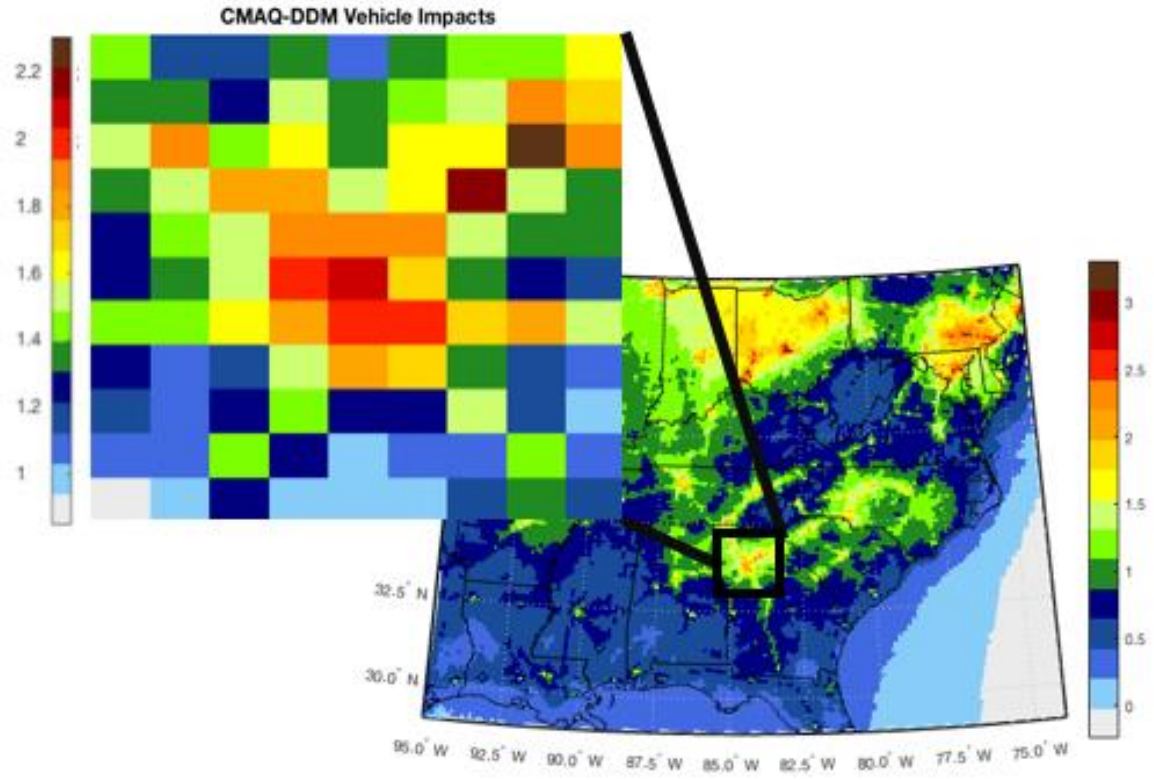

Figure 7-3. CMAQ-DDM (µg m^{-3}) identified vehicle source impacts (on-road gasoline + on-road diesel) on $PM_{2.5}$ in Atlanta, GA (extracted from previously developed data for eastern United States (J. Bates, Weber, et al., 2018)) averaged from June 1, 2012 through April 30, 2013.

All three OP^{DTT} measurement sites exist within one 12km x 12km CMAQ-DDM grid, so the daily CMAQ-DDM vehicle source impacts were combined with the annual-average OBS-RLINE data using the previously described model fusion method to obtain results at a 250m resolution. The daily CMAQ-DDM results from June 2012 through July 2013, providing temporal information, were fused with 2011 annual-average (temporally static) OBS-RLINE, providing fine spatial resolution data, resulting in daily estimates for on-road primary and secondarily-formed vehicle $PM_{2.5}$ at a 250m resolution in Atlanta, GA from June 2012 through April 2013 (Figure 7-4).

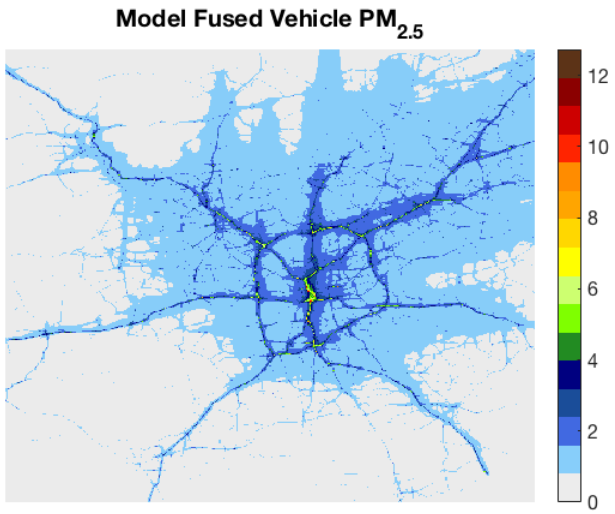

Figure 7-4. Model fused $PM_{2.5}$ (µg m^{-3}) from vehicles in Atlanta,GA , averaged from June 1, 2012 through April 30, 2013.

7.2.4 Estimation of OP^{DTT} spatial fields

Previous work has investigated the intrinsic OP^{DTT} of vehicle-derived $PM_{2.5}$ using CMAQ-DDM source impacts (J. Bates, Weber, et al., 2018). The intrinsic OP^{DTT} of on-road gasoline and on-road diesel were found to be 0.022 nmol min^{-1} μg_{gas}^{-1} and 0.067 nmol min^{-1} μg_{dies}^{-1}, respectively, with an average of 0.045 nmol min^{-1} μg_{veh}^{-1}. This average value of intrinsic OP^{DTT} for mobile-source $PM_{2.5}$ was applied to the model fused $PM_{2.5}$ values to estimate intraurban spatial trends in on-road mobile source-related OP^{DTT} in Atlanta, GA (Figure 7-5). Comprehensive water-soluble OP^{DTT} from multiple sources was also etimated by adding source-specific OP^{DTT} for fires, natrual gas combustion, and regional sources to the on-road mobile source-related OP^{DTT}. These sources have been previously found to be the major contributors to OP^{DTT} in the eastern United States (J. Bates, Weber, et al., 2018). Source-specific OP^{DTT} was obtained by interpolating source-specific $PM_{2.5}$ concentrations from CMAQ-DDM at a 12km resolution to a 250m resolution matching the grids of the

model-fused data using triangulation based linear interpolation. These interpolated $PM_{2.5}$ fields were multiplied by their respective intrinsic OP^{DTT} values obtained from previous work (Figure D-1) and then added to the vehicle-derived OP^{DTT} etimates to obtain OP^{DTT} of ambient $PM_{2.5}$ from comprehensive emission sources in Atlanta, GA (Figure 7-5). Source-specific intrinsic OP^{DTT} values were obtained from the coefficients in a regression relating fires, natural gas combustion, on-road diesel, and on-road gasoline to OP^{DTT} and from the intercept for the regional source (J. Bates, Weber, et al., 2018). The intrinsic values are 0.11 nmol min^{-1} μg_{fire}^{-1}, 0.056 nmol min^{-1} $\mu g_{natrual\_gas}^{-1}$, and 0.17 nmol min^{-1} $\mu g_{regional}^{-1}$ for the fire, natural gas combustion, and regional sources, respectively.

7.3 Results

The three OP^{DTT} measurement locations in Atlanta, GA span across ~3km. The ratios in the OP^{DTT} measurements for RS/JST and GT/JST are 1.12 ± 0.37 and 0.81 ± 0.18, respectively, with maximum of daily ratios of 2.16 and 1.33, respectively. The ratios in vehicle impacts on $PM_{2.5}$ is significantly higher, with RS/JST values of 6.1 and 3.0 for primary OBS-RLINE $PM_{2.5}$ and model-fused vehicle $PM_{2.5}$ and GT/JST values of 1.4 for both primary OBS-RLINE $PM_{2.5}$ and model-fused vehicle $PM_{2.5}$ during the OP^{DTT} measurement time periods. OP^{DTT} has been found to be more spatially uniform than other OP assays due to contributions from secondary organic species, which are more homogeneously distributed than other species, like metals (Verma et al., 2014; Yang et al., 2015). The OP^{DTT} measurements used in this work were performed on total water-soluble $PM_{2.5}$, not just vehicle-related $PM_{2.5}$, and includes contributions from more spatially homogeneous source impacts, such as aged prescribed burning. When additional source impacts (fires, natural gas combustion, regional sources) are included in estimated OP^{DTT}

across Atlanta (Figure 7-5), the ratios of OP^{DTT} between sites become smaller, with an average of 1.5 for RS/JST and 1.1 for GT/JST, suggesting that these additional sources make OP^{DTT} more spatially uniform within Atlanta. However, there is still significant intraurban spatial variability in estimated OP^{DTT} that can affect exposure analyses for epidemiologic studies (Figure 7-5).

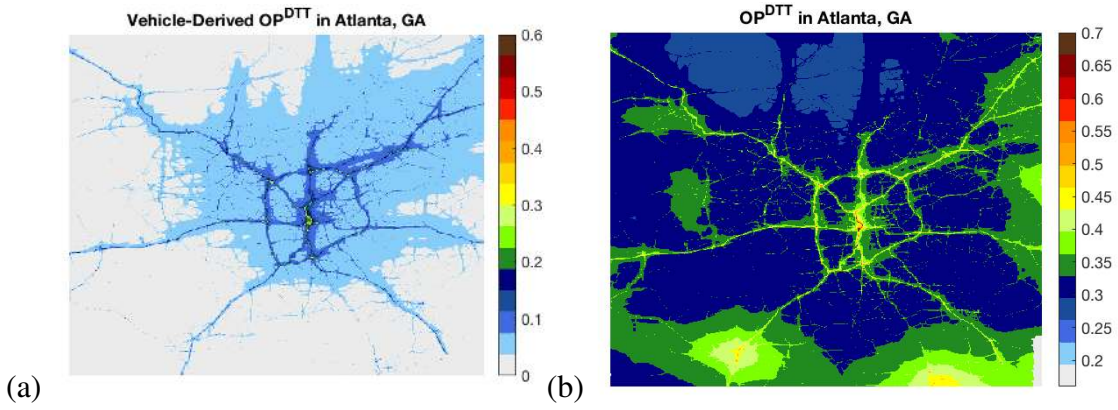

Figure 7-5. Estimated OP^{DTT} (nmol min^{-1} m^{-3}) due to (a) on-road vehicles and (b) all sources (fires, natural gas, on-road vehicles, regional) in Atlanta, GA averaged from June 1, 2012 through April 30, 2013. Note the differences in color bar on each plot to better show spatial distribution.

Spatial correlation analyses were used to investigate the relationship between water-soluble OP^{DTT} observations and primary $PM_{2.5}$ vehicle source impacts from OBS-RLINE and primary and secondary $PM_{2.5}$ vehicle source impacts from the model fused results (Figure 7-4). The spatial Pearson's linear correlations between OP^{DTT} and OBS-RLINE and model fused $PM_{2.5}$ data are 0.55 and 0.48, respectively. Interestingly, the primary roadway impacts from OBS-RLINE have a slightly higher spatial correlation with OP^{DTT} than the primary and secondary impacts from the model fusion data. There may be

a heterogeneous intraurban component to OP^{DTT} driven by primary roadway emissions, e.g., driven by copper.

The normalized mean biases in estimated vehicle-driven OP^{DTT} are -76%, -57%, and -31% at JST, GT, and RS, respectively, and the temporal Pearson's linear correlation coefficients between estimated and measured OP^{DTT} are 0.41, 0.36, and 0.29 at JST, GT, and RS, respectively. The very negative biases are expected because the estimated OP^{DTT} is only from vehicle impacts, not total water-soluble $PM_{2.5}$ impacts that include highly OP^{DTT}-active sources like biomass burning. The biases increase in negativity the farther away from the roadway due to the increase in contribution from other sources to OP^{DTT}. When other sources, such as fires and natural gas burning, are added to the OP^{DTT} estimates, the normalized mean biases in estimated OP^{DTT} increase to 1.0%, 47%, and 45% at JST, GT, and RS, respectively, and the temporal Pearson's linear correlation coefficients between estimated and measured OP^{DTT} become 0.59, 0.39, and 0.29 at JST, GT, and RS, respectively. These results suggest that the model fused data with all included sources of OP^{DTT} can estimate OP^{DTT} at urban sites, like JST, with fairly high accuracy. However, the estimates are biased high at the roadway measurement site. The high bias at the RS site for OP^{DTT} estimates from all sources (vehicles, fires, natural gas combustion, and regional sources) could be due to biases in the model fused $PM_{2.5}$ estimates (driven by high biases in OBS-RLINE) on roadways causing an overestimation of $PM_{2.5}$ on roads. An alternate hypothesis for the high bias is that primary vehicle emissions may not contribute signficantly to ambient OP^{DTT}, so using one inrinsic value for vehicle-driven OP^{DTT} may overestimate OP^{DTT}. In other words, the intrinsic vehicle OP^{DTT} may increase with photochemical aging, causing it to vary spatially and be potentially lower on roadways. It

is also possible that one intrinsic value cannot be used for the entire vehicle fleet. If gasoline and diesel engines have significnatly different intrinsic OP^{DTT} values, the contribution of on-road vehicles to OP^{DTT} will depend upon the vehicle fleet makeup.

Table 7-1. Normalized mean biases of OP^{DTT} estimates using different source impacts at each measurement site.

	JST	GT	RS
OP^{DTT} from vehicles	-76%	-57%	-31%
OP^{DTT} from all sources	1.0%	47%	45%

7.4 Discussion

Generally, the intraurban spatial distribution of estimated vehicle-driven OP^{DTT} is greater than the variation observed in OP^{DTT} measurements, but the measurements incorporate OP^{DTT} from other sources, such as biomass burning, that are more spatially homogeneous than vehicle $PM_{2.5}$. Inclusion of fires, natural gas combustion, and regional sources in the OP^{DTT} estimates resulted in a more spatially homogeneous field with smaller ratios between urban and roadside observational sites. Nevertheless, there is still significant heterogeneity within Atlanta in the estimated OP^{DTT} fields that could lead to disproportionate exposures.

A source of uncertainty in the estimated OP^{DTT} fields (Figure 7-5) is the "total" vehicle intrinsic OP^{DTT} value averaged from gasoline and diesel emission estimates.

Different engines may produce $PM_{2.5}$ with significantly different OP^{DTT}, meaning the vehicle fleet composition will affect ambient OP^{DTT}. The vehicle impact on the spatial distribution of OP^{DTT} is further complicated by the different components of vehicle emissions. Metal emissions (e.g., copper from brake and tire wear) will be highest near the roadway, but photochemical aging of diesel $PM_{2.5}$ has been shown to increase OP^{DTT} due to quinone formation from poly aromatic hydrocarbons (PAHs), reducing the rapid decrease in OP^{DTT} away from roadways that would be expected from copper emissions (Antinolo et al., 2015; J. Bates, Fang, et al., 2018; McWhinney, Gao, Zhou, & Abbatt, 2011). Future work with OBS-RLINE and fused data focusing on individual diesel and gasoline sources and possibly spatially varying intrinsic OP^{DTT} estimates would be valuable to discerning the different impacts of each vehicle type on OP^{DTT} spatial distribution.

Furthermore, it should be noted that there are signficinatly more data at the JST site than the other two measurement locations. The limited OP^{DTT} measurements at each site do not incorporate each season at each location. Because OP^{DTT} varies temporally, with higher values in the winter than summer, the temporal correlations presented in this work may be affected by the lack of data. For example, during the GT measurement time period (July 2012 through August 2012) and RS measurement time period (September 2012 through October 2012 and January 2012 through February 2013), the correlations between JST measurements and OP^{DTT} estimates are -0.01 and 0.61, respectively, (compared to 0.59 during the JST measurement period) showing a significant difference for the GT measurement time period, i.e. the summer. The model-fused results may not capture temporal variability in OP^{DTT} as well in summer.

Overall, these results suggest that vehicles signficantly contribute to ambient OP^{DTT} at urban and roadside sites, and this model fusion approach with intrinsic OP^{DTT} values appears to accurately estimate OP^{DTT} at urban sites, though more measurement data would be useful for further evaluation. The model fused results overpredict OP^{DTT} at the roadside site possibly due to overestimation of intrinsic OP^{DTT} of the vehicle fleet by averaging gasoline and diesel intrinsic OP^{DTT}, assumption of a spatially static intrinsic OP^{DTT} for vehicle emissions, or high biases in OBS-RLINE estimated primary $PM_{2.5}$ on roadways. Nevertheless, OP^{DTT} is an area of research with growing interest and increasing evidence of epidemiologic relevance, so the modeling techniques presented in this work could provide useful tools for estimating ambient intraurban OP^{DTT} spatial concentration fields for exposure and epidemiologic analyses.

CHAPTER 8.

SUMMARY OF CONCLUSIONS AND FUTURE RESEARCH

8.1 Summary of Conclusions

The dissertation presents the development, application, and evaluation of models capable of simulating historical and regional spatiotemporal trends in OP^{DTT} of ambient $PM_{2.5}$ for epidemiologic and environmental justice studies. OP^{DTT} of daily ambient $PM_{2.5}$ was estimated from August 1, 1998 through December 31, 2010 at a measurement site in Atlanta, GA and from June 1, 2012 through July 30, 2013 across the eastern United States using multivariate regressions with two source apportionment techniques: the receptor model CMB and the chemical transport model CMAQ-DDM. Each of these source impact analyses found biomass burning and vehicles with both gasoline and diesel engines to significantly impact ambient OP^{DTT}. The estimated OP^{DTT} concentration fields across the eastern United States suggest widespread exposure to $PM_{2.5}$ sources with elevated OP^{DTT}, with populations in urban areas and near fires having highest exposures. Further, OP^{DTT} was found to be higher in the winter and spring in the southeastern United States due to increased prescribed burning.

The estimated OP^{DTT} historical time series in Atlanta, GA was used in an epidemiologic analysis that showed OP^{DTT} to have higher risk ratios for asthma/wheezing and congestive heart failure emergency department visits than $PM_{2.5}$ mass in both one- and two-pollutant models. These results provide epidemiologic evidence of a biologically plausible mechanism, oxidative stress, that may be responsible, in part, for specific

cardiorespiratory effects of $PM_{2.5}$ and that OP^{DTT} is a health-relevant property of $PM_{2.5}$ useful for future health research. Work performed globally corroborates these conclusions by presenting strong associations between OP^{DTT} and adverse health outcomes, such as microvascular function, asthma, and ischemic heart disease. OP_{SLF}^{GSH} has also been associated with adverse health outcomes, such as lung cancer, while no significant links between OP_{SLF}^{AA} or OP^{AA} and cardiorespiratory outcomes have been found. Therefore, OP^{DTT} and OP_{SLF}^{GSH} appear to be the acellular assays that capture the redox reactions most relevant to cardiorespiratory endpoints. The CMAQ-DDM modeling technique for OP^{DTT} presented in this dissertation can be useful for integrating future measurements of OP, including assays other than the DTT assay, and developing large-scale spatial fields of OP with limited observational data for future multi-city and/or regional epidemiologic analyses.

Additionally, two methods were developed for modeling fine-scale spatial fields of urban air pollutants, including $PM_{2.5}$, CO, NOx, and OP^{DTT}. First, a statistical model was developed under a Bayesian hierarchal framework to downscale daily 12km CMAQ using either fine scale (250m resolution) annual-averaged mobile source emission fields or primary roadway pollutant concentration fields from RLINE as land-use regression variables. The model was applied to estimate daily $PM_{2.5}$ at geocoded locations in Atlanta, GA in 2010. While the approach combining the raw emissions with CMAQ led to viable results, using the RLINE fields led to unphysical results with higher $PM_{2.5}$ concentrations in rural areas than on roadways. This phenomenon was linked to the limited observational data on which to train the model and the spatial correlations between the CMAQ and RLINE fields. In other words, the CMAQ fields captured sufficient spatial variation in

$PM_{2.5}$ concentration so that the RLINE and CMAQ data spatially covaried. The CMAQ inputs also provided temporal data, while the RLINE data was temporally static, driving the model to rely more heavily on the CMAQ data and estimate a negative coefficient for RLINE.

Model fusion methods were also developed and applied to estimate daily 24 h averaged $PM_{2.5}$, 1 h maximum NOx, 1 h maximum CO, and 24 h averaged OP^{DTT} at a 250m resolution in Atlanta, GA. The model fusion methods used linear combinations of CMAQ and RLINE to develop concentration fields at a fine spatial resolution without sacrificing chemical formation and regional emissions, which can be a large component of pollutants like $PM_{2.5}$ in the southeastern United States. Two approaches were developed to fuse CMAQ and RLINE due to model biases: an additive method that was applied to $PM_{2.5}$ and a multiplicative method that was applied to NOx, CO, and OP^{DTT}. The model fusion estimates for $PM_{2.5}$, NOx, and CO in Atlanta showed high concentrations on and near roadways, decreasing rapidly with distance from roads with spatial gradients in line with observations. Model fusion estimates had higher spatial and temporal correlations with observations than CMAQ and RLINE, suggesting that these methods have potential for creating air pollutant concentration estimates with minimal biases for exposure and epidemiologic analyses. These fine scale data could be useful for assessing disproportionate pollutant exposures within an urban area and are currently being used in city planning, environmental justice, and health analyses. The speed of these model fusion algorithms allow rapid application to long time series of data and the flexibility of these methods allows application to other model inputs, pollutants, and study areas.

The multiplicative model fusion method was applied to estimate within-city spatial variation of OP^{DTT} of ambient $PM_{2.5}$ in Atlanta, GA from June 2, 2012 through July 30, 2013. The model fusion method used daily CMAQ-DDM $PM_{2.5}$ on-road vehicle source impacts (gasoline and diesel) and annual-averaged primary $PM_{2.5}$ from RLINE to estimate total (primary and secondary) on-road vehicle-related $PM_{2.5}$ at a 250m resolution in Atlanta, GA. This on-road $PM_{2.5}$ impact was multiplied by an estimate of intrinsic OP^{DTT} from vehicles to estimate intraurban spatial variation of vehicle-driven OP^{DTT}. This result was then added to OP^{DTT} estimates of other sources found to significantly impact OP^{DTT}, including fires, natural gas combustion, and regional sources, that were calculated by multiplying their source-specific intrinsic OP^{DTT} values by their $PM_{2.5}$ contributions linearly interpolated to a 250m spatial resolution. The intraurban spatial fields of OP^{DTT} are relatively spatially uniform due to source impacts like biomass burning and regional sources, but there are peaks on roadways driven by vehicle emissions. High spatial correlations between OP^{DTT} and RLINE or model-fused vehicle $PM_{2.5}$ imply that vehicle concentrations can potentially be used to estimate small-scale spatial variations in OP^{DTT}. A small bias in OP^{DTT} estimates at an urban site but a high bias in OP^{DTT} estimates at a roadway site imply overestimation of OP^{DTT} near roadways possibly due to biased-high RLINE $PM_{2.5}$ results, a need for separate intrinsic values for gasoline and diesel vehicles, or an overestimation of intrinsic OP^{DTT} values. The intrinsic OP^{DTT} of vehicle emissions increases with photochemical aging, so assuming a static intrinsic OP^{DTT} of vehicles may overestimate the impact of primary emissions from traffic. Nevertheless, this research presents the first insight into within-city variation of ambient OP^{DTT} in Atlanta driven by

vehicles and this model fusion method provides a solid foundation for future work investigating small-scale spatial variations of OP for health analyses.

Overall, the models developed in this dissertation as well as their associated spatiotemporal fields of air pollutant concentrations can be valuable tools for future epidemiologic, environmental justice, and city planning studies wanting to develop exposure data using information beyond the limited observational data available.

8.2 Future Research

8.2.1 OP^{DTT} measurements for further evaluation of source impact results

Because biomass burning was found to be a significant contributor to ambient OP^{DTT} in the southeastern United States, fires may be a major focus of future health research. With decreasing vehicle emissions, biomass burning is becoming an increasing fraction of OP^{DTT} (Figure 8-1), making exposure to biomass burning a growing concern.

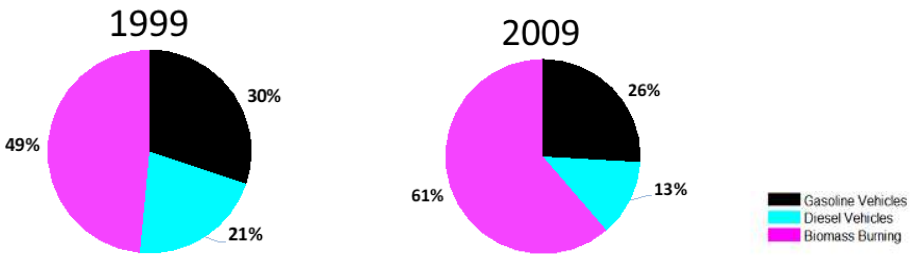

Figure 8-1. Annual average contributions to apportioned OP^{DTT} in Atlanta, GA for 1999 (left) and 2009 (right).

Heavily populated cities may be significantly impacted by health-related particulate matter from fires if aging increases OP^{DTT} as the fire impacts that hit cities often have travelled far and aged significantly. OP^{DTT} measurements in and downwind of fire

plumes would be useful for assessing the change in toxicity over time and if population exposures in urban areas should be a concern. Such studies could investigate the interaction of fire plumes with anthropogenic emissions and how the resulting chemistry alters the OP of the resulting particulate matter. Additionally, OP^{DTT} measurements in and near fires could also be used to further evaluate the CMAQ-DDM-estimated spatiotemporal fields of OP^{DTT} presented in chapter 4. In that work, wildfires and prescribed burning were the major driver of the spatial variation in OP^{DTT} across the eastern United States, but these fires may not have impacted the OP^{DTT} measurement sites from which the observational data was gathered to train the model. Having OP^{DTT} measurements in and near fires would help assess if the high OP^{DTT} estimates near fires produced using CMAQ-DDM modeling are within reason.

OP^{DTT} measurements of ambient $PM_{2.5}$ outside of the southeastern United States could also be useful in evaluating the eastern United States OP^{DTT} spatial fields presented in chapter 4 and for adjusting these fields using data assimilation techniques, OP^{DTT} measurements across multiple sites in Atlanta, GA could be used to further evaluate results presented in chapter 7. Measurements could be used to test the assumption that a regression trained on data from only four OP^{DTT} measurement sites in the southeastern United States can be applied across the entire eastern United States. In other words, OP^{DTT} measurements in northern states, like Illinois, could be used to evaluate the hypothesis that source-specific intrinsic OP^{DTT} values are similar across the United States, if not globally. Furthermore, any additional OP^{DTT} measurements could be integrated into the model development process presented in chapter 4. More observations would increase the size of the model training data set and improve upon the robustness of the model. Especially useful would

be measurements near localized emissions, like residential burning and construction sites with heavy diesel truck impacts, that may not be represented at the OP^{DTT} measurement sites used in chapter 4. There is growing interest in OP in Europe, Canada, China, and elsewhere, and OP^{DTT} measurements globally could be used in a similar fashion to the method presented in chapter 4 to model OP^{DTT}, or other OP assays, in other regions.

Each source-impact model developed in this dissertation has large intercepts, suggesting model misspecification and possibly missing sources. As described in chapter 3, the intercept could be driven by artifacts that condensed on the OP^{DTT} filters but not on the filters collected post-denuder used for speciated measurements in CMB. Future measurements of OP^{DTT} on both filters collected using denuded and non-denuded systems could be used to test this hypothesis while providing evidence of whether volatile organic species are OP^{DTT}-active or not.

Another area of interest for future work would be collecting total OP^{DTT} data, rather than water-soluble OP^{DTT} data. The models developed in chapters 3 and 4 related $PM_{2.5}$ source impacts to water-soluble OP^{DTT} to derive source-specific intrinsic OP^{DTT} values. These intrinsic values assume that the ratio of water-soluble OP^{DTT} to total $PM_{2.5}$ is constant. Using total OP^{DTT} measurements to train the models would build upon our knowledge on the relationship between OP^{DTT} and source impacts, though water-soluble results may be more relevant to health.

8.2.2 Updated Source Impact Analysis

The distinction between intrinsic OP^{DTT} of diesel and gasoline vehicles is uncertain and differs between the CMB and CMAQ-DDM approaches presented in chapters 3 and 4.

The CMAQ-DDM method estimates a larger contribution from diesel vehicles than gasoline vehicles while the CMB method predicts a larger contribution from gasoline vehicles than diesel vehicles in Atlanta, GA. It would be useful to update the CMB profiles using speciated data collected more recently than 2001 and 2002 (the time period that the source profiles used in chapter 3 were developed for). If the profiles for gasoline and/or diesel changed significantly from 2003 to the present, the intrinsic OP^{DTT} of vehicles may also have changed. These updated profiles could be used to re-run the analysis in chapter 3 to determine if the impacts of gasoline and/or diesel vehicles on OP^{DTT} have changed over time.

The impacts of secondary concentrations versus primary emissions on OP^{DTT} are also of increasing interest. As sources and organic species age, their intrinsic OP^{DTT} values increase. A CMAQ-DDM approach with multivariate regression, like presented in chapter 4, may be useful in modeling this phenomenon. The organic carbon component of each source identified by CMAQ-DDM can be separated into primary and secondary organics. These components could then be used as separate independent variables in the OP^{DTT} source impact model, resulting in individual coefficients (i.e., intrinsic OP^{DTT} estimates) for primary and secondary organic carbon for each source. Also, certain species, like ammonium sulfate or ozone, can be used as markers of photochemical activity and/or age of pollutants. Integrating an "aging" term in the OP^{DTT} source impact model may improve performance and minimize the intercept. Introducing a seasonal variable may provide insight into the causal link (or lack thereof) between natural gas combustion and OP^{DTT} and may reduce the intercept.

8.2.3 *Integrating new measurements and updated modeling for intraurban pollutant concentration estimates*

One major limitation of the statistical downscaling model presented in chapter 5 is the lack of observational data on which to train the model. However, since the time of the original model evaluation, additional near-road monitoring sites have been established in the Atlanta area that could be used in the model training data set. Further, RLINE could be run on a daily basis, rather than an annual-average basis, and then input to the statistical downscaler. Providing temporally variable fine-scale data may potentially alleviate the problem of the statistical downscaler relying too heavily on CMAQ. Further, the statistical downscaler was applied to $PM_{2.5}$, a relatively spatially homogeneous pollutant. CMAQ can capture the spatial variation in $PM_{2.5}$ with 12km grids but may not be able to capture the spatial patterns of more heterogeneous pollutants, like NOx and CO. Applying the statistical downscaler to a more heterogeneous pollutant may result in RLINE becoming more informative in the model and lead to more realistic results. The existing model framework could also be adjusted to have spatially and temporally varying regression coefficients for RLINE, rather than the current fixed-effect regression coefficients that are used for land-use variables, that could minimize spatial biases in RLINE (especially high biases on roadways). Non-linear relationship terms may also be introduced as previous work has shown that calibrating RLINE with CMB-derived source impacts using monitor data is best done with non-linear fits (Zhai et al., 2016).

The model fusion methods for estimating intraurban spatial fields of OP^{DTT} in Atlanta, GA presented in chapter 7 relied upon RLINE data that used emissions from the total vehicle fleet, including gasoline and diesel vehicles, and an intrinsic OP^{DTT} value that

had been averaged between diesel and gasoline estimates. Future work running RLINE with separate gasoline and diesel emissions would improve upon the estimates produced in chapter 7 as these two engine types have different intrinsic OP^{DTT} values. The model fusion method could be run twice in Atlanta, GA, once for diesel and once for gasoline vehicles, then multiplied by their respective intrinsic OP^{DTT} values and added together. This update could be especially important around the Downtown Connector, where the vehicle fleet is dominated by gasoline engines, and I-285, a major route for diesel 18-wheelers. Further, the OP^{DTT} estimates and CMAQ-DDM results used in the model fusion process are from 2012 through 2013, but the RLINE data was only available for 2011 at the time of the study. The gasoline and diesel RLINE impacts could be run for 2012 and 2013 to match the CMAQ-DDM and OP^{DTT} data sets. Finally, a static intrinsic OP^{DTT} value was used in the work presented in chapter 7. However, it has been shown that photochemical aging and exposure to ozone increases OP^{DTT} of diesel exhaust. Flexible intrinsic OP^{DTT} values that change with distance from roadway and/or ozone concentration may improve intraurban OP^{DTT} estimates. Near-roadway intrinsic OP^{DTT} estimates could be obtained by applying the method developed in chapter 3 using CMB source impact analysis with urban OP^{DTT} data to roadside OP^{DTT} data.

8.2.4 Global OP research initiatives

Current research suggests that the DTT assay and glutathione assay in surrogate lung fluid (GSH_{SLF}) are the most relevant acellular OP assays for health outcomes, while the ascorbic acid assay, no matter if SLF is used or not, has no association with adverse cardiorespiratory outcomes. Because OP^{DTT} is significantly impacted by organic species, but it does not appear that OP^{AA} is, the cumulative health study results may suggest that

organic species play a significant role in cardiorespiratory impacts due to PM-mediated oxidative stress, a hypothesis worthy of future research. Additionally, the utility of SLF in OP assays, or if direct assessment of OP from filters is sufficient for health associations, may be an area for future review. Additional epidemiologic studies to confirm the relationship between OP and cardiorespiratory endpoints, as well as to explore other health outcomes that are known to be affected by particulate matter exposure, such as birth defects, would be useful to further asses the oxidative stress hypothesis of particulate matter, determine the utility of OP in health studies, and improve our understanding on the relationship between particulate matter and health.

APPENDIX A.

SUPPLEMENTAL MATERIAL FOR CHAPTER 3

To correct for temporal misalignment between DTT measurements collected from 12 pm (noon) to 11 am and source impact estimates from midnight to midnight, the sources identified were scaled by fixed ratios. For example, suppose total $PM_{2.5}$ used for source impact estimation was measured from midnight to midnight on day 1 on filter 1 and from midnight to midnight on day 2 on filter 2. The filter used to measure DTT activity of WS-$PM_{2.5}$ was collected from noon on day 1 to 11 am on day 2 on filter 3. To achieve a measurement of total $PM_{2.5}$ from noon to 11 am matching the filter collection period of filter 3, we would multiply $12/24*PM_{2.5\_filter1} + 11/24*PM_{2.5\_filter2}$, making the total weighting $23/24*PM_{2.5}$ to match the 23-hr integrated samples of WS-$PM_{2.5}$ DTT activity.

Table A-1. Coefficients, standard errors (in parentheses) and *p* values for the DTT regression with all sources and for the regression with only sources that have statistically significant coefficients used to create the historical DTT estimates for the epidemiologic study.

	Intercept	**LDGV**	**HDDV**	**SDUST**	**BURN**	**AMSULF**	**AMBSLF**	**AMNITR**	**OTHER_OC**
Coefficients	0.004	0.12	0.051	0.017	0.061	0.032	0.0072	0.014	0.007
nmol min^{-1} μg^{-1}	(0.028)	(0.023)	(0.029)	(0.015)	(0.013)	(0.0095)	(0.017)	(0.018)	(0.010)
p values	0.90	<0.01	0.084	0.26	<0.01	<0.01	0.67	0.45	0.53
Coefficients	0.066	0.12	0.061		0.074				
nmol min^{-1} μg^{-1}	(0.021)	(0.022)	(0.025)	-	(0.010)	-	-	-	-
p values	<0.01	<0.01	0.018	-	<0.01	-	-	-	-

Table A-2. Pearson correlation coefficients between volume normalized DTT (DTTv, nmol min^{-1} m^{-3}) and species concentration and mass normalized DTT (DTTm, nmol min^{-1} μg^{-1}) and species concentration measured from June 2012 – April 2013.

	Total $PM_{2.5}$	SO_4^{2-}	NO_3^-	NH_4^+	EC	OC	Al	Ca	Cu	Fe	K	Mn	Pb	Si	Ti	Zn
DTTv	0.56	0.33	0.30	0.44	0.54	0.49	0.05	0.27	0.50	0.39	0.51	0.36	0.34	0.14	0.12	0.52
DTTm	-0.25	-0.34	0.22	-0.02	-0.03	-0.22	0.09	0.42	0.20	0.35	0.14	0.32	0.11	0.23	0.17	0.24

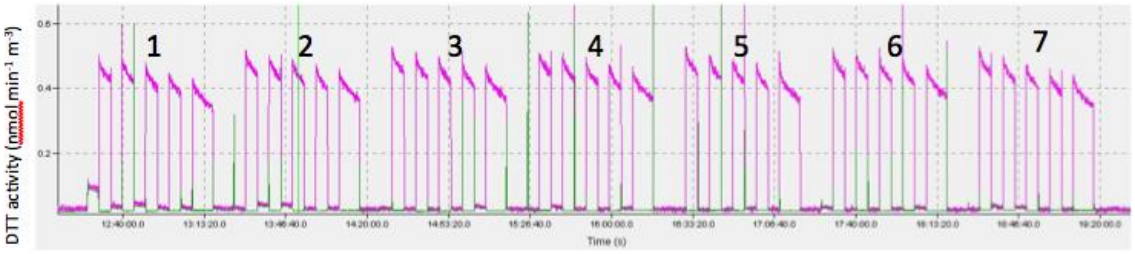

Figure A-8-2. Results from an experiment comparing the DTT activity of a blank filter (filter 1) to filters with water-soluble sulfate (filters 2-7) showing that there is no significant difference between the blank filters and water-soluble sulfate filters.

APPENDIX B.

SUPPLEMENTAL MATERIAL FOR CHAPTER 4

Table B-1. A description of each of the 16 emission source categories used in the CMAQ-DDM modeling.

Source	Description of Included Source Categories
Agriculture	Industrial processes and miscellaneous area sources: food and agriculture, agricultural production (livestock and crops), eggs and poultry production, manure handling, beef cattle feedlots, fertilizer application, domestic and wild animal waste emissions, country grain elevators
Aircraft	Mobile sources, miscellaneous area sources, and internal combustion engines: aircraft, aircraft/rocket engine firing and testing, fixed and rotary wing aircraft L & TO Exhaust
Biogenic	Primary and secondary biogenic PM resulting from volatile organic carbon (VOC) emissions from vegetation and nitrogen oxide (NO) emissions from soil estimated from the Biogenic Emissions Inventory System (BEIS) in SMOKE coupled with CMAQ to use WRF meteorology

Table B-1 continued

Coal	External combustion boilers, industrial processes, stationary source fuel combustion, waste disposal: electric generation with coal (anthracite, bituminous/subbituminous, lignite, waste coal), commercial units, space heaters, residential units, government solid waste disposal
Dust	Industrial processes, miscellaneous area sources, mobile sources, and waste disposal: construction, paved and unpaved roads, agricultural production of crops, paved and unpaved haul roads with gasoline and diesel traffic at industrial, landfill and construction sites, demolitions
Fire	Waste disposal, treatment, and recovery and miscellaneous area sources: open burning, agricultural field burning, forest wildfires, managed burning (logging debris), prescribed burning for forest management, prescribed burning on rangeland
Fuel Oil	External combustion boilers, internal combustion engines, stationary source fuel combustion, and industrial processes (residual oil, distillate oil): electric generation, oil and gas production, commercial/institutional units, space heaters, residential units, engine testing, chemical manufacturing plants, food and agricultural equipment, metal production equipment, mineral production equipment, process heaters, flares, pulp and paper mill equipment, rubber and plastic production equipment, miscellaneous manufacturing industrial equipment,

Table B-1 continued

Metal	Industrial processes and miscellaneous area sources: primary and secondary metal production, fabricated metal products, repair shops, welding repair shops
Natural Gas Combustion	External combustion boilers, internal combustion engines, industrial processes, petroleum and solvent evaporation, waste disposal, stationary source fuel combustion: electric generation, industrial processes, oil and gas production, commercial/institutional units, space heaters, engine testing, chemical manufacturing equipment, food and agriculture equipment, metal production equipment, mineral production equipment, petroleum industry (process heaters, flares, incinerators), pulp and paper and wood production equipment, rubber and plastic production equipment, surface coating operational equipment, organic solvent evaporation equipment, miscellaneous manufacturing industrial equipment (heaters, incinerators, and flares), solid waste disposal (government, commercial/institutional, and industrial)
Non-road Diesel	Mobile sources and internal combustion engines: off-highway diesel vehicles, marine vessels, pleasure craft, military marine vessels, diesel railroad equipment, diesel industrial equipment (fork lifts)
Non-road Gasoline	Mobile sources: off-highway gasoline vehicles, marine vessels, pleasure craft, gasoline railroad equipment

Table B-1 continued

On-road Diesel	Mobile sources: Highway diesel vehicles
On-road Gasoline	Mobile sources: Highway gasoline vehicles
Wood burning	Waste disposal, external combustion boilers, industrial processes, stationary source fuel combustion: solid waste incineration, trench burner for wood, firefighting, wood pallet burning, open burning of wood solid waste at commercial/institutional sites, electric generation with wood/bark waste, space heaters, in-process wood fuel use at industrial facilities, wood boilers for electric utility, industrial sites, and commercial/institutional facilities, residential wood burners
Seasalt	Estimated from PM sodium and chloride concentrations
Other	All remaining emission sources

Table B-2. Normalized mean biases in $PM_{2.5}$ species after bias correction algorithms and temporal interpolation have been applied. Biases presented in the table are averaged over all CSN and SEARCH sites (146 sites) across the eastern United States and across the OP^{DTT} measurement sites (4 sites).

	$PM_{2.5}$	**OC**	**EC**	**NO_3^-**	**NH_4^+**	**SO_4^-**	**Na**	**Al**	**Si**	**K**	**Ca**	**Ti**	**Mn**	**Fe**	**Cu**	**Zn**	**Pb**
CSN and SEARCH sites	-0.05	0.01	0.27	0.01	0.01	0.00	0.14	0.62	0.90	0.31	0.92	1.34	-0.28	-0.26	0.40	0.41	-0.60
OP^{DTT} measure-ment sties	-0.02	-0.01	0.17	0.17	-0.05	-0.01	0.16	-0.36	0.17	0.20	1.63	1.20	-0.19	0.00	0.61	0.58	-0.68

Table B-3. Pearson's linear correlation coefficients between CMAQ-DDM source impacts used in regression development.

	AC	AG	BI	CL	DU	FI	FO	MT	NAT	OG	NG	OD	ND	OT	SS	WO
AC	1	-0.03	0.14	-0.02	0.07	0.12	-0.02	0.18	0.14	-0.02	0.13	0.14	0.06	0.26	0.08	-0.09
AG		1	-0.38	0.13	-0.20	0.08	0.00	0.13	0.50	0.30	0.17	0.42	0.17	-0.22	0.16	0.26
BI			1	0.10	0.22	-0.10	0.18	0.08	-0.30	0.00	0.33	0.01	0.07	0.43	-0.21	-0.32
CL				1	-0.12	0.04	0.40	0.36	0.30	0.19	0.38	0.38	0.41	0.07	0.02	0.11
DU					1	0.03	-0.18	-0.10	-0.14	-0.09	-0.04	0.03	-0.02	0.12	-0.10	-0.10

Table B-3 continued

FI	1	0.02	-0.09	0.16	0.11	-0.06	0.19	0.11	0.15	0.22	0.00
FO		1	0.15	0.10	0.16	0.25	0.11	0.13	0.25	0.01	-0.11
MT			1	0.22	0.08	0.42	0.24	0.21	0.10	-0.11	0.06
NAT				1	0.28	0.15	0.39	0.39	-0.03	0.23	0.41
OG					1	0.34	0.43	0.41	0.07	0.17	0.16
NG						1	0.52	0.60	0.32	-0.05	-0.01
OD							1	0.69	0.27	0.13	0.23
ND								1	0.26	0.05	0.24
OT									1	-0.03	-0.03
SS										1	0.22
WO											1

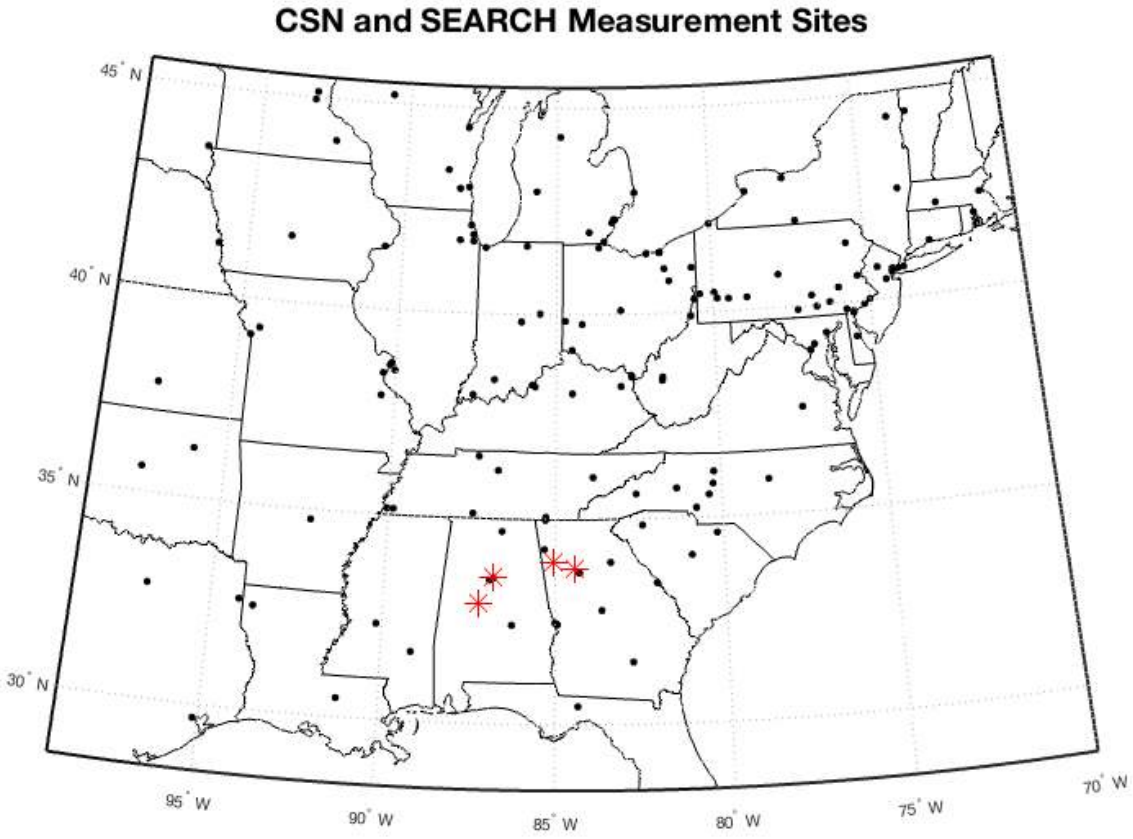

Figure B-1. Locations of CSN and SEARCH monitoring sites within the study domain whose data were used to minimize bias in CMAQ-DDM estimates. CSN sites are represented as black dots and SEARCH sites are represented as red asterisks. SEARCH site locations are also where OP^{DTT} measurement sites are.

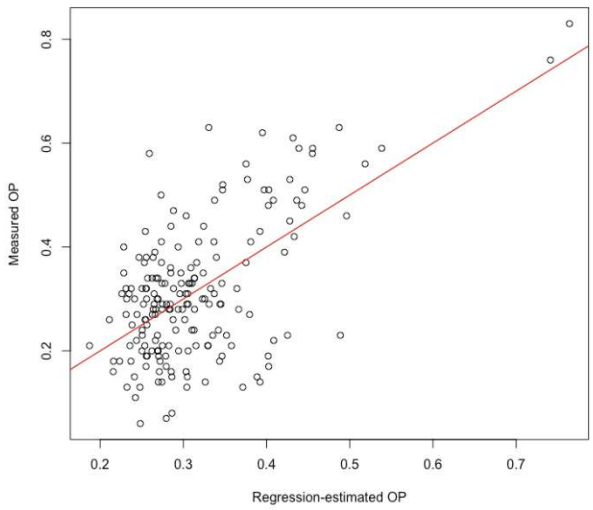

Figure B-2. Measured OP^{DTT} versus regression-estimated OP^{DTT} with the 1:1 line in red.

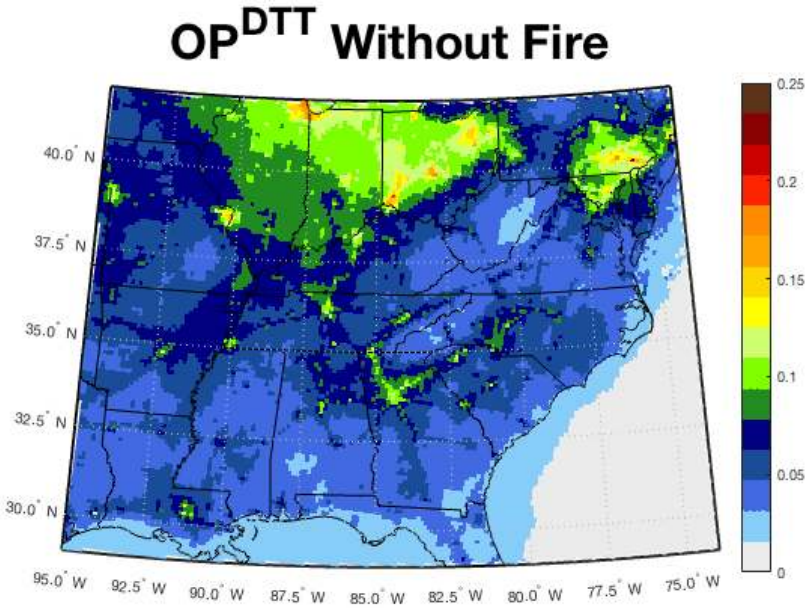

Figure B-3. OP^{DTT} driven by natural gas combustion, on-road diesel, and on-road gasoline (no fire impacts) averaged from June 2012 to July 2013.

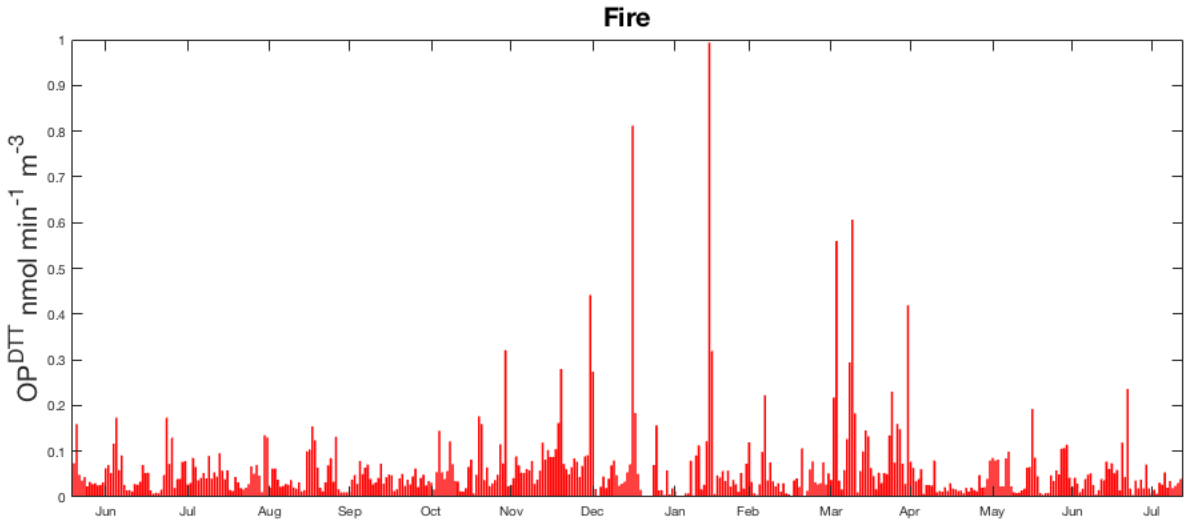
Fire
OP^DTT nmol min^-1 m^-3
0
0.1
0.2
0.3
0.4
0.5
0.6
0.7
0.8
0.9
1
Jun
Jul
Aug
Sep
Oct
Nov
Dec
Jan
Feb
Mar
Apr
May
Jun
Jul

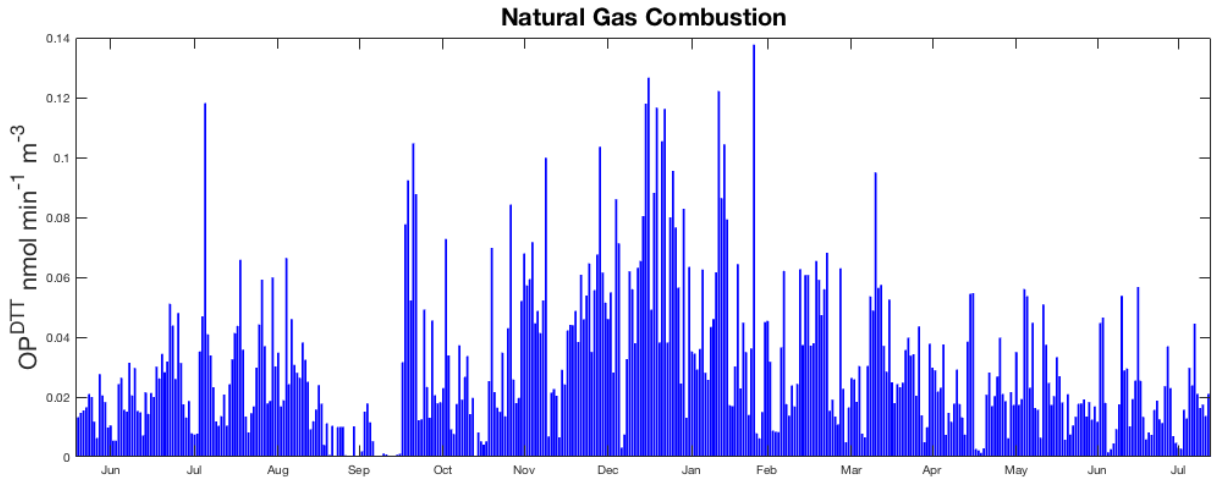
Natural Gas Combustion
OP^DTT nmol min^-1 m^-3
0
0.02
0.04
0.06
0.08
0.1
0.12
0.14
Jun
Jul
Aug
Sep
Oct
Nov
Dec
Jan
Feb
Mar
Apr
May
Jun
Jul

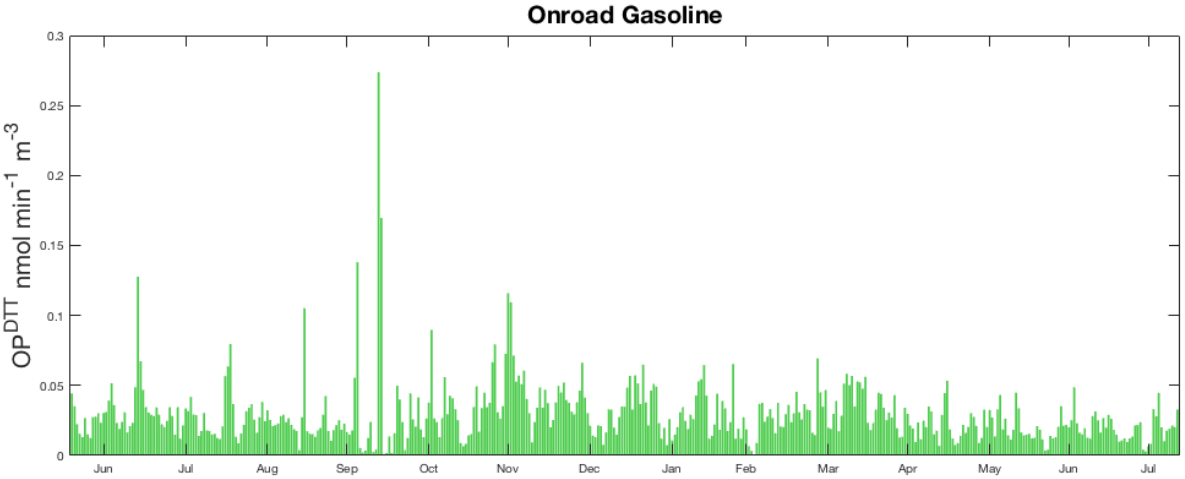
Onroad Gasoline
OP^DTT nmol min^-1 m^-3
0
0.05
0.1
0.15
0.2
0.25
0.3
Jun
Jul
Aug
Sep
Oct
Nov
Dec
Jan
Feb
Mar
Apr
May
Jun
Jul

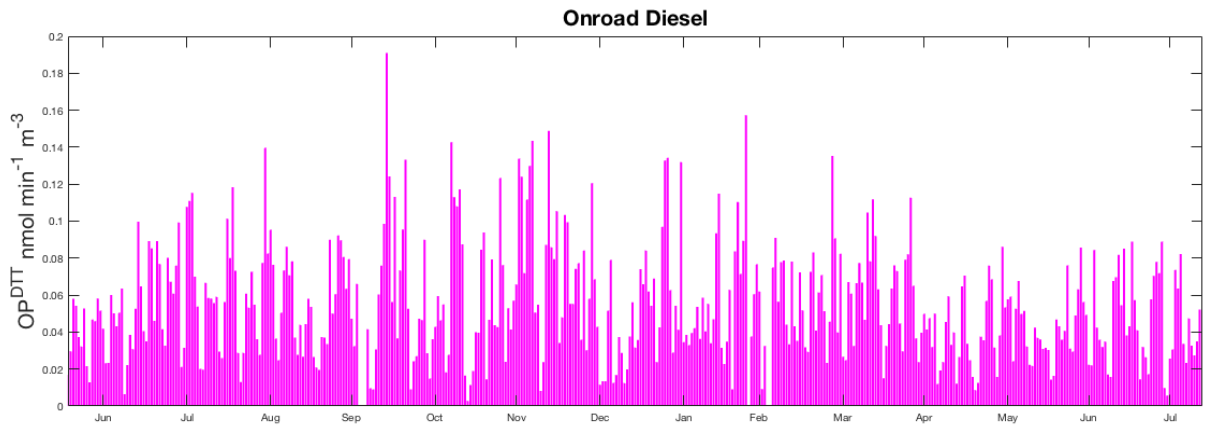

Figure B-4. Temporal trends in source impacts on estimated OP^{DTT} at the Atlanta, GA measurement site. Note: The plots are on different y-scales to show daily variations in OP^{DTT}.

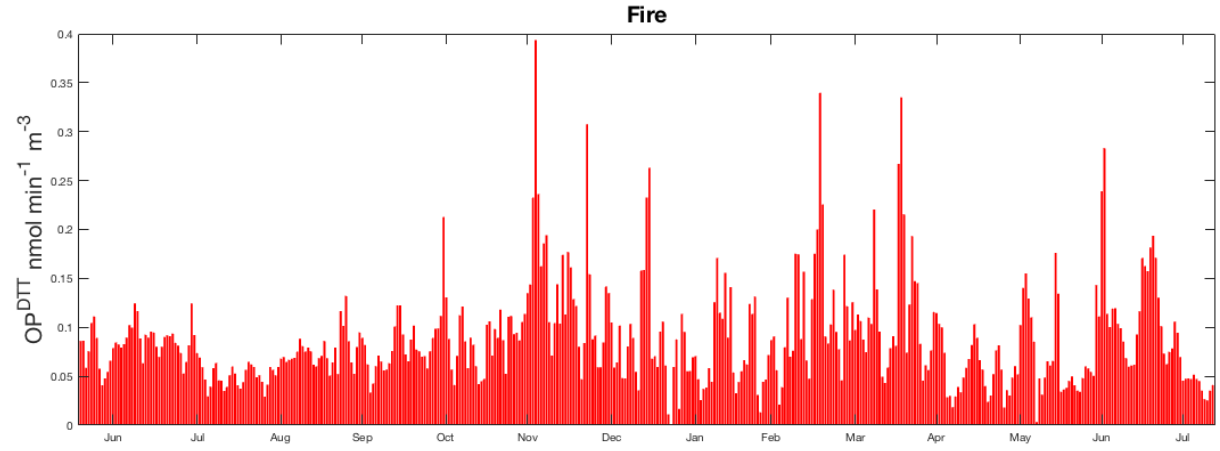

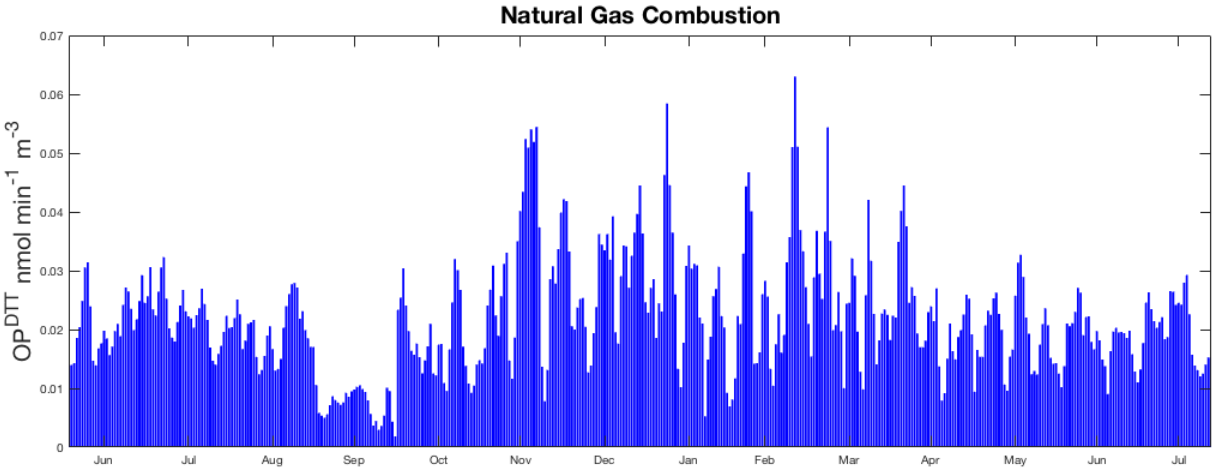

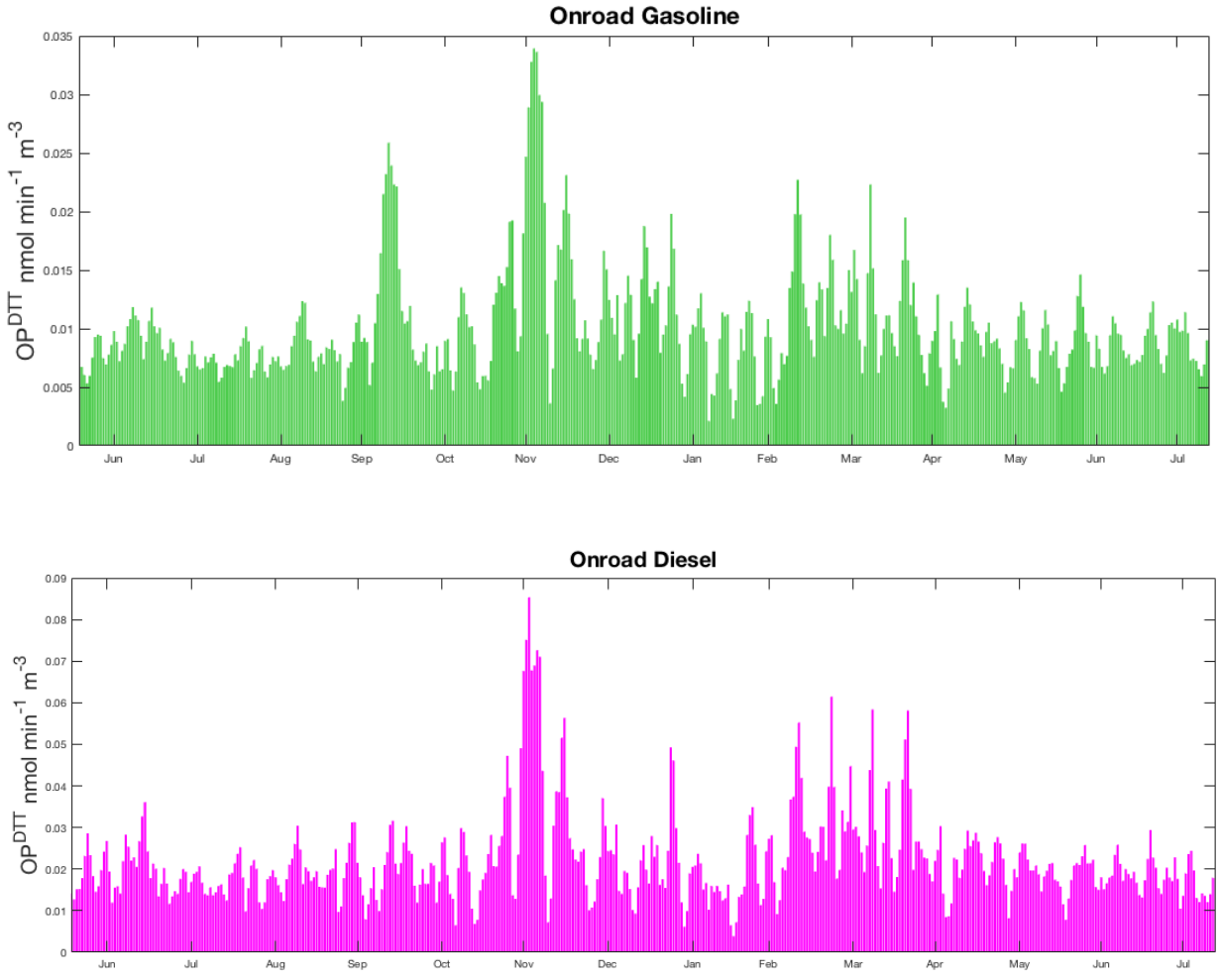

Figure B-5. Temporal trends in source impacts on estimated OP^{DTT} across the modeling domain. Note: The plots are on different y-scales to show daily variations in OP^{DTT}.

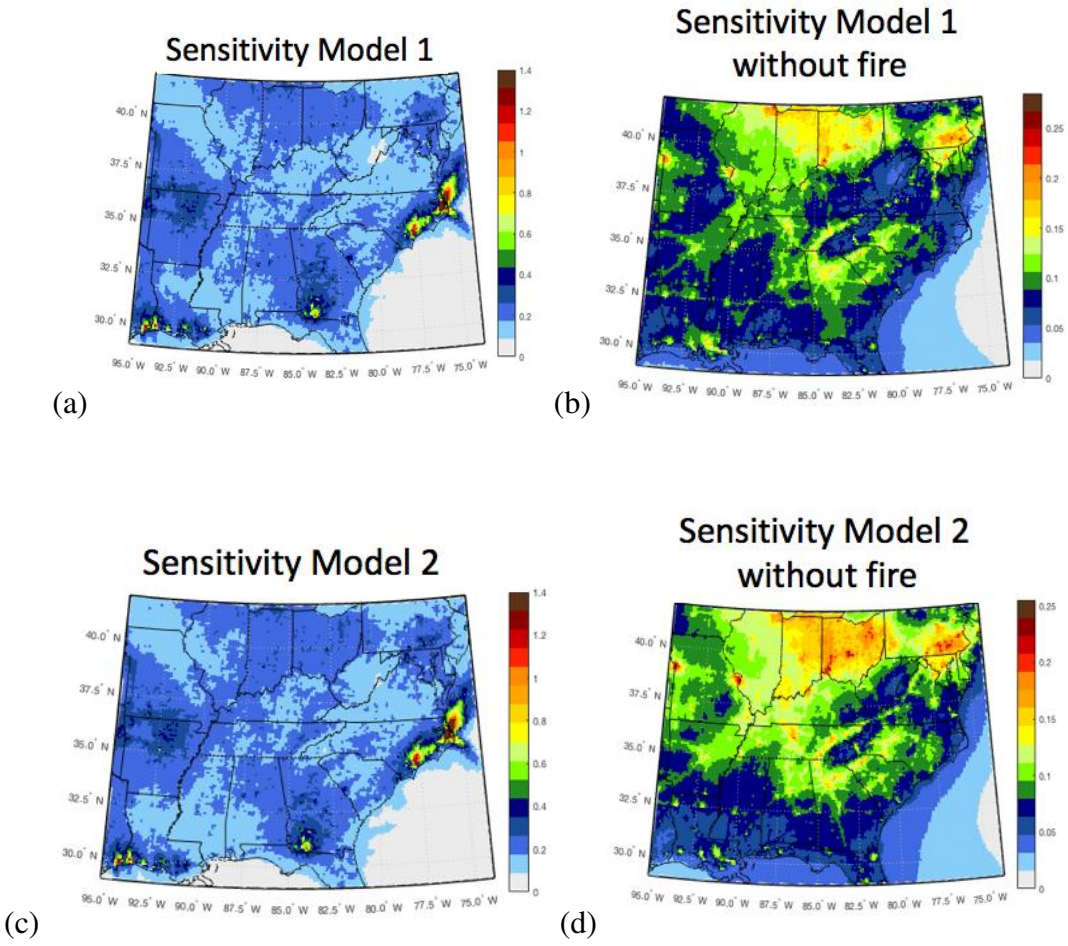

Figure B-6. OP^{DTT} estimated using source impacts and coefficients in sensitivity models 2 ((a) and (b)) and 3 ((c) and (d)), with ((a) and (c)) and without ((b) and (d)) fire impacts to see the spatial distributions without large concentrations from wildfires.

APPENDIX C.

SUPPLEMENTAL MATERIAL FOR CHAPTER 6

When applying the additive method to 1 h maximum CO and NOx, it was found that the method produced negative values at a small amount of 250m grid cells on certain days. For daily estimates during 2005, 49 and 259 days for CO and NOx, respectively, produced at least one negative value in the final results, with a maximum of 15% of the 329,472 grid cells over Atlanta below zero. These negative values are driven by the fact that the 12km average of OBS-RLINE is higher than the 12km OBS-CMAQ at certain locations, driving negative background concentrations. At specific locations, OBS-RLINE can be biased high when wind direction aligns with a link of emissions and OBS-CMAQ can be biased low if vertical diffusion occurs too rapidly. Specifically for 2005 annual average results, 36 and 75 out of 143 urban background grid cells for CO and NOx, respectively, were below zero after the subtraction step (CTM- $\overline{DISP}_{\text{coarse}}$), implying, unrealistically, that 25% and 52% of the urban background concentrations for CO and NOx, respectively, were negative. This negative urban background is then interpolated and added to 250m RLINE, which are not high enough to bring the estimates above zero at some grid locations.

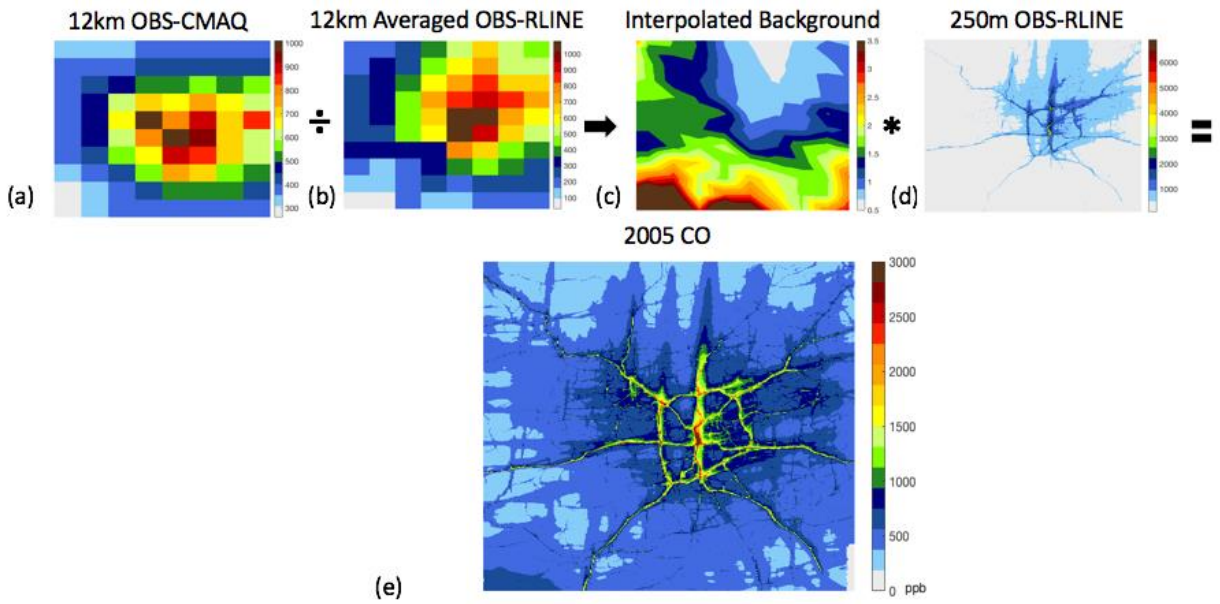

Figure C-1. Multiplicative model fusion steps and results for 2005 annual average CO. First, the fine resolution (250m) OBS-RLINE field is averaged to a 12km grid matching the OBS-CMAQ grid (b). OBS-CMAQ 12km field (a) is divided by the 12km OBS-RLINE (b). These results are spatially interpolated to 250m resolution matching the OBS-RLINE grid resolution (c) and then multiplied by the 250m resolution OBS-RLINE field (d) to provide a 250m resolution model-fused annual average CO field (e). Note: each plot has a different color scale in order to show the spatial distribution clearly.

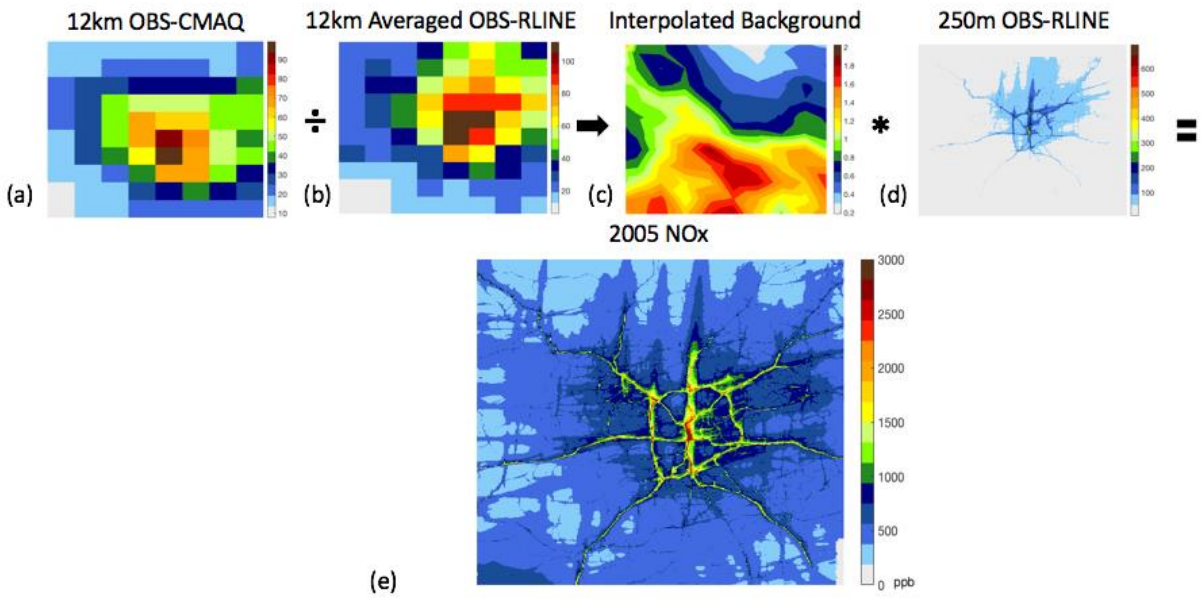

Figure C-2. Multiplicative model fusion steps and results for 2005 annual average NOx. First, the fine resolution (250m) OBS-RLINE field is averaged to a 12km grid matching the OBS-CMAQ grid (b). OBS-CMAQ 12km field (a) is divided by the 12km OBS-RLINE (b). These results are spatially interpolated to 250m resolution matching the OBS-RLINE grid resolution (c) and then multiplied by the 250m resolution OBS-RLINE field (d) to provide a 250m resolution model-fused annual average NOx field (e). Note: each plot has a different color scale in order to show the spatial distribution clearly.

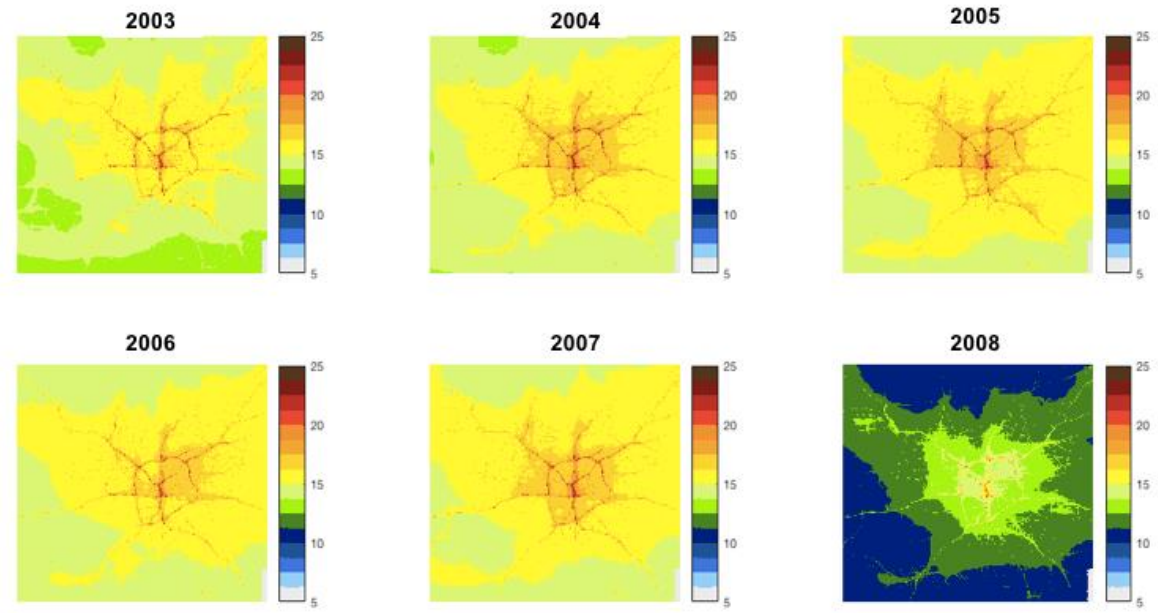

Figure C-3. Annual average $PM_{2.5}$ concentrations ($\mu g/m^3$) estimated using the additive model fusion process for each year of the study period (2003 through 2008).

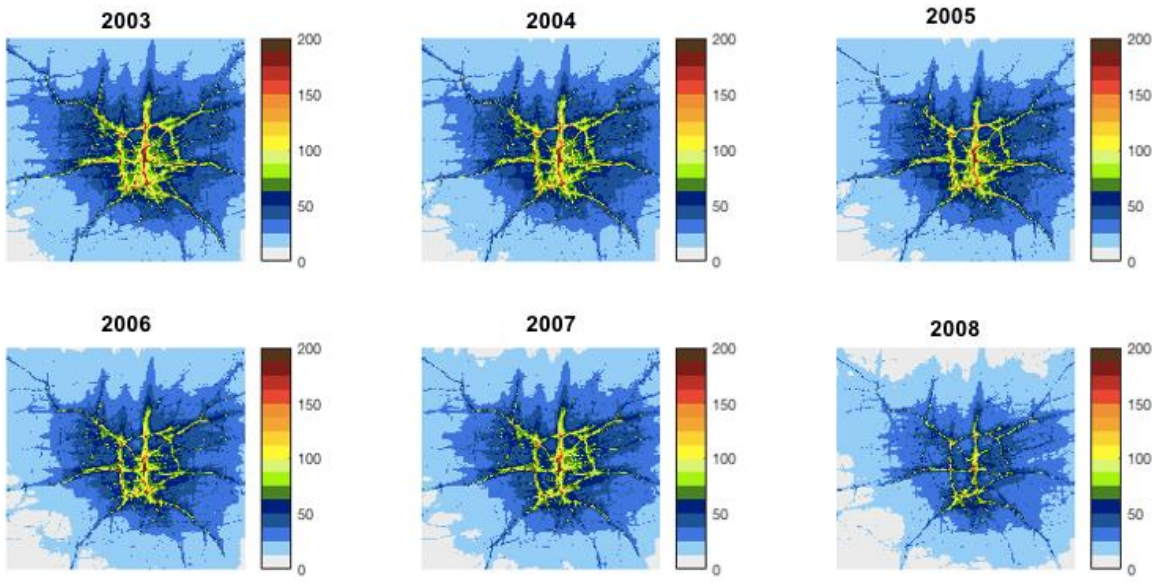

Figure C-4. Annual average 1-hr maximum NOx concentrations (ppb) estimated using the multiplicative model fusion process for each year of the study period (2003 through 2008).

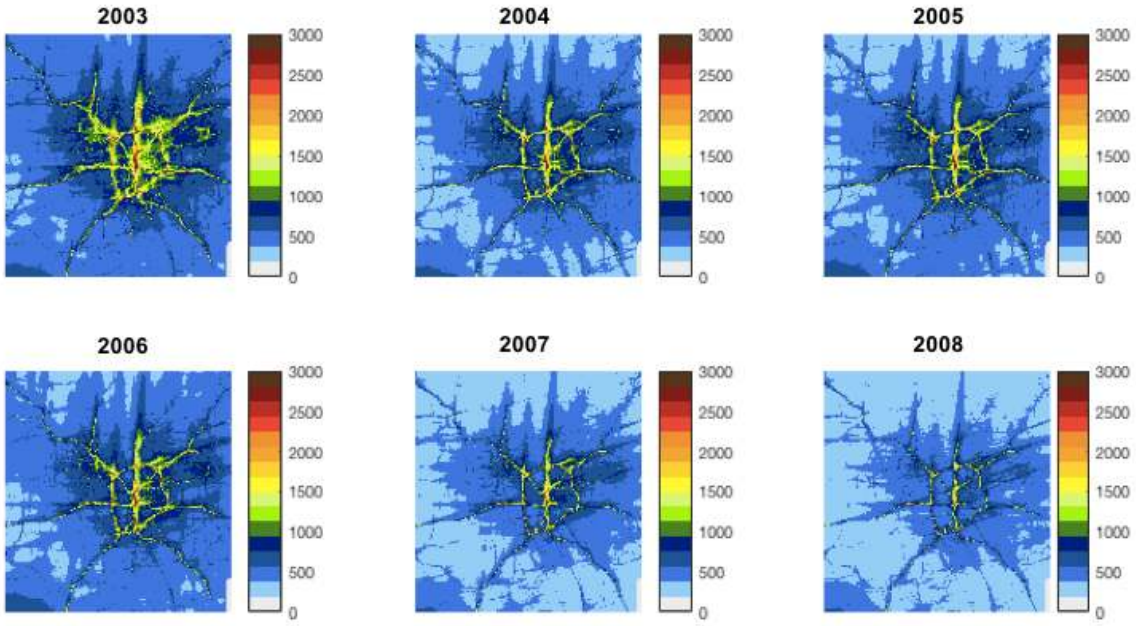

Figure C-5. Annual average 1-hr maximum CO concentrations (ppb) estimated using the multiplicative model fusion process for each year of the study period (2003 through 2008).

Table C-1. Monitor information, including network names, whether the monitor is located in an urban or rural location, and years that data are available. If there is no month listed, data are available for the entire year.

Species	*Site Name*	*Network(s)*	*Location type*	*Years Available*
$PM_{2.5}$	JST	SEARCH	urban	2003-2008
	YRK	SEARCH, GA EPD	rural	2003-2008
	SDK	CSN, GA EPD	urban	2003-2008
	Forest Park	CSN	rural	2003-2008
	Kennesaw	CSN	urban	2003-2008

Table C-1 continued

	Doraville	CSN	urban	2003-2008
	E. Rivers	CSN	urban	2003-2008
	Fire Station 8	CSN	urban	2003-2006; 2008
NO_X	JST	SEARCH	urban	2003-2008
	YRK	SEARCH, CSN	rural	2003-2008
	SDK	CSN	urban	2003-2008
	Tucker	CSN	urban	2003-2006
	Georgia Tech	CSN	urban	2003-2008
	Conyers	CSN	rural	2003-2008
CO	JST	SEARCH	urban	2003-2008
	YRK	SEARCH	rural	2003-2008
	SDK	CSN	urban	05/2003-08/2008
	Roswell Rd	CSN	urban	2003-2008

***JST: Jefferson Street; YRK: Yorkville; SDK: South Dekalb**

Table C-2. Evaluation statistics for model fused estimates of $PM_{2.5}$ (µg/m^3), CO (ppb), and NOx (ppb) using each model fusion method.

	$PM_{2.5}$	***CO***	***NOx***
Mean			
Multiplicative Method	17.9 (14.0—18.4)	737.4 (528.5—890.7)	56.5 (41.6—61.0)
Additive Method	16.7 (13.7—17.0)	725.5 (511.8—881.9)	55.6 (40.4—59.4)
Observations	15.7 (11.0—16.1)	787.8 (477.3—928.2)	68.8 (48.1—77.3)
RMSE[a]			
Multiplicative Method	5.4 (4.0—6.2)	206.3 (138.6—250.1)	36.8 (31.2—38.0)
Additive Method	1.9 (1.8—2.3)	206.1 (146.0—244.0)	37.6 (33.7—39.4)
Mean Bias[b]			
Multiplicative Method	2.0 (1.1—2.6)	-51.6 (-98.1— -36.5)	-13.9 (-15.3— -8.4)
Additive Method	1.0 (0.2—1.3)	-66.0 (-107.9— -45.0)	-15.3 (-16.9— -9.7)

Table C-2 continued

Normalized Mean Bias[c]			
Multiplicative Method	11.3 (5.3—15.9)	0.2 (-1.7—8.4)	4.3 (0.9—22.2)
Additive Method	6.9 (1.5—8.0)	-0.6 (-5.2—8.3)	2.4 (-0.7—20.8)
Mean Error[d]			
Multiplicative Method	4.6 (3.5—5.3)	143.5 (105.3—181.5)	24.9 (22.6—27.6)
Additive Method	1.5 (1.4—1.9)	152.5 (121.4—191.8)	27.3 (25.3—29.6)
Normalized Mean Error[e]			
Multiplicative Method	29.9 (27.0—34.6)	23.8 (15.6—25.7)	39.6 (35.3—55.3)
Additive Method	9.9 (9.0—12.1)	25.0 (17.7—27.4)	42.4 (38.0—57.0)
Temporal R[f]			
Multiplicative Method	0.99 (0.92—0.99)	0.93 (0.92—0.95)	0.98 (0.89—1.0)

Table C-2 continued

Additive Method	0.99 (0.92—0.99)	0.94 (0.94—0.96)	0.97 (0.96—0.98)

[a]Root-mean squared error: $\sqrt{mean((C_m - C_o)^2)}$; C_o: observed concentration; C_m: modeled concentration

[b]Mean bias: $mean(C_m - C_o)$; C_o: observed concentration; C_m: modeled concentration

[c]Normalized mean bias: $\left(\frac{mean(C_m)}{mean(C_o)} - 1\right) * 100$; C_o: observed concentration; C_m: modeled concentration

[d]Mean error: $mean(|C_m - C_o|)$; C_o: observed concentration; C_m: modeled concentration

[e]Normalized mean error: $\frac{\sum|C_m - C_o|}{\sum C_o} * 100$; C_o: observed concentration; C_m: modeled concentration

[f]Pearson's correlation coefficient

APPENDIX D.

SUPPLEMENTAL MATERIAL FOR CHAPTER 7

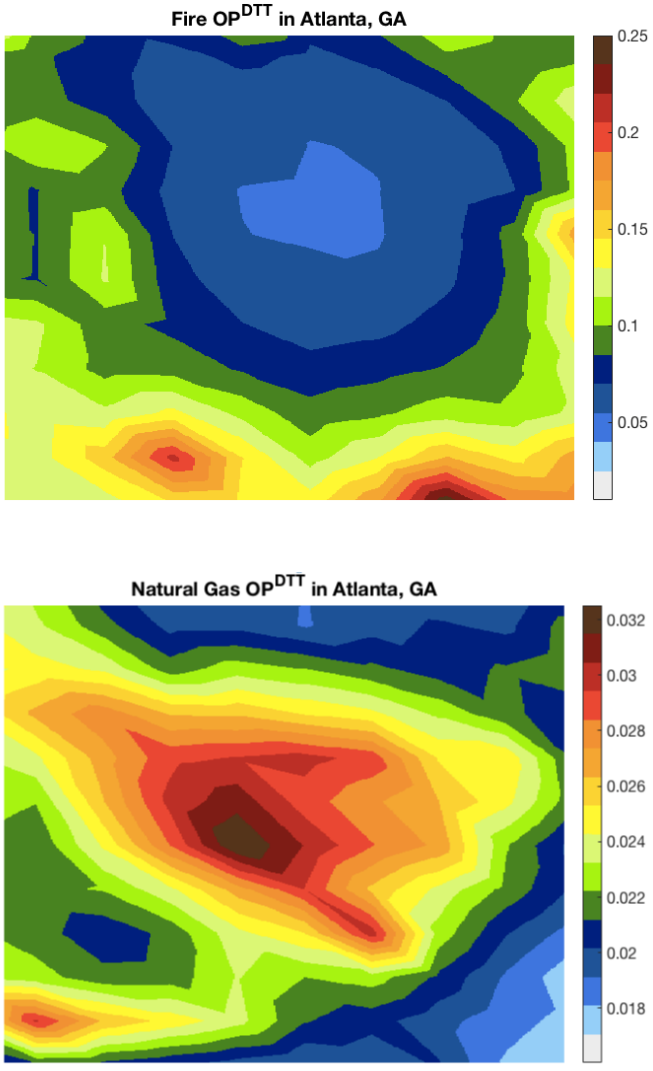

Figure D-1. Estimated OP^{DTT} of fires (top) and natural gas combustion (bottom) in Atlanta, GA.

REFERENCES

Abrams, J. Y., Weber, R. J., Klein, M., Samat, S. E., Chang, H. H., Strickland, M. J., . . . Tolbert, P. E. (2017). Associations between Ambient Fine Particulate Oxidative Potential and Cardiorespiratory Emergency Department Visits. *Environmental Health Perspectives, 125*(10). doi:10.1289/ehp1545

Akhtar, U. S., McWhinney, R. D., Rastogi, N., Abbatt, J. P. D., Evans, G. J., & Scott, J. A. (2010). Cytotoxic and proinflammatory effects of ambient and source-related particulate matter (PM) in relation to the production of reactive oxygen species (ROS) and cytokine adsorption by particles. *Inhalation Toxicology, 22*, 37-47. doi:10.3109/08958378.2010.518377

Alaghmand, M., & Blough, N. V. (2007). Source-dependent variation in hydroxyl radical production by airborne particulate matter. *Environmental Science & Technology, 41*(7), 2364-2370. doi:10.1021/es061902o

Antinolo, M., Willis, M. D., Zhou, S. M., & Abbatt, J. P. D. (2015). Connecting the oxidation of soot to its redox cycling abilities. *Nature Communications, 6*, 7. doi:10.1038/ncomms7812

Antonini, J. M., Clarke, R. W., Murthy, G. G. K., Sreekanthan, P., Jenkins, N., Eagar, T. W., & Brain, J. D. (1998). Freshly generated stainless steel welding fume induces greater lung inflammation in rats as compared to aged fume. *Toxicology Letters, 98*(1-2), 77-86. doi:10.1016/s0378-4274(98)00103-9

Appendix L to Part 50-Reference Method for the Determination of Fine Particulate Matter as PM2.5 in the Atmosphere, (2001).

Arangio, A. M., Tong, H. J., Socorro, J., Poschl, U., & Shiraiwa, M. (2016). Quantification of environmentally persistent free radicals and reactive oxygen species in atmospheric aerosol particles. *Atmospheric Chemistry and Physics, 16*(20), 13105-13119. doi:10.5194/acp-16-13105-2016

Arunachalam, S., Valencia, A., Akita, Y., Serre, M. L., Omary, M., Garcia, V., & Isakov, V. (2014). A Method for Estimating Urban Background Concentrations in Support of Hybrid Air Pollution Modeling for Environmental Health Studies. *International Journal of Environmental Research and Public Health, 11*(10), 10518-10536. doi:10.3390/ijerph111010518

Atkinson, R. W., Samoli, E., Analitis, A., Fuller, G. W., Green, D. C., Anderson, H. R., . . . Mudway, I. S. (2016). Short-term associations between particle oxidative potential and daily mortality and hospital admissions in London. *International Journal of Hygiene and Environmental Health, 219*(6), 566-572. doi:10.1016/j.ijheh.2016.06.004

Autrup, H., Daneshvar, B., Dragsted, L. O., Gamborg, M., Hansen, A. M., Loft, S., . . . Knudsen, L. E. (1999). Biomarkers for exposure to ambient air pollution - Comparison of carcinogen-DNA adduct levels with other exposure markers and markers for oxidative stress. *Environmental Health Perspectives, 107*(3), 233-238. doi:10.2307/3434514

Balachandran, S., Pachon, J. E., Hu, Y. T., Lee, D., Mulholland, J. A., & Russell, A. G. (2012). Ensemble-trained source apportionment of fine particulate matter and method uncertainty analysis. *Atmospheric Environment, 61*, 387-394. doi:10.1016/j.atmosenv.2012.07.031

Ball, J. C., Straccia, A. M., Young, W. C., & Aust, A. E. (2000). The formation of reactive oxygen species catalyzed by neutral, aqueous extracts of NIST ambient particulate matter and diesel engine particles. *Journal of the Air & Waste Management Association, 50*(11), 1897-1903.

Bates, J., Fang, T., Verma, V., Zeng, L., Weber, R. J., Tolbert, P. E., . . . Russell, A. (2018). Review of acellular assays of ambient particulate matter oxidative potential: methods and their relationships with composition, sources, and health effects. *Environmental Science & Technology*.

Bates, J., Pennington, A. F., Zhai, X., Friberg, M., Metcalf, F., Darrow, L., . . . Russell, A. (2018). Application and evaluation of two model fusion approaches to obtain ambient air pollutant concentrations at a fine spatial resolution (250m) in Atlanta. *Environmental Modelling and Software*. doi:https://doi.org/10.1016/j.envsoft.2018.06.008

Bates, J., Weber, R. J., Verma, V., Fang, T., Ivey, C., Liu, C., . . . Russell, A. (2018). Source Impact Modeling of Spatiotemporal Trends In PM2.5 Oxidative Potential across the Eastern United States. *Atmospheric Environment*.

Bates, J. T., Weber, R. J., Abrams, J., Verma, V., Fang, T., Klein, M., . . . Russell, A. G. (2015). Reactive Oxygen Species Generation Linked to Sources of Atmospheric Particulate Matter and Cardiorespiratory Effects. *Environmental Science & Technology, 49*(22), 13605-13612. doi:10.1021/acs.est.5b02967

Baulig, A., Garlatti, M., Bonvallot, V., Marchand, A., Barouki, R., Marano, F., & Baeza-Squiban, A. (2003). Involvement of reactive oxygen species in the metabolic pathways triggered by diesel exhaust particles in human airway epithelial cells. *American Journal of Physiology-Lung Cellular and Molecular Physiology, 285*(3), L671-L679. doi:10.1152/ajplung.00419.2002

Beevers, S. D., Kitwiroon, N., Williams, M. L., Kelly, F. J., Anderson, H. R., & Carslaw, D. C. (2013). Air pollution dispersion models for human exposure predictions in London. *Journal of Exposure Science and Environmental Epidemiology, 23*(6), 647-653. doi:10.1038/jes.2013.6

Berrocal, V. J., Craigmile, P. F., & Guttorp, P. (2012). Regional climate model assessment using statistical upscaling and downscaling techniques. *Environmetrics, 23*(5), 482-492. doi:10.1002/env.2145

Berrocal, V. J., Gelfand, A. E., & Holland, D. M. (2010a). A bivariate Space-time downscaler uneder space and time misalignment *Annals of Applied Statistics, 4*(4), 1942-1975. doi:10.1214/10-aoas351

Berrocal, V. J., Gelfand, A. E., & Holland, D. M. (2010b). A Spatio-Temporal Downscaler for Output From Numerical Models. *Journal of Agricultural Biological and Environmental Statistics, 15*(2), 176-197. doi:10.1007/s13253-009-0004-z

Biswas, S., Verma, V., Schauer, J. J., Cassee, F. R., Cho, A. K., & Sioutas, C. (2009). Oxidative Potential of Semi-Volatile and Non Volatile Particulate Matter (PM) from Heavy-Duty Vehicles Retrofitted with Emission Control Technologies. *Environmental Science & Technology, 43*(10), 3905-3912. doi:10.1021/es9000592

Boogaard, H., Janssen, N. A. H., Fischer, P. H., Kos, G. P. A., Weijers, E. P., Cassee, F. R., . . . Hoek, G. (2012). Contrasts in Oxidative Potential and Other Particulate Matter Characteristics Collected Near Major Streets and Background Locations. *Environmental Health Perspectives, 120*(2), 185-191. doi:10.1289/ehp.1103667

Brunekreef, B., & Holgate, S. T. (2002). Air pollution and health. *Lancet, 360*(9341), 1233-1242. doi:10.1016/s0140-6736(02)11274-8

Byun, D., & Schere, K. L. (2006). Review of the governing equations, computational algorithms, and other components of the models-3 Community Multiscale Air Quality (CMAQ) modeling system. *Applied Mechanics Reviews, 59*(1-6), 51-77. doi:10.1115/1.2128636

Caiazzo, F., Ashok, A., Waitz, I. A., Yim, S. H. L., & Barrett, S. R. H. (2013). Air pollution and early deaths in the United States. Part I: Quantifying the impact of major sectors in 2005. *Atmospheric Environment, 79*, 198-208. doi:10.1016/j.atmosenv.2013.05.081

Calas, A., Uzu, G., Kelly, F., Houdier, S., Martins, J. M. F., Thomas, F., . . . Jaffrezo, J.-L. (2018). Comparison between five acellular oxidative potential measurement assays performed with detailed chemistry on PM10 samples from the city of Chamonix (France). *Atmospheric Chemistry and Physics Discussion*.

Calas, A., Uzu, G., Martins, J. M. F., Voisin, D., Spadini, L., Lacroix, T., & Jaffrezo, J. L. (2017). The importance of simulated lung fluid (SLF) extractions for a more relevant evaluation of the oxidative potential of particulate matter. *Scientific Reports, 7*. doi:10.1038/s41598-017-11979-3

Canova, C., Minelli, C., Dunster, C., Kelly, F., Shah, P. L., Caneja, C., . . . Burney, P. (2014). PM10 Oxidative Properties and Asthma and COPD. *Epidemiology, 25*(3), 467-468. doi:10.1097/ede.0000000000000084

CEP. (2003). *Sparse Matrix Operator Kernel Emissions Modeling System (SMOKE) User Manual*. Chapel HIll, NC, USA: Carolina Environmental Program-The University of North Carolina at Chapel Hill.

Cesaroni, G., Forastiere, F., Stafoggia, M., Andersen, Z. J., Badaloni, C., Beelen, R., . . . Peters, A. (2014). Long term exposure to ambient air pollution and incidence of acute coronary events: prospective cohort study and meta-analysis in 11 European cohorts from the ESCAPE Project. *Bmj-British Medical Journal, 348*. doi:10.1136/bmj.f7412

Chang, H. H., Hu, X. F., & Liu, Y. (2014). Calibrating MODIS aerosol optical depth for predicting daily PM2.5 concentrations via statistical downscaling. *Journal of Exposure Science and Environmental Epidemiology, 24*(4), 398-404. doi:10.1038/jes.2013.90

Chang, H. H., Reich, B. J., & Miranda, M. L. (2012). Time-to-Event Analysis of Fine Particle Air Pollution and Preterm Birth: Results From North Carolina, 2001-2005. *American Journal of Epidemiology, 175*(2), 91-98. doi:10.1093/aje/kwr403

Chang, S. Y., Vizuete, W., Serre, M., Vennam, L. P., Omary, M., Isakov, V., . . . Arunachalam, S. (2017). Finely resolved on-road PM2.5 and estimated premature mortality in central North Carolina. *Risk Analysis, 17*(12), 2420-2434.

Chang, S. Y., Vizuete, W., Serre, M., Vennam, L. P., Omary, M., Isakov, V., . . . Arunachalam, S. (2017). Finely Resolved On-Road PM2.5 and Estimated Premature Mortality in Central North Carolina. *Risk Analysis*. doi:10.1111/risa.12775

Chang, S. Y., Vizuete, W., Valencia, A., Naess, B., Isakov, V., Palma, T., . . . Arunachalam, S. (2015). A modeling framework for characterizing near-road air pollutant concentration at community scales. *Science of the Total Environment, 538*, 905-921. doi:10.1016/j.scitotenv.2015.06.139

Charrier, J. G., & Anastasio, C. (2011). Impacts of antioxidants on hydroxyl radical production from individual and mixed transition metals in a surrogate lung fluid. *Atmospheric Environment, 45*(40), 7555-7562. doi:10.1016/j.atmosenv.2010.12.021

Charrier, J. G., & Anastasio, C. (2012). On dithiothreitol (DTT) as a measure of oxidative potential for ambient particles: evidence for the importance of soluble transition metals. *Atmospheric Chemistry and Physics, 12*(19), 9321-9333. doi:10.5194/acp-12-9321-2012

Charrier, J. G., & Anastasio, C. (2015). Rates of Hydroxyl Radical Production from Transition Metals and Quinones in a Surrogate Lung Fluid. *Environmental Science & Technology, 49*(15), 9317-9325. doi:10.1021/acs.est.5b01606

Charrier, J. G., McFall, A. S., Richards-Henderson, N. K., & Anastasio, C. (2014). Hydrogen Peroxide Formation in a Surrogate Lung Fluid by Transition Metals and Quinones Present in Particulate Matter. *Environmental Science & Technology, 48*(12), 7010-7017. doi:10.1021/es501011w

Charrier, J. G., McFall, A. S., Vu, K. K. T., Baroi, J., Olea, C., Hasson, A., & Anastasio, C. (2016). A bias in the "mass-normalized" DTT response - An effect of non-linear concentration-response curves for copper and manganese. *Atmospheric Environment, 144*, 325-334. doi:10.1016/j.atmosenv.2016.08.071

Charrier, J. G., Richards-Henderson, N. K., Bein, K. J., McFall, A. S., Wexler, A. S., & Anastasio, C. (2015). Oxidant production from source-oriented particulate matter - Part 1: Oxidative potential using the dithiothreitol (DTT) assay. *Atmospheric Chemistry and Physics, 15*(5), 2327-2340. doi:10.5194/acp-15-2327-2015

Chen, X., & Hopke, P. K. (2009). A chamber study of secondary organic aerosol formation by linalool ozonolysis. *Atmospheric Environment, 43*(25), 3935-3940. doi:10.1016/j.atmosenv.2009.04.033

Cheung, K. L., Polidori, A., Ntziachristos, L., Tzamkiozis, T., Samaras, Z., Cassee, F. R., . . . Sioutas, C. (2009). Chemical Characteristics and Oxidative Potential of Particulate Matter Emissions from Gasoline, Diesel, and Biodiesel Cars. *Environmental Science & Technology, 43*(16), 6334-6340. doi:10.1021/es900819t

Chirizzi, D., Cesari, D., Guascito, M. R., Dinoi, A., Giotta, L., Donateo, A., & Contini, D. (2017). Influence of Saharan dust outbreaks and carbon content on oxidative potential of water-soluble fractions of PM2.5 and PM10. *Atmospheric Environment, 163*, 1-8. doi:10.1016/j.atmosenv.2017.05.021

Cho, A. K., Sioutas, C., Miguel, A. H., Kumagai, Y., Schmitz, D. A., Singh, M., . . . Froines, J. R. (2005). Redox activity of airborne particulate matter at different sites in the Los Angeles Basin. *Environmental Research, 99*(1), 40-47. doi:10.1016/j.envres.2005.01.003

Choi, Y., Osterman, G., Eldering, A., Wang, Y. H., & Edgerton, E. (2010). Understanding the contributions of anthropogenic and biogenic sources to CO enhancements and outflow observed over North America and the western Atlantic Ocean by TES and MOPITT. *Atmospheric Environment, 44*(16), 2033-2042. doi:10.1016/j.atmosenv.2010.01.029

Chung, M. Y., Lazaro, R. A., Lim, D., Jackson, J., Lyon, J., Rendulic, D., & Hasson, A. S. (2006). Aerosol-borne quinones and reactive oxygen species generation by particulate matter extracts. *Environmental Science & Technology, 40*(16), 4880-4886. doi:10.1021/es0515957

Cimorelli, A. J., Perry, S. G., Venkatram, A., Weil, J. C., Paine, R. J., Wilson, R. B., . . . Brode, R. W. (2005). AERMOD: A dispersion model for industrial source applications. Part I: General model formulation and boundary layer

characterization. *Journal of Applied Meteorology, 44*(5), 682-693. doi:10.1175/jam2227.1

Cohan, D. S., Hakami, A., Hu, Y. T., & Russell, A. G. (2005). Nonlinear response of ozone to emissions: Source apportionment and sensitivity analysis. *Environmental Science & Technology, 39*(17), 6739-6748. doi:10.1021/es05664m

Cohn, C. A., Simon, S. R., & Schoonen, M. A. A. (2008). Comparison of fluorescence-based techniques for the quantification of particle-induced hydroxyl radicals. *Particle and Fibre Toxicology, 5*, 9. doi:10.1186/1743-8977-5-2

Cong, X. C., Qu, J. H., & Yang, G. S. (2016). On-road measurements of pollutant concentration profiles inside Yangkou tunnel, Qingdao, China. *Environmental Geochemistry and Health*, 1-12. doi:10.1007/s10653-016-9885-2

Crilley, L. R., Knibbs, L. D., Miljevic, B., Cong, X. C., Fairfull-Smith, K. E., Bottle, S. E., . . . Morawska, L. (2012). Concentration and oxidative potential of on-road particle emissions and their relationship with traffic composition: Relevance to exposure assessment. *Atmospheric Environment, 59*, 533-539. doi:10.1016/j.atmosenv.2012.05.039

Crooks, J., & Isakov, V. (2013). A wavelet-based approach to blending observations with deterministic computer models to resolve the intraurban air pollution field A wavelet-based approach to blending observations with deterministic computer models to resolve the intraurbanair pollution field. *Journal of the Air & Waste Management Association, 63*(12), 1369-1385. doi:10.1080/10962247.2012.758061

D'Onofrio, D. (2016). Atlanta Roadside Emissions Exposure Study - Methodology & Project Overview. Retrieved from http://www.atlantaregional.com/environment/air/arees-near-road-emissions

Darrow, L. A., Klein, M., Strickland, M. J., Mulholland, J. A., & Tolbert, P. E. (2011). Ambient Air Pollution and Birth Weight in Full-Term Infants in Atlanta, 1994-2004. *Environmental Health Perspectives, 119*(5), 731-737. doi:10.1289/ehp.1002785

Davis, T., Lawla, A., Servadio, J., Bates, J. T., Ramaswami, A., Convertino, M., . . . Russell, A. (2017). *Demographic Inequalities in Health Outocmes and Air Pollution Exposure in the Atlanta Aera and its Relationship to Urban Infrastructure*.

Delfino, R. J., Sioutas, C., & Malik, S. (2005). Potential role of ultrafine particles in associations between airborne particle mass and cardiovascular health. *Environmental Health Perspectives, 113*(8), 934-946. doi:10.1289/ehp.7938

Delfino, R. J., Staimer, N., Tjoa, T., Gillen, D. L., Schauer, J. J., & Shafer, M. M. (2013). Airway inflammation and oxidative potential of air pollutant particles in a pediatric

asthma panel. *Journal of Exposure Science and Environmental Epidemiology, 23*(5), 466-473. doi:10.1038/jes.2013.25

Dellinger, B., Pryor, W. A., Cueto, R., Squadrito, G. L., Hegde, V., & Deutsch, W. A. (2001). Role of free radicals in the toxicity of airborne fine particulate matter. *Chemical Research in Toxicology, 14*(10), 1371-1377. doi:10.1021/tx010050x

Dionisio, K. L., Isakov, V., Baxter, L. K., Sarnat, J. A., Sarnat, S. E., Burke, J., . . . Ozkaynak, H. (2013). Development and evaluation of alternative approaches for exposure assessment of multiple air pollutants in Atlanta, Georgia. *Journal of Exposure Science and Environmental Epidemiology, 23*(6), 581-592. doi:10.1038/jes.2013.59

DiStefano, E., Eiguren-Fernandez, A., Delfino, R. J., Sioutas, C., Froines, J. R., & Cho, A. K. (2009). Determination of metal-based hydroxyl radical generating capacity of ambient and diesel exhaust particles. *Inhalation Toxicology, 21*(8-11), 731-738. doi:10.1080/08958370802491433

Donaldson, K., Brown, D. M., Mitchell, C., Dineva, M., Beswick, P. H., Gilmour, P., & MacNee, W. (1997). Free radical activity of PM10: Iron-mediated generation of hydroxyl radicals. *Environmental Health Perspectives, 105*, 1285-1289. doi:10.2307/3433548

Donaldson, K., Stone, V., Seaton, A., & MacNee, W. (2001). Ambient particle inhalation and the cardiovascular system: Potential mechanisms. *Environmental Health Perspectives, 109*, 523-527. doi:10.2307/3454663

Dou, J., Lin, P., Kuang, B. Y., & Yu, J. Z. (2015). Reactive Oxygen Species Production Mediated by Humic-like Substances in Atmospheric Aerosols: Enhancement Effects by Pyridine, Imidazole, and Their Derivatives. *Environmental Science & Technology, 49*(11), 6457-6465. doi:10.1021/es5059378

Dunker, A. M. (1981). EFFICIENT CALCULATION OF SENSITIVITY COEFFICIENTS FOR COMPLEX ATMOSPHERIC MODELS. *Atmospheric Environment, 15*(7), 1155-1161. doi:10.1016/0004-6981(81)90305-x

Dunker, A. M. (1984). THE DECOUPLED DIRECT METHOD FOR CALCULATING SENSITIVITY COEFFICIENTS IN CHEMICAL-KINETICS. *Journal of Chemical Physics, 81*(5), 2385-2393. doi:10.1063/1.447938

Edgerton, E. S., Hartsell, B. E., Saylor, R. D., Jansen, J. J., Hansen, D. A., & Hidy, G. M. (2005). The southeastern aerosol research and characterization study: Part II. Filter-based measurements of fine and coarse particulate matter mass and composition. *Journal of the Air & Waste Management Association, 55*(10), 1527-1542.

Eiguren-Fernandez, A., Kreisberg, N., & Hering, S. (2017). An online monitor of the oxidative capacity of aerosols (o-MOCA). *Atmospheric Measurement Techniques, 10*(2), 633-644. doi:10.5194/amt-10-633-2017

Eiguren-Fernandez, A., Shinyashiki, M., Schmitz, D. A., DiStefano, E., Hinds, W., Kumagai, Y., . . . Froines, J. R. (2010). Redox and electrophilic properties of vapor- and particle-phase components of ambient aerosols. *Environmental Research, 110*(3), 207-212. doi:10.1016/j.envres.2010.01.009

ENVIRON International Corporation. (2014). *User's Guide to the Comprehensive Air Quality Model with Extensions Version 6.1*. Retrieved from www.camx.com/files/camxusersguide_v6-10.pdf

Fang, T., Guo, H. Y., Zeng, L. H., Verma, V., Nenes, A., & Weber, R. J. (2017). Highly Acidic Ambient Particles, Soluble Metals, and Oxidative Potential: A Link between Sulfate and Aerosol Toxicity. *Environmental Science & Technology, 51*(5), 2611-2620. doi:10.1021/acs.est.6b06151

Fang, T., Verma, V., Bates, J. T., Abrams, J., Klein, M., Strickland, M. J., . . . Weber, R. J. (2016). Oxidative potential of ambient water-soluble PM2.5 in the southeastern United States: contrasts in sources and health associations between ascorbic acid (AA) and dithiothreitol (DTT) assays. *Atmospheric Chemistry and Physics, 16*(6), 3865-3879.

Fang, T., Verma, V., Guo, H., King, L. E., Edgerton, E. S., & Weber, R. J. (2015). A semi-automated system for quantifying the oxidative potential of ambient particles in aqueous extracts using the dithiothreitol (DTT) assay: results from the Southeastern Center for Air Pollution and Epidemiology (SCAPE). *Atmospheric Measurement Techniques, 8*(1), 471-482. doi:10.5194/amt-8-471-2015

Fang, T., Zeng, L. H., Gao, D., Verma, V., Stefaniak, A. B., & Weber, R. J. (2017). Ambient Size Distributions and Lung Deposition of Aerosol Dithiothreitol-Measured Oxidative Potential: Contrast between Soluble and Insoluble Particles. *Environmental Science & Technology, 51*(12), 6802-6811. doi:10.1021/acs.est.7b01536

Fletcher, R. (1987). *Practical Methods of Optimization*. Cornwall, UK: John Wiley and Sons.

Fonken, L. K., Xu, X., Weil, Z. M., Chen, G., Sun, Q., Rajagopalan, S., & Nelson, R. J. (2011). Air pollution impairs cognition, provokes depressive-like behaviors and alters hippocampal cytokine expression and morphology. *Molecular Psychiatry, 16*(10), 987-995. doi:10.1038/mp.2011.76

Fox, J. R., Cox, D. P., Drury, B. E., Gould, T. R., Kavanagh, T. J., Paulsen, M. H., . . . Kaufman, J. D. (2015). Chemical characterization and in vitro toxicity of diesel exhaust particulate matter generated under varying conditions. *Air Quality Atmosphere and Health, 8*(5), 507-519. doi:10.1007/s11869-014-0301-8

Franklin, M., Zeka, A., & Schwartz, J. (2007). Association between PM2.5 and all-cause and specific-cause mortality in 27 US communities. *Journal of Exposure Science and Environmental Epidemiology, 17*(3), 279-287. doi:10.1038/sj.jes.7500530

Friberg, M. D., Zhai, X. X., Holmes, H. A., Chang, H. H., Strickland, M. J., Sarnat, S. E., . . . Mulholland, J. A. (2016). Method for Fusing Observational Data and Chemical Transport Model Simulations To Estimate Spatiotemporally Resolved Ambient Air Pollution. *Environmental Science & Technology, 50*(7), 3695-3705. doi:10.1021/acs.est.5b05134

Fuentes, M., & Raftery, A. E. (2005). Model evaluation and spatial interpolation by Bayesian combination of observations with outputs from numerical models. *Biometrics, 61*(1), 36-45. doi:10.1111/j.0006-341X.2005.030821.x

Fujitani, Y., Furuyama, A., Tanabe, K., & Hirano, S. (2017). Comparison of Oxidative Abilities of PM2.5 Collected at Traffic and Residential Sites in Japan. Contribution of Transition Metals and Primary and Secondary Aerosols. *Aerosol and Air Quality Research, 17*, 574-587.

Fuller, S. J., Wragg, F. P. H., Nutter, J., & Kalberer, M. (2014). Comparison of on-line and off-line methods to quantify reactive oxygen species (ROS) in atmospheric aerosols. *Atmospheric Environment, 92*, 97-103. doi:10.1016/j.atmosenv.2014.04.006

Fushimi, A., Saitoh, K., Hayashi, K., Ono, K., Fujitani, Y., Villalobos, A. M., . . . Schauer, J. J. (2017). Chemical characterization and oxidative potential of particles emitted from open burning of cereal straws and rice husk under flaming and smoldering conditions. *Atmospheric Environment, 163*, 118-127. doi:10.1016/j.atmosenv.2017.05.037

Gao, D., Fang, T., Verma, V., Zeng, L. G., & Weber, R. J. (2017). A method for measuring total aerosol oxidative potential (OP) with the dithiothreitol (DTT) assay and comparisons between an urban and roadside site of water-soluble and total OP. *Atmospheric Measurement Techniques, 10*(8), 2821-2835. doi:10.5194/amt-10-2821-2017

Gass, K., Balachandran, S., Chang, H. H., Russell, A. G., & Strickland, M. J. (2015). Ensemble-Based Source Apportionment of Fine Particulate Matter and Emergency Department Visits for Pediatric Asthma. *American Journal of Epidemiology, 181*(7), 504-512. doi:10.1093/aje/kwu305

Geller, M. D., Ntziachristos, L., Mamakos, A., Samaras, Z., Schmitz, D. A., Froines, J. R., & Sioutas, C. (2006). Physicochemical and redox characteristics of particulate matter (PM) emitted from gasoline and diesel passenger cars. *Atmospheric Environment, 40*(36), 6988-7004. doi:10.1016/j.atmosenv.2006.06.018

Georgia Department of Transportation. (2005). 2005 Annual Average Daily Traffic Report (AADT).

Ghio, A. J., Carraway, M. S., & Madden, M. C. (2012). COMPOSITION OF AIR POLLUTION PARTICLES AND OXIDATIVE STRESS IN CELLS, TISSUES,

AND LIVING SYSTEMS. *Journal of Toxicology and Environmental Health-Part B-Critical Reviews, 15*(1), 1-21. doi:10.1080/10937404.2012.632359

Gill, P. E., Murray, W., & Wright, M. H. (1981). *Practical Optimization*. London, UK: Academic Press.

Godoi, R. H. M., Polezer, G., Borillo, G. C., Brown, A., Valebona, F. B., Silva, T. O. B., . . . Godoi, A. F. L. (2016). Influence on the oxidative potential of a heavy-duty engine particle emission due to selective catalytic reduction system and biodiesel blend. *Science of the Total Environment, 560*, 179-185. doi:10.1016/j.scitotenv.2016.04.018

Godri, K. J., Duggan, S. T., Fuller, G. W., Baker, T., Green, D., Kelly, F. J., & Mudway, I. S. (2010). Particulate Matter Oxidative Potential from Waste Transfer Station Activity. *Environmental Health Perspectives, 118*(4), 493-498. doi:10.1289/ehp.0901303

Godri, K. J., Green, D. C., Fuller, G. W., Dall'Osto, M., Beddows, D. C., Kelly, F. J., . . . Mudway, I. S. (2010). Particulate Oxidative Burden Associated with Firework Activity. *Environmental Science & Technology, 44*(21), 8295-8301. doi:10.1021/es1016284

Godri, K. J., Harrison, R. M., Evans, T., Baker, T., Dunster, C., Mudway, I. S., & Kelly, F. J. (2011). Increased Oxidative Burden Associated with Traffic Component of Ambient Particulate Matter at Roadside and Urban Background Schools Sites in London. *Plos One, 6*(7). doi:10.1371/journal.pone.0021961

Goldman, G. T., Mulholland, J. A., Russell, A. G., Strickland, M. J., Klein, M., Waller, L. A., & Tolbert, P. E. (2011). Impact of exposure measurement error in air pollution epidemiology: effect of error type in time-series studies. *Environmental Health, 10*, 11. doi:10.1186/1476-069x-10-61

Gryparis, A., Paciorek, C. J., Zeka, A., Schwartz, J., & Coull, B. A. (2009). Measurement error caused by spatial misalignment in environmental epidemiology. *Biostatistics, 10*(2), 258-274. doi:10.1093/biostatistics/kxn033

Hansen, D. A., Edgerton, E., Hartsell, B., Jansen, J., Burge, H., Koutrakis, P., . . . Rasmussen, R. (2006). Air quality measurements for the aerosol research and inhalation epidemiology study. *Journal of the Air & Waste Management Association, 56*(10), 1445-1458.

Hansen, D. A., Edgerton, E. S., Hartsell, B. E., Jansen, J. J., Kandasamy, N., Hidy, G. M., & Blanchard, C. L. (2003). The southeastern aerosol research and characterization study: Part 1-overview. *Journal of the Air & Waste Management Association, 53*(12), 1460-1471.

HEI Panel on the Health Effects of Traffic-Related Air Pollution. (2010). *Traffic-Related Air Pollution: A Critical Review of the Literature on Emissions, Exposure, and Health Effects* (17). Retrieved from Boston, MA:

Hellack, B., Quass, U., Nickel, C., Wick, G., Schins, R. P. F., & Kuhlbusch, T. A. J. (2015). Oxidative potential of particulate matter at a German motorway. *Environmental Science-Processes & Impacts, 17*(4), 868-876. doi:10.1039/c4em00605d

Hellack, B., Yang, A., Cassee, F. R., Janssen, N. A. H., Schins, R. P. F., & Kuhlbusch, T. A. J. (2014). Intrinsic hydroxyl radical generation measurements directly from sampled filters as a metric for the oxidative potential of ambient particulate matter. *Journal of Aerosol Science, 72*, 47-55. doi:10.1016/j.jaerosci.2014.02.003

Hidy, G. M., Blanchard, C. L., Baumann, K., Edgerton, E., Tanenbaum, S., Shaw, S., . . . Walters, J. (2014). Chemical climatology of the southeastern United States, 1999-2013. *Atmospheric Chemistry and Physics, 14*(21), 11893-11914. doi:10.5194/acp-14-11893-2014

Hogervorst, J. G. F., de Kok, T., Briede, J. J., Wesseling, G., Kleinjans, J. C. S., & van Schayck, C. P. (2006). Relationship between radical generation by urban ambient particulate matter and pulmonary function of school children. *Journal of Toxicology and Environmental Health-Part a-Current Issues, 69*(3), 245-262. doi:10.1080/15287390500227431

Holder, A. L., Carter, B. J., Goth-Goldstein, R., Lucas, D., & Koshland, C. P. (2012). Increased cytotoxicity of oxidized flame soot. *Atmospheric Pollution Research, 3*(1), 25-31. doi:10.5094/apr.2012.001

Hu, S., Polidori, A., Arhami, M., Shafer, M. M., Schauer, J. J., Cho, A., & Sioutas, C. (2008). Redox activity and chemical speciation of size fractioned PM in the communities of the Los Angeles-Long Beach harbor. *Atmospheric Chemistry and Physics, 8*(21), 6439-6451.

Hu, Y., Balachandran, S., Pachon, J. E., Baek, J., Ivey, C., Holmes, H., . . . Russell, A. G. (2014). Fine particulate matter source apportionment using a hybrid chemical transport and receptor model approach. *Atmospheric Chemistry and Physics, 14*(11), 5415-5431. doi:10.5194/acp-14-5415-2014

Huang, W., Zhang, Y. X., Zhang, Y., Fang, D. Q., & Schauer, J. J. (2016). Optimization of the Measurement of Particle-Bound Reactive Oxygen Species with 2 ',7 '-dichlorofluorescin (DCFH). *Water Air and Soil Pollution, 227*(5), 10. doi:10.1007/s11270-016-2860-9

Hudman, R. C., Murray, L. T., Jacob, D. J., Millet, D. B., Turquety, S., Wu, S., . . . Sachse, G. W. (2008). Biogenic versus anthropogenic sources of CO in the United States. *Geophysical Research Letters, 35*(4), 5. doi:10.1029/2007gl032393

Hung, H. F., & Wang, C. S. (2001). Experimental determination of reactive oxygen species in Taipei aerosols. *Journal of Aerosol Science, 32*(10), 1201-1211. doi:10.1016/s0021-8502(01)00051-9

Isakov, V., Irwin, J. S., & Ching, J. (2007). Using CMAQ for exposure Modeling and characterizing the subgrid variability for exposure estimates. *Journal of Applied Meteorology and Climatology, 46*(9), 1354-1371. doi:10.1175/jam2538.1

Ivey, C., Holmes, H., Hu, Y. T., Mulholland, J. A., & Russell, A. G. (2014). *Spatial and Temporal Extension of a Novel Hybrid Source Apportionment Model*.

Ivey, C. E., Holmes, H. A., Hu, Y. T., Mulholland, J. A., & Russell, A. G. (2016). A method for quantifying bias in modeled concentrations and source impacts for secondary particulate matter. *Frontiers of Environmental Science & Engineering, 10*(5), 12. doi:10.1007/s11783-016-0866-6

Janssen, N. A. H., Strak, M., Yang, A., Hellack, B., Kelly, F. J., Kuhlbusch, T. A. J., . . . Hoek, G. (2015). Associations between three specific a-cellular measures of the oxidative potential of particulate matter and markers of acute airway and nasal inflammation in healthy volunteers. *Occupational and Environmental Medicine, 72*(1), 49-56. doi:10.1136/oemed-2014-102303

Janssen, N. A. H., Yang, A. L., Strak, M., Steenhof, M., Hellack, B., Gerlofs-Nijland, M. E., . . . Cassee, F. (2014). Oxidative potential of particulate matter collected at sites with different source characteristics. *Science of the Total Environment, 472*, 572-581. doi:10.1016/j.scitotenv.2013.11.099

Jedynska, A., Hoek, G., Wang, M., Yang, A., Eeftens, M., Cyrys, J., . . . Kooter, I. M. (2017). Spatial variations and development of land use regression models of oxidative potential in ten European study areas. *Atmospheric Environment, 150*, 24-32. doi:10.1016/j.atmosenv.2016.11.029

Jeng, H. A. (2010). Chemical composition of ambient particulate matter and redox activity. *Environmental Monitoring and Assessment, 169*(1-4), 597-606. doi:10.1007/s10661-009-1199-8

Jiang, H. H., Jang, M., Sabo-Attwood, T., & Robinson, S. E. (2016). Oxidative potential of secondary organic aerosols produced from photooxidation of different hydrocarbons using outdoor chamber under ambient sunlight. *Atmospheric Environment, 131*, 382-389. doi:10.1016/j.atmosenv.2016.02.016

Jung, H., Guo, B., Anastasio, C., & Kennedy, I. M. (2006). Quantitative measurements of the generation of hydroxyl radicals by soot particles in a surrogate lung fluid. *Atmospheric Environment, 40*(6), 1043-1052. doi:10.1016/j.atmosenv.2005.11.015

Karavalakis, G., Gysel, N., Schmitz, D. A., Cho, A. K., Sioutas, C., Schauer, J. J., . . . Durbin, T. D. (2017). Impact of biodiesel on regulated and unregulated emissions, and redox and proinflammatory properties of PM emitted from heavy-duty

vehicles. *Science of the Total Environment, 584*, 1230-1238. doi:10.1016/j.scitotenv.2017.01.187

Khurshid, S. S., Siegel, J. A., & Kinney, K. A. (2014). Technical Note: Particulate reactive oxygen species concentrations and their association with environmental conditions in an urban, subtropical climate. *Atmospheric Chemistry and Physics, 14*(13), 6777-6784. doi:10.5194/acp-14-6777-2014

King, L. E., & Weber, R. J. (2013). Development and testing of an online method to measure ambient fine particulate reactive oxygen species (ROS) based on the 2 ',7 '-dichlorofluorescin (DCFH) assay. *Atmospheric Measurement Techniques, 6*(7), 1647-1658. doi:10.5194/amt-6-1647-2013

Kleindienst, T. E., Lewandowski, M., Offenberg, J. H., Edney, E. O., Jaoui, M., Zheng, M., . . . Edgerton, E. S. (2010). Contribution of Primary and Secondary Sources to Organic Aerosol and PM2.5 at SEARCH Network Sites. *Journal of the Air & Waste Management Association, 60*(11), 1388-1399. doi:10.3155/1047-3289.60.11.1388

Kodavanti, U. P., Schladweiler, M. C., Ledbetter, A. D., Hauser, R., Christiani, D. C., McGee, J., . . . Costa, D. L. (2002). Temporal association between pulmonary and systemic effects of particulate matter in healthy and cardiovascular compromised rats. *Journal of Toxicology and Environmental Health-Part A, 65*(20), 1545-1569. doi:10.1080/00984100290071667

Koehler, K. A., Shapiro, J., Sameenoi, Y., Henry, C., & Volckens, J. (2014). Laboratory Evaluation of a Microfluidic Electrochemical Sensor for Aerosol Oxidative Load. *Aerosol Science and Technology, 48*(5), 489-497. doi:10.1080/02786826.2014.891722

Kramer, A. J., Rattanavaraha, W., Zhang, Z. F., Gold, A., Surratt, J. D., & Lin, Y. H. (2016). Assessing the oxidative potential of isoprene-derived epoxides and secondary organic aerosol. *Atmospheric Environment, 130*, 211-218. doi:10.1016/j.atmosenv.2015.10.018

Kuang, X. M., Scott, J. A., da Rocha, G. O., Betha, R., Price, D. J., Russell, L. M., . . . Paulson, S. E. (2017). Hydroxyl radical formation and soluble trace metal content in particulate matter from renewable diesel and ultra low sulfur diesel in at-sea operations of a research vessel. *Aerosol Science and Technology, 51*(2), 147-158. doi:10.1080/02786826.2016.1271938

Kunzli, N., Mudway, I. S., Gotschi, T., Shi, T. M., Kelly, F. J., Cook, S., . . . Borm, P. J. A. (2006). Comparison of oxidative properties, light absorbance, and total and elemental mass concentration of ambient PM2.5 collected at 20 European sites. *Environmental Health Perspectives, 114*(5), 684-690. doi:10.1289/ehp.8584

Li, N., Sioutas, C., Cho, A., Schmitz, D., Misra, C., Sempf, J., . . . Nel, A. (2003). Ultrafine particulate pollutants induce oxidative stress and mitochondrial damage. *Environmental Health Perspectives, 111*(4), 455-460. doi:10.1289/ehp.6000

Li, Y., Zhu, T., Zhao, J. C., & Xu, B. Y. (2012). Interactive Enhancements of Ascorbic Acid and Iron in Hydroxyl Radical Generation in Quinone Redox Cycling. *Environmental Science & Technology, 46*(18), 10302-10309. doi:10.1021/es301834r

Lim, S. S., Vos, T., & Flaxman, A. D. (2013). A comparative risk assessment of burden of disease and injury attributable to 67 risk factors and risk factor clusters in 21 regions, 1990-2010: a systematic analysis for the Global Burden of Disease Study 2010 (vol 380, pg 2224, 2012). *Lancet, 381*(9874), 1276-1276.

Lim, S. S., Vos, T., Flaxman, A. D., Danaei, G., Shibuya, K., Adair-Rohani, H., . . . Ezzati, M. (2012). A comparative risk assessment of burden of disease and injury attributable to 67 risk factors and risk factor clusters in 21 regions, 1990-2010: a systematic analysis for the Global Burden of Disease Study 2010. *Lancet, 380*(9859), 2224-2260. doi:10.1016/s0140-6736(12)61766-8

Liu, Q. Y., Baumgartner, J., Zhang, Y. X., Liu, Y. J., Sun, Y. J., & Zhang, M. G. (2014). Oxidative Potential and Inflammatory Impacts of Source Apportioned Ambient Air Pollution in Beijing. *Environmental Science & Technology, 48*(21), 12920-12929. doi:10.1021/es5029876

Liu, Q. Y., Zhang, Y. X., Liu, Y. J., & Zhang, M. G. (2014). Characterization of springtime airborne particulate matter-bound reactive oxygen species in Beijing. *Environmental Science and Pollution Research, 21*(15), 9325-9333. doi:10.1007/s11356-014-2843-6

Ma, S. X., Ren, K., Liu, X. W., Chen, L. G., Li, M., Li, X. Y., . . . Xu, Z. C. (2015). Production of hydroxyl radicals from Fe-containing fine particles in Guangzhou, China. *Atmospheric Environment, 123*, 72-78. doi:10.1016/j.atmosenv.2015.10.057

Ma, Y., Cheng, Y., Qiu, X., Cao, G., Fang, Y., Wang, J., . . . Hu, D. (2017a). Sources and oxidative potential of water-soluble humic-like substances (HULISWS) in fine particulate matter (PM2.5) in Beijing. *Atmospheric Chemistry and Physics Discussion*.

Ma, Y., Cheng, Y., Qiu, X., Cao, G., Fang, Y., Wang, J., . . . Hu, D. (2017b). Sources of oxidative potential of water-soluble humic-like substances (HULISws) in fine particulate matter (PM2.5) in Beijing. *Atmospheric Chemistry and Physics Discussion*.

Maikawa, C. L., Weichenthal, S., Wheeler, A. J., Dobbin, N. A., Smargiassi, A., Evans, G., . . . Pollitt, K. J. G. (2016). Particulate Oxidative Burden as a Predictor of Exhaled Nitric Oxide in Children with Asthma. *Environmental Health Perspectives, 124*(10), 1616-1622. doi:10.1289/ehp175

Makino, K., Hagiwara, T., Hagi, A., Nishi, M., & Murakami, A. (1990). Cautionary note for DMPO spin trapping in teh presence of iron-ion *Biochemical and Biophysical*

Research Communications, 172(3), 1073-1080. doi:10.1016/0006-291x(90)91556-8

Marshall, J. D., Nethery, E., & Brauer, M. (2008). Within-urban variability in ambient air pollution: Comparison of estimation methods. *Atmospheric Environment, 42*(6), 1359-1369. doi:10.1016/j.atmosenv.2007.08.012

McHugh, C. A., Carruthers, D. J., & Edmunds, H. A. (1997). ADMS-Urban: an air quality management system for traffic, domestic and industrial pollution. *International Journal of Environment and Pollution, 8*(3-6), 666-674.

McWhinney, R. D., Badali, K., Liggio, J., Li, S. M., & Abbatt, J. P. D. (2013). Filterable Redox Cycling Activity: A Comparison between Diesel Exhaust Particles and Secondary Organic Aerosol Constituents. *Environmental Science & Technology, 47*(7), 3362-3369. doi:10.1021/es304676x

McWhinney, R. D., Gao, S. S., Zhou, S. M., & Abbatt, J. P. D. (2011). Evaluation of the Effects of Ozone Oxidation on Redox-Cycling Activity of Two-Stroke Engine Exhaust Particles. *Environmental Science & Technology, 45*(6), 2131-2136. doi:10.1021/es102874d

McWhinney, R. D., Zhou, S., & Abbatt, J. P. D. (2013). Naphthalene SOA: redox activity and naphthoquinone gas-particle partitioning. *Atmospheric Chemistry and Physics, 13*(19), 9731-9744. doi:10.5194/acp-13-9731-2013

Michanowicz, D. R., Shmool, J. L. C., Tunno, B. J., Tripathy, S., Gillooly, S., Kinnee, E., & Clougherty, J. E. (2016). A hybrid land use regression/AERMOD model for predicting intra-urban variation in PM2.5. *Atmospheric Environment, 131*, 307-315. doi:10.1016/j.atmosenv.2016.01.045

Miljevic, B., Hedayat, F., Stevanovic, S., Fairfull-Smith, K. E., Bottle, S. E., & Ristovski, Z. D. (2014). To Sonicate or Not to Sonicate PM Filters: Reactive Oxygen Species Generation Upon Ultrasonic Irradiation. *Aerosol Science and Technology, 48*(12), 1276-1284. doi:10.1080/02786826.2014.981330

Miljevic, B., Heringa, M. F., Keller, A., Meyer, N. K., Good, J., Lauber, A., . . . Ristovski, Z. D. (2010). Oxidative Potential of Logwood and Pellet Burning Particles Assessed by a Novel Profluorescent Nitroxide Probe. *Environmental Science & Technology, 44*(17), 6601-6607. doi:10.1021/es100963y

Moldanova, J., Fridell, E., Winnes, H., Holmin-Fridell, S., Boman, J., Jedynska, A., . . . Niessner, R. (2013). Physical and chemical characterisation of PM emissions from two ships operating in European Emission Control Areas. *Atmospheric Measurement Techniques, 6*(12), 3577-3596. doi:10.5194/amt-6-3577-2013

Moreno, T., Kelly, F. J., Dunster, C., Oliete, A., Martins, V., Reche, C., . . . Querol, X. (2017). Oxidative potential of subway PM2.5. *Atmospheric Environment, 148*, 230-238. doi:10.1016/j.atmosenv.2016.10.045

Mugica, V., Ortiz, E., Molina, L., De Vizcaya-Ruiz, A., Nebot, A., Quintana, R., . . . Alcantara, E. (2009). PM composition and source reconciliation in Mexico City. *Atmospheric Environment, 43*(32), 5068-5074. doi:10.1016/j.atmosenv.2009.06.051

Napelenok, S. L., Cohan, D. S., Hu, Y. T., & Russell, A. G. (2006). Decoupled direct 3D sensitivity analysis for particulate matter (DDM-3D/PM). *Atmospheric Environment, 40*(32), 6112-6121. doi:10.1016/j.atmosenv.2006.05.039

NOAA National Centers for Environmental Information. (2012). State of the Climate: Wilfires. Retrieved from https://www.ncdc.noaa.gov/sotc/fire/201211

Ntziachristos, L., Froines, J., Cho, A., & Sioutas, C. (2007). Relationship between redox activity and chemical speciation of size-fractionated particulate matter. *Particle and Fibre Toxicology, 4*(5).

Obrien, P. J. (1991). MOLECULAR MECHANISMS OF QUINONE CYTOTOXICITY. *Chemico-Biological Interactions, 80*(1), 1-41. doi:10.1016/0009-2797(91)90029-7

Paciorek, C. J. (2012). Combining spatial information sources while accounting for systematic errors in proxies. *Journal of the Royal Statistical Society Series C-Applied Statistics, 61*, 429-451. doi:10.1111/j.1467-9876.2011.01035.x

Pant, P., Baker, S. J., Shukla, A., Maikawa, C., Pollitt, K. J. G., & Harrison, R. M. (2015). The PM10 fraction of road dust in the UK and India: Characterization, source profiles and oxidative potential. *Science of the Total Environment, 530*, 445-452. doi:10.1016/j.scitotenv.2015.05.084

Patel, A., & Rastogi, N. (2018). Oxidative potential of ambient fine aerosol over a semi-urban site in the Indo-Gangetic Plain. *Atmospheric Environment, 175*, 127-134. doi:10.1016/j.atmosenv.2017.12.004

Pavovic, J., Holder, A. L., & Yelyerton, T. L. B. (2015). Effects of Aftermarket Control Technologies on Gas and Particle Phase Oxidative Potential from Diesel Engine Emissions. *Environmental Science & Technology, 49*(17), 10544-10552. doi:10.1021/acs.est.5b01487

Perrone, M. G., Zhou, J., Malandrino, M., Sangiorgi, G., Rizzi, C., Ferrero, L., . . . Bolzacchini, E. (2016). PM chemical composition and oxidative potential of the soluble fraction of particles at two sites in the urban area of Milan, Northern Italy. *Atmospheric Environment, 128*, 104-113. doi:10.1016/j.atmosenv.2015.12.040

Pope, C. A., Burnett, R. T., Thun, M. J., Calle, E. E., Krewski, D., Ito, K., & Thurston, G. D. (2002). Lung cancer, cardiopulmonary mortality, and long-term exposure to fine particulate air pollution. *Jama-Journal of the American Medical Association, 287*(9), 1132-1141. doi:10.1001/jama.287.9.1132

Pope, C. A., Ezzati, M., & Dockery, D. W. (2009). Fine-Particulate Air Pollution and Life Expectancy in the United States. *New England Journal of Medicine, 360*(4), 376-386. doi:10.1056/NEJMsa0805646

Pourkhesalian, A. M., Stevanovic, S., Rahman, M. M., Faghihi, E. M., Bottle, S. E., Masri, A. R., . . . Ristovski, Z. D. (2015). Effect of atmospheric aging on volatility and reactive oxygen species of biodiesel exhaust nano-particles. *Atmospheric Chemistry and Physics, 15*(16), 9099-9108. doi:10.5194/acp-15-9099-2015

Pourkhesalian, A. M., Stevanovic, S., Salimi, F., Rahman, M. M., Wang, H., Pham, P. X., . . . Ristovski, Z. D. (2014). Influence of Fuel Molecular Structure on the Volatility and Oxidative Potential of Biodiesel Particulate Matter. *Environmental Science & Technology, 48*(21), 12577-12585. doi:10.1021/es503160m

Prahalad, A. K., Inmon, J., Dailey, L. A., Madden, M. C., Ghio, A. J., & Gallagher, J. E. (2001). Air pollution particles mediated oxidative DNA base damage in a cell free system and in human airway epithelial cells in relation to particulate metal content and bioreactivity. *Chemical Research in Toxicology, 14*(7), 879-887. doi:10.1021/tx010022e

Rahman, M. M., Stevanovic, S., Islam, M. A., Heimann, K., Nabi, M. N., Thomas, G., . . . Ristovski, Z. D. (2015). Particle emissions from microalgae biodiesel combustion and their relative oxidative potential. *Environmental Science-Processes & Impacts, 17*(9), 1601-1610. doi:10.1039/c5em00125k

Rattanavaraha, W., Rosen, E., Zhang, H. F., Li, Q. F., Pantong, K., & Kamens, R. M. (2011). The reactive oxidant potential of different types of aged atmospheric particles: An outdoor chamber study. *Atmospheric Environment, 45*(23), 3848-3855. doi:10.1016/j.atmosenv.2011.04.002

Rowangould, G. M. (2013). A census of the US near-roadway population: Public health and environmental justice considerations. *Transportation Research Part D-Transport and Environment, 25*, 59-67. doi:10.1016/j.trd.2013.08.003

Saffari, A., Daher, N., Shafer, M. M., Schauer, J. J., & Sioutas, C. (2014a). Global Perspective on the Oxidative Potential of Airborne Particulate Matter: A Synthesis of Research Findings. *Environmental Science & Technology, 48*(13), 7576-7583. doi:10.1021/es500937x

Saffari, A., Daher, N., Shafer, M. M., Schauer, J. J., & Sioutas, C. (2014b). Seasonal and spatial variation in dithiothreitol (DTT) activity of quasi-ultrafine particles in the Los Angeles Basin and its association with chemical species. *Journal of Environmental Science and Health Part a-Toxic/Hazardous Substances & Environmental Engineering, 49*(4), 441-451. doi:10.1080/10934529.2014.854677

Saffari, A., Hasheminassab, S., Shafer, M. M., Schauer, J. J., Chatila, T. A., & Sioutas, C. (2016). Nighttime aqueous-phase secondary organic aerosols in Los Angeles and

its implication for fine particulate matter composition and oxidative potential. *Atmospheric Environment, 133*, 112-122. doi:10.1016/j.atmosenv.2016.03.022

Samake, A., Uzu, G., Martins, J. M. F., Calas, A., Vince, E., Parat, S., & Jaffrezo, J. L. (2017). The unexpected role of bioaerosols in the Oxidative Potential of PM. *Scientific Reports, 7*. doi:10.1038/s41598-017-11178-0

Samara, C. (2017). On the Redox Activity of Urban Aerosol Particles: Implications for Size Distribution and Relationships with Organic Aerosol Components. *Atmosphere, 8*(10). doi:10.3390/atmos8100205

Sameenoi, Y., Koehler, K., Shapiro, J., Boonsong, K., Sun, Y. L., Collett, J., . . . Henry, C. S. (2012). Microfluidic Electrochemical Sensor for On-Line Monitoring of Aerosol Oxidative Activity. *Journal of the American Chemical Society, 134*(25), 10562-10568. doi:10.1021/ja3031104

Sameenoi, Y., Panymeesamer, P., Supalakorn, N., Koehler, K., Chailapakul, O., Henry, C. S., & Volckens, J. (2013). Microfluidic Paper-Based Analytical Device for Aerosol Oxidative Activity. *Environmental Science & Technology, 47*(2), 932-940. doi:10.1021/es304662w

Samuël, W., Gaëlle, U., Calas, A., Chevrier, F., Besombes, J.-L., Charron, A., . . . Jaffrezo, J.-L. (2018). An apportionment method for the Oxydative Potential to the atmospheric PM sources: application to a one-year study in Chamonix, France. *Atmospheric Chemistry and Physics Discussion*.

Sarnat, J. (2017a). *Developing multipollutant exposure indicators of traffice pollution: The Dorm Room Inhalation to Vehicle Emissions (DRIVE) study*. Health Effects Institute.

Sarnat, J. (2017b). Developing multipollutant exposure indicators of traffice pollution: The Dorm Room Inhalation to Vehicle Emissions (DRIVE) study. Health Effects Institute. *In Press*.

Sarnat, J. A., Marmur, A., Klein, M., Kim, E., Russell, A. G., Sarnat, S. E., . . . Tolbert, P. E. (2008). Fine particle sources and cardiorespiratory morbidity: An application of chemical mass balance and factor analytical source-apportionment methods. *Environmental Health Perspectives, 116*(4), 459-466. doi:10.1289/ehp.10873

Sarnat, S. E., Klein, M., Sarnat, J. A., Flanders, W. D., Waller, L. A., Mulholland, J. A., . . . Tolbert, P. E. (2010). An examination of exposure measurement error from air pollutant spatial variability in time-series studies. *Journal of Exposure Science and Environmental Epidemiology, 20*(2), 135-146. doi:10.1038/jes.2009.10

Secrest, M. H., Schauer, J. J., Carter, E. M., Lai, A. M., Wang, Y. Q., Shan, M., . . . Baumgartner, J. (2016). The oxidative potential of PM2.5 exposures from indoor and outdoor sources in rural China. *Science of the Total Environment, 571*, 1477-1489. doi:10.1016/j.scitotenv.2016.06.231

Shen, H., & Anastasio, C. (2011). Formation of hydroxyl radical from San Joaquin Valley particles extracted in a cell-free surrogate lung fluid. *Atmospheric Chemistry and Physics, 11*(18), 9671-9682. doi:10.5194/acp-11-9671-2011

Shen, H., Barakat, A. I., & Anastasio, C. (2011). Generation of hydrogen peroxide from San Joaquin Valley particles in a cell-free solution. *Atmospheric Chemistry and Physics, 11*(2), 753-765. doi:10.5194/acp-11-753-2011

Shen, H. Y., & Anastasio, C. (2012). A comparison of hydroxyl radical and hydrogen peroxide generation in ambient particle extracts and laboratory metal solutions. *Atmospheric Environment, 46*, 665-668. doi:10.1016/j.atmosenv.2011.10.006

Shi, T. M., Schins, R. P. F., Knaapen, A. M., Kuhlbusch, T., Pitz, M., Heinrich, J., & Borm, P. J. A. (2003). Hydroxyl radical generation by electron paramagnetic resonance as a new method to monitor ambient particulate matter composition. *Journal of Environmental Monitoring, 5*(4), 550-556. doi:10.1039/b303928p

Shinyashiki, M., Eiguren-Fernandez, A., Schmitz, D. A., Di Stefano, E., Li, N., Linak, W. P., . . . Cho, A. K. (2009). Electrophilic and redox properties of diesel exhaust particles. *Environmental Research, 109*(3), 239-244. doi:10.1016/j.envres.2008.12.008

Shirmohammadi, F., Hasheminassab, S., Wang, D. B., Schauer, J. J., Shafer, M. M., Delfino, R. J., & Sioutas, C. (2016). The relative importance of tailpipe and non-tailpipe emissions on the oxidative potential of ambient particles in Los Angeles, CA. *Faraday Discussions, 189*, 361-380. doi:10.1039/c5fd00166h

Shirmohammadi, F., Wang, D. B., Hasheminassab, S., Verma, V., Schauer, J. J., Shafer, M. M., & Sioutas, C. (2017). Oxidative potential of on-road fine particulate matter (PM2.5) measured on major freeways of Los Angeles, CA, and a 10-year comparison with earlier roadside studies. *Atmospheric Environment, 148*, 102-114. doi:10.1016/j.atmosenv.2016.10.042

Snyder, M. G., Venkatram, A., Heist, D. K., Perry, S. G., Petersen, W. B., & Isakov, V. (2013). RLINE: A line source dispersion model for near-surface releases. *Atmospheric Environment, 77*, 748-756. doi:10.1016/j.atmosenv.2013.05.074

Solomon, P. A., Crumpler, D., Flanagan, J. B., Jayanty, R. K. M., Rickman, E. E., & McDade, C. E. (2014). U.S. National PM2.5 Chemical Speciation Monitoring Networks—CSN and IMPROVE: Description of networks. *Journal of the Air & Waste Management Association, 64*(12), 1410-1438. doi:10.1080/10962247.2014.956904

Solomon, P. A., Crumpler, D., Flanagan, J. B., Jayanty, R. K. M., Rickman, E. E., & McDade, C. E. (2014). US National PM2.5 Chemical Speciation Monitoring Networks-CSN and IMPROVE: Description of networks. *Journal of the Air & Waste Management Association, 64*(12), 1410-1438. doi:10.1080/10962247.2014.956904

Son, Y., Mishin, V., Welsh, W., Lu, S. E., Laskin, J. D., Kipen, H., & Meng, Q. M. (2015). A Novel High-Throughput Approach to Measure Hydroxyl Radicals Induced by Airborne Particulate Matter. *International Journal of Environmental Research and Public Health, 12*(11), 13678-13695. doi:10.3390/ijerph121113678

Sorensen, M., Daneshvar, B., Hansen, M., Dragsted, L. O., Hertel, O., Knudsen, L., & Loft, S. (2003). Personal PM2.5 exposure and markers of oxidative stress in blood. *Environmental Health Perspectives, 111*(2), 161-165. doi:10.1289/ehp.5646

Stein, A. F., Isakov, V., Godowitch, J., & Draxler, R. R. (2007). A hybrid modeling approach to resolve pollutant concentrations in an urban area. *Atmospheric Environment, 41*(40), 9410-9426. doi:10.1016/j.atmosenv.2007.09.004

Stevanovic, S., Miljevic, B., Surawski, N. C., Fairfull-Smith, K. E., Bottle, S. E., Brown, R., & Ristovski, Z. D. (2013). Influence of Oxygenated Organic Aerosols (OOAs) on the Oxidative Potential of Diesel and Biodiesel Particulate Matter. *Environmental Science & Technology, 47*(14), 7655-7662. doi:10.1021/es4007433

Stocker, J., Hood, C., Carruthers, D., Seaton, M., & Jockel, K. (2014, October 27-29, 2014). *The Development and Evaluation of an Automated System for Nesting ADMS-Urban Regional Photochemical Models.* Paper presented at the 13th Annual CMAS Conference, Chapel HIll, NC.

Strak, M., Janssen, N. A. H., Godri, K. J., Gosens, I., Mudway, I. S., Cassee, F. R., . . . Hoek, G. (2012). Respiratory Health Effects of Airborne Particulate Matter: The Role of Particle Size, Composition, and Oxidative Potential-The RAPTES Project. *Environmental Health Perspectives, 120*(8), 1183-1189. doi:10.1289/ehp.1104389

Strickland, M. J., Darrow, L. A., Klein, M., Flanders, W. D., Sarnat, J. A., Waller, L. A., . . . Tolbert, P. E. (2010). Short-term Associations between Ambient Air Pollutants and Pediatric Asthma Emergency Department Visits. *American Journal of Respiratory and Critical Care Medicine, 182*(3), 307-316. doi:10.1164/rccm.200908-1201OC

Szigeti, T., Ovari, M., Dunster, C., Kelly, F. J., Lucarelli, F., & Zaray, G. (2015). Changes in chemical composition and oxidative potential of urban PM2.5 between 2010 and 2013 in Hungary. *Science of the Total Environment, 518*, 534-544. doi:10.1016/j.scitotenv.2015.03.025

Theobald, M. R., Simpson, D., & Vieno, M. (2016). Improving the spatial resolution of air-quality modelling at a European scale - development and evaluation of the Air Quality Re-gridder Model (AQR v1.1). *Geoscientific Model Development, 9*(12), 4475-4489. doi:10.5194/gmd-9-4475-2016

Tian, D., Hu, Y. T., Wang, Y. H., Boylan, J. W., Zheng, M., & Russell, A. G. (2009). Assessment of Biomass Burning Emissions and Their Impacts on Urban and Regional PM2.5: A Georgia Case Study. *Environmental Science & Technology, 43*(2), 299-305. doi:10.1021/es801827s

Totlandsdal, A. I., Lag, M., Lilleaas, E., Cassee, F., & Schwarze, P. (2015). Differential Proinflammatory Responses Induced by Diesel Exhaust Particles with Contrasting PAH and Metal Content. *Environmental Toxicology, 30*(2), 188-196. doi:10.1002/tox.21884

Tuet, W. Y., Chen, Y. L., Xu, L., Fok, S., Gao, D., Weber, R. J., & Ng, N. L. (2017). Chemical oxidative potential of secondary organic aerosol (SOA) generated from the photooxidation of biogenic and anthropogenic volatile organic compounds. *Atmospheric Chemistry and Physics, 17*(2), 839-853. doi:10.5194/acp-17-839-2017

U. S. Environmental Protection Agency. (1997). *The STability ARray Program*.

U. S. Environmental Protection Agency. (2009). *Motor Vehicle Emission Simulator (MOVES) 2010: User Guide*.

U. S. Environmental Protection Agency. (2012). Motor Vehicle Emissions Simulator (MOVES) User Guide for MOVES 2010b.

U.S. Environmental Protection Agency. (2004). *User's Guide for the AERMOD Meteorological Processor (AERMET)*.

U.S. Environmental Protection Agency. (2015). *AERMINUTE User's Guide*.

U.S. EPA. (2009). *Integrated Science Assessment (ISA) for Particulate Matter*. (EPA/600/R-08/139F). Washington, DC: U.S. Environmental Protection Agency,.

United Nations, Department of Economic and Social Affairs, & Population Division. (2014). World Urbanization Prospects: The 2014 Revision, Highlights. (ST/ESA/SER.A/352).

Valavanidis, A., Salika, A., & Theodoropoulou, A. (2000). Generation of hydroxyl radicals by urban suspended particulate air matter. The role of iron ions. *Atmospheric Environment, 34*(15), 2379-2386. doi:10.1016/s1352-2310(99)00435-5

Velali, E., Papachristou, E., Pantazaki, A., Choli-Papadopoulou, T., Planou, S., Kouras, A., . . . Samara, C. (2016). Redox activity and in vitro bioactivity of the water-soluble fraction of urban particulate matter in relation to particle size and chemical composition. *Environmental Pollution, 208*, 774-786. doi:10.1016/j.envpol.2015.10.058

Venkatachari, P., & Hopke, P. K. (2008). Development and laboratory testing of an automated monitor for the measurement of atmospheric particle-bound reactive oxygen species (ROS). *Aerosol Science and Technology, 42*(8), 629-635. doi:10.1080/02786820802227345

Venkatachari, P., Hopke, P. K., Brune, W. H., Ren, X. R., Lesher, R., Mao, J. Q., & Mitchel, M. (2007). Characterization of wintertime reactive oxygen species

concentrations in Flushing, New York. *Aerosol Science and Technology, 41*(2), 97-111. doi:10.1080/02786820601116004

Venkatachari, P., Hopke, P. K., Grover, B. D., & Eatough, D. J. (2005). Measurement of particle-bound reactive oxygen species in Rubidoux aerosols. *Journal of Atmospheric Chemistry, 50*(1), 49-58. doi:10.1007/s10874-005-1662-z

Verma, V., Fang, T., Guo, H., King, L., Bates, J. T., Peltier, R. E., . . . Weber, R. J. (2014). Reactive oxygen species associated with water-soluble PM2.5 in the southeastern United States: spatiotemporal trends and source apportionment. *Atmospheric Chemistry and Physics, 14*(23), 12915-12930. doi:10.5194/acp-14-12915-2014

Verma, V., Fang, T., Xu, L., Peltier, R. E., Russell, A. G., Ng, N. L., & Weber, R. J. (2015). Organic Aerosols Associated with the Generation of Reactive Oxygen Species (ROS) by Water-Soluble PM2.5. *Environmental Science & Technology, 49*(7), 4646-4656. doi:10.1021/es505577w

Verma, V., Ning, Z., Cho, A. K., Schauer, J. J., Shafer, M. M., & Sioutas, C. (2009). Redox activity of urban quasi-ultrafine particles from primary and secondary sources. *Atmospheric Environment, 43*(40), 6360-6368. doi:10.1016/j.atmosenv.2009.09.019

Verma, V., Pakbin, P., Cheung, K. L., Cho, A. K., Schauer, J. J., Shafer, M. M., . . . Sioutas, C. (2011). Physicochemical and oxidative characteristics of semi-volatile components of quasi-ultrafine particles in an urban atmosphere. *Atmospheric Environment, 45*(4), 1025-1033. doi:10.1016/j.atmosenv.2010.10.044

Verma, V., Polidori, A., Schauer, J. J., Shafer, M. M., Cassee, F. R., & Sioutas, C. (2009). Physicochemical and Toxicological Profiles of Particulate Matter in Los Angeles during the October 2007 Southern California Wildfires. *Environmental Science & Technology, 43*(3), 954-960. doi:10.1021/es8021667

Verma, V., Rico-Martinez, R., Kotra, N., King, L., Liu, J. M., Snell, T. W., & Weber, R. J. (2012). Contribution of Water-Soluble and Insoluble Components and Their Hydrophobic/Hydrophilic Subfractions to the Reactive Oxygen Species-Generating Potential of Fine Ambient Aerosols. *Environmental Science & Technology, 46*(20), 11384-11392. doi:10.1021/es302484r

Verma, V., Wang, Y., El-Afifi, R., Fang, T., Rowland, J., Russell, A. G., & Weber, R. J. (2015). Fractionating ambient humic-like substances (HULIS) for their reactive oxygen species activity - Assessing the importance of quinones and atmospheric aging. *Atmospheric Environment, 120*, 351-359. doi:10.1016/j.atmosenv.2015.09.010

Vidrio, E., Jung, H., & Anastasio, C. (2008). Generation of hydroxyl radicals from dissolved transition metals in surrogate lung fluid solutions. *Atmospheric Environment, 42*(18), 4369-4379. doi:10.1016/j.atmosenv.2008.01.004

Visentin, M., Pagnoni, A., Sarti, E., & Pietrogrande, M. C. (2016). Urban PM2.5 oxidative potential: Importance of chemical species and comparison of two spectrophotometric cell-free assays. *Environmental Pollution, 219*, 72-79. doi:10.1016/j.envpol.2016.09.047

Vreeland, H., Schauer, J. J., Russell, A. G., Marshall, J. D., Fushimi, A., Jain, G., . . . Bergin, M. H. (2016). Chemical characterization and toxicity of particulate matter emissions from roadside trash combustion in urban India. *Atmospheric Environment, 147*, 22-30. doi:10.1016/j.atmosenv.2016.09.041

Vreeland, H., Weber, R., Bergin, M., Greenwald, R., Golan, R., Russell, A. G., . . . Sarnat, J. A. (2017). Oxidative potential of PM2.5 during Atlanta rush hour: Measurements of in-vehicle dithiothreitol (DTT) activity. *Atmospheric Environment, 165*, 169-178. doi:10.1016/j.atmosenv.2017.06.044

Wang, Y., Arellanes, C., Curtis, D. B., & Paulson, S. E. (2010). Probing the Source of Hydrogen Peroxide Associated with Coarse Mode Aerosol Particles in Southern California. *Environmental Science & Technology, 44*(11), 4070-4075. doi:10.1021/es100593k

Wang, Y., Hopke, P., Sun, L., Chalupa, D. C., & Utell, M. J. (2011). Laboratory and Field Testing of an Automated Atmospheric Particle-Bound Reactive Oxygen Species Sampling-Analysis System. *Journal of Toxicology, 2011*.

Wang, Y., Kim, H., & Paulson, S. E. (2011). Hydrogen peroxide generation from alpha- and beta-pinene and toluene secondary organic aerosols. *Atmospheric Environment, 45*(18), 3149-3156. doi:10.1016/j.atmosenv.2011.02.060

Wang, Y., Plewa, M., Mukherjee, U., & Verma, V. (2018). Assessing the cytotoxicity of ambient partiuclate matter (PM) using Chinese hamster ovary (CHO) cells and its relationship with the PM chemical composition and oxidative potential. *Atmospheric Environment, 179*, 132-141.

Weichenthal, S., Crouse, D. L., Pinault, L., Godri-Pollitt, K., Lavigne, E., Evans, G., . . . Burnett, R. T. (2016). Oxidative burden of fine particulate air pollution and risk of cause-specific mortality in the Canadian Census Health and Environment Cohort (CanCHEC). *Environmental Research, 146*, 92-99. doi:10.1016/j.envres.2015.12.013

Weichenthal, S., Lavigne, E., Evans, G., Pollitt, K., & Burnett, R. T. (2016). Ambient PM2.5 and risk of emergency room visits for myocardial infarction: impact of regional PM2.5 oxidative potential: a case-crossover study. *Environmental Health, 15*, 9. doi:10.1186/s12940-016-0129-9

Weijers, E. P., Khlystov, A. Y., Kos, G. P. A., & Erisman, J. W. (2004). Variability of particulate matter concentrations along roads and motorways determined by a moving measurement unit. *Atmospheric Environment, 38*(19), 2993-3002. doi:10.1016/j.atmosenv.2004.02.045

Wilson, J. G., Kingham, S., Pearce, J., & Sturman, A. P. (2005). A review of intraurban variations in particulate air pollution: Implications for epidemiological research. *Atmospheric Environment, 39*(34), 6444-6462. doi:10.1016/j.atmosenv.2005.07.030

Winquist, A., Schauer, J. J., Turner, J. R., Klein, M., & Sarnat, S. E. (2015). Impact of ambient fine particulate matter carbon measurement methods on observed associations with acute cardiorespiratory morbidity. *Journal of Exposure Science and Environmental Epidemiology, 25*(2), 215-221. doi:10.1038/jes.2014.55

Wragg, F. P. H., Fuller, S. J., Freshwater, R., Green, D. C., Kelly, F. J., & Kalberer, M. (2016). An automated online instrument to quantify aerosol-bound reactive oxygen species (ROS) for ambient measurement and health-relevant aerosol studies. *Atmospheric Measurement Techniques, 9*(10), 4891-4900. doi:10.5194/amt-9-4891-2016

Xiong, Q. S., Yu, H. R., Wang, R. R., Wei, J. L., & Verma, V. (2017). Rethinking Dithiothreitol-Based Particulate Matter Oxidative Potential: Measuring Dithiothreitol Consumption versus Reactive Oxygen Species Generation. *Environmental Science & Technology, 51*(11), 6507-6514. doi:10.1021/acs.est.7b01272

Yang, A., Janssen, N. A. H., Brunekreef, B., Cassee, F. R., Hoek, G., & Gehring, U. (2016). Children's respiratory health and oxidative potential of PM2.5: the PIAMA birth cohort study. *Occupational and Environmental Medicine, 73*(3), 154-160. doi:10.1136/oemed-2015-103175

Yang, A., Jedynska, A., Hellack, B., Rooter, I., Hoek, G., Brunekreef, B., . . . Janssen, N. A. H. (2014). Measurement of the oxidative potential of PM2.5 and its constituents: The effect of extraction solvent and filter type. *Atmospheric Environment, 83*, 35-42. doi:10.1016/j.atmosenv.2013.10.049

Yang, A., Wang, M., Eeftens, M., Beelen, R., Dons, E., Leseman, D., . . . Hoek, G. (2015). Spatial Variation and Land Use Regression Modeling of the Oxidative Potential of Fine Particles. *Environmental Health Perspectives, 123*(11), 1187-1192. doi:10.1289/ehp.1408916

Yanosky, J. D., Tonne, C. C., Beevers, S. D., Wilkinson, P., & Kelly, F. J. (2012). Modeling Exposures to the Oxidative Potential of PM10. *Environmental Science & Technology, 46*(14), 7612-7620. doi:10.1021/es3010305

Yu, H., Russell, A., Mulholland, J., Odman, T., Hu, Y., Chang, H. H., & Kumar, N. (2018). Cross-comparison and evaluation of air pollution field estimation methods. *Atmospheric Environment, 179*, 49-60.

Yu, H. R., Wei, J. L., Cheng, Y. L., Subedi, K., & Verma, V. (2018). Synergistic and Antagonistic Interactions among the Particulate Matter Components in Generating

Reactive Oxygen Species Based on the Dithiothreitol Assay. *Environmental Science & Technology, 52*(4), 2261-2270. doi:10.1021/acs.est.7b04261

Zhai, X. X., Mulholland, J., Russell, A., & Holmes, H. (2017). Spatial and temporal source apportionment of PM2.5 in Georgia, 2002 to 2013. *Atmospheric Environment, 161*, 112-121.

Zhai, X. X., Russell, A. G., Sampath, P., Mulholland, J. A., Kim, B., Kim, Y., & D'Onofrio, D. (2016). Calibrating R-LINE model results with observational data to develop annual mobile source air pollutant fields at find spatial resolution: Application in Atlanta. *Atmospheric Environment, 147*, 446-457. doi:http://dx.doi.org/10.1016/j.atmosenv.2016.10.015

Zhang, X., Staimer, N., Tjoa, T., Gillen, D. L., Schauer, J. J., Shafer, M. M., . . . Delfino, R. J. (2016). Associations between microvascular function and short-term exposure to traffic-related air pollution and particulate matter oxidative potential. *Environmental Health, 15*, 16. doi:10.1186/s12940-016-0157-5

Zhu, Y. F., Hinds, W. C., Kim, S., & Sioutas, C. (2002). Concentration and size distribution of ultrafine particles near a major highway. *Journal of the Air & Waste Management Association, 52*(9), 1032-1042. doi:10.1080/10473289.2002.10470842

Zomer, B., Colle, L., Jedynska, A., Pasterkamp, G., Kooter, I., & Bloemen, H. (2011). Chemiluminescent reductive acridinium triggering (CRAT)-mechanism and applications. *Analytical and Bioanalytical Chemistry, 401*(9), 2945-2954. doi:10.1007/s00216-011-5342-3